LIGHT-DRIVEN METAL-CATALYZED ASYMMETRIC TRANSFORMATIONS

Eugenio Gandolfo

UNIVERSITAT ROVIRA i VIRGILI

Light-driven Metal-catalyzed Asymmetric Transformations

EUGENIO GANDOLFO

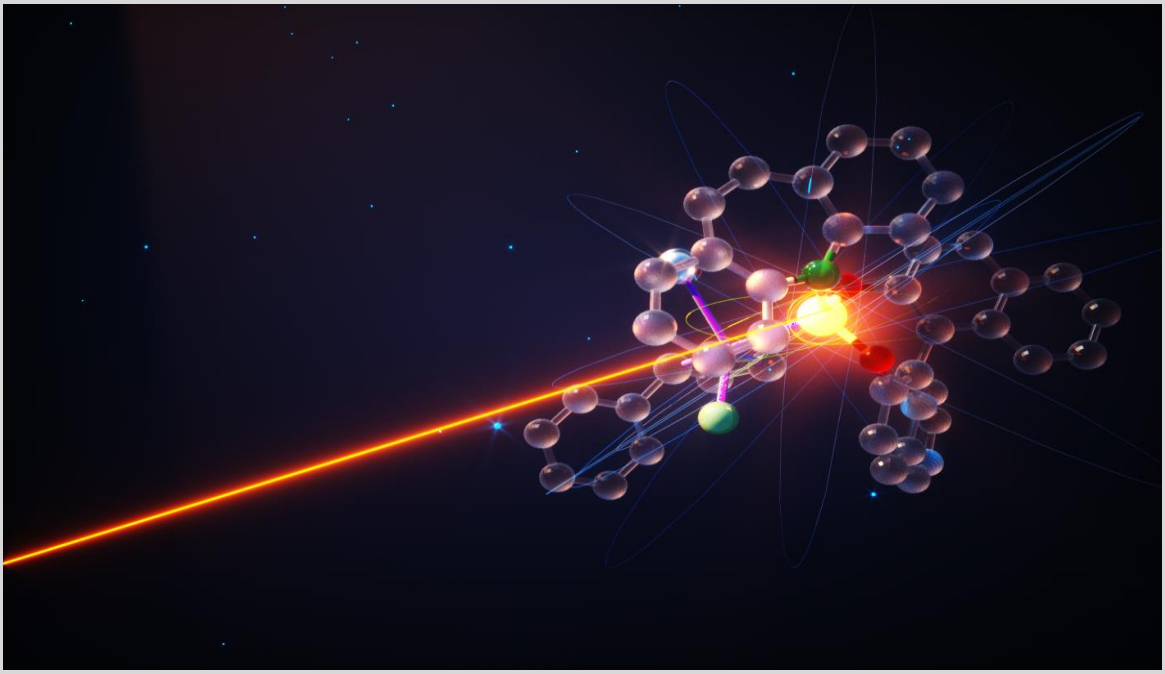

DOCTORAL THESIS
2021

Eugenio Gandolfo

Light-driven Metal-catalyzed Asymmetric Transformations

Doctoral Thesis

Supervised by Prof. Paolo Melchiorre

ICIQ – Institut Català d'Investigació Química

UNIVERSITAT
ROVIRA i VIRGILI

Tarragona
2021

UNIVERSITAT ROVIRA i VIRGILI

ICIQ Institut Català d'Investigació Química

Prof. Paolo Melchiorre, ICREA Research Professor & ICIQ Group Leader

I STATE that the present study, entitled "Light-driven Metal-catalyzed Asymmetric Transformations", presented by EUGENIO GANDOLFO for the award of the degree of Doctor, has been carried out under my supervision at the Institut Català d'Investigació Química (ICIQ).

Tarragona, June the 22nd, 2021

Doctoral Thesis Supervisor

Prof. Paolo Melchiorre

Acknowledgements

I would like to thank my supervisor Professor Paolo Melchiorre for giving me the opportunity to join his research group and take part in this exciting trip.

Additionally, I would like to thank all the former and current members of the Melchiorre group for sharing their knowledge and helping me going through my doctoral studies. I want to thank Dr Lorna Piazzi, Maria Checa and Núria Planella for the administrative support.

I would like to thank all the research support units at ICIQ, in particular I am indebted to the NMR-staff, the spectroscopy unit and the chromatography unit. I would also like to acknowledge the financial support from the Institute of Chemical Research of Catalonia (ICIQ) from the European Research Council for the ERC starting grant (278541-ORGA-NAUT) and ERC consolidator grant (681840-CATA-LUX).

Additionally, I am personally grateful to:

- ICIQ PhD Fellowship
- PHOTOORGANO CAT supported by MICINN-Agencia Estatal de Investigación (CTQ2016-75520-P)

List of Publications

- **Gandolfo, E**., Tang, X., Roy, S. R., Melchiorre, P. "Photochemical Asymmetric Nickel-Catalyzed Acyl Cross-Coupling" *Angew. Chem. Int. Ed.* **2019**, *58*, 16854-16858.

- Crisenza, G. E. M., Faraone, A., **Gandolfo, E.**, Mazzarella, D., Melchiorre, P. "Catalytic asymmetric C–C cross-couplings enabled by photoexcitation" *Nat. Chem.* **2021**. DOI: *10.1038/s41557-021-00683-5*.

A Flavia e Fiorella

Table of Contents

Chapter I

General Overview

1.1 Introduction

This chapter provides a general overview on photochemistry and how its merger with established catalytic tools served to develop new synthetic strategies. Photochemistry is the branch of chemistry that studies the effects of the interaction between light and matter. For this interaction to be fruitful, it has to satisfy the first principle of photochemistry (the *Grotthuss-Draper law*), which states that only the light absorbed by a molecule can induce a photochemical process.[1] As necessary condition, the incident light has to fit to the Bohr equation (Equation 1.1, where h is Planck's constant and E_i and E_f are the initial and final orbital energies):[1]

$$h\nu = E_f - E_i \qquad \text{(Eq. 1.1)}$$

In a simple way, only the photons possessing the right energy ($h\nu$) can effectively promote the HOMO-LUMO transition. E_f and E_i represents the energy of the excited- and ground-state wave functions Ψ_f and Ψ_i, respectively (Figure 1.1a). These functions describe the state of the electron in the respective orbitals.[2]

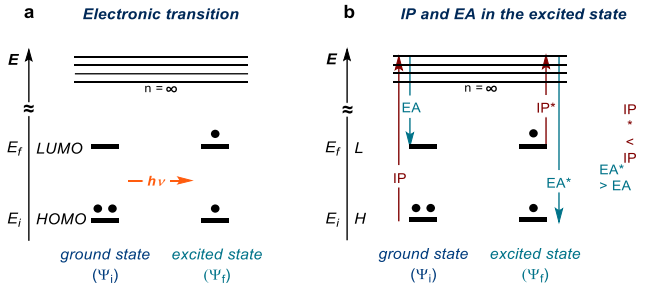

Figure 1.1: a) The energy of a photon ($h\nu$) induces the transition of an electron from the HOMO (H) to the LUMO (L); b) differences in EA and IP between the ground state and the excited state (marked with *).

[1] Balzani, V., Ceroni, P., Juris, A., "Photochemistry and Photophysics: Concept, Research and Applications", Weinheim, Wiley-VCH, 2014
[2] Turro, N. J., Ramamurthy, V., Scaiano, J. C., "Principles of Molecular Photochemistry: An Introduction", University Science Books, 2009

Therefore, upon light excitation, the electrons in the highest occupied molecular orbital (HOMO, H) can be promoted to the lowest unoccupied molecular orbital (LUMO, L) through a vertical transition (Franck-Condon principle).[2] Due to an enhanced electron affinity (EA) of the HOMO and a lower ionization potential (IP) of the LUMO (Figure 1.1b), an excited-state molecule has a completely different reactivity than in the ground state; for example, it becomes both a better oxidant and a better reductant. Hence, a molecule in its excited state has to be considered a completely different compound than in its ground state.[3]

An excited molecule can take part in different pathways (Figure 1.2): i) unimolecular ones, ii) bi-molecular ones, and iii) radiative and nonradiative processes. The unimolecular processes include isomerization, fragmentation, and rearrangement; the bi-molecular ones include photoadditions, single-electron transfer[4] (SET), energy transfer[5] (EnT), and atom transfer[6] (AT). Alternatively, the excited-state molecule can return back to the ground state through fluorescence, phosphorescence (radiative), or thermal degradation (nonradiative) pathways.

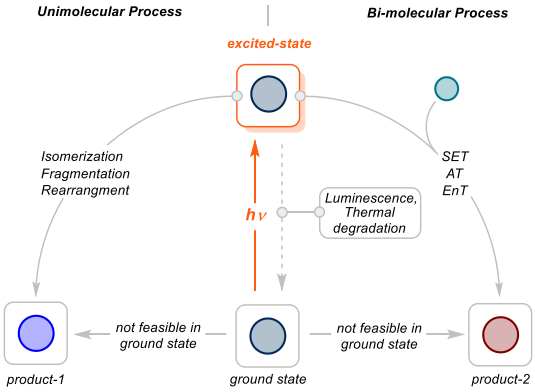

Figure 2.2: Fundamental steps in Light-Matter interaction

[3] Albini, A., Fagnoni, M. "Photochemically Generated Intermediates In Synthesis" 2013, John Wiley & Sons
[4] Kavarnos, G. J. "Fundamentals of Photoinduced Electron Transfer" 1993, VCH.
[5] Strieth-Kalthoff, F., James, M. J., Teders, M., Pitzer, L., Glorius, F. "Energy Transfer Catalysis Mediated by Visible Light: Principles, Applications, Directions" Chem. Soc. Rev. 2018, 47, 7190-7202.
[6] Capaldo, L., Lafayette Quadri, L., Ravelli, D., "Photocatalytic Hydrogen Atom Transfer: the Philosopher's Stone for Late-Stage Functionalization?" *Green Chem.* **2020**, *22*, 3376.

Overall, the excitation of molecules can open up new opportunities in chemistry, which are inaccessible under thermal conditions. For example, the bimolecular processes, which will be extensively discussed in this thesis, provide an easy way to generate open-shell intermediates under mild conditions, which can then be leveraged to design radical processes.

The potential of photochemistry was recognized a long ago.[7] However, it is only with Giacomo Ciamician, at the beginning of the 20th century, that synthetic photochemistry was exploited to effectively synthesize molecules.[8] Nevertheless, photochemistry remained a niche field with limited applications for a long time.[9] In early 2000, the situation changed. Photochemistry experienced a new youth, capitalizing upon the techno-scientific advancements, such as the development of light-emitting diodes (LEDs)[10] and the application of transition metal photocatalysts.[11] Those innovations provided new momentum for photochemistry.

In modern synthetic photochemistry, a reaction is generally initiated through two main strategies (Figure 1.3):[12]

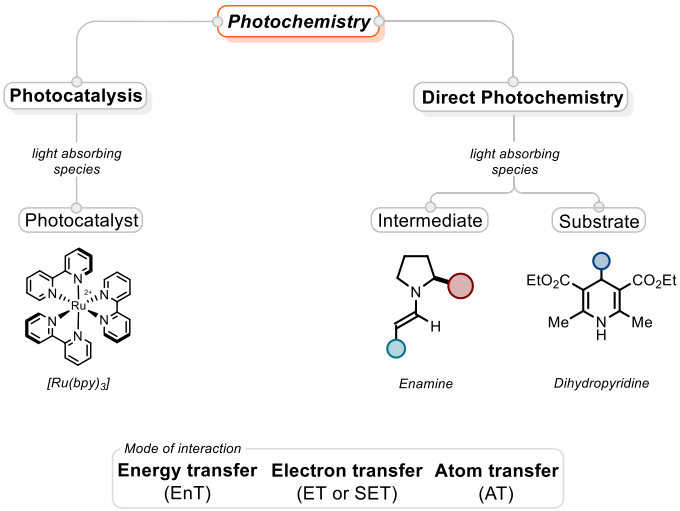

Figure 3.3: Branches of modern synthetic photochemistry

[7] Roth, H. D., "The Beginnings of Organic Photochemistry", Angew. Chem. Int. Ed. 1989, 28, 1193.
[8] Ciamician, G., "The Photochemistry of the Future" Science 1912, 36, 385.
[9] Albini, A., "Photochemistry: Past, Present and Future", Berlin Heidelberg, Springer-Verlag, 2016;
[10] Sender, M., Ziegenbald, D., "Light Sources for Photochemical Processes – Estimation of Technological Potentials" *Chem. Ing. Tech.* **2017**, *89*, 1159.
[11] Paris, J. P., Brandt, W. W., "Charge Transfer Luminescence of a Ruthenium(II) Chelate" *J. Am. Chem. Soc.* **1959**, *81*, 5001.
[12] Buzzetti, L., Crisenza, G. E. M., Melchiorre, P., "Mechanistic Studies in Photocatalysis" *Angew. Chem. Int. Ed.* **2019**, *58*, 3730.

i) *photocatalysis*, which employs the ability of a colored catalyst to absorb light and then activate achromatic substrates (the catalyst is regenerated during the reaction without undergoing any permanent chemical change); ii) *direct photochemistry*, which consists in the direct excitation of colored substrates or reaction intermediates to trigger a photochemical process in the excited state.

Within the photocatalytic approach, a photocatalyst harvests the energy of light to drive the formation of open-shell intermediates via the aforementioned bi-molecular processes (SET, EnT and AT). *Photoredox catalysis* uses SET events to trigger the formation of radicals or reactive intermediates; this approach has been fruitfully merged with other ground-state catalytic tools (e.g. organocatalysis, nickel catalysis) to address synthetic challenges not achievable via classical ground-state chemistry.[13]

A general scheme for photoredox catalytic processes is depicted in Scheme 1.1.

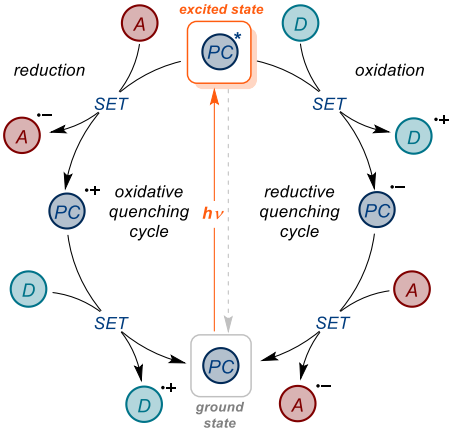

Scheme 4.1: Quenching cycles in photoredox catalysis.

The electronically excited photocatalyst (PC*) is a better oxidant and reductant than in the ground state and can trigger SET events to activate ground-state substrates via an oxidative or a reductive quenching mechanism. In the reductive quenching cycle, the PC* initially acts as oxidant with a suitable electron donor (**D**), leading to the formation of the radical cation of the donor ($\mathbf{D}^{\bullet+}$) and the reduced form of the photocatalyst $PC^{\bullet-}$. The latter intermediate is now a good reductant and can transfer an electron to a suitable acceptor (**A**), forming the radical anionic $\mathbf{A}^{\bullet-}$ while returning the ground-state PC and closing the

[13] Shaw, M. H., Twilton, J., MacMillan, D. W. C., "Photoredox Catalysis in Organic Chemistry" *J. Org. Chem.* **2016**, *81*, 6898.

catalytic cycle. In the alternative oxidative cycle, the PC* is a reducing species that transfers an electron to a suitable acceptor **A**. This event delivers the radical anion of the acceptor $\mathbf{A}^{\bullet-}$ and the oxidized form of the photocatalyst ($PC^{\bullet+}$). This intermediate acts as an oxidant to trigger a SET event with a suitable donor **D**, completing the photoredox catalytic cycle. In both catalytic cycles the radical intermediates, generated upon SET events from the photocatalyst, undergo following transformations to afford the final product. In a seminal study,[14] MacMillan showcased the beneficial features of combining photoredox catalysis with classical enantioselective enamine **I** catalysis (Scheme 1.2). This dual catalytic approach delivered the α-alkylated aldehyde **3**, unobtainable under thermal conditions, in high yields and enantiomeric excess.

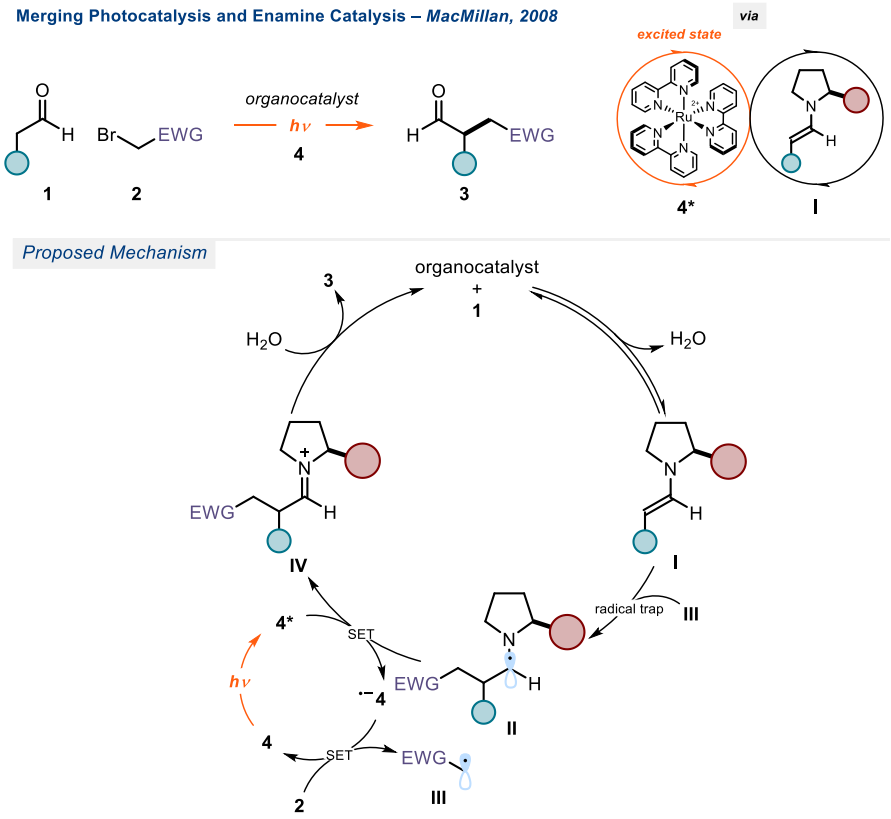

Scheme 5.2: First example on the merge of photoredox catalysis and organocatalysis; EWG: electron-withdrawing group.

[14] Nicewicz, D. A., MacMillan, D. W. C. "Merging Photoredox Catalysis with Organocatalysis: the Direct Asymmetric Alkylation of Aldehydes" Science 2008, 322, 77-80.

The proposed catalytic cycle starts with the photoexcitation of the photoredox catalyst **4**, which oxidizes via SET a sacrificial amount of enamine **I**. This event produces a strong reducing Ru(I) complex (**4**$^{\bullet-}$), able to transfer an electron to the electron-poor alkyl bromide **2**. This step regenerates **4** and leads to the formation of the electrophilic radical intermediate **III**, after bromide anion loss. Stereocontrolled trap of **III** by the transient electron-rich chiral enamine **I** produces the α-amino radical **II**. The latter is oxidized by the photoexcited complex **4** to form the iminium **IV**. Hydrolysis of **IV** delivers product **3** and turns over the organocatalyst. Recently, the group of Yoon[15] demonstrated that this process is taking place via a self-propagating radical chain manifold in which the photocatalyst is acting as an initiator to generate the first electrophilic radical **III**.

The example detailed in Scheme 1.2 paved the way to the development of other reactions, where visible light excitation of a photocatalyst was successfully combined with ground-state catalytic tools to activate achromatic substrates.[16] On this vein, photoredox catalysis was also successfully merged with metal-catalysis. Inspired by previous works,[17] the groups of Molander,[18] Doyle and MacMillan[19] demonstrated that the iridium-based photocatalysts (**9** and **10**) could expand the cross-coupling partners of nickel catalysis (Scheme 1.3). Moreover, this approach solved some of the drawbacks of classical nickel cross-coupling (e.g. harsh conditions, hazardous organometallic reagents) combining aryl halides **5** with bench-stable alkyl radical precursors **6** to deliver products **7**. Besides nickel, the combination of photoredox catalysis with metal catalysis - termed as *metallaphotoredox catalysis* - was also successfully expanded to include other transition metals, such as palladium[20], copper,[21] and gold. [22]

---

[15] Cismesia, M. A.; Yoon, T. P. "Characterizing Chain Processes in Visible Light Photoredox Catalysis" *Chem. Sci.* **2015**, *6*, 5426.

[16] a) Prier, C. K., Rankic, D. A., MacMillan, D. W. C., " Visible Light Photoredox Catalysis with Transition Metal Complexes: Applications in Organic Synthesis" *Chem. Rev.* **2013**, *113*, 5322; b) Tucker, J. W., Stephenson, C. R. J., "Shining Light on Photoredox Catalysis: Theory and Synthetic Applications", *J. Org. Chem.* **2012**, *77*, 1617.

[17] a) Kalyani, D., McMurtrey, K. B., Neufeldt, S. R., Sanford, M. S. "Room-Temperature C-H Arylation: Merger of Pd-Catalyzed C-H Functionalization and Visible-Light Photocatalysis" *J. Am. Chem. Soc.* **2011**, *133*, 18566.

[18] Tellis, J. C., Primer, D. N., Molander, G. A., "Single-Electron Transmetalation in Organoboron Cross-Coupling by Photoredox/Nickel Dual Catalysis", *Science* **2014**, *345*, 433.

[19] Zuo, Z., Ahneman, D.T., Chu, L., Terret, J. A., Doyle, A. G., MacMillan, D. W. C., 'Merging Photoredox with Nickel Catalysis: Coupling of α-Carboxyl Sp^3-Carbons with Aryl Halides', *Science* **2014**, *345*, 437

[20] Shee, M., Singh, N. D. P., "Cooperative Photoredox and Palladium Catalysis: Recent Advances in Various Functionalization Reactions" *Catal. Sci. Technol.* **2021**, *11*, 742.

[21] Hossain, A., Bhattacharyya, A., Reiser O., "Copper's Rapid Ascent in Visible-Light Photoredox Catalysis" *Science* **2019**, *364,* 450.

[22] Hopkinson, M. N., Tlahuext-Aca, A., Glorius, F., "Merging Visible Light Photoredox and Gold Catalysis" *Acc. Chem. Res.* **2016**, *49*, 2261. For a review see: a) Twilton, J., Le, C., Zhang, P., Shaw, M.

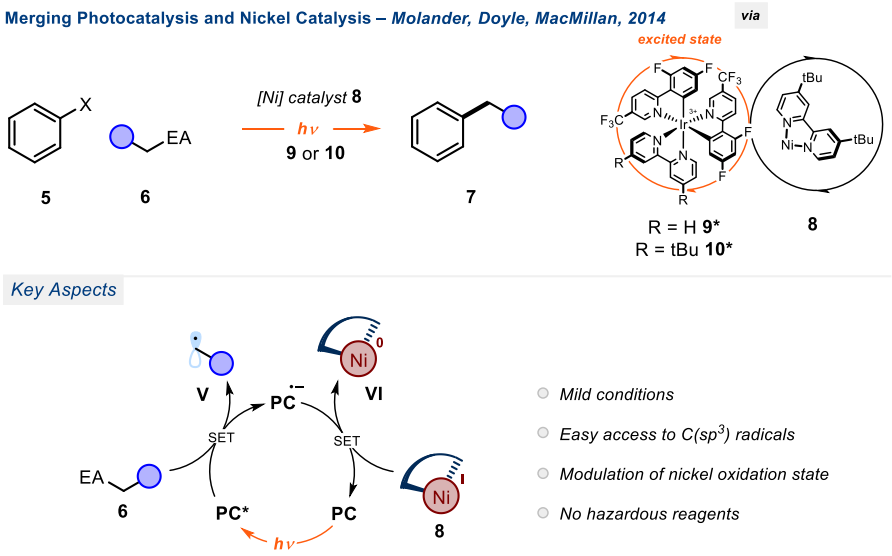

Scheme 6.3: First example on the merge of photoredox catalysis and nickel catalysis; EA: electron auxiliary

The second strategy of central relevance to this thesis is the *direct photochemistry* approach (Scheme 1.4). It exploits the new reactivity acquired in the excited-state by some colored catalytic intermediates and substrates, which can initiate radical processes. An intriguing feature of this approach is that it can repurpose catalytic intermediates with an established reactivity in the ground-state to achieve completely new processes. This is because photoexcitation can switch on new catalytic properties that significantly diverge from ground-state polar reactivity.

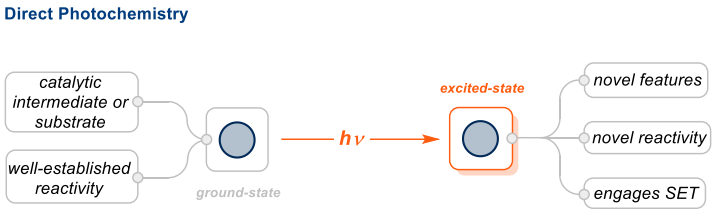

Scheme 7.4: Direct excitation approach

H., Evans, R. W., MacMillan, D. W. C., "The merger of transition Metal and Photocatalysis", *Nat. Rev. Chem.,* **2017**, *52*, 1; b) Skubi, K. L., Blum, T. R., Yoon, T. P. 'Dual Catalysis Strategies in Photochemical Synthesis" *Chem. Rev.* **2016**, *116*, 17, 10035.

Our research group is active in studying and exploiting the photochemical properties of certain colored (chiral) organic intermediates, which can harvest the energy of photons to trigger the formation of radicals upon SET activation of substrates. Stereocontrolled trapping of these open-shell intermediates yields the desired enantioenriched chiral product. In this strategy, the chiral organocatalytic intermediate plays the dual role of photo-activator and stereo-induction carrier. For example, we recently demonstrated how an electron-rich chiral enamine **II**, on light excitation, unveils new catalytic properties and triggers radical reactivity (Scheme 1.5).[23]

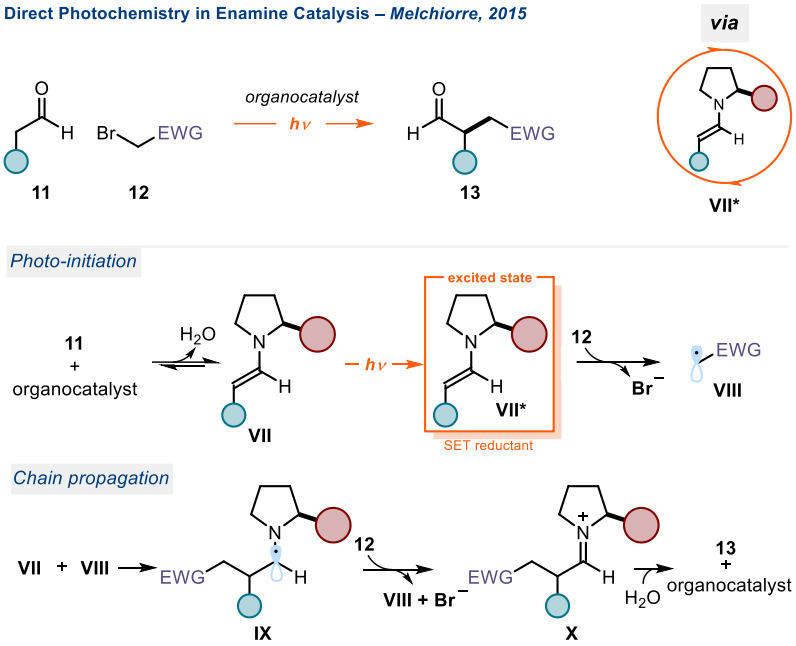

Scheme 8.5: Direct excitation of enamine **VII** reveals its reducing properties.

The proposed mechanism[24] starts with the condensation of the organocatalyst with aldehyde **11** to generate the chiral enamine **VII**. A sacrificial amount of **VII**, by absorbing

[23] a) Silvi, M., Arceo, E., Jurberg, I. D., Cassani, C., Melchiorre, P. "Enantioselective Organocatalytic Alkylation of Aldehydes and Enals Driven by the Direct Photoexcitation of Enamines" *J. Am. Chem. Soc.* **2015**, *137*, 6120; b) Filippini, G., Silvi, M., Melchiorre, P. "Enantioselective Formal α-Methylation and α-Benzylation of Aldehydes by Means of Photo-organocatalysis" *Angew. Chem. Int. Ed.* **2017**, *56*, 4447.

[24] Bahamonde, A., Melchiorre, P. "Mechanism of the Stereoselective α-Alkylation of Aldehydes Driven by the Photochemical Activity of Enamines" *J. Am. Chem. Soc.* **2016**, *138*, 8019.

light in the near-UV region (till about 400 nm), reaches the excited state (**VII***) to become a strong SET reductant. This means that the excited enamine can activate electron-poor alkyl halides (e.g. bromomalonates and α-iodosulfones), which would be unreactive towards the nucleophilic ground-state enamine.The emerging electrophilic radical **VIII** is then intercepted by the ground-state chiral enamine **VII**, delivering the α-amino radical **IX**. This intermediate transfers an electron to **12,** starting a radical chain process while giving the iminium ion **X**. Hydrolysis of the latter releases the enantioenriched product **13** and the organocatalyst (Scheme 1.5).

The discovery of photoexcited enamine catalysis prompted us to seek for other colored organocatalytic intermediates, which exhibit new catalytic properties upon light excitation. We demonstrated that chiral iminium ions **XI**[25, 26] — well-known electrophilic intermediates in the ground state[27] — become powerful oxidants upon visible-light excitation ($E^*(\mathbf{XI}^{\bullet+}/\mathbf{XI}^*)$ = +2.40 V vs Ag/AgCl, in CH_3CN). (Scheme 1.6). Intermediate **XI*** can oxidize, *via* an SET event, a wide variety of non-nucleophilic radical precursors **15**[28] (Scheme 1.6). The two open-shell intermediates, **XII** and **XIII**, undergo a stereocontrolled radical-radical combination affording the enantioenriched product **16**

[25] Silvi, M.; Verrier, C.; Rey, Y. P.; Buzzetti, L; Melchiorre, P. "Visible-light Excitation of Iminium Ions Enables the Enantioselective Catalytic β-Alkylation of Enals" *Nat. Chem.*, **2017**, *9*, 868.
[26] Silvi, M., Melchiorre, P., "Enhancing the Potential of Enantioselective Organocatalysis with Light", *Nature* **2018**, *554*, 41.
[27] Erkkilä, A., Majander, I., Pihko, P. M., "Iminium Catalysis", *Chem. Rev.* **2007**, *107*, 5416.
[28] Selected examples: a) Mazzarella, D., Crisenza, G. E. M., Melchiorre, P., "Asymmetric Photocatalytic C–H Functionalization of Toluene and Derivatives" *J. Am. Chem. Soc.* **2018**, *140*, 8439; b) Verrier, C., Alandini, N., Pezzetta, C., Moliterno, M., Buzzetti, L., Hepburn, H. B., Vega-Peñaloza, A., Silvi, M., Melchiorre, P., "Direct Stereoselective Installation of Alkyl Fragments at the β-Carbon of Enals via Excited Iminium Ion Catalysis" *ACS Catal.,* **2018**, *8*, 1062.

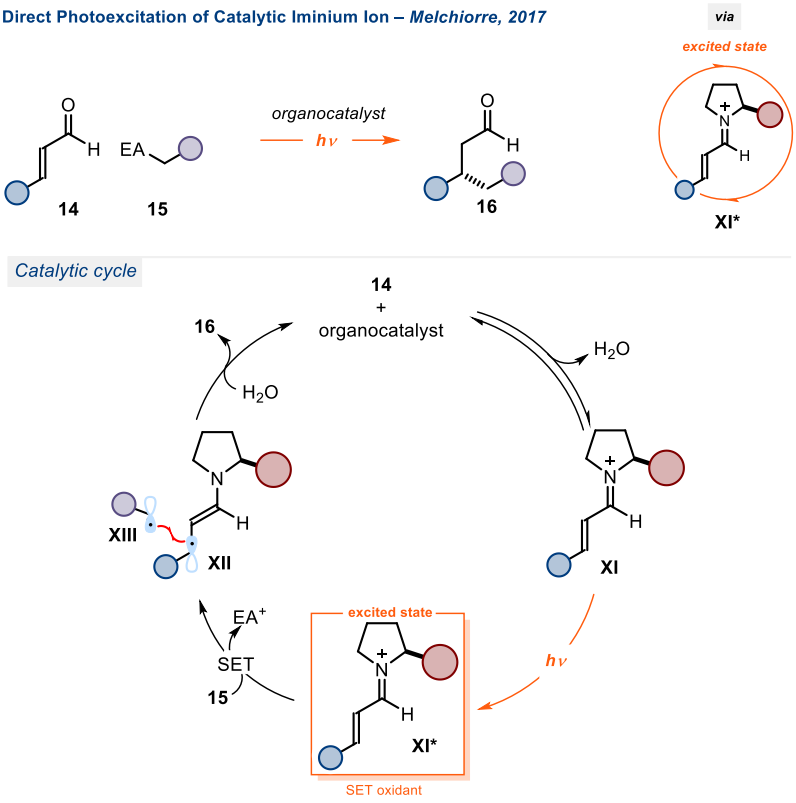

Scheme 1.6: Direct excitation of iminium ion **XI** reveals its oxidative properties.

In analogy to the photoexcitation of reaction intermediates, light excitation of colored substrates could be used to turn them into better oxidants and reductants capable to undergo SET events unleashing radical reactivity. For example, it was demonstrated that light-excitation of 1,4-dihydropyridine (DHP) **20** (Scheme 1.7), primarily known as ground-state hydride source, turns it into a strong photo-reductant that can engage in SET manifolds.[29]

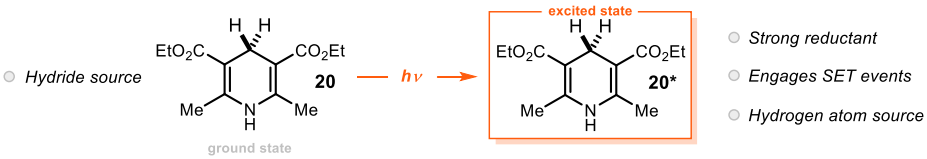

Scheme 1.7: Direct excitation of **20** reveals new reactivity.

[29] Jung, J., Kim, J., Park, G., You, Y., Cho, E. J., "Selective Debromination and α-Hydroxylation of α-Bromo Ketones Using Hantzsch Esters as Photoreductants", Adv. Synth. Catal. 2016, 358, 74–80.

Our group expanded this finding to the excitation of 4-alkyl-1,4-dihydropyridines **21** which, on excitation, develops a dual reactivity profile (Scheme 1.8). Acting as a photo-reductant, the excited substrate **21*** triggers an SET event with suitable oxidants, leading to the formation of the unstable radical cation **XIV**. After fragmentation of this fleeting intermediate, an alkyl radical **XV** is released.[30]

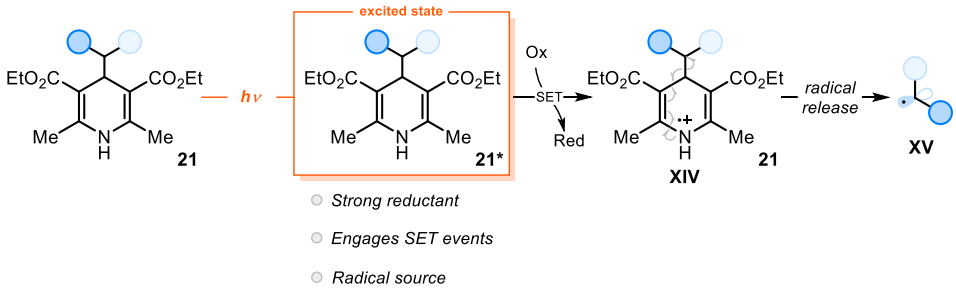

Scheme 1.8: Direct excitation of **21** reveals new reactivity.

We exploited this photochemical behavior to develop an array of nickel catalyzed carbon-carbon bond forming processes (Scheme 1.9). The proposed mechanism for the nickel-catalyzed radical cross-coupling is shown in Scheme1.9. The strong reducing properties of the excited DHP **21*** allow the SET reduction of the nickel(II) pre-catalyst **24** to the active nickel(0) intermediate **XVI**. The concomitant formation of the unstable radical-cation **XIV** triggers, upon fragmentation, the release of radical **XV**. The active Ni(0) catalyst **XVI** intercepts alkyl radical **XV** forming a nickel(I) organometallic intermediate **XVII**, which then undergoes oxidative addition with the aryl bromide **22**. This leads to intermediate **XVIII**, which, after reductive elimination, yields the cross-coupled product **23**. Finally, SET transfer from the excited state **21** to the inactive Ni(I) complex **XIX** closes the nickel catalytic cycle while regenerating the radical intermediate **XV**.

[30] Buzzetti, L., Prieto, A., Raha Roy, S., Melchiorre, P., "Radical-Based C−C Bond-Forming Processes Enabled by the Photoexcitation of 4-Alkyl-1,4-dihydropyridines" *Angew. Chem. Int. Ed.* **2017**, *56*, 15039.

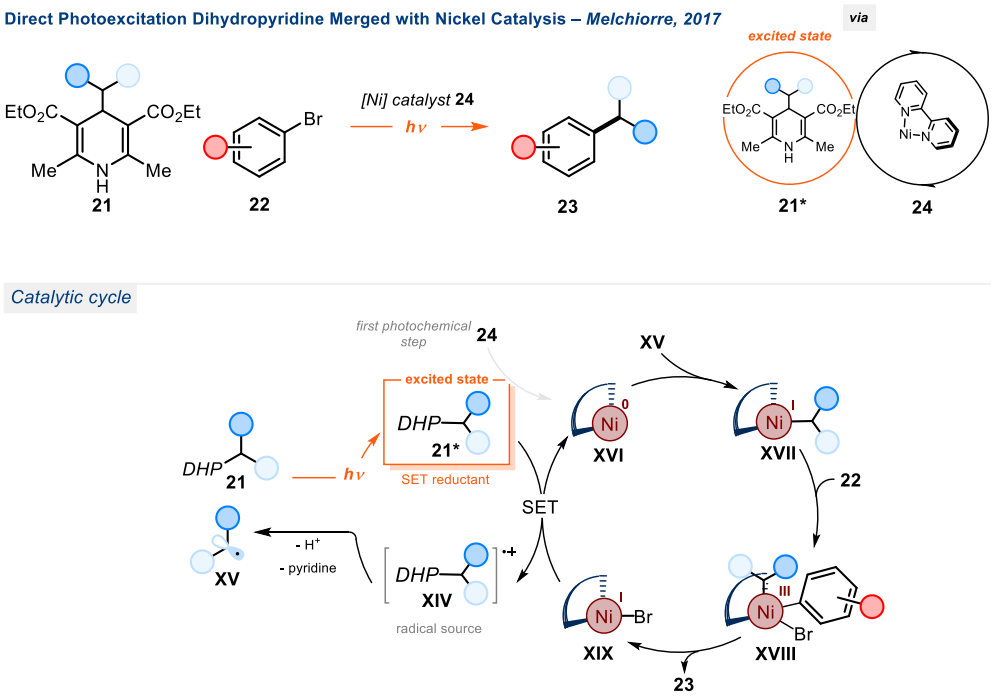

Scheme 1.9: Merging ground state nickel catalysis and direct excitation of dihydropyridines **21** to forge new carbon-carbon bonds.

The direct excitation of substrates and catalytic intermediates (*direct photochemistry*) represents the foundation of the chemistry discussed in this doctoral thesis.

1.2. General Objectives and Summary

The main objective of this doctoral research was to exploit the direct excitation of substrates and catalytic intermediates to develop metal-catalyzed asymmetric methodologies. 4-Alkyl-1,4-dihydropyridines (4-alkyl-DHPs) **21** were extensively used as versatile source of electrons and radicals. An overview on the rich chemistry of DHPs in both their excited and ground state is detailed in Chapter 2 of the thesis. These substrates have been instrumental to the chemistry developed during my research efforts.

In the first project, I exploited the excited-state properties of 4-alkyl-DHPs **21** to develop a photochemical enantioselective nickel catalyzed acyl cross-coupling process with symmetrical anhydrides. In the second part of my doctoral studies, I exploited the photochemistry of a catalytic chiral organo-iridium complex that, upon light excitation,

becomes a strong oxidant capable to promote SET events and generate radicals from DHP precursors. This photochemical strategy enables an enantioselective alkyl-alkyl cross-coupling reaction between allylic alcohols and 4-alkyl-DHPs **21**, unobtainable under thermal conditions.

1.2.1. Photochemical Asymmetric Nickel-catalyzed Acyl Cross-coupling

Chapter III reports the development of a photochemical strategy based on the direct excitation of DHPs **21** (Scheme 1.10), in combination with the ground-state reactivity of a chiral nickel complex **XX**. The synergistic combination of photochemistry and nickel-catalysis offers a useful asymmetric platform for the preparation of enantioenriched chiral α-alkylated ketones **26**. This Visible light-promoted strategy avoids the use of any external photocatalyst or stoichiometric reducing agents, providing the desired chiral products **26** in good yields and excellent enantiomeric excess. We used the direct excitation of DHPs **21** to generate alkyl radicals (**XV**) and to modulate the oxidation state of the nickel catalyst (**XX**), while readily available symmetrical anhydrides **25** served as electrophilic partners. This strategy allowed to stereoselectively install heteroatom-containing fragments within the final products **26**, such as indole and carbazole moieties. I also performed photophysical (UV-Vis) and electrochemical mechanistic studies to elucidate the dual role of DHPs **21**, which acted as both SET reductants and radical precursors.[31]

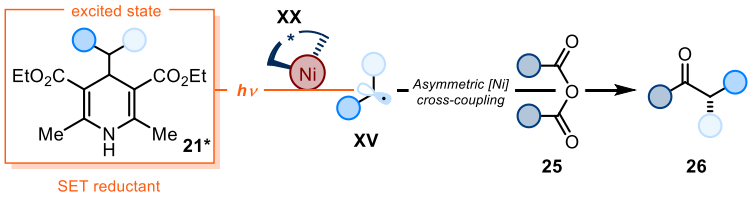

Scheme 9.10: Photoexcitation of dihydropyridine **21** merged with ground-state asymmetric nickel catalysis to prepare α-substituted enantioenriched ketones **26**.

[31] This work was published in collaboration with Dr Sudipta Raha Roy, who conducted the initial studies and part of the optimization process, Dr. Xinjun Tang, who carried out part of the reaction scope, photophysical and electrochemical studies. I performed extensive optimization studies, method development and photophysical and electrochemical studies.

1.2.2. Catalytic Asymmetric C-C Cross-couplings Enabled by the Photoexcitation of an Allyl-iridium Complex

The fourth chapter describes how light excitation could divert the well-established polar reactivity of the chiral organo-iridium complex **XXII**, switching on novel catalytic functions and enabling mechanistically new radical-based enantioselective pathways (Scheme 1.11). Complex **XXII** is a privileged intermediate in asymmetric catalysis since it is largely used to promote enantioselective allylation substitution processes[32] acting as a chiral electrophile. We found that light excitation of this chiral (η^3-allyl)iridium(III) complex reveals its ability to trigger SET pathways, enabling the oxidation of alkyl-DHPs **21**, thereby overriding the classical cross-coupling mechanism. These finding were exploited to realize an enantioselective alkyl-alkyl radical cross-coupling reaction between allylic alcohols **27** and 4-alkyl-1,4-dihyropyridines **21**, which acted as radical precursors. This methodology allowed the preparation of a wide range of cross-coupled products **28**, also bearing biological relevant scaffolds and complex structures derived from drugs. Photophysical, electrochemical, and other studies provided mechanistic insights of the overall process.

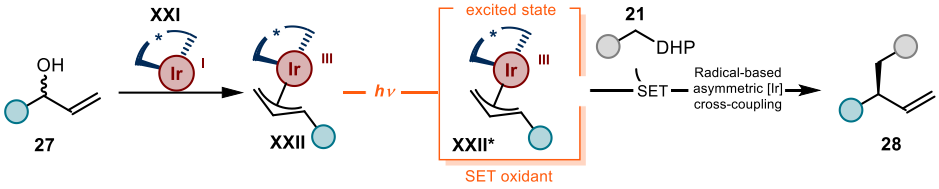

Scheme 10.11: Direct excitation of *in-situ* generated complex **XXII** reveals its oxidant properties. This tool was employed to activate non-nucleophilic substrates **21** in asymmetric radical cross-couplings.

[32] Cheng, Q., Tu, H-F., Zheng, C., Qu, J-P., Helmchen, G., You, S-L., "*Iridium-Catalyzed Asymmetric Allylic Substitution Reactions*" *Chem. Rev.* **2019**, *119*, 1855.

Chapter II

The Chemistry of 1,4-Dihydropyridines

This doctoral study has largely used 1,4-dihydropiridines (DHPs) as photoreductants and radical precursors. This chapter aims to provide the basic concepts and benchmark examples in the chemistry of DHPs. In the first part, I will discuss the role of DHPs as ground-state reagents, whereas in the second part the excited-state chemistry of these versatile compounds is detailed.

2.1 Introduction

2.2.1 General Properties

1,4-dihydropyridines (DHPs) are versatile compounds. For example, their fundamental scaffold is found in drugs[1] and bioactive compounds[2] (Scheme 2.1 a and b). The lone pair of the nitrogen atom within the DHP scaffold is in conjugation with the unsaturated system, exerting a stabilizing effect on the molecule. Adorning positions 3 and 5 (Scheme 2.1c) with electron-withdrawing groups increases the resonance effect, leading to a further stabilization.[3] However, once these substrates are activated, the driving force of aromatization makes them powerful reagents, which are capable to carry out multiple roles.[4]

1,4-DHPs are bench-stable compounds that can be easily handled and prepared from simple staring materials. The first synthesis was reported by Artur Hantzsch in 1881, who used DHPs as intermediate for the preparation of pyridines **5** (Scheme 2.1 c).[5,6]

---

[1] Lavilla. R. "Recent Developments in the Chemistry of Dihydropyridines" *J. Chem. Soc. Per. Trans. 1* **2002**, *9*, 1141

[2] Stout, D. M., Meyers, A. I. "Recent Advances in the Chemistry of Dihydropyridines" *Chem. Rev.* **1982**, *2*, 223.

[3] Eisner, U., Kuthan, J. "Chemistry of Dihydropyridines" *Chem. Rev.* **1972**, *72*, 1, 1.

[4] Walton, J. C., Studer, A. "Evolution of Functional Cyclohexadiene-Based Synthetic Reagents: The Importance of Becoming Aromatic" *Acc. Chem. Res.* **2005**, *38*, 10, 794.

[5] Hantzsch, A. "Condensationsprodukte Aus Aldehydammoniak Und Ketonartigen Verbindungen" *Ber. Dtsch. Chem. Ges.* **1881**, *14*, 2, 1637.

[6] A photochemical methodology to access 4-alkyl-1,4-DHPs from alkyl iodides has been recently reported: Liu, X-G., Dong, C-S., Li, F., Zhang, B. "Manganese-Mediated Direct Functionalization of Hantzsch Esters with Alkyl Iodides via an Aromatization−Dearomatization Strategy" DOI: 10.1021/acs.orglett.1c01210.

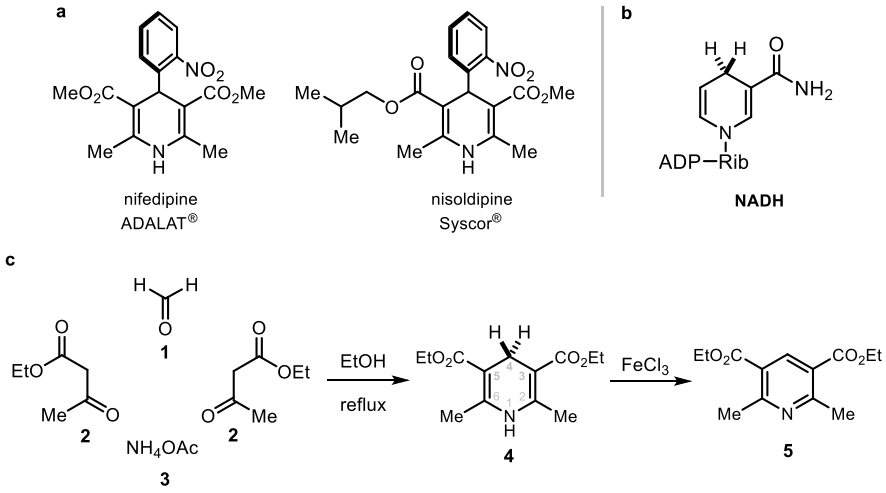

Scheme 2.1. DHP scaffold in (a) pharmaceutical drugs and (b) in natural enzyme cofactor, nicotinamide adenine dinucleotide (NADH); (c) First synthesis of Hantzsch esters by Hantzsch.

Since then, this scaffold has found application in a plethora of transformations because of its multipurpose properties. We can recognize five distinct reactivities (Scheme 2.2), mostly arising from the ground-state reactivity. DHPs may serve as: *i*) hydride sources; *ii*) alkyl transfer reagents; *iii*) electron donors; *iv*) hydrogen atom donors; *v*) alkyl radical precursors (only when bearing an alkyl substituent at 4 position). The different reactivity manifolds available to DHPs will be discussed in the next section.

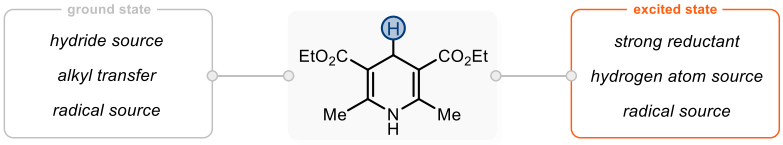

Scheme 2.2. Ground-state and excited-state reactivity of DHPs.

2.2 Reactivity of DHPs in the Ground State

2.2.1 1,4-Dihydropyridines as Biomimetic Hydride Sources

Nicotinamide adenine dinucleotide (NADH) is the most abundant molecule bearing the 1,4-dihydropyridine moiety. This enzyme cofactor plays multiple roles in biological

systems acting as redox mediator by transferring hydride ions to the surrounding substrates, in a process referred to as *transfer hydrogenation*. (Scheme 2.3).[7]

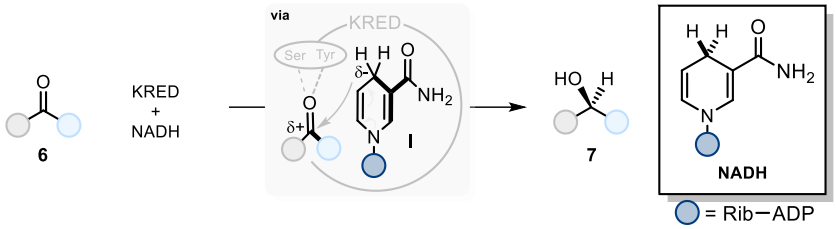

Scheme 2.3: Transfer hydrogenation of cofactor NADH in KRED enzymes. Rib: ribose; ADP: adenine diphosphate; KRED: ketoreductase.

The structural similarity of DHPs with NADH cofactor stimulated the idea of using these reagents as mild and safe hydride source.[8] For example, as shown in Scheme 2.4, H-DHP **4** can transfer a hydride ion (H^-) to a suitable electrophile with concomitant aromatization followed by proton transfer to the resulting carbanion **III**.

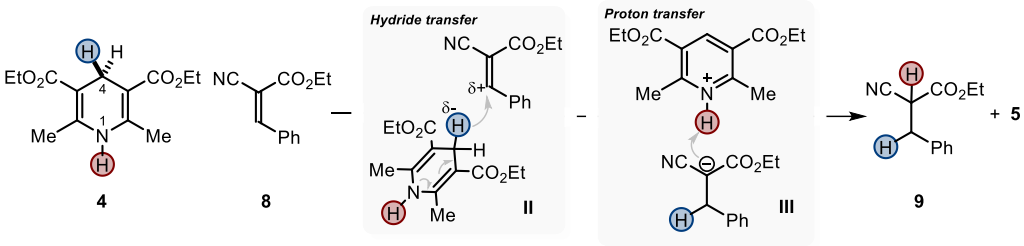

Scheme 2.4.: Hydride transfer mechanism from H-DHP **4** to ester **8**.

Since the dihydropyridine H-DHP **4** bears two hydrogen atoms (at the 1- and 4-position), several studies have been performed to determine which hydrogen atom is transferred as hydride and which as proton. Through kinetic and thermodynamic investigations, Zhu and Cheng studied the sequence of the hydride transfer mechanism of H-DHP **4** to substrate **8**.[9] The results pointed to a first hydride transfer from the C-4 position (blue

[7] Huisman, G, W., Liang, J., Krebber, A. "Practical Chiral Alcohol Manufacture Using Ketoreductases" *Curr. Opin. Chem. Biol.* **2010**, 14, 122.
[8] Yasui, S., Ohno, A. "Model Studies with Nicotinamide Derivatives" *Bioorg. Chem.* **1986**, *14*, 70.
[9] Selected examples: a) Zhu, X.-Q., Liu, Y.-C., Cheng, J.-P. "Which Hydrogen Atom Is First Transferred in the NAD(P)H Model Hantzsch Ester Mediated Reactions via One-Step and Multistep Hydride Transfer?" *J. Org. Chem* **1999**, *64*, 8980; b) Zhu, X.-Q., Liu, H.-L., Yuan, P.-W., Liu, Y., Cao,

circle in Scheme 2.4) followed by proton loss from the *N*-position (red circle in Scheme 2.4) to deliver pyridine **5** and the corresponding product **9**.

Recently, with the advent of organocatalysis, dihydropyridines have found broad application as reducing agents in organocatalytic enantioselective reactions.[10] In independent efforts, Rueping[11] and List[12] exploited asymmetric Brønsted acid catalysis to develop a biomimetic enantioselective reduction of imines (Scheme 2.5).

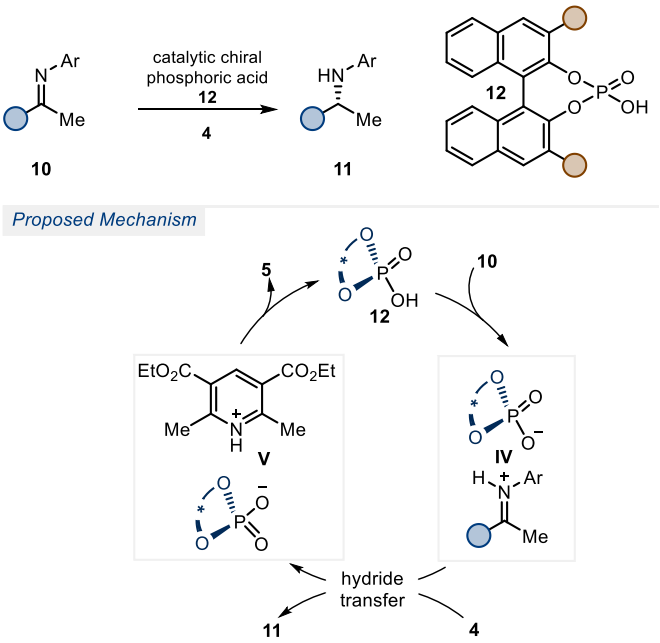

Scheme 2.5.: Application of H-DHP in organocatalytic asymmetric C=N bond reduction

Both authors proposed the mechanism depicted in Scheme 2.5. The catalytic chiral phosphoric acid **12** activates the imine derivative **10** by forming the ion pair **IV**. At this point, H-DHP **4**, acting as hydride source, reduces the electrophilic iminium ion within the ionic pair **IV**, affording the desired enantioenriched amine **11** along with the

L., Cheng, J.-P. "A Detailed Investigation into the Oxidation Mechanism of Hantzsch 1,4-Dihydropyridines by Ethyl α-Cyanocinnamates and Benzylidenemalononitriles" *J. Chem. Soc., Perkin Trans.* **2000**, *2,* 1857.

[10] Rueping, M., Dufour, J., Schoepke, F. R. "Advances in Catalytic Metal-Free Reductions: From Bio-inspired Concepts to Applications in the Organocatalytic Synthesis of Pharmaceuticals and Natural Products" *Green Chem.* **2011**, *13*, 1084.

[11] Rueping, M., Sugiono, E., Azap, C., Theissman, T., Bolte, M. "Enantioselective Brønsted Acid Catalyzed Transfer Hydrogenation: Organocatalytic Reduction of Imines" *Org. Lett.* **2005**, *7*, 17, 3781

[12] Hoffmann, S., Seayad, A. M., List, B. "A Powerful Brønsted Acid Catalyst for the Organocatalytic Asymmetric Transfer Hydrogenation of Imines" *Angew. Chem. Int. Ed.* **2005**, *44*, 7424.

pyridinium salt **V**. Proton transfer within the ion pair **V** regenerates catalyst **12** and liberates pyridine **5**.

Dihydropyridine **4** served has hydride source also within the iminium ion activation strategy. For example, MacMillan[13] and List[14] independently reported a protocol for asymmetric transfer hydrogenation of α,β-unsaturated aldehydes **13** (Scheme 2.6).

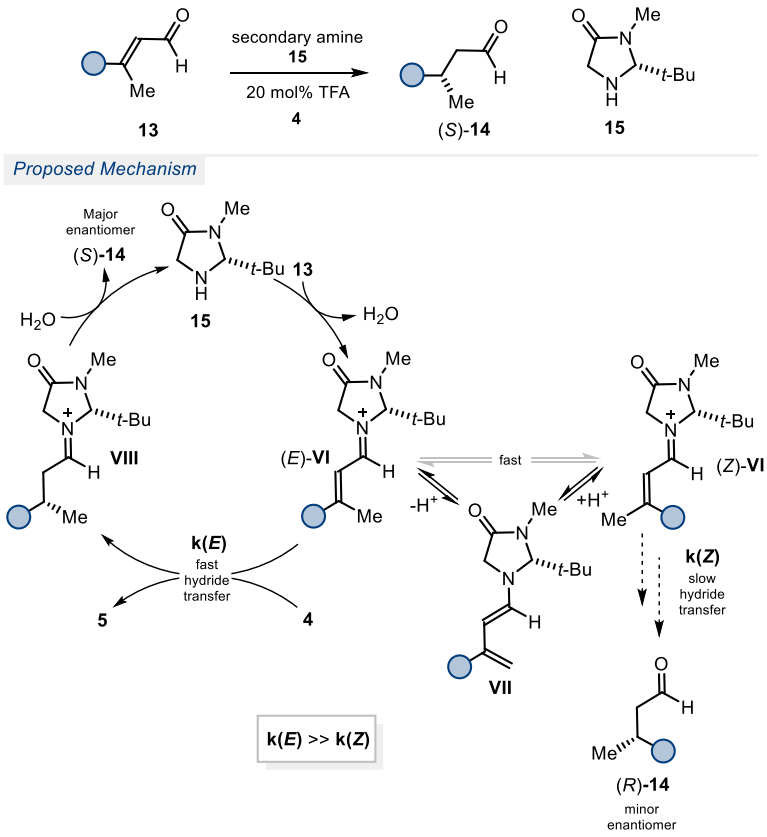

Scheme 2.6 Application of H-DHP in enantioselective C=C bond reduction

In this approach, the condensation of a chiral secondary amine catalyst **15** with enal **13** generates the electron poor iminium ion **VI**. Hydride transfer from H-DHP **4** to the

[13] Ouellet, S. G., Tuttle, J. B., MacMillan, D.W. C. "Enantioselective Organocatalytic Hydride Reduction" *J. Am. Chem. Soc.* **2005**, *127*, 1, 32.

[14] Yang, J. M., Hechavarria Fonseca, M. T., Vignola, N., List, B. "Metal-Free, Organocatalytic Asymmetric Transfer Hydrogenation of α,β-Unsaturated Aldehydes" *Angew. Chem. Int. Ed.* **2005**, *44*, 108.

electrophilic intermediate **VI** and hydrolysis of iminium **VII** yields the highly enantioenriched product **14** and regenerate the organocatalyst **15**. Intriguingly, this protocol proceeds by an enantioconvergent pathway, since geometry of the double bond in enal **13** is not relevant for the enantioselectivity of the final product. This is because the iminium ion **VI** can rapidly interconvert via formation of the enamine intermediate **VII**. The rate-determining hydride-transfer (k(*Z*) or k(*E*), see Scheme 2.6) takes place preferentially with the (*E*)-**VI** isomer (k(*E*)>>k(*Z*)), conveying both iminium ion isomers **VI** towards the major enantiomer (*S*)-**14**.

2.2.2 1,4-Alkyl-dihydropyridines as Alkyl Transfer Reagents

Beside serving as hydride source, 1,4-dihydropyridines can also act as alkyl transfer reagents, when adorned with alkyl groups at C-4 position. Recently, the group of Tang exploited this behavior to design a Lewis acid-catalyzed alkylation of imines **17** (Scheme 2.7).[15] The authors proposed a concerted mechanism where the heterolytic cleavage of the alkyl fragment in dihydropyridine **16** generates incipient carbanionic species **X**, which adds into the Lewis acid-activated imine **IX** delivering product **18**. This hypothesis is supported by experiments conducted in the presence of radical scavengers and Brønsted acids, which did not affect the efficiency of the reaction, ruling out either a radical or a free-carbanion based-mechanism.

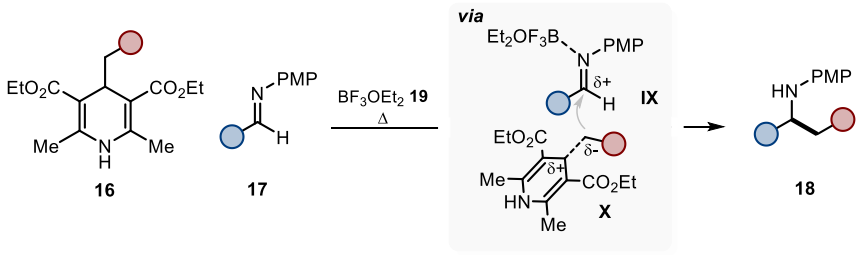

Scheme 2.7.: 4-alkyl-DHPs as alkylation reagents.

2.2.3 1,4-Dihydropyridines as Electron and Hydrogen Atom Donors

Within the field of photoredox catalysis, DHPs have found a novel application serving as electron and hydrogen atom source. Indeed, the low oxidation potential of H-DHP **4** (E^{ox}~

[15] Li, G., Chen, R., Wu, L., Fu, Q., Zhang, X., Tang, Z. "Alkyl Transfer from C–C Cleavage" *Angew. Chem. Int. Ed.* **2013**, *52*, 8432.

0.8-1 V) [16] is within the operative range of many excited-state photocatalysts. The general mode of action of H-DHP **4**, in photoredox catalysis, is depicted in Scheme 2.8. An excited-state photocatalyst (PC) oxidizes, via SET event, H-DHP **4** leading to the formation of radical cation **XI**. This reactive intermediate rapidly undergoes aromatization by delivering a hydrogen atom to the environment. Eventually, the cationic pyridinium **XII** serves as proton source.

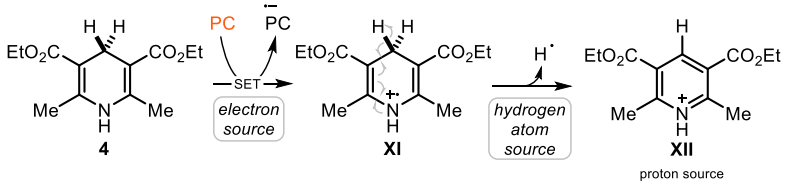

Scheme 2.8.: H-DHP **4** as electron and hydrogen atom donor in the ground state.

The first application of DHPs derivatives in this role dates back to the late 1970s.[17] Kellogg exploited the reducing features of the N-methylated DHP **24**, in combination with the ruthenium-based photocatalyst **23**, to promote the light-driven desulfonylation of substrate **20** (Scheme 2.9). Although detailed mechanistic studies were not provided by the authors, it is assumed that DHP **24** serves as electron source for the excited photocatalyst **23** and as a hydrogen atom source to yield product **21**.

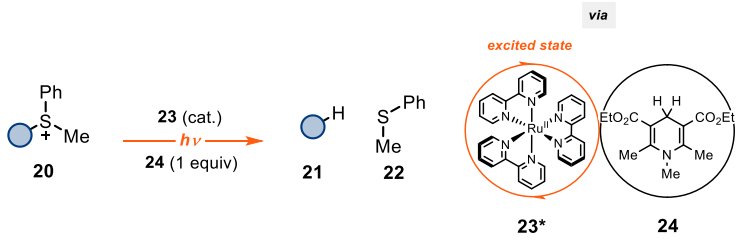

Scheme 2.9.: First application of H-DHP **24** as electron and hydrogen atom source.

More recently, the group of Stephenson revived the role of DHPs as electron and hydrogen atom source by reporting a reductive dehalogenation of the unactivated organic halides **25** (Scheme 2.10).[18] Upon light absorption, the excited state photocatalyst

[16] Huang, W., Cheng, X. "Hantzsch Esters as Multifunctional Reagents in Visible-Light Photoredox Catalysis" *Synlett* **2017**, *28*, 148.
[17] Hedstrand, D. M., Kruizinga, W. M., Kellogg, R. M. "Light Induced and Dye Accelerated Reductions of Phenacyl Onium Salts by 1,4-Dihydropyridines" *Tetrahedron Lett.* **1978**,*19*, 1255.
[18] Narayanam, J. M. R., Tucker J. W., Stephenson C. R. J. 'Electron-Transfer Photoredox Catalysis: Development of a Tin-Free Reductive Dehalogenation Reaction', *J. Am. Chem. Soc.* **2009**, *131*, 8756.

23*oxidizes, via SET, H-DHP **4** delivering the Ru(I)-photocatalyst (**23**$^{\bullet-}$) along with the radical cation **XI**. The reduction of substrate **25**, mediated by the Ru(I) photocatalyst, leads to the homolytic fragmentation of the carbon-bromide bond and provides the alkyl radical **XIII** that, upon HAT from radical cation **XI**, yields the desired product **26**.

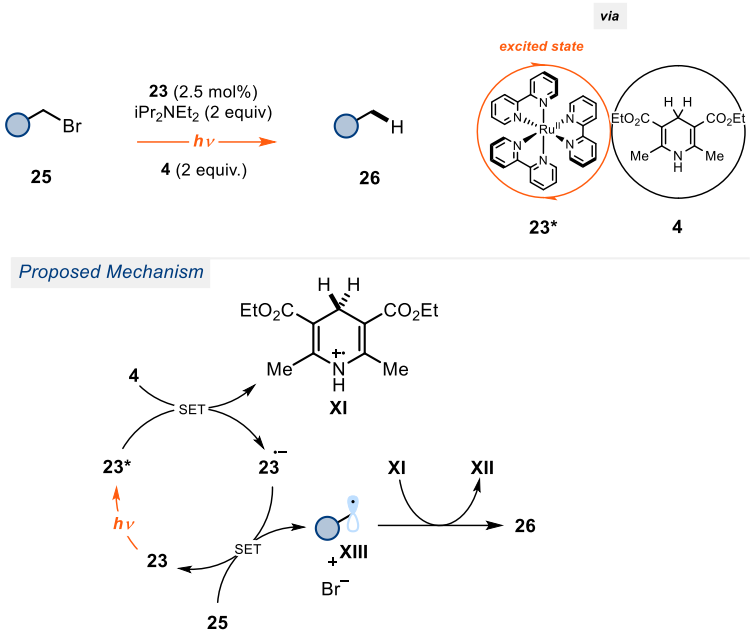

Scheme 2.10.:H-DHP **4** as electron and hydrogen donor in a photoredox dehalogenative protocol.

2.2.4 1,4-Dihydropyridines as Radical Precursors

The reactivity manifolds of 4-alkyl-DHPs **16** can also be expanded when used in combination with photoredox catalysis,[19] since they can serve as electron donor and carbon-centered radical source. Similarly to simple DHPs, 4-alkyl-DHPs **16** have a low oxidation potential (E^{ox} ~1-1.3 V), which can be reached by many photocatalysts in the excited state. Therefore, **16** can be easily activated by SET. A general reactivity manifold is shown in Scheme 2.11. Upon SET oxidation of substrate **16**, the fleeting radical cation **XIV** is formed. This latter, differently from intermediate **XI** (Scheme 2.8) which delivers a hydrogen atom, releases the carbon-centered radical **XV** upon aromatization.

[19] Wang, P. Z., Chen, J. R., Xiao, W. J. "Hantzsch Esters: An Emerging Versatile Class of Reagents in Photoredox Catalyzed Organic Synthesis" *Org. Biomol. Chem.* **2019**, *17*, 6936.

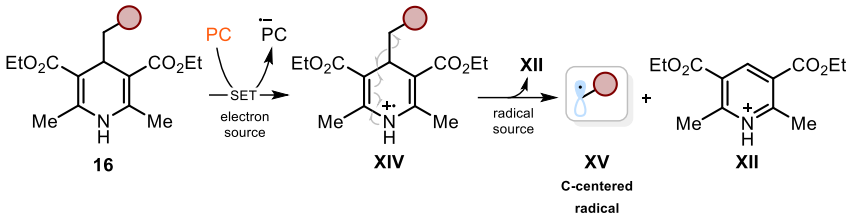

Scheme 2.11.: 4-alkyl-DHP **16** as electron and carbon-centered radical donor in photoredox catalysis.

In 2016, this reactivity manifold has been exploited by the group of Molander to develop a nickel catalyzed C(sp^3)-C(sp^2) coupling between 4-alkyl-DHPs **27** and aryl halides **28** (Scheme 2.12).[20]

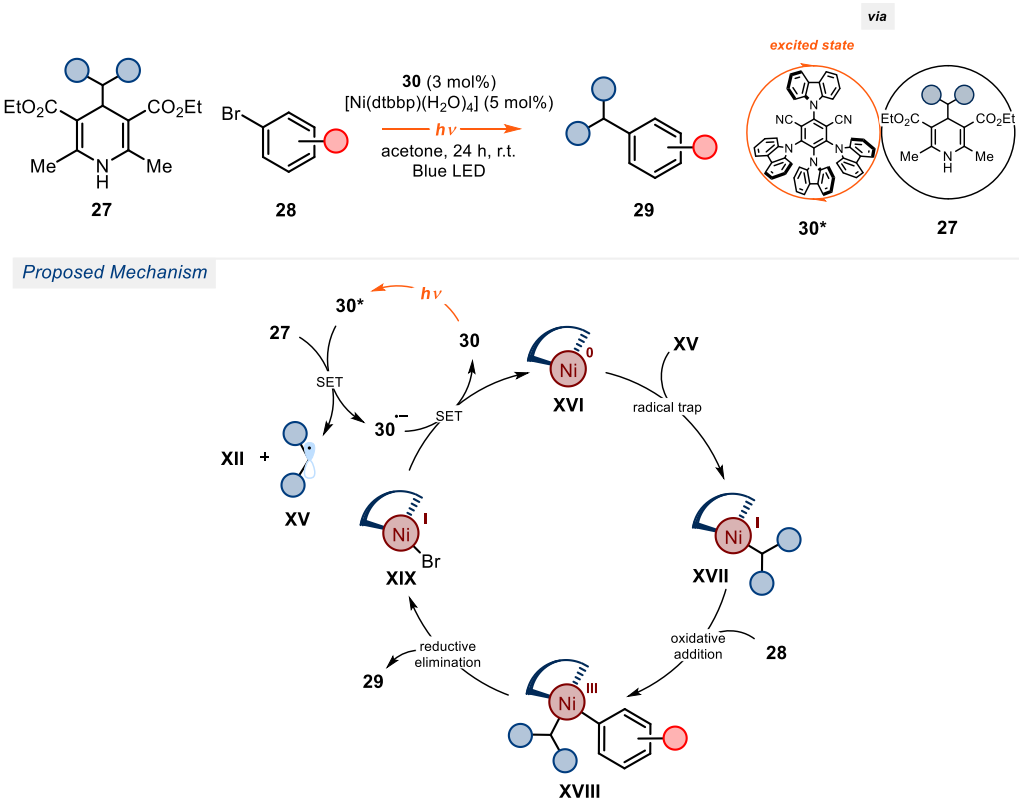

Scheme 2.12.: DHP **27** as an electron and alkyl radical source in metallaphotoredox catalysis.

[20] Gutiérrez-Bonet, Á., Tellis, J. C., Matsui, J. K., Vara, B. A., Molander, G. A. "1,4-Dihydropyridines as Alkyl Radical Precursors: Introducing the Aldehyde Feedstock to Nickel/Photoredox Dual Catalysis" *ACS Catal.* **2016**, *6*, 8004.

Upon light absorption, the organic photocatalyst **30** triggers the SET oxidation of dihydropyridine **27**, leading to the formation of the alkyl radical **XV**. Concomitantly, the emerging Ni(0) complex **XVI** traps the newly formed intermediate **XV**, resulting in the Ni(I) complex **XVII**. This latter intermediate undergoes oxidative addition with the aryl bromide **28** and, upon reductive elimination from the Ni(III) complex **XVIII**, the desired product **29** is released. SET from the reduced form of the photocatalyst to Ni(I) complex **XIX**, regenerates the Ni(0) active catalyst, closing the catalytic cycle.

2.3 Reactivity of DHPs in the Excited State

2.3.1 1,4-Dihydropyridines as Photoreductants and Hydrogen Atom Source

After the discovery of NADH and the understanding of its role in biological systems, different model compounds mirroring this coenzyme, such as DHPs, were studied and utilized in transfer hydrogenation reactions.[21] However, these transformations were limited to the ability of dihydropyridines to deliver a hydride ion (H^-) only to strongly electrophilic partners.[22] The direct excitation of dihydropyridines offered novel reactivity frameworks, beyond the sole transfer hydrogenation reactions. [23]

The photoactivity of dihydropyridine **4** was first observed by Westheimer in 1961,[24] who reported on the photochemical reduction of bromotrichloromethane **29** in the presence of H-DHP **4** (Scheme 2.13).

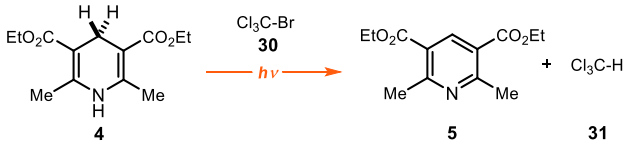

Scheme 2.13.: First use of H-DHP **4** as a photoreductant.

The products of the reaction, pyridine **5** and trichloromethane **31**, account for a formal reduction of the electron poor **30** and oxidation of H-DHP **4**. However, due to the absence of further mechanistic studies, the exact role of the excited DHP **4** remained unclear.[25]

---

[21] Eisner, U., Kuthan, J. "Chemistry of Dihydropyridines" *Chem. Rev.* **1972**, *72*, 1, 1.
[22] Zheng, C., You, S-L., "Transfer hydrogenation with Hantzsch esters and related organic hydride donors" *Chem. Soc. Rev.* **2012**, *41*, 2498.
[23] Sammes, J. D., Widdowson, D. A. "Hydrogen Transfer in NADH Models. An Intramolecular Photochemical Redox Reaction" *J. C. S. Chem. Comm.*, **1972**, *18*, 1023
[24] Kurz, J. L., Robert Hutton, R., Westheimer, F. H. "The Photochemical Reduction of Bromotrichloromethane by Derivatives of 1,4-Dihydropyridine", *J. Am. Chem. Soc.* **1961**, *83*, 584
[25] Selected examples: a) Jin, M.-Z., Yang, L., Wu, L.-M., Liu, Y.-C., Liu, Z.-L. "Novel Photoinduced Aromatization of Hantzsch 1,4-dihydropyridines" *Chem. Commun.* **1998**, 2451. b) Zhang, J., Jin, M.-Z.,

In 1983, Fukuzumi reported[26] on the empowered reductive features of 1-benzyl-1,4-dihydronicotinamide (BNAH) **32**, another substrate mimicking the NADH cofactor. In this case, the author studied the photochemical dehalogenation of alkyl bromides **33** operated by the photoexcited BNAH **32** (Scheme 2.14). Through kinetic and spectroscopic techniques, the authors established the excited-state reduction potential of BNAH **32** to be around -2.60 V vs SCE, whereas its ground-state reduction potential was measured to be $E(BNAH^{\bullet+}/BANH)$= +0.57 V vs SCE. The marked photoreductant properties of substrate **32** enabled an exergonic SET to the alkyl bromide **33**, which would not have been feasible in the ground state.

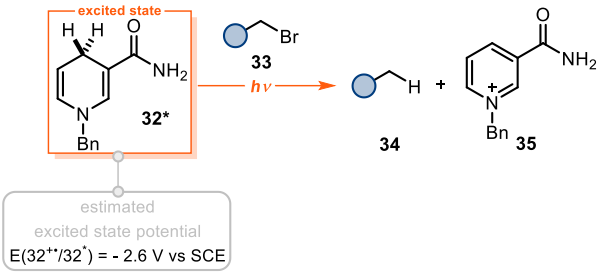

Scheme 2.14.: Estimation of the excited-state redox potential of BNAH **32**.

These seminal studies inspired the group of Cho[27] to evaluate the reductive power of photoexcited H-DHP **4**. Differently from Fukuzumi, Cho exploited a commonly used method, based on the Rehm-Weller formalism,[28] that combines spectroscopic and electrochemical analysis to *estimate* the excited-state potential of a substrate. For a given molecule **A**, the Rehm-Weller theory (Eq. 2.1) considers the excited-state potential ($E_{1/2}$*(**A**)) as a correction of the ground-state potential ($E_{1/2}$(**A**)), which can measured by cyclic voltammetry.

Zhang, W., Yang, L., Liu, Z.-L. "Photoinduced Transformation of α,β-epoxyketones to β-hydroxyketones by Hantzsch 1, 4-dihydropyridine" *Tetrahedron Lett.* **2002**, *43*, 9687.

[26] a) Fukuzumi, S., Hironaka, K., and Tanaka, T. "Photoreduction of Alkyl Halides by an NADH Model Compound. An Electron-Transfer Chain Mechanism", *J. Am. Chem. Soc.* **1983**, 105, 14, 4722. b) Fukuzumi, S., Inada, O., Suenobu, T. "Mechanisms of Electron-Transfers Oxidation of NADH Analogues and Chemiluminescence. Detection of the Keto and Enol Radical Cations", *J. Am. Chem. Soc.* **2003**, *125*, 4808.

[27] Jung, J., Kim, J., Park, G., You, Y., Cho, E. J. "Selective Debromination and α-Hydroxylation of α-Bromo Ketones Using Hantzsch Esters as Photoreductants", *Adv. Synth. Catal.* **2016**, *358*, 74.

[28] Calculated using the Rehm-Weller equation; Rehm, D., Weller, A. "Kinetics of Fluorescence Quenching by Electron and H-atom Transfer", *Isr. J. Chem.* **1970**, *8*, 259.

$$E^{*}_{1/2}(\mathbf{A}^{*}) = E_{1/2}(\mathbf{A}) \pm E_{00}(\mathbf{A}) \qquad \text{Eq. 2.1}$$

Such correction factor is given by the E_{00} value of **A**, which is the energy difference between the lowest vibrational level of the excited state and the corresponding ground state (Scheme 2.15, left). This value is estimated by UV-Vis spectroscopy considering the long wavelength tail of the UV-Vis absorption spectrum (Scheme 2.15, right).[29] The sign of the correction factor (E_{00}) is defined by the role of **A** acting as photooxidant (sign +) or photoreductant (sign -). In case of H-DHP **4**, since it behaves as a photoreductant, the corresponding Rehm-Weller equation for the excited-state potential is written as in Eq. 2.2.

$$E^{ox}_{1/2}(\mathbf{4}^{*}) = E^{ox}_{1/2}(\mathbf{4}) - E_{00}(\mathbf{4}) \qquad \text{Eq 2.2}$$

By the difference of the measured ground-state potential ($E_{1/2}$(**4**) = +0.79 V vs SCE) and the estimated value of E_{00}(**4**) (+3.07 eV), the group of Cho evaluated the excited-state potential of H-DHP **4** to be ≈ -2.28 V vs SCE.

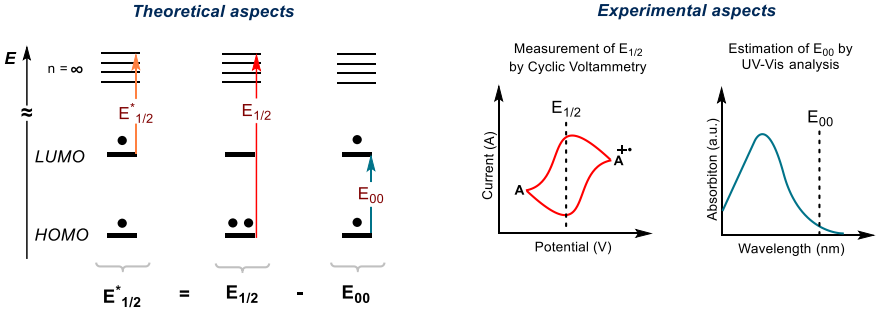

Scheme 2.15.: Theoretical and experimental aspects of the Rehm-Weller formalism.

Supported by this evaluation, the authors developed a photochemical protocol for the dehalogenation of α-bromoketones **36** based on the direct excitation of H-DHP **4** (Scheme 2.16). In the proposed mechanism, the excited H-DHP **4** triggers a SET reduction of ketone **36**, leading to the formation of the radical cation **XI** and the carbon-centered radical **XX**. **XX** undergoes HAT from the unstable **XI** to deliver the reduced product **37**.

[29] A more precise method to estimate the E_{00} can be done by overlapping the absorption spectrum and the emission spectrum of the fluorophore. The wavelength at which the two spectra overlap can be considered as the E_{00}. Nevertheless, this method cannot be always applied. For further details see: Balzani, V., Ceroni, P., Juris, A. "Photochemistry and photophysics: concepts, research, applications". 2014; John Wiley & Sons.

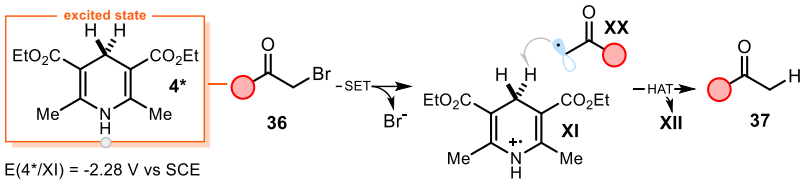

Scheme 2.16.: Photoexcitation of H-DHP **4** for the reductive debromination of α-bromoketones **36**.

The group of Hyster, inspired by the work of Fukuzumi on photoexcited BNAH, investigated the photoactivity of nicotinamide co-factors (NADPH) to develop an enzymatic, enantioselective radical dehalogenation of α-bromolactones **38** (Scheme 2.17). [30]

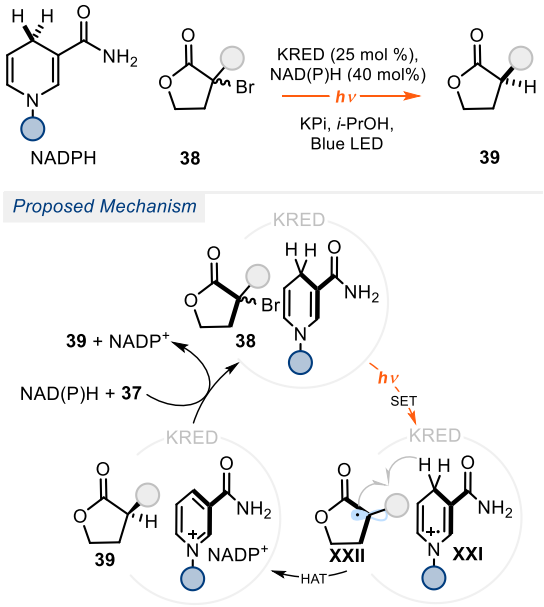

Scheme 2.17.: Photochemistry of NADPH co-factor in a stereoselective debromination reaction.

In the proposed mechanism, substrate **38** and co-factor NADPH are embedded within the chiral pocket of the ketoreductase enzyme (KRED). A photoinduced electron transfer from the NADPH co-factor to the □□haloketones **38** leads to the formation of the prochiral radical intermediate **XXII** and the radical cation **XXI**. Spatially-controlled HAT

[30] Emmanuel, M. A., Greenberg, N. R., Oblinsky, D. G., Hyster, T. K. "Accessing Non-Natural Reactivity by Irradiating Nicotinamide-Dependent Enzymes with Light", *Nature* **2016**, *540*, 414.

from **XXI** to the α-ketoradical **XXII** delivers the enantioenriched product **39** and the electron poor $NADP^+$. Restoration of NADPH and release of the enantioenriched ester **38** regenerates the active enzymatic pocket (Scheme 2.17).

Recently, our group proved that the direct excitation of 4-substituted-DHPs **40** (Scheme 2.18) brings up a dual reactivity profile, retaining the reducing features while serving as source of carbon-centered radicals.

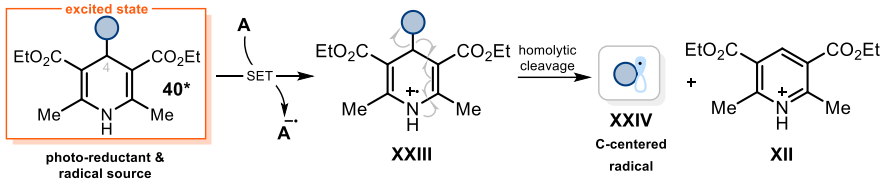

Scheme 2.18.: Dual reactivity profile of photoexcited 4-substituted-DHPs.

Similarly to H-DHP **4**, 4-substituted-DHPs **40**, upon light excitation, become strong photo-reductants that can transfer an electron to a suitable ground-state acceptor (**A**). This event drives the formation of the unstable radical cation **XXIII**, which upon aromatization delivers the carbon-centered radical **XXIV** (Scheme 2.18).

We exploited the facile modification of the C4-substituent to access alkyl- (**XV**) [31] acyl- (**XXV**),[32] and carbamoyl- (**XXVII**) radicals[33] under very mild conditions (Scheme 2.19).

[31] Buzzetti, L., Prieto, A., Roy, S. R., Melchiorre, P. "Radical-Based C–C Bond-Forming Processes Enabled by the Photoexcitation of 4-Alkyl-1,4-Dihydropyridines", *Angew. Chem. Int. Ed.* **2017**, *56*, 15039.

[32] Goti, G., Bieszczad B., Vega-Peñaloza, A., Melchiorre, P., "Stereocontrolled Synthesis of 1,4-Dicarbonyl Compounds by Photochemical Organocatalytic Acyl Radical Addition to Enals" *Angew. Chem. Int. Ed.* **2019**, *58*, 1213.

[33] Nurtalya Alandini, Doctoral Thesis **2020** "1,4-Dihydropyridines as Versatile Reagents in Photochemical Carbon-Carbon Bond-Forming Processes

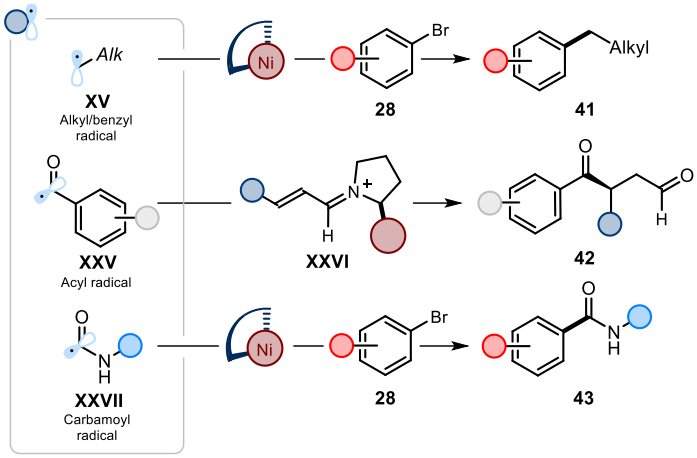

Scheme 2.19.: Radicals generated via the direct excitation of 4-substituted-DHPs **40** and applications thereof.

These open-shell intermediates have been used in different organo- and metal- catalyzed transformations. For example, we applied the dual reactivity profile of photo-excited DHP **44** to promote a nickel-catalyzed carbamoylation of aryl bromide **29** (Scheme 2.20).

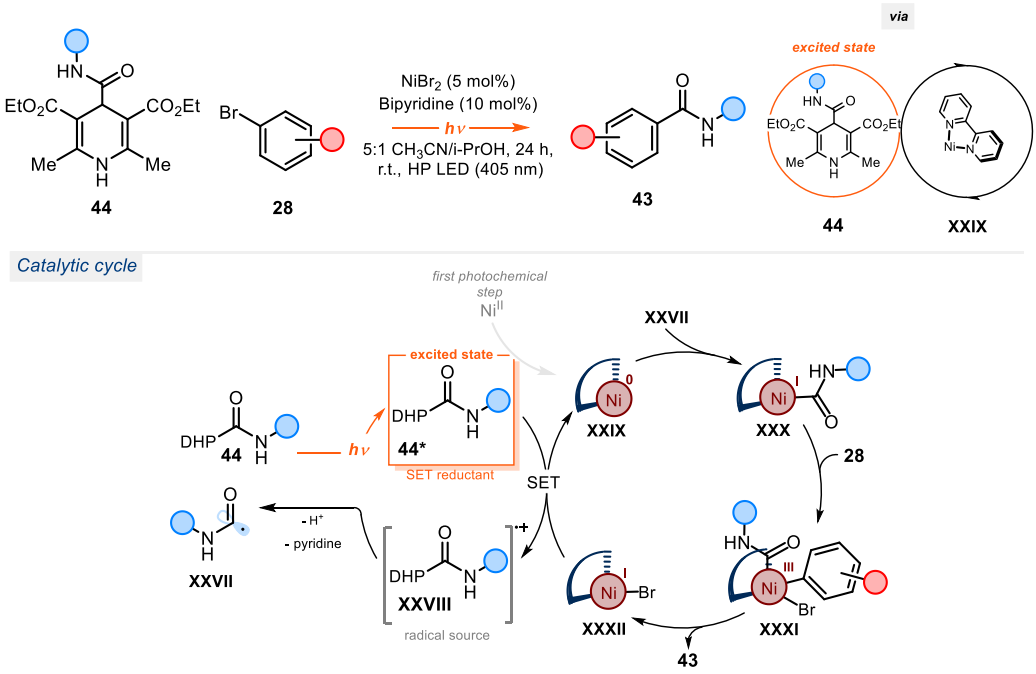

Scheme 2.20: The excited-state reactivity of 4-carbamoyl-DHP **44** triggers a nickel-catalyzed carbamoylation of aryl bromides **28**.

Upon light irradiation, dihydropyridine **44*** reduces the N(II) precatalyst by two discrete sequential SET event, yielding the active Ni(0) complex **XXIX**. Concomitantly, the radical cation **XXVIII**, upon aromatization, releases the carbamoyl radical **XXVII**, which is intercepted by the Ni(0) complex yielding the N(I) intermediate **XXX**. This latter undergoes oxidative addition with the aryl bromide 28 producing complex **XXXI**, which after reductive elimination deliver product **43**. Reduction of the emerging Ni(I) complex **XXXII** by an excited state DHPs regenerate the active Ni(0) complex **XXIX**.

During my research work, I further exploited both the ground-state and the excited-state reactivity of 1,4-dihydropyridines, and their ability to serve as photoreductants, electron donors and radical precursors. In the chemistry discussed in Chapter III, alkyl-DHPs were exploited as excited-state reductants and radical sources to develop a nickel-catalyzed asymmetric acyl cross-coupling for the synthesis of enantioenriched ketones. In Chapter IV, alkyl-DHPs served as ground-state reductants and α-amino radical sources in a photo-driven iridium-catalyzed asymmetric alkyl-alkyl cross-coupling.

Chapter III

Photochemical Asymmetric Nickel-catalyzed Acyl Cross-coupling.

Target

Developing a photochemical asymmetric nickel-catalyzed acyl cross-coupling for the synthesis of chiral α,α-disubstituted ketones.

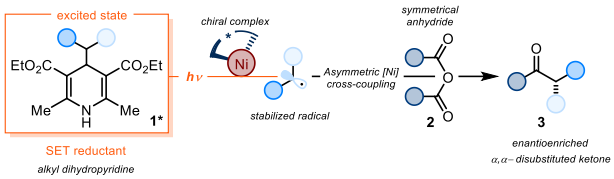

Tools

Exploiting the ability of photoexcited 4-alkyl DHPs **1** to act as SET reductants and radical sources in combination with ground-state nickel asymmetric catalysis.[1]

3.1 Introduction

In the past decades, the use of nickel to catalyze cross-couplings reactions has gained prominence, either by the use of traditional cross-coupling processes (featuring nucleophiles and electrophiles) and, more recently, by reductive-coupling reactions (featuring two electrophiles and a reductant). Researchers took advantage of the peculiar characteristics of this Earth-abundant metal providing elegant and powerful synthetic solutions, which effectively complemented traditional palladium-based technologies.[2] Amongst the most valuable features of nickel, we can include: cost-effectiveness, facile oxidative addition and reductive elimination, slow β-hydride elimination, and different oxidation states available ($Ni^{0/I/II/III/IV}$) (Figure 3.1).[3] This latter accounts for the tendency of nickel to participate in radical processes, allowing the expansion of cross-coupling reactions beyond the traditional $C(sp^2)$-$C(sp^2)$ bond formation, e.g. enabling difficult-to-realize $C(sp^3)$-$C(sp^3)$ couplings. Diversifying the way in which nickel catalysis could be

[1] Part of the project discussed in this Chapter has been conducted in collaboration with Dr Xinjun Tang and Dr Sudipta Raha Roy. Part of the work has been published, see: Gandolfo, E., Tang, X., Roy, S. R., Melchiorre, P. "Photochemical Asymmetric Nickel-Catalyzed Acyl Cross-Coupling" *Angew. Chem. Int. Ed.* **2019**, *58*, 16854.

[2] a) Tamaru, Y. "Modern Organonickel Chemistry" Weinheim, Wiley-VCH, 2005; b) Iwasaki, T., Kambe, N. "Ni-Catalyzed C–C Couplings Using Alkyl Electrophiles" *Top. Curr. Chem.* **2016**, *374*, 66.

[3] Tasker, S. Z., Standley, E. A., Jamison, T. F. "Recent Advances in Homogeneous Nickel Catalysis" *Nature* **2014**, *509*, 299.

integrated with radical reactivity served as a driving force for innovation (Scheme 3.1, left). For example, the recent merge with photoredox catalysis provided novel and mild ways to access radical intermediates via single-electron transfer (SET) events; at the same time, the photoredox catalyst modulated the oxidation state of the nickel catalyst. To date, photoredox and nickel dual catalysis has provided valuable synthetic solutions not achievable under classical thermal conditions (Scheme 3.1, right).[4]

Recently, our group reported a complementary photochemical methodology to promote light-driven nickel cross-coupling processes without the need of an external photoredox catalyst (Scheme 3.1, center-bottom).[5] Specifically, we used the tendency of the 4-alkyl-1,4-dihydropyridines (DHPs) **1** to act, upon direct photoexcitation, as both radical sources and SET reductants, thus modulating the oxidation state of the nickel catalyst.

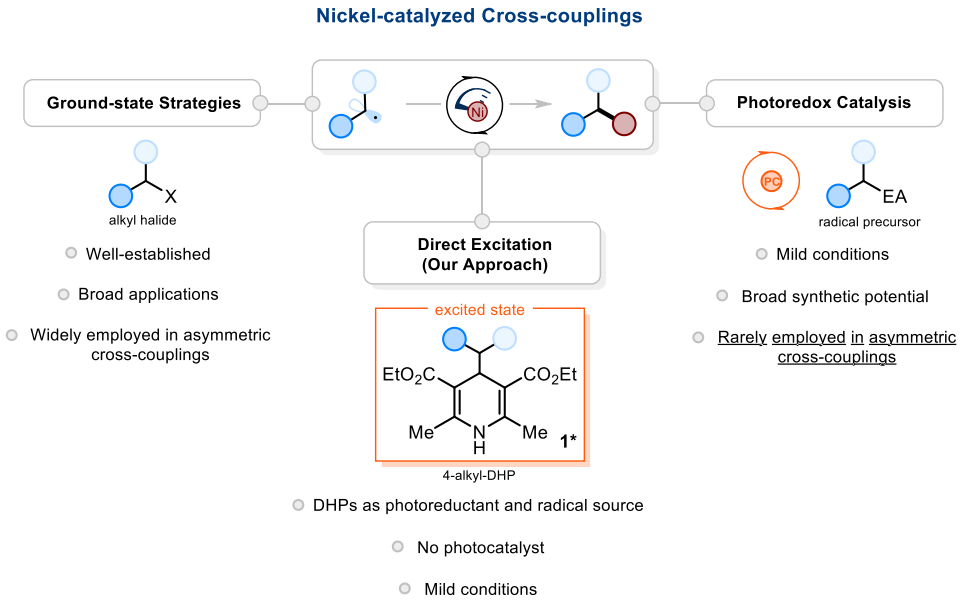

Scheme 3.1: Traditional and photochemical strategies to access radical reactivity in nickel-catalyzed cross-couplings

In the first part of my Ph.D., I explored the possibility to harness this photochemical platform to expand the potential of asymmetric nickel catalyzed cross-couplings. More in general, the combination of photoredox and asymmetric nickel catalysis has been rarely

[4] Zhu, C., Yue, H., Chu, L., Rueping, M. "Recent Advances in Photoredox and Nickel Dualcatalyzed Cascade Reactions: Pushing the Boundaries of Complexity" *Chem. Sci.* **2020**, *11*, 4051.
[5] Buzzetti, L., Prieto, A., Raha Roy, S., Melchiorre, P. "Radical-Based C−C Bond-Forming Processes Enabled by the Photoexcitation of 4-Alkyl-1,4-dihydropyridines" *Angew. Chem. Int. Ed.* **2017**, *56*, 15039.

employed hampering the development of nickel-based methodologies to access stereogenic centers.[6] Therefore, we sought the opportunity to expand the asymmetric nickel catalysis toolbox by capitalizing upon the excited-state chemistry of DHPs. In particular, we showcased the utility of this photochemical method through the stereocontrolled synthesis of α,α-disubstituted enantioenriched chiral ketones **3** via enantioselective acyl cross-coupling (Scheme 3.2).

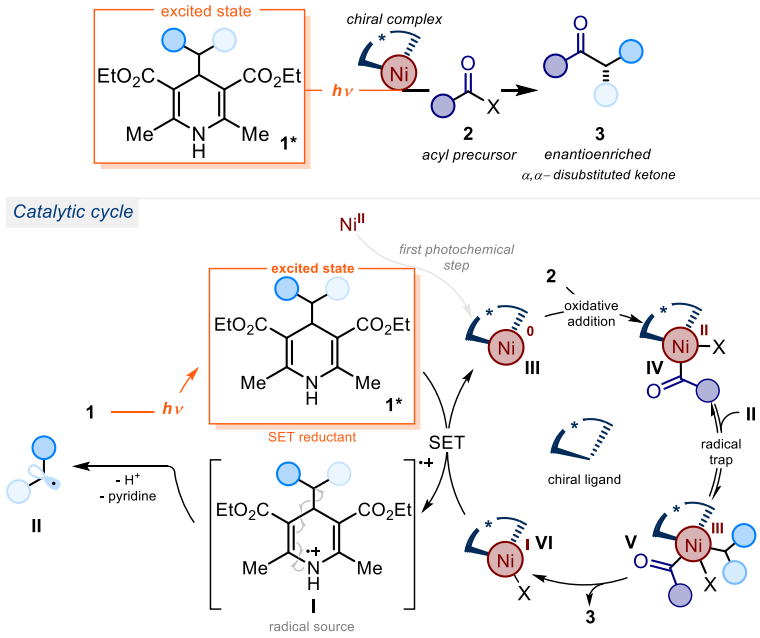

Scheme 3.2: Merging the direct excitation of DHP **1** with nickel asymmetric catalysis for the synthesis of enantioenriched chiral ketones **3**.

We surmised a mechanistic scenario where the use of an appropriate chiral ligand, which adorned the nickel catalyst, could secure the C(sp^3)-C(sp^2) bond formation in a stereocontrolled fashion. Upon photoexcitation, DHP 1 becomes a strong SET reductant able to reduce the chiral nickel(II) pre-catalyst generating the nickel(0) intermediate III. This event leads to the concomitant formation of the unstable radical-cation I which, upon fragmentation, releases the radical II. The active chiral Ni(0) catalyst III intercepts the alkyl radical III forming the nickel(I) intermediate IV, which then undergoes oxidative addition with the electrophilic partner producing the Ni(III) species V. This latter, after

[6] Lipp, A., Badir, S. O., Molander, G. A. "Stereoinduction in Metallaphotoredox Catalysis" *Angew. Chem. Int. Ed.* **2021**, *60*, 1714

stereoselective reductive elimination, yields the enantioenriched ketone product 3. Finally, SET from the excited state DHP 1 to the inactive Ni(I) complex VI closes the nickel catalytic cycle while regenerating the radical intermediate II.

3.2 Nickel-catalyzed Asymmetric Cross-couplings

Asymmetric nickel catalysis is a powerful tool to prepare chiral molecules.[7] Different nickel catalytic strategies have been developed, based on traditional asymmetric cross-coupling (Scheme 3.3, a), asymmetric reductive cross-coupling (Scheme 3.3, b), and recently electrophile-olefin asymmetric cross-coupling (Scheme 3.3, c).

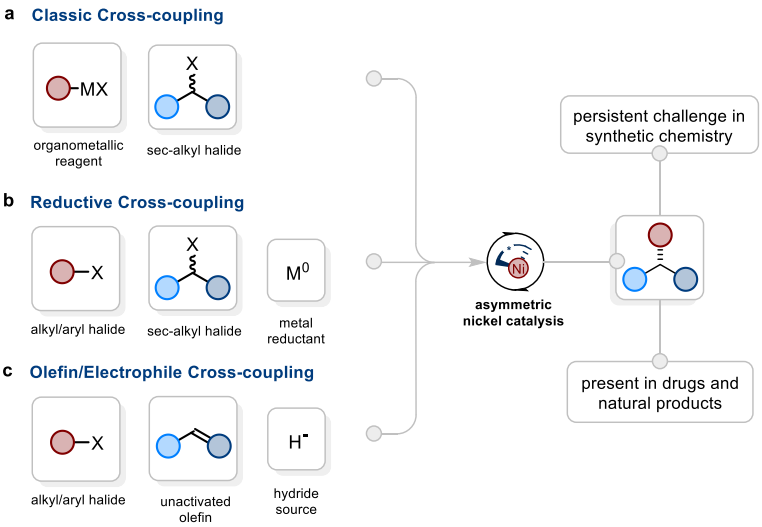

Scheme 3.3: Different approaches in nickel asymmetric catalysis.

With regard to traditional cross-coupling, fundamental contributions came from the group of Fu in 2005[8], who reported the first example of an asymmetric cross-coupling between a racemic secondary electrophile **4** and a primary alkyl nucleophile **5** (Scheme 3.4). Until then, nickel-catalyzed asymmetric cross-coupling used primary electrophiles and secondary organometallic nucleophiles, which limited the synthetic application of this

[7] a) Choi, J., Fu, G. C. "Transition Metal–Catalyzed Alkyl-Alkyl bond Formation: another Dimension in Cross-Coupling Chemistry" *Science* **2017**, *356*, 152; b) Cherney, A. H., Kadunce, N. T., Reisman, S. E. "Enantioselective and Enantiospecific Transition-Metal-Catalyzed Cross-Coupling Reactions of Organometallic Reagents To Construct C−C Bonds" *Chem. Rev.* **2015**, *115*, 9587; c) Pellissier, H. "Enantioselective Nickel-Catalyzed Transformations" RSC Catalysis Series No. 26, 2016.

[8] Fischer, C., Fu, G. C. "Asymmetric Nickel-Catalyzed Negishi Cross-Couplings of Secondary α-Bromo Amides with Organozinc Reagents" *J. Am. Chem. Soc.* **2005**, *127*, 4595.

tool. Here the authors used α-bromo amides **4** as electrophiles, and alkyl zinc **5** as nucleophiles. The reaction proceeds under mild conditions, affording the desired products **6** in high yields and enantioselectivities. The proposed mechanistic cycle starts with a SET reduction of the electrophilic α-bromo amides **4** by the Ni (I) complex **VII**, leading to radical intermediates **VIII**. The emerging Ni(II) intermediate **IX** undergoes transmetallation with the alkyl zinc nucleophile **5** delivering complex **X**. The latter captures the α-amide radical **VIII** and undergoes reductive elimination to release the enantioenriched α,α-disubstituted amide product **6** and Ni(I) complex **VII**, which restarts the catalytic cycle.

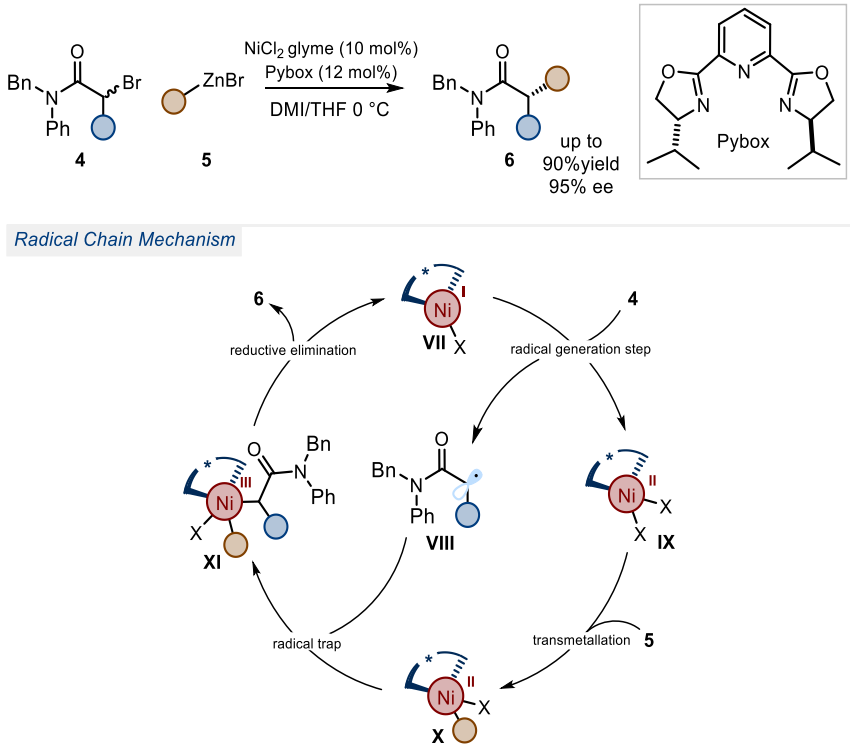

Scheme 3.4: First example of a nickel catalyzed enantioconvergent coupling of a racemic secondary electrophile **4**.

Further mechanistic studies demonstrated the formation of carbon-centered radicals and their roles as key intermediates of the enantioconvergent pathway.[9] After this initial

[9] a) Fu, G. C. "Transition-Metal Catalysis of Nucleophilic Substitution Reactions: A Radical Alternative to S_N1 and S_N2 Processes" *ACS Cent. Sci.* **2017**, *3*, 692; b) Schley, N. D., Fu, G. C. "Nickel-Catalyzed Negishi Arylations of Propargylic Bromides: A Mechanistic Investigation" *J. Am. Chem. Soc.* **2014**, *136*,

report, this catalytic platform was further exploited in a plethora of asymmetric transformations using different combinations of nucleophiles and racemic alkyl halides (e.g. benzylic, unactivated alkyl, and allylic halides).[10]

The reductive cross-coupling approach experienced a more limited development. Only recently, the Reisman group reported the first enantioselective example using acyl chlorides **7** and secondary benzylic chloride **8** as cross-coupling partners in the presence of a chiral bisoxazoline (Box) ligand to access the enantioenriched α,α-disubstituted ketones **9** (Scheme 3.5).[11] Manganese powder served as terminal stoichiometric reductant to generate the nickel(0) complex as the active catalyst. The proposed catalytic cycle starts with oxidative addition of the acyl chloride **7** with the active Ni(0) complex **XII**, formed in-situ by the reducing properties of manganese. The emerging Ni(II) complex **XIII** is then reduced by manganese to Ni(I) intermediate **XIV**. A second oxidative addition of benzylic chloride **8** with complex **XV** yields the Ni(III) intermediate **XVI**. This latter undergoes reductive elimination delivering the α,α-disubstituted ketones **9** and nickel catalyst **XII**, restarting the cycle.[12]

16588; c) Yin, H., Fu, G. C. "Mechanistic Investigation of Enantioconvergent Kumada Reactions of Racemic α-Bromoketones Catalyzed by a Nickel/Bis(oxazoline) Complex" *J. Am. Chem. Soc.* **2019**, *141*, 15433; for a general review on nickel mechanisms in catalysis see: Diccianni, J. B., Diao, T. "Mechanisms of Nickel-Catalyzed Cross-Coupling Reactions" *Trends Chem*, **2019**, *1*, 830.

[10]Use of benzylic alkyl halides: a) Arp, F. O., Fu, G. C. "Catalytic Enantioselective Negishi Reactions of Racemic Secondary Benzylic Halides" *J. Am. Chem. Soc.* **2005**, *127*, 10482. Use of unactivated alkyl halides: b) Saito, B. Fu, G. C. "Enantioselective Alkyl−Alkyl Suzuki Cross-Couplings of Unactivated Homobenzylic Halides" *J. Am. Chem. Soc.* **2008**, *28*, 6694. Use of allylic halides: c) Son, S., Fu, G. C. "Nickel-Catalyzed Asymmetric Negishi Cross-Couplings of Secondary Allylic Chlorides with Alkylzincs" *J. Am. Chem. Soc.* **2008**, *9*, 2756. For a recent example of asymmetric cross-coupling in a double convergent protocol: d) Huo, H., Gorsline, B. J., Fu, G. C. "Catalyst-Controlled Doubly Enantioconvergent Coupling of Racemic Alkyl Nucleophiles and Electrophiles" *Science* **2020**, *367*, 559.

[11] Cherney, A. H., Kadunce, N. T., Reisman, S. E. "Catalytic Asymmetric Reductive Acyl Cross-Coupling: Synthesis of Enantioenriched Acyclic α,α-Disubstituted Ketones" *J. Am. Chem. Soc.* **2013**, *135*, 7442.

[12] For reviews on nickel-catalyzed reductive cross-coupling see: a) Poremba, K. E., Dibrell, S. E., Reisman, S. E. "Nickel-Catalyzed Enantioselective Reductive Cross-Coupling Reactions" *ACS Catal.* **2020**, *10*, 8237; b) Knappke, C. E. I., Grupe, S., Gärtner, D.,. Corpet, M., Gosmini, C., von Wangelin, A. J. "Reductive Cross-Coupling Reactions between Two Electrophiles" *Chem. Eur. J.* **2014**, *20*, 6828.

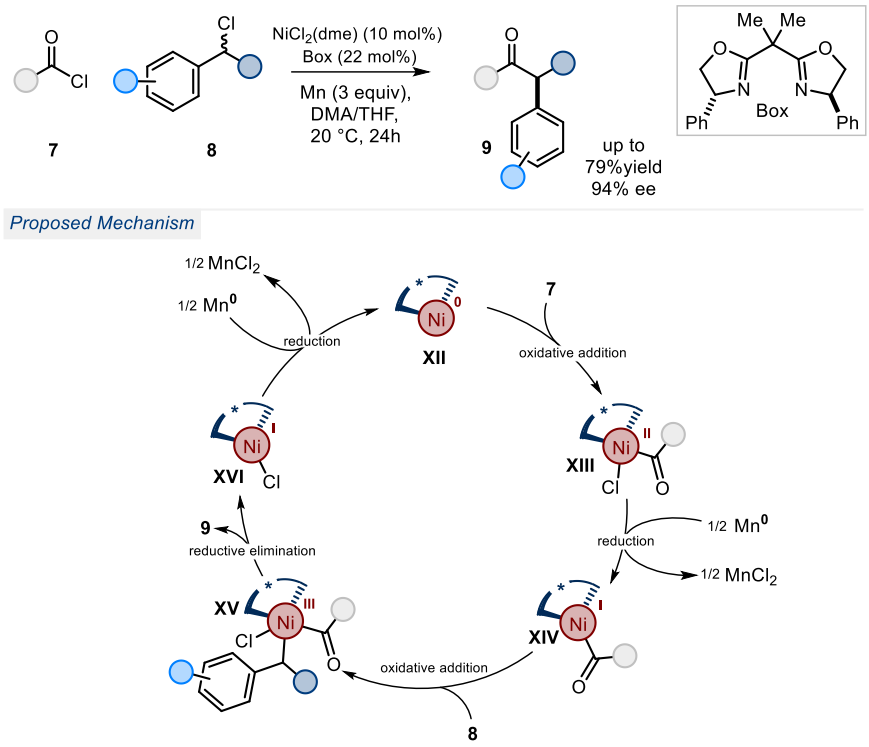

Scheme 3.5: First example of asymmetric nickel reductive-coupling and proposed mechanism.

Lastly, in 2018, the group of Fu reported a novel asymmetric nickel-catalyzed process of secondary or tertiary alkyl halides and simple olefins to access highly enantioenriched compounds (Scheme 3.6). A major perk of this approach, compared to the previously presented protocols, lies in the use of stable and commercially available reagents and the absence of stoichiometric reducing agents. The authors studied the reactivity between the electrophilic amide **10** and unactivated olefin **11** to access enantioenriched α,α-disubstituted amides **12**.[13] In contrast to the classic nickel cross-coupling processes, tertiary alkyl halides could be used for the first time in an enantioconvergent coupling. Such peculiar reactivity enabled the difficult preparation of enantioenriched quaternary stereocenters. For this transformation, the authors proposed the mechanism depicted in Scheme 3.6. The catalytic cycle begins with an SET from the Ni(I) complex **XVII** to the electrophilic amide **10**. This event leads to the formation of the tertiary radical **XVIII** and the Ni(II) complex **XIX**. This latter undergoes σ-bond metathesis with silane **13**

[13] "Wang, Z., Yin, H., Fu, G. C. "Catalytic Enantioconvergent Coupling of Secondary and Tertiary Electrophiles with Olefins" *Nature* **2018**, *563*, 379.

producing the Ni(II)-hydride intermediate **XX**, which activates olefin **11** via β-migratory insertion. The emerging Ni(II) intermediate **XXI** traps radical **XVIII** to produce a Ni(III) complex **XXII**, which after reductive elimination delivers the enantioenriched amide **12**.

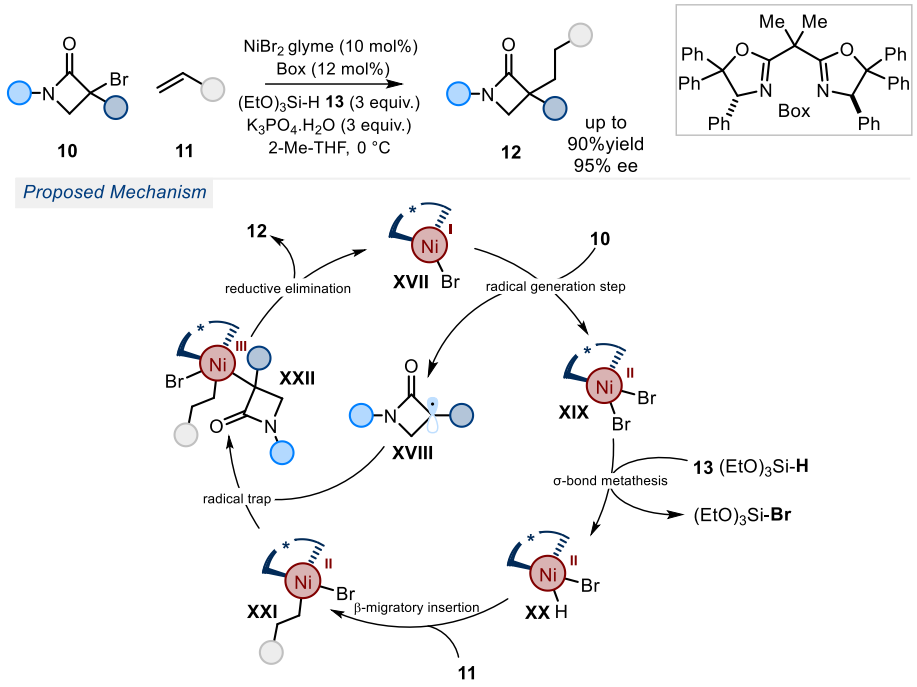

Scheme 3.6: First example of asymmetric electrophile-olefin cross-coupling.

3.3 Merging Photoredox and Asymmetric Nickel-catalyzed Cross-couplings

The methodologies presented so far have the drawback of using either organometallic reagents or stoichiometric amounts of metallic reductants to modulate the oxidation state of the chiral nickel catalyst and promote the formation of radical intermediates. The combination of nickel and photoredox catalysis emerged as a powerful tool to overcome these issues. Moreover, this approach broadened the scope of reaction partners to include substrates that were unreactive under the thermal conditions.[14] In fact, by the means of an excited-state photocatalyst, it is possible to access, via SET or hydrogen atom transfer

[14] a) Prier, C. K., Rankic, D. A., MacMillan, D. W. C. "Visible Light Photoredox Catalysis with Transition Metal Complexes: Applications in Organic Synthesis" *Chem. Rev.* **2013**, *113*, 5322; b) Twilton, J., Le, C., Zhang, P., Shaw, M. H., Evans, R. W., MacMillan, D. W. C. "The Merger of Transition Metal and Photocatalysis" *Nat. Rev. Chem.* **2017**, *52*, 1.

(HAT) pathways, radical intermediates while tuning the oxidation state of the nickel catalyst (Scheme 3.7).

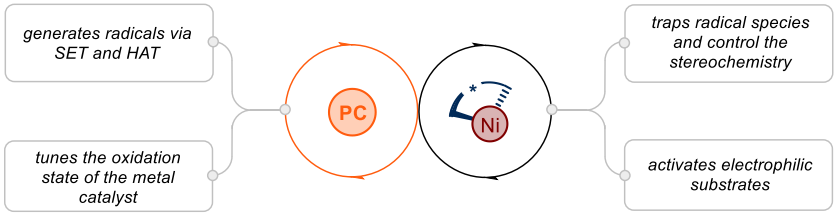

Scheme 3.7: Working modes of photoredox in nickel asymmetric catalysis. PC, photocatalyst.

Despite the practical advantages of this approach, only few examples have been reported regarding nickel- catalyzed asymmetric transformations.[15] The first merge of photoredox catalysis and nickel asymmetric catalysis was reported by Molander in the pioneering report on *metallaphotoredox catalysis*.[16] In this work, an iridium based photocatalyst allowed the direct coupling between aryl halides and primary alkyl potassium trifluoroborate salts **14**, which are generally recalcitrant reagents under thermal conditions (Scheme 3.8).

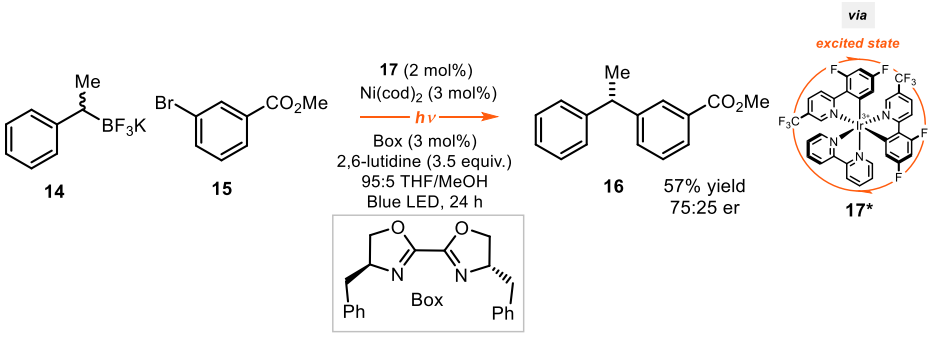

Scheme 3.8: First merge of asymmetric nickel catalysis and photoredox catalysis.

[15] For a review see: reference 6; For other examples not discussed here see: a) Stache, E. E., Rovis, T., Doyle, A. G. "Dual Nickel- and Photoredox-Catalyzed Enantioselective Desymmetrization of Cyclic meso-Anhydrides" *Angew. Chem. Int. Ed.* **2017**, *56*, 3679; b) Zhou, Q-Q., Lu, F-D., Liu, D., Lu L-Q., Xiao, W-J. "Dual Photoredox and Nickel-Catalyzed Desymmetric C–O Coupling Reactions: Visible Light-Mediated Enantioselective Synthesis of 1,4-Benzodioxanes" *Org. Chem. Front.* **2018**, *5*, 3098; c) Guan, H., Zhang, Q., Walsh, P. J., Mao, J. "Nickel/Photoredox-Catalyzed Asymmetric Reductive Cross-Coupling of Racemic a-Chloro Esters with Aryl Iodides" *Angew. Chem. Int. Ed.* **2020**, *59*, 5172.
[16] Tellis, J. C., Primer, D. N., Molander, G. A. "Single-Electron Transmetalation in Organoboron Cross-Coupling by Photoredox/Nickel Dual Catalysis" *Science* **2014**, *345*, 433.

The activation mode exploited in this process relies on the low oxidation potential of substrates **14**, which are activated via SET from the excited photocatalyst **17**. In a single example, the authors proved that, when adorning the nickel catalyst with a chiral bisoxazoline (Box) ligand, a modest level of stereocontrol could be achieved (50% ee).
In 2016, Fu and MacMillan reported the first extensive application of this photoredox approach [17] by stereoselectively coupling natural abundant carboxylic acids **18** and (hetero)aryl bromides **19** (Scheme 3.9).

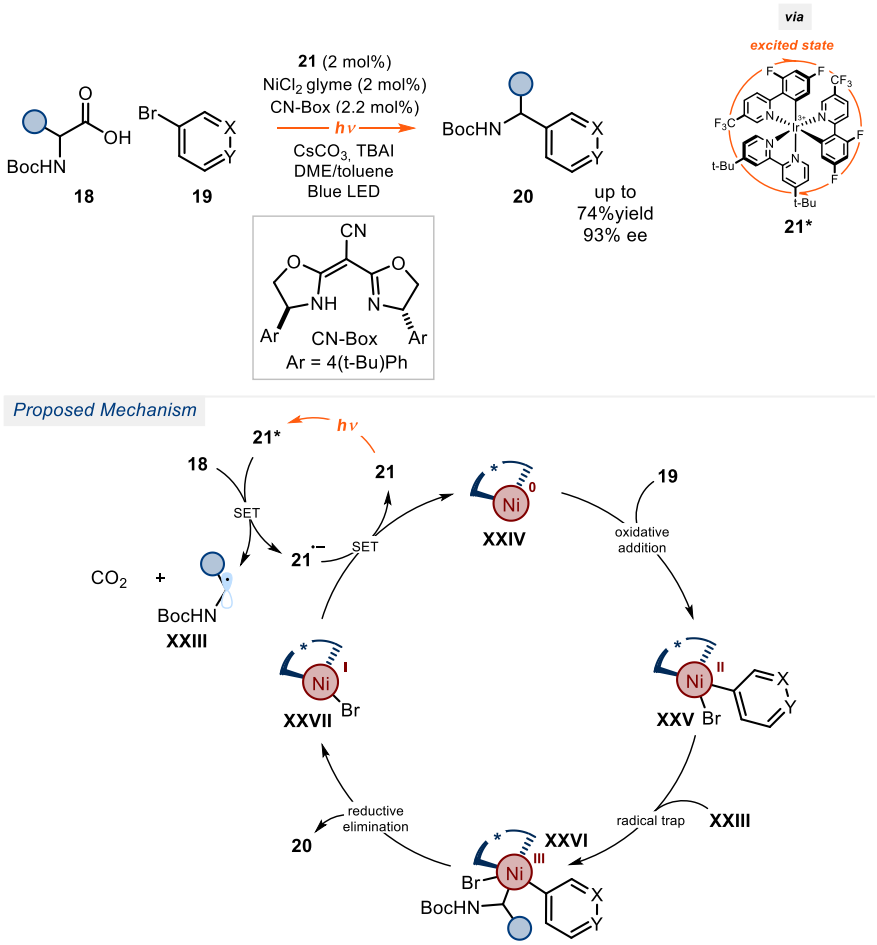

Scheme 3.9: First general application of photoredox catalysis in enantioselective nickel catalysis.

[17] Zuo, Z., Cong, H., Li, W., Choi, J., Fu, G. C., MacMillan, D. W. C. "Enantioselective Decarboxylative Arylation of α-Amino Acids via the Merger of Photoredox and Nickel Catalysis" *J. Am. Chem. Soc.* **2016**, *138*, 1832. For another report employing a similar strategy see: Pezzetta, C., Bonifazi, D., Davidson, R. W. M. "Enantioselective Synthesis of N-Benzylic Heterocycles: A Nickel and Photoredox Dual Catalysis Approach" *Org. Lett.* **2019**, *21*, 8957.

Also here, the photochemical activation exploits the SET oxidation of substrate **17** by the excited photocatalyst **21**. The feasibility of this coupling, although in a non-asymmetric version, was already demonstrated.[18] In the current case, the use of a substituted semicorrin-like chiral ligand (CN-Box) provided the chiral information enabling the preparation of α-aryl amines with high enantioselectivity.

The proposed mechanism for this transformation is depicted in Scheme 3.9. Upon light excitation, the iridium-based photocatalyst **21*** oxidizes the anion of the carboxylic acid derivative **18**, which upon decarboxylation delivers the α-amino radical **XXIII**. The reduced form of the photocatalyst (**21**$^{\bullet-}$) is now able to reduce, *via* SET, the Ni(I) pre-catalyst **XXVII** to Ni(0). The emerging nickel complex **XXIV** undergoes oxidative addition with the aryl bromide **19** generating the Ni(II) intermediate **XXV**. This latter traps the α-amino radical **XXIII** leading to the Ni(III) complex **XXVI**, which after reductive elimination yields the enantioenriched product **20** in high enantiomeric excesses and yields.

More recently, Lu and co-workers coupled nickel asymmetric catalysis with photo-induced hydrogen atom transfer (HAT) catalysis (Scheme 3.10). This study, by introducing a novel activation strategy of radical precursors beyond SET activation, broadened the scope of reaction partners.[19] Simple benzylic derivatives **22** were coupled with aryl bromides **23** in the presence of the iridium-based photocatalyst **21**, which served to tune the oxidation state of the nickel, and aryl ketone **25**, which acted as the HAT co-catalyst. Moreover, the bis-imidazoline ligand (Biim) was crucial to secure high level of enantioselectivity. The proposed mechanism involves a double intersection between the nickel and the photoredox catalytic cycles. In the first interplay, the reduced form of the photocatalyst **21**$^{\bullet-}$ generates the Ni(0) catalyst **XXX** via an SET, which undergoes oxidative addition with the aryl bromide **23**, delivering the Ni(II) complex **XXXI**. At this point, the excited-state photocatalyst **21*** oxidizes complex **XXXI** triggering the

[18] Zuo, Z., Ahneman, D. T., Chu, L., Terrett, J. A., Doyle, A. G., MacMillan, D. W. "Merging photoredox with nickel catalysis: Coupling of α-carboxyl sp3-carbons with aryl halides" *Science* **2014**, *345*, 437.

[19] Cheng, X., Lu, H., Lu, Z. "Enantioselective Benzylic C–H Arylation via Photoredox and Nickel Dual Catalysis" Nat. Comunn. **2019**, *10,* 1. For another photoredox-nickel catalyzed asymmetric cross-coupling employing HAT catalysis see: Fan, P., Lan, Y., Zhang, C., Wang, C. "Nickel/Photo-Cocatalyzed Asymmetric Acyl-Carbamoylation of Alkenes" *J. Am. Chem. Soc.* **2020**, *142*, 5, 2180.

formation of a bromine radical, via Ni(III)-Br homolytic cleavage.[20] Ketone **25**,[21] activates the benzylic substrate **22** delivering the stabilized benzyl radical **XXXII**. This is then trapped by the Ni(II) complex **XXXIII** that, upon reductive elimination, yields the α-arylated product **24** in high yields and enantioselectivity.

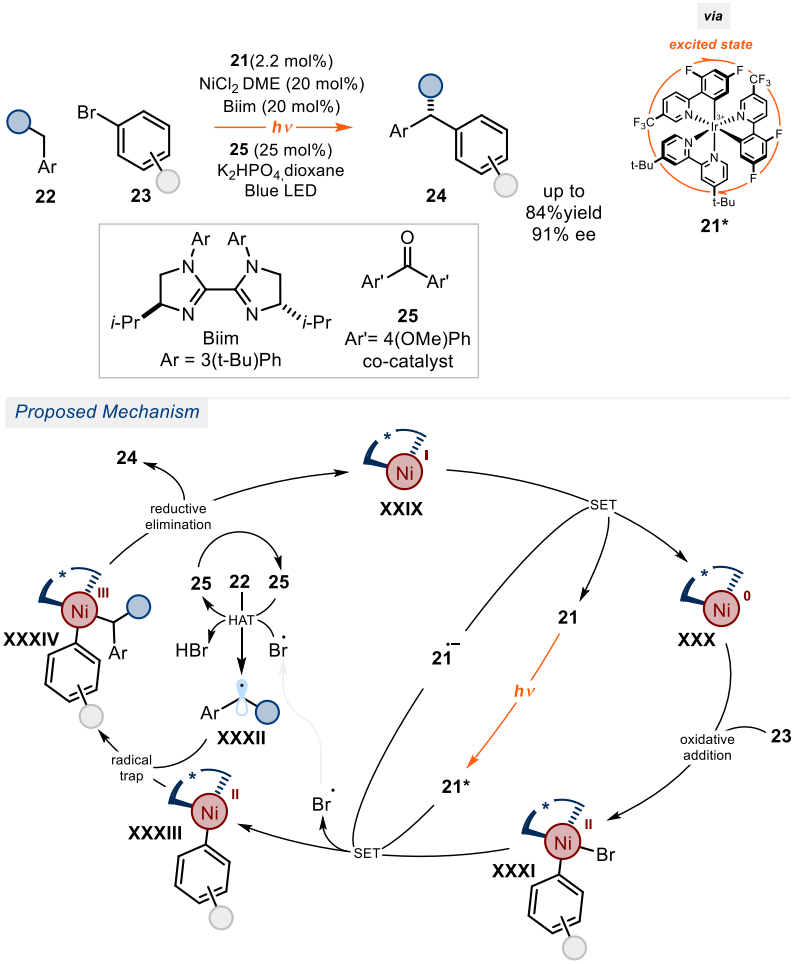

Scheme 3.10.: Combination of asymmetric metallaphotoredox and HAT catalysis.

[20] A plausible energy transfer (EnT) mechanism for the generation of the bromine radical cannot be excluded, for further details see: Heitz, D. R., Tellis, J. C., Molander, G. A., "Photochemical Nickel-Catalyzed C−H Arylation: Synthetic Scope and Mechanistic Investigations" *J. Am. Chem. Soc.* **2016**, *138*, 12715.

[21] For a prior example merging photochemical HAT activation by aromatic ketones in combination with nickel catalysis see: Shen, Y., Gu, Y., Martin, R., "sp3 C–H Arylation and Alkylation Enabled by the Synergy of Triplet Excited Ketones and Nickel Catalysts" *J. Am. Chem. Soc. 2018*, *140*, 12200.

3.4 Design and Target of the Project

Recently, our laboratory reported a complementary photochemical methodology for nickel catalyzed cross-coupling reactions that exploits the direct excitation of DHPs **1** to generate radicals, without the use of external photocatalysts (Scheme 3.11).[5] This protocol was exploited in C(sp^3)-C(sp^2) cross-coupling with aryl halides and acyl chlorides to synthetize products **28** and ketones **29**, respectively.

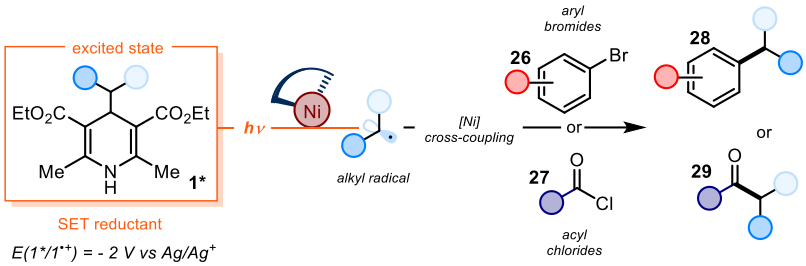

Scheme 3.11: Merging DHPs **1** direct excitation in nickel catalysis.

In this approach, the excited DHPs **1** serve a dual role: it acts as a strong SET reductant to reduce the nickel catalyst and as a radical source, providing one of the cross-coupling partners. The proposed mechanism for this nickel-catalyzed radical cross-coupling is shown in Scheme 3.12. The strong reducing properties of the excited DHP **1*** ($E(\mathbf{1}^*/\mathbf{1}^{\bullet+})$ ~ -2 V vs Ag/AgCl in CH_3CN) allow an exergonic SET reduction of the nickel(II) pre-catalyst (E^{red} (Ni^{2+}/Ni^0) $= -1.2/-1.3$ vs SCE in DMF)[22] to the active nickel(0) intermediate **XXXV**. The concomitant formation of the unstable radical-cation **I** triggers, upon fragmentation, the release of radical **II**. The active Ni(0) catalyst **XXXV** intercepts alkyl radical **II** forming a nickel(I) organometallic intermediate X**XXVI**, which then undergoes oxidative addition with the electrophilic partner, for example acyl chloride **27**. This would lead to intermediate **XXXVII**, which, after reductive elimination, yields the cross-coupled product **29**. Finally, SET transfer from the excited DHP **1** to the inactive Ni(I) complex **XXXVIII** closes the nickel catalytic cycle while regenerating the radical intermediate **II**.

[22] a) Johnston, P., Smith, R. T., Allmendinger, S., MacMillan, D. W. C. "Metallaphotoredox-catalysed Sp3–Sp3 Cross-coupling of Carboxylic Acids with Alkyl Halides" *Nature* **2016**, *536*, 322; b) de Franca, K.W. R., Navarro, M., Leonel, E., Durandetti, M., Nedelec, J-Y. "Electrochemical Homocoupling of 2-Bromomethylpyridines Catalyzed by Nickel Complexes" *J. Org. Chem.* **2002**, *67*, 1838.

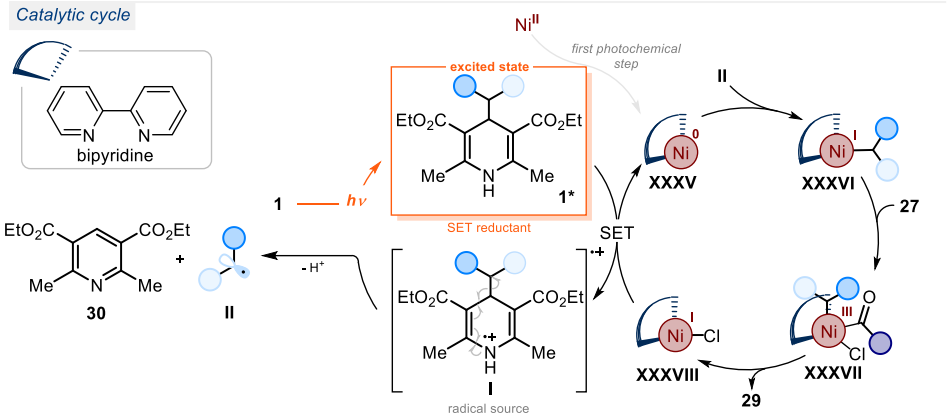

Scheme 3.12: Proposed mechanistic cycle for the merge of the excited-state chemistry of DHP **1** and nickel catalysis.

We sought to exploit this dual reactivity profile of excited DHPs to expand the synthetic potential of asymmetric nickel-catalyzed cross-couplings. As showed in the previous paragraphs, the exploitation of asymmetric nickel cross-couplings within the photochemical framework is rare. To date, this promising area is still lacking of an extensive use, thus hampering the development of practical and simple ways to access stereogenic centers. Nevertheless, this approach has its main drawback in the need of expensive photocatalysts to trigger reactivity and modulate the oxidation state of the nickel catalyst. Our photochemical has the potential to overcome this issue since the sole photo-excited DHP **1** sustains the nickel catalytic cycle and concurrently generates radicals. Moreover, this work represents one of the few examples of light-driven asymmetric nickel cross-coupling, and the first using the direct excitation approach. We applied this idea to the development of an enantioselective acyl cross-coupling for the preparation of α,α-disubstituted alkyl ketones, which are important and versatile compounds for the synthesis of natural products and pharmaceutical (Scheme 3.13).[23]

[23] Cano, R., Zakarian, A., McGlacken, G. P. "Direct Asymmetric Alkylation of Ketones: Still Unconquered" *Angew. Chem. Int. Ed.* **2017**, *56*, 9278.

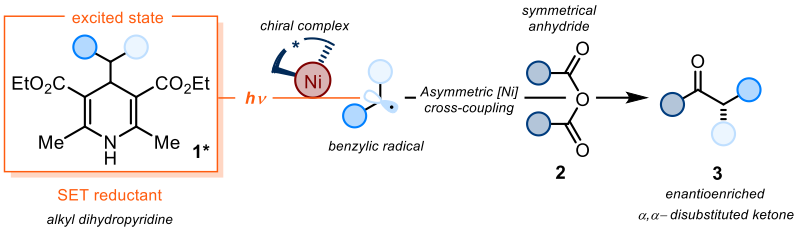

Scheme 3.13: Our target photochemical asymmetric nickel catalyzed process.

3.5 Results and Discussion

3.5.1 Photophysical Characterization of DHPs 1a and 1b

The crucial mechanistic aspect of our photochemical plan is the ability of an excited DHP to act as a strong reducing agent, firstly towards a Ni(II) pre-catalyst, to generate the catalytically active Ni (0), and later to turn over the nickel catalytic cycle. Therefore, at the onset of our investigation, I deemed as essential to determine if our model DHP substrates **1a** and **1b** (Scheme 3.14), upon light excitation, could serve as suitable reductants for a Ni(II) pre-catalyst (E (Ni^{2+}/Ni^{0}) = −1.2/ −1.3 V vs SCE in DMF).

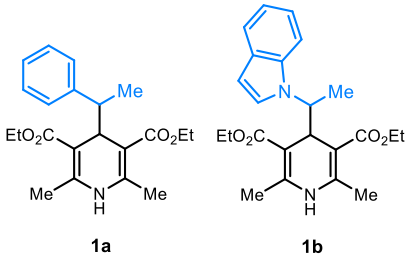

Scheme 3.14: Structures of substrates **1a** and **1b**.

To this end, we exploited the Rehm-Weller formalism, which relies on UV-Visible spectroscopy and electrochemical analysis (see Chapter II for details), to establish the excited-state reduction potential of **1a** and **1b**.

UV-Visible spectroscopy of a diluted sample (concentration, 3 mM) of **1a**, in CH_3CN, confirmed its ability to absorb visible light up to 420 nm (Figure 3.1). Similar observation was made for substrate **1b** (Figure 3.2) under the same experimental conditions.

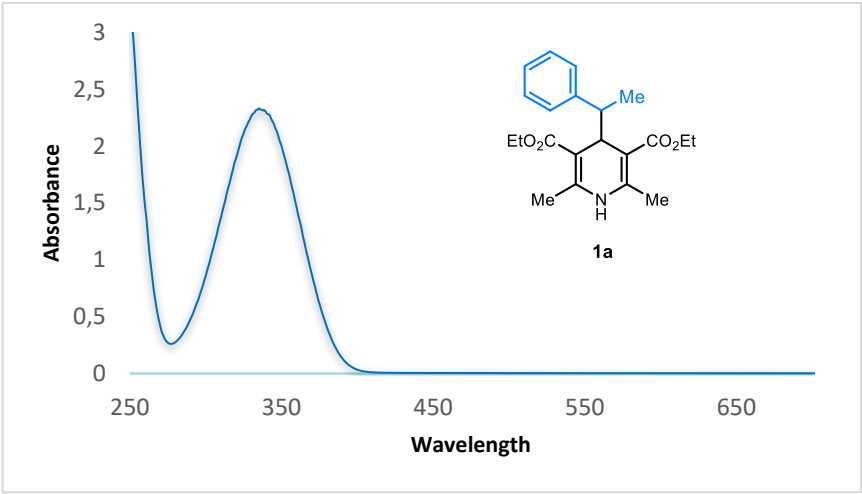

Figure 3.1: Absorption spectrum of **1a** ([**1a**] = 3 mM in CH_3CN): λ_{max} = 337 nm. The tail wavelength of absorption was considered at 420 nm.

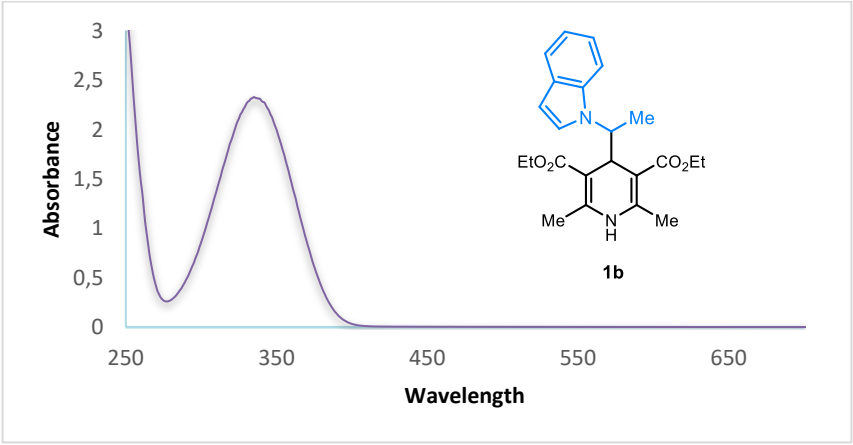

Figure 3.2: Absorption spectrum of **1b** ([**1b**] = 3 mM in CH_3CN): λ_{max} = 339 nm. The tail wavelength of absorption was considered at 420 nm.

We then performed electrochemical characterization of substrate **1a** via cyclic voltammetry (CV). The measurement indicated an irreversible oxidation peak (Figure 3.3) with an $E_p^A = E_{ox}$ (**1a**$^{\cdot+}$/**1a**) = +1.30 V vs Ag/AgCl. This is rationalized by the propensity of DHP **1a** to undergo fragmentation upon SET oxidation.[24] Compound **1b**

[24] Wang, P. Z., Chen, J. R., Xiao, W. J. "Hantzsch Esters: An Emerging Versatile Class of Reagents in Photoredox Catalyzed Organic Synthesis", *Org. Biomol. Chem.* **2019**, *17*, 6936

displayed an akin irreversible oxidation peak (Figure 3.4) with an $E_p^A = E^{ox}$ (**1b**$^{\bullet+}$/**1b**) = + 1.3 V vs. Ag/AgCl.

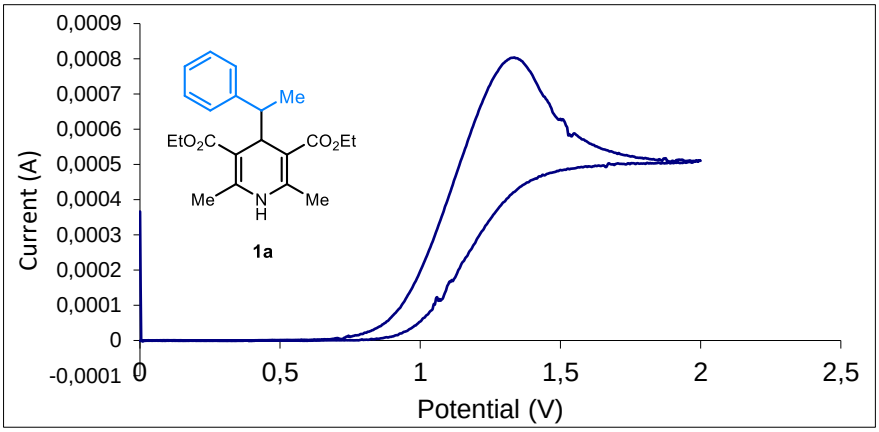

Figure 3.3: Cyclic voltammogram of 0.02M [**1a**] in 0.1 M $TBAPF_6$ in CH_3CN. Sweep rate: 200 mV/s. Working electrode: glassy-carbon electrode, reference electrode: Ag/AgCl (NaCl saturated), auxiliary electrode: Pt wire. Irreversible oxidation. $E_p^A = E_{ox}$ (**1a**$^{\cdot+}$/**1a**) = +1.3 V; E_p^A is the anodic peak potential, while E_{ox} value describes the electrochemical properties of **1a**.

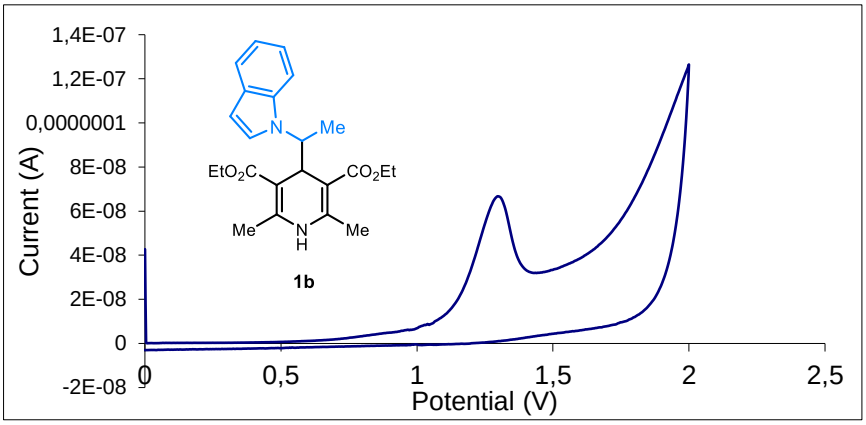

Figure 3.4: Cyclic voltammogram of 0.02 M [**1b**] in 0.1 M $TBAPF_6$ in CH_3CN. Sweep rate: 200 mV/s. glassy-carbon electrode working electrode, Ag/AgCl (NaCl saturated) reference electrode, Pt wire auxiliary electrode. Irreversible oxidation. $E_p^A = E_{ox}$ (**1b**$^{\cdot+}$/**1b**) = +1.3 V; E_p^A is the anodic peak potential, while E_{ox} value describes the electrochemical properties of **1b**

On the basis of the spectroscopic and electrochemical measurements, and applying the Rehm-Weller approximation,[25] the reduction potential for the excited **1a** was estimated to be ~ − 1.6 V vs Ag/AgCl. This estimation confirmed that the SET reduction of a Ni(II) precatalyst (E^{red} (Ni^{II}/Ni^{0}) = - 1.2 V vs. SCE in DMF) by DHP **1a** under visible-light irradiation was feasible. This was a crucial step in our design plan. Comparable estimation was made also for substrate **1b**: (**1b**$^{\bullet+}$/**1b***) = − 1.6 V vs Ag/AgCl.

3.6 Optimization of the Reaction Conditions

After establishing the ability of dihydropyridine **1a** to act as suitable photo-reductant upon light excitation, we examined if it could participate in asymmetric nickel catalyzed acyl cross-coupling. We started our investigation using acyl chloride **27** as readily available acyl precursors (Scheme 3.15).

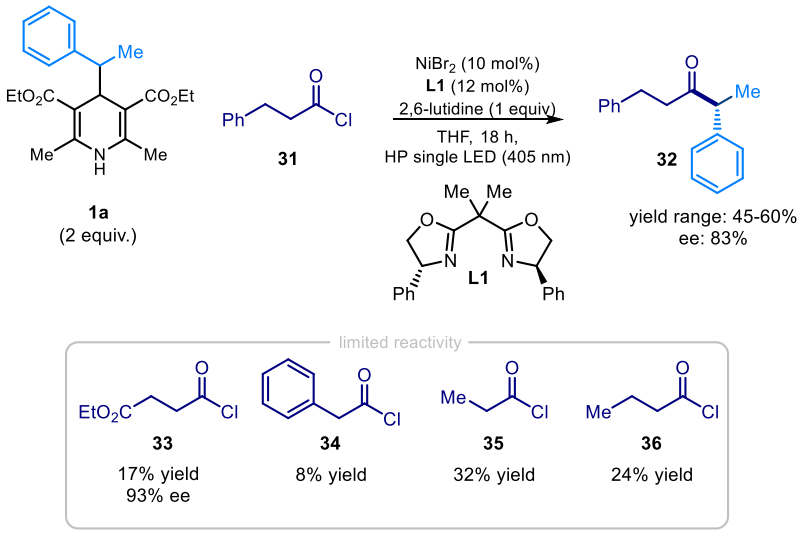

Scheme 3.15: Initial results obtained with acyl chlorides.

This choice was informed by the success of our previous protocol using direct excitation of 4-alkyl-DHPs, in combination with acyl chlorides, to trigger a nickel-catalyzed acyl cross-coupling.[5] We adorned the nickel complex with the chiral Box ligand **L1** (Scheme

[25] For DHP **1a**, we estimated from the UV-Vis analysis a $E_{00}(\mathbf{1a})$ = +2.9 eV, whereas from the CV analysis we measured a $E_{1/2}(\mathbf{1a})$ = +1.3 V vs Ag/Ag^{+}. Applying this results to the Rehm-Weller equation: $E^{*}_{1/2}(1a^{*}) = E_{1/2}(\mathbf{1a}) - E_{00}(\mathbf{1a})$, we obtained the following equation: $E^{*}_{1/2}(\mathbf{1a}^{*}) = 1.3 - 2.9 = -1.6\,V$ which corresponds to the estimated excited-state reduction potential of DHP **1a**. An akin procedure was applied to DHP **1b**, founding a similar value for a $E^{*}_{1/2}(\mathbf{1b}^{*}) = -1.6\,V$. For further details see: Rehm, D., Weller, A. "Kinetics of Fluorescence Quenching by Electron and H-Atom Transfer" *Isr. J. Chem.* **1970**, *8*, 259.

3.15) in order to induce stereocontrol. The choice of this ligand was suggested by the privileged role that Box chiral scaffolds have held in nickel asymmetric cross-couplings.[26] Submitting DHP **1a** and acyl chloride **31** to the reaction conditions, the desired product **32** was formed in modest yield and but with high ee. Despite the initial encouraging results, we realized that the use of acyl chlorides as substrates did not secure reproducible results. Moreover, the reactivity was limited only to few substrates (Scheme 3.15).

We then identified symmetrical anhydrides as more suitable acyl precursors. The use of these electrophilic substrates was already reported in nickel-photoredox methodologies.[27,15a] Initial experiments were conducted using the commercially available butyric anhydride **2a** in THF, using $NiBr_2$ as the nickel source and the chiral Box ligand **L1** under irradiation of a single high-power LED (λ_{max} = 405 nm) at room temperature (Table 3.1).[28]

Table 3.1: Screening of the temperature

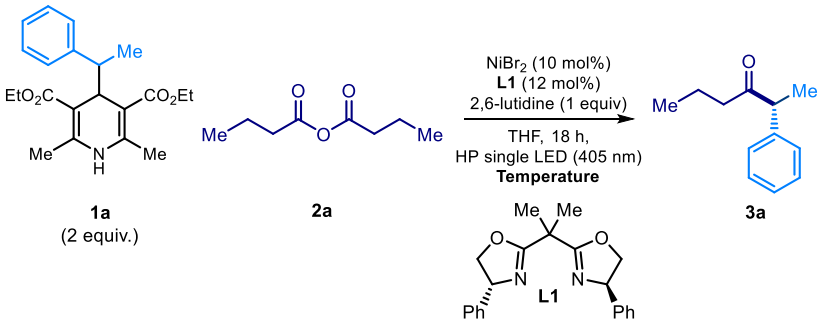

entry	temperature	yield (%)[a]	ee(%)
1	24°C	73	87
2	+10 °C	66	95
3	-10 ° C	65	95

Reaction performed on a 0.1 mmol scale in THF (0.167 M) using 1 equiv. of 2,6-lutidine under illumination by a single high-power (HP) LED (λ_{max} = 405 nm) for 18 hours. [a] Yields of isolated **3a**.

[26] For a general review on Box ligands in asymmetric catalysis see: Desimoni, G., Faita, G., Jørgensen, K. A. "C2-Symmetric Chiral Bis(Oxazoline) Ligands in Asymmetric Catalysis" *Chem. Rev.* **2006**, *106*, 3561. For a selected example of Box ligands in nickel asymmetric cross-coupling see: reference 11.
[27] Joe, C.L., Doyle, A. G. "Direct Acylation of C(sp^3)-H Bonds Enabled by Nickel and Photoredox Catalysis" *Angew. Chem. Int. Ed.* **2016**, *55*, 4040.
[28] For more details on the reaction set-up see page 62.

After 18 hours, the reaction delivered product **3a** with in an encouraging 73% yield (isolated product) and 87% of enantiomeric excess (Table 3.1, entry 1). In order to increase the enantioselectivity, we tested the effects of lower temperature. Performing the reaction at +10° C increased the enantiomeric excess to 95%, albeit with a slight reduction in yield (Table 3.1, entry 2). A lower temperature (-10 °C) did not provide any improvement (Table 3.1, entry 3). In light of the excellent enantiomeric excess and the good yield obtained, we decide to continue the optimization employing +10° C as the reaction temperature.

Other parameters, including the nickel source, solvents, and the chiral ligands, were screened (Table 3.2). Different nickel sources promoted the cross-coupling reaction, although with lower yield and ee (entries 2 and 3). We then studied the influence of different solvents: polar solvents, such as dimethyl acetamide (DMA) and dimethyl formamide (DMF), delivered product **3a** with lower yield albeit with similar stereocontrol (entries 4 and 5). Dimethoxyethane (DME) afforded the product only in trace amounts but with excellent stereocontrol (entry 6). Acetonitrile (ACN) provided only 18% of product **3a** (entry 7); in this case the enantiomeric excess was not determined. Lastly, we examined different chiral ligands belonging to the Box (bisoxazoline) family. In all cases, the nature of the substituents strongly affected the yields and enantiopurity of the product (entries 7-10). These studies confirmed the originally tested chiral ligand **L1** as the best performing.

Table 3.2: Screening of nickel sources, solvents, and chiral ligands

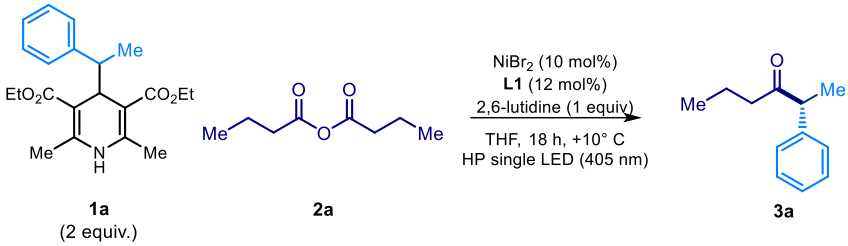

Chiral ligands tested

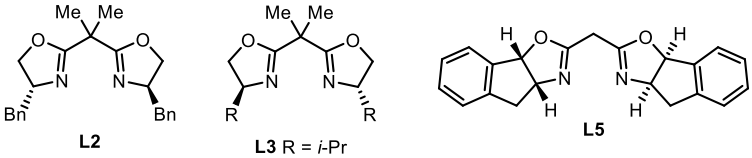

entry	deviation	Yield[a] (%)	ee(%)
1	none	66	95
2	$NiBr_2$dme instead of $NiBr_2$	62	95
3	$NiCl_2$dme instead of $NiBr_2$	62	91
4	DMA instead of THF	44	87
5	DMF instead of THF	61	93
6	DME instead of THF	7[b]	95[c]
7	ACN instead of THF	18[b]	n.d.
8	**L2** instead of **L1**	10[b]	66[c]
9	**L3** instead of **L1**	26	-28
10	**L4** instead of **L1**	20	-65
11	**L5** instead of **L1**	38	0

Reaction performed on a 0.1 mmol scale in THF (0.167 M) using 1 equiv. of 2,6-lutidine as base under illumination by a single high-power (HP) LED (λ_{max} = 405 nm) for 18 hours. [a] Yields of isolated **3a**. [b]Yield of **3a** determined by ^{1}H NMR analysis of the crude mixture using mesitylene as the internal standard. [c]The enantiomeric excess was measured after purification of the crude mixture using preparative thin layer chromatography (TLC) technique.

We then studied the reactivity of the indole-containing racemic DHP **1b** (Table 3.3). This radical precursor was selected because it would form product **3b** bearing a stereogenic center α to the indole nitrogen. This structural motif is synthetically interesting because

it is found in many natural products and pharmaceutical drugs.[29] However, it is a difficult synthetic target as testified to by the paucity of asymmetric catalytic procedures available for the preparation of enantioenriched *N*-alkylated indoles [30] Under the optimized conditions identified in Table 3.2, entry 1, product **3b** was formed only in a modest 22% yield (Table 3.3, entry 1). Increasing the reaction time to 48 hours had a beneficial effect on the reaction, providing **3b** in 53% yield and 80% ee (entry 2). After a fast screening of other nickel sources, we found that $NiCl_2$ afforded the best performance in terms of yield (product **3b** formed in 56% yield) but with somehow reduced stereocontrol (75 % ee, entry 3). To obtain a good compromise between reactivity and enantioselectivity, we tested $NiCl_2$ in other reaction conditions. No improvement was observed when using other solvents (entries 5 and 6) or chiral ligands (entries 7 and 8). Importantly, exclusion of catalyst and light completely suppressed the formation of the product (8 and 9). With the optimized conditions in hand (Table 3.2, entry 1 and Table 3.3, entry 3), we tested the generality of this chemistry.

[29] a) T.V. Sravanthi, S.L. Manju, "Indoles - A Promising Scaffold for Drug Development" *Eur.J. Pharm. Sci.* **2016**, *91*, 1; b) Fernandez, L. S., Buchanan, M. S., Carroll, A.R., Feng, Y. J., Quinn, R. J., "Flinderoles A−C: Antimalarial Bis-indole Alkaloids from Flindersia Species" Quinn, *Org. Lett.* **2009**, *11*, 329.

[30] a) Ye, Y., Kim, S.-T., Jeong, J., Baik, M.-H., Buchwald, S. L., "CuH-Catalyzed Enantioselective Alkylation of Indole Derivatives with Ligand-Controlled Regiodivergence" *J. Am. Chem. Soc.* **2019**, *14*, 3901; b) Kim, S.W., Schempp, T. T., Zbieg, J. R., Stivala, C.E., Krische, M. J., "Regio- and Enantioselective Iridium-Catalyzed N-Allylation of Indoles and Related Azoles with Racemic Branched Alkyl-Substituted Allylic Acetates" *Angew. Chem. Int. Ed.* **2019**, *58*, 7762; c) Allen, J. R., Bahamonde, A., Furukawa, Y., Sigman, M. S., "Enantioselective N-Alkylation of Indoles via an Intermolecular Aza-Wacker-Type Reaction" *J. Am. Chem. Soc.* **2019**, *141*, 8670; d) Kainz, Q. M., Matier, C. D., Bartoszewicz, A., Zultanski, S. L., Peters, J. C., Fu, G. C., "Asymmetric copper-catalyzed C-N cross-couplings induced by visible light" *Science* **2016**, *351*, 681.

Table 3.3: Optimization studies using DHP **1b**

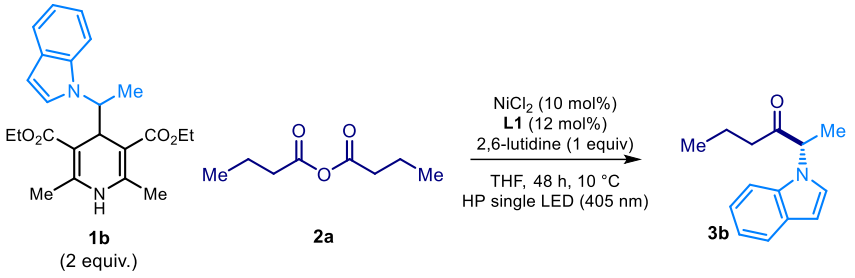

Chiral ligands tested

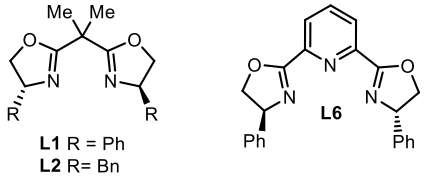

entry	deviation	yield (%)[a]	ee(%)
1	As in table 3.2 entry 1	22	80
2	$NiBr_2$ for 48 hours	53	80
3	none	65 (56)[b]	75
4	$NiCl_2$ dme instead of $NiCl_2$	48	80
5	acetonitrile instead of THF	43	28
6	1,4-dioxane instead of THF	38	77
7	L2 instead of L3	31	12
8	L6 instead of L3	34	0
9	No catalyst or light	0	-

Reactions performed on a 0.1 mmol scale in THF (0.167 M) using 1 equiv. of 2,6-lutidine as base under illumination by a single HP LED (λ_{max} = 405 nm) for 48 hours. [a] Yield of **3b** determined by ^{1}H NMR analysis of the crude mixture using mesitylene as the internal standard. [b] Yields of isolated **3b**.

3.7 Scope of the Radical Precursors

Firstly, we evaluated the generality of the methodology by testing an array of DHPs bearing benzyl substituents, in combination with butyric anhydride **2a**, under the reaction conditions depicted in Figure 3.5. Alkyl chains of different length were installed in the final ketone product (**37-39**).

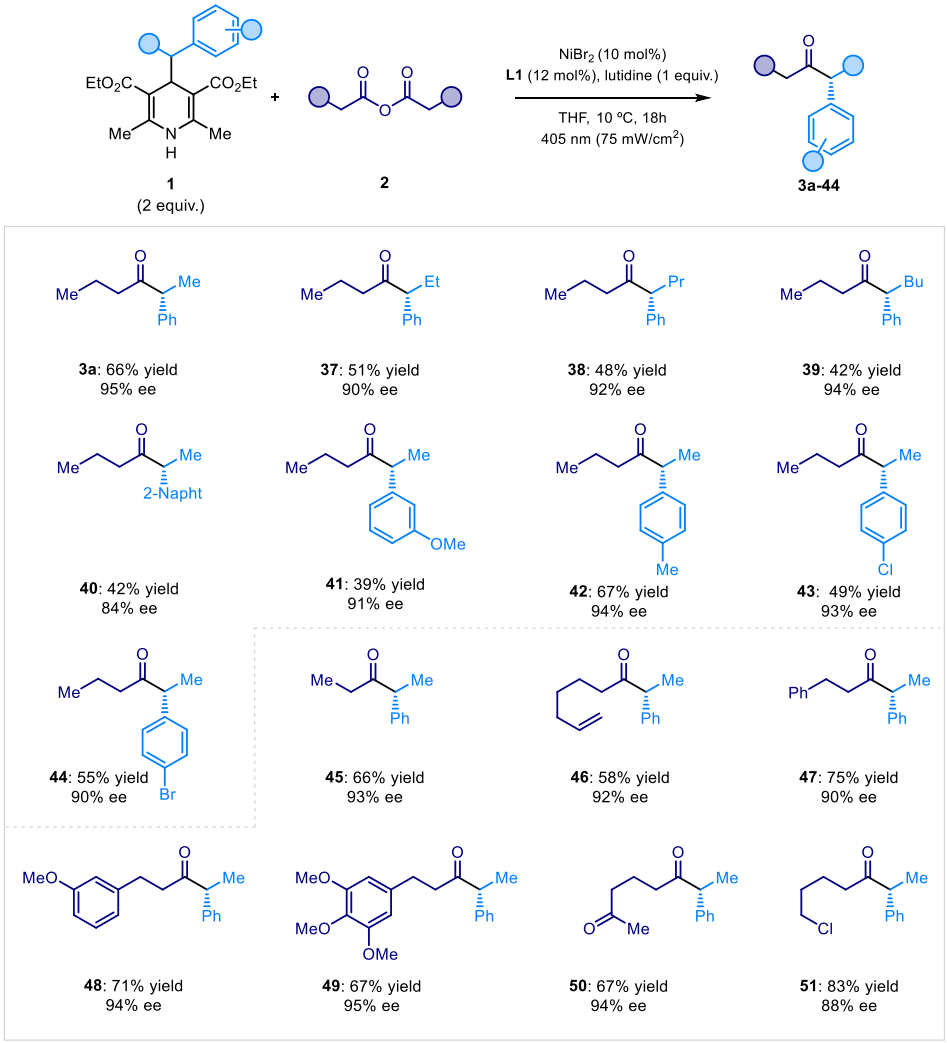

Figure 3.5: Survey of benzyl DHPs and anhydride precursors that can participate in the photochemical reaction. Reactions performed on a 0.1 mmol scale, at +10 °C for 18 hours, in THF (0.125 M) using 2 equiv. of **1** and an irradiance of 75 mW/cm², as controlled by an external power supply (full details of the illumination set-up are reported in the experimental section 3.12.2). Yields and enantiomeric excesses of the isolated products are indicated below each entry.

A variety of α-methyl-α-aryl ketones were prepared in high enantiomeric excess and good yields. The process tolerated aromatic rings bearing electron-donating substituents (**42**) and electron-withdrawing halides (**43**, **44**) in para position, while a meta-substituted ring decreases the yield (**41**). A naphthyl ring was also tolerated, albeit a modest decrease in enantiomeric excess was observed (**40**). Validation of the methodology was continued testing DHP **1a** in combination with different anhydrides. A shorter alkyl chain did not affect the reactivity (product **45**). Olefin (**46**) and electron-rich aromatic rings (**47** to **49**) were included in the final products in good yields and excellent stereocontrol. Functional groups known to take part in transition metal cross-coupling reactions, such as preinstalled ketones (**50**) and primary alkyl chloride (**51**), were tolerated.

We then investigated the reactivity of the heteroaromatic derived radical precursors of type **1b** in combination with butyric anhydride **2**a (Figure 3.6). The corresponding cross-coupled product (**3b** to **62**) bears a structural motif – an indole α to a stereocenter - frequently found in natural and pharmaceutical products.[31] More in general, asymmetric protocols to build *N*-alkylated indoles are scarce.[32] The methodology tolerated different halogen substituents on the indole moiety, delivering the corresponding products in good yields and enantiomeric excess (**52-54**). Another biological relevant scaffold, such as carbazole, could be readily installed, albeit with a significant drop in stereocontrol (product **56**). Similar drop in enantiomeric excess, but with a higher yield, was observed when installing the tetrahydrocarbazole fragment (**55**). We then tested modifications on the acyl fragment. Primary alkyl chlorides (product **57**) and different aryl functionality were tolerated (**59**, **61** and **62**). Aromatic and alkyl ketones (**58** and **60**), which are sensitive functional groups under traditional cross-coupling conditions, were tolerated by this protocol.

32

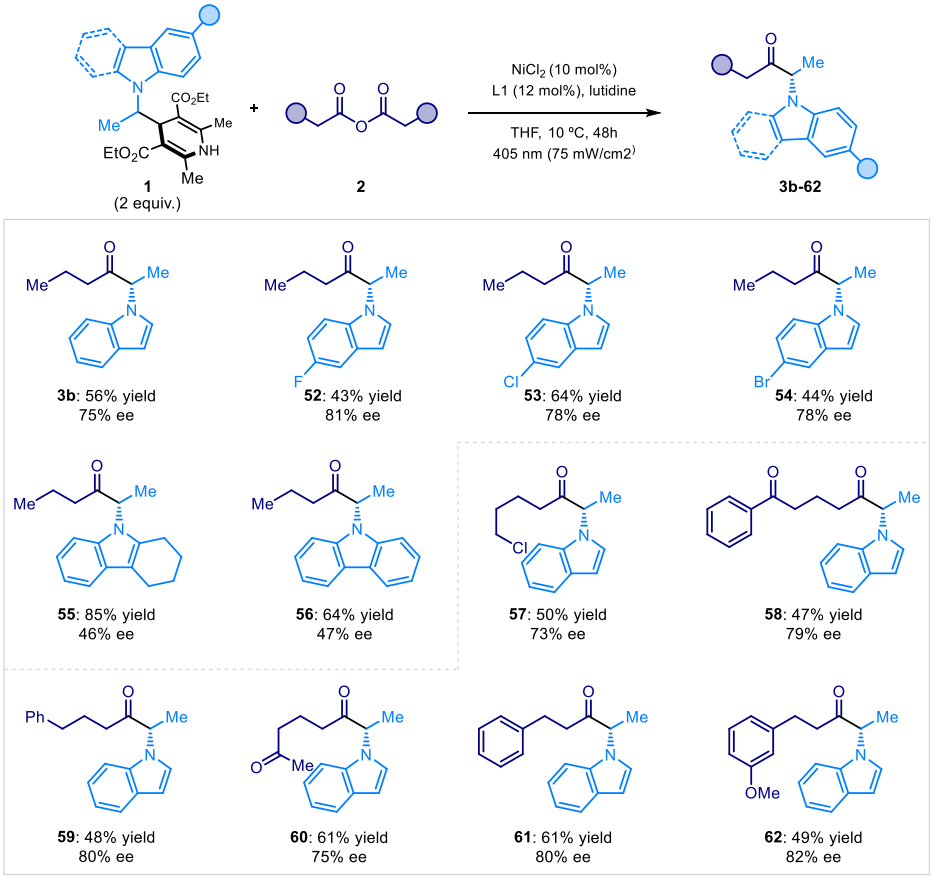

Figure 3.6: Survey of α-amino DHPs and anhydride precursors that can participate in the photochemical process. Reactions performed on a 0.1 mmol scale, at +10 °C for 48 hours in THF (0.6 mL), using 2 equiv. of 1 and an irradiance of 75 mW/cm². Yields and enantiomeric excess of the isolated products are indicated below each entry.

3.8 Limitations of the Methodology

The methodology presented some limitations (Figure 3.7). With regard to the *radical precursors*: i) we could not install simple alkyl fragments (**63**, **64**) or aryl moiety bearing *ortho*-substituents (**65**); ii) the synthesis of indole-derived DHPs bearing alkyl groups other than methyl was unsuccessful (**66**); iii) electron-poor α-amino radicals did not react in the cross-coupling protocol (**68**). With regard to the *acyl precursors*: i) functionalization of benzoic anhydrides (**69**) or alkyl anhydrides bearing α-substituents (**70**) was not possible; ii) the use of other acyl sources, such as acyl chlorides (**71**), mixed

(**72**) or cyclic anhydrides (**73**), and activated amides (**74**), did not deliver any product or provided irreproducible results.

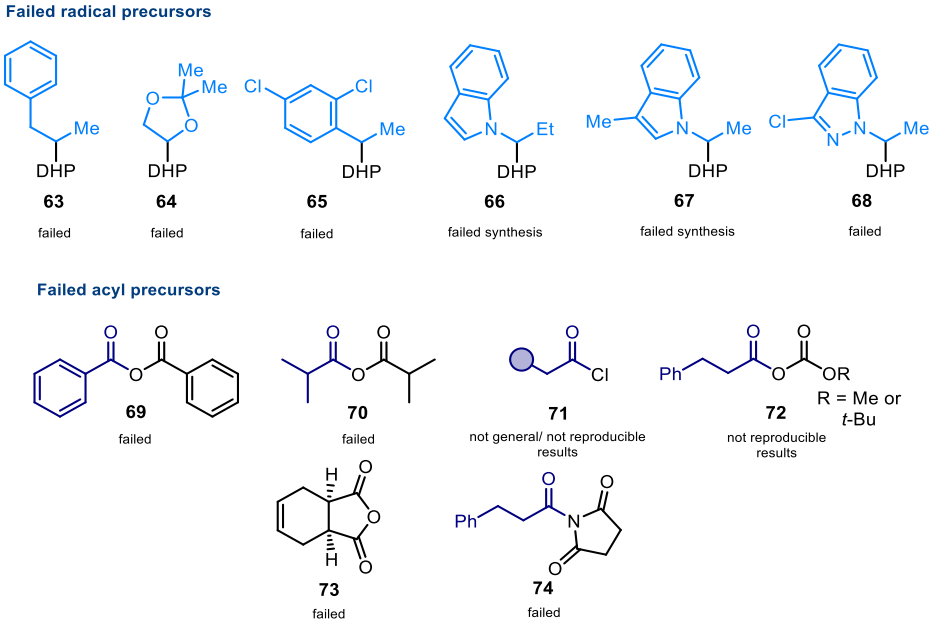

Figure 3.7: Radical precursors and acyl precursors that failed to react under the optimized conditions or the synthesis of which was unsuccessful.

3.9 Proposed Mechanism

The proposed mechanism for this asymmetric nickel catalyzed acyl cross-coupling is depicted in Figure 3.18. The process starts with the photoexcitation of racemic DHP **1**, which, in its excited state, becomes a strong reductant ((**1a**$^{\bullet+}$/**1a***) = - 1.6 V vs Ag/AgCl). DHP **1*** is able to reduce, by two discrete SET events, the Ni^{II} chiral pre-catalyst affording the active chiral Ni(0) complex **IV**(E^{red} (Ni^{II}/Ni^{0}) = −1.2/ −1.3 V vs. SCE in DMF) adorned with ligand **L1**. After the SET process, the unstable radical cation **II**, upon fragmentation, delivers the stabilized benzyl radical **III** and the pyridine **30** byproduct. The chiral Ni (0) complex **IV** begins its catalytic cycle undergoing oxidative addition with the acyl electrophile **2**, delivering the Ni(II)-acyl intermediate **V**. The latter intermediate intercepts radical **II**, affording the Ni(III) complex **VI** which undergoes

reductive elimination[33] releasing the enantioenriched product **3** and the Ni(I)-Box chiral complex **VII**. This is turned over to the active catalyst by another photoexcited DHP **1*** restarting the cycle.

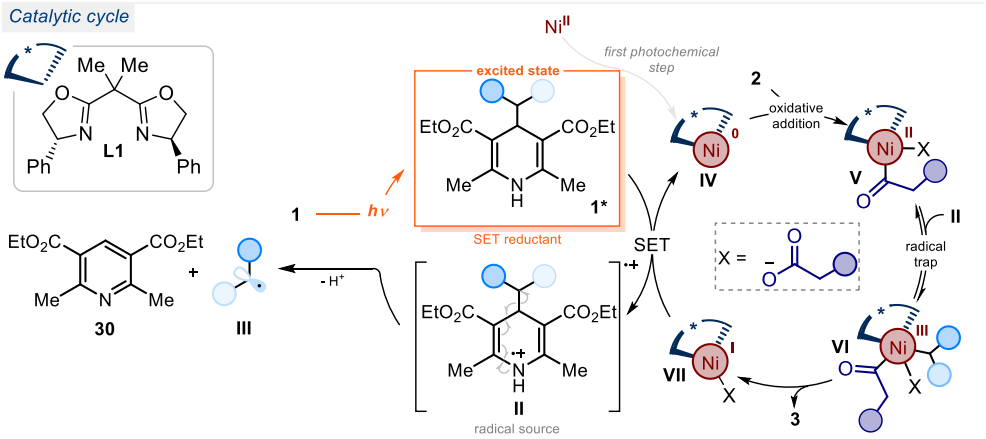

Scheme 3.18: Proposed mechanism for the photo-driven, nickel-catalyzed asymmetric acyl-coupling.

3.10 Conclusions

In this chapter, I detailed the development of a photo-driven nickel catalyzed asymmetric acyl cross-coupling process. This methodology allowed the synthesis of α,α-disubstituted ketones **3** with high levels of stereocontrol under mild photochemical conditions, without using an external photocatalyst. The chemistry exploits the excited-state properties of 4-alkyl-1,4-dihydropyridines, which can act as both strong SET reductants and radical precursors. We have used this approach to stereoselectively couple radicals with symmetric anhydrides. The resulting chiral ketones, which contain different groups at the α-stereogenic center, including an (1*H*-indol-1-yl) moiety, are synthesized with good stereocontrol. This approach represents one of the few examples of asymmetric nickel catalysis developed in the photochemical framework. It is also the first one to proceed via direct excitation of substrates, without the need of a photocatalyst. We believe that this strategy can provide a reliable platform for other applications in enantioselective catalytic cross-coupling processes.

[33] A mechanistic study on the nickel-catalyzed cross-coupling of photoredox-generated radicals suggested the reductive elimination as being the stereo-determining step of the process, see: O. Gutierrez, J. C. Tellis, D. N. Primer, G.A. Molander, M. C. Kozlowski, *J. Am. Chem. Soc.* **2015**, *137*, 4896. Given the similarities with our radical-based system, this mechanistic scenario might also apply here.

3.11 Experimental Section

General Information. The ^{1}H NMR, ^{13}C NMR spectra and UPC^2 traces are available in the literature[1] and are not reported in the present thesis.

The NMR spectra were recorded at 400 MHz and 500 MHz for ^{1}H or at 100 MHz and 125 MHz for ^{13}C, respectively. High temperature NMR analyses were recorded at 328 K in $CDCl_3$ in a 500 MHz with cryoprobe spectrometer. The chemical shifts (δ) for ^{1}H and ^{13}C are given in ppm relative to residual signals of the solvents ($CHCl_3$ @ 7.26 ppm ^{1}H NMR, 77.36 ppm ^{13}C NMR). Coupling constants are given in Hz. The following abbreviations are used to indicate the multiplicity: s, singlet; d, doublet; t, triplet; q, quartet; m, multiplet; br s, broad signal.

High-resolution mass spectra (HRMS) were obtained from the ICIQ High Resolution Mass Spectrometry Unit on MicroTOF Focus and Maxis Impact (Bruker Daltonics) with electrospray ionization. Optical rotations were measured on a Polarimeter Jasco P-1030 and are reported as follows: $[\alpha]_D^T$ (*c* in g per 100 mL, solvent).

UV-vis measurements were carried out on a Shimadzu UV-2401PC spectrophotometer equipped with photomultiplier detector, double beam optics and D2 and W light sources.

Cyclic voltammetry studies were carried out on a Princeton Applied Research PARSTAT 2273 potentiostat offering compliance voltage up to ± 100 V (available at the counter electrode), ± 10 V scan range and ± 2 A current range.

General Procedures. All reactions were set up under an argon atmosphere in oven-dried glassware using standard Schlenk techniques, unless otherwise stated. Synthesis grade solvents were used as purchased. Anhydrous solvents were taken from a commercial SPS solvent dispenser. Chromatographic purification of products was accomplished using force-flow chromatography (FC) on silica gel (35-70 mesh). For thin layer chromatography (TLC) analysis throughout this work, Merck precoated TLC plates (silica gel 60 GF254, 0.25 mm) were used, using UV light as the visualizing agent and and either phosphomolybdic acid in EtOH, dinitrophenylhydrazine in EtOH/H_2O or basic aqueous potassium permangante ($KMnO_4$), and heat as developing agents. Organic solutions were concentrated under reduced pressure on a Büchi rotary evaporator (in vacuo at 40 ºC, ~5 mbar).

In order to get consistent results, the nickel dibromide ($NiBr_2$) pre-catalyst was weighted and pre-dosed under inert atmosphere (glovebox technique).

Determination of Enantiomeric Purity: UPC^2 analysis on chiral stationary phase was performed on a Waters Acquity instrument using IC, CEL1, IE and AMY1 chiral columns. The exact conditions for the analyses are specified within the characterization section. UPC^2 traces were compared to racemic samples prepared by running the reaction

in the presence of a catalytic amount (12 mol%) of 2,2-bipyridyl as the ligand, which is commercially available form Sigma Aldrich.

Materials: Commercial grade reagents and solvents were purchased at the highest commercial quality from Sigma Aldrich, Fluka, Acros Organics, Fluorochem or Alfa Aesar and used as received, unless otherwise stated. All the ligand tested were purchased from Sigma Aldrich or Fluorochem. The chiral Box ligand (**L1**) was purchased from Fluorochem. The nickel sources employed in the scope ($NiCl_2$ and $NiBr_2$) were purchased from Sigma Aldrich.

3.11.1. Substrate Synthesis

Synthesis of the 4-alkyl-1,4-Dihydropyridines 1

4-alkyl-1,4-dihydropyridines **1** were synthesized according to procedures reported in the literature. [34] The following 4-alkyl-1,4-dihydropyridines were prepared from the corresponding aldehydes using the General procedure 1 in the Scheme 3.19:

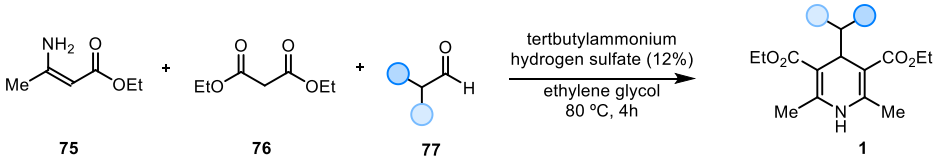

Scheme 3.19 Preparation of 4-alkyl 1,4-dihydropyridines **1.**

General procedure 1: Ethyl-3-aminocrotonate **75** (1 equiv.) and ethylene glycol (2.5 M) were added to a flask under nitrogen. Next, ethyl acetoacetate **76** (1 equiv.) was added followed by the sequential addition of aldehyde **77** (1 equiv.) and tetrabutylammonium hydrogen sulfate (12 mol%). The resulting solution was heated up to 80 °C and stirred for 4 hours, then cooled to ambient temperature and diluted with ethyl acetate. Brine was added and the mixture was extracted using ethyl acetate (3 x 50 mL). The organic layers were combined, dried ($MgSO_4$), and concentrated. The crude material was purified by flash column chromatography to furnish the desired 4-alkyl-1,4-dihydropyridine **1**.

[34] Gutiérrez-Bonet, Á., Tellis, J. C., Matsui, J. K., Vara, B. A., Molander, G. A. "1,4-Dihydropyridines as Alkyl Radical Precursors: Introducing the Aldehyde Feedstock to Nickel/Photoredox Dual Catalysis" *ACS Catal.* **2016**, *6*, 8004.

Synthesis of the Symmetrical Anhydrides 2

The following anhydrides were synthesized according to the procedures reported in the literature[35] from the corresponding carboxylic acids using the procedure detailed in Scheme 3.20:

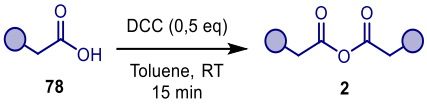

Scheme 3.20 Preparation of symmetrical anhydrides

General Procedure 2: Dicyclohexylcarbodiimide DCC (0,50-0,55 equiv.) was added to a solution of the appropriate carboxylic acid **78** (1 equiv.) in toluene (0.3 M). The solution was stirred at room temperature for 15 min. The suspension was filtered and concentrated under vacuum to give the crude product, which was used without further purification.

3.11.2. General Procedures for the Photochemical Synthesis of α-Amino and α-Aryl Ketones

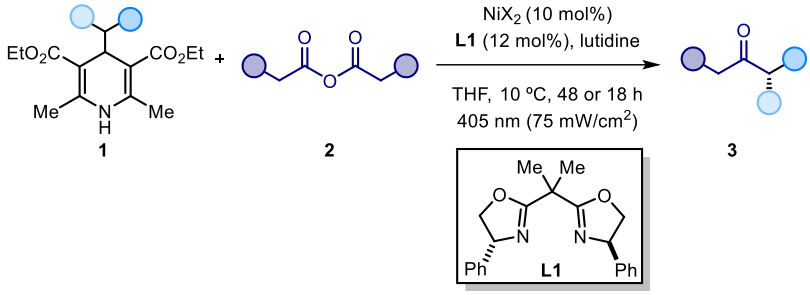

Scheme 3.21 Photochemical Synthesis of α-Amino and α-Aryl Ketones.

General Procedure 3: To a vial containing 10 mol% of the nickel salt pre-catalyst ($NiCl_2$ or $NiBr_2$) was added a solution of the chiral ligand **L1** (0,12 mol%) in THF (0.6 mL). The solution was added into a Schlenck tube containing the appropriate 4-alkyl dihydropyridine **1** (2 equiv.), anhydride **2** (1 equiv.), and lutidine (1 equiv.). The mixture was placed under an atmosphere of argon, cooled to –78 °C, and degassed via vacuum evacuation (5 min), backfilled with argon, and warmed to room temperature. The freeze-

[35] Stark, D. G., Morrill, L. C., Cordes, D. B., Slawin, A. M. Z., O'Riordan, T. J. C., Smith, A. D. "Enantioselective Synthesis of 3,5,6-Substituted Dihydropyranones and Dihydropyridinones using Isothiourea-Mediated Catalysis" *Chem. : Asian J.* **2016**, *11*, 395.

pump-thaw cycle was repeated three times, and then the Schlenk tube was sealed with Parafilm and placed into a 3D-printed plastic support mounted on an aluminium block fitted with a 405 nm high-power single LED (λ = 405 nm, the full setup is detailed in Figure 3.8. The irradiance was fixed at 75±3 mW/cm^2 (1200 μA), as controlled by an external power supply and measured using a photodiode light detector at the start of each reaction. The temperature was kept constant at +10 °C with a chiller connected to the irradiation plate (temperature was measured within a reaction vial provided with a thermometer). The reaction was stirred for 18-48 hours, then the crude was filtered on a plug of silica using ethyl acetate as eluent, and the solvent evaporated. The crude mixture was purified on silica gel to furnish the chiral product.

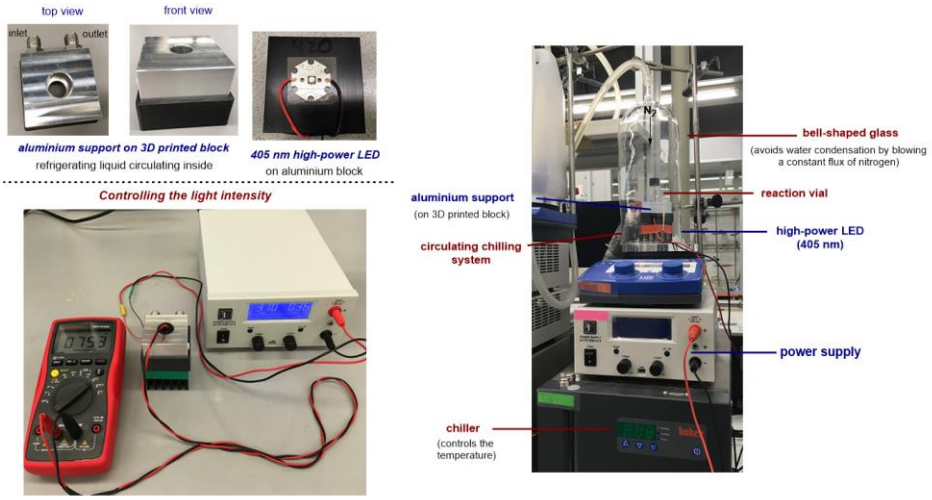

Figure 3.8. Detailed set-up and illumination system. The light source for illuminating the reaction vessel consisted in a 405 nm high-power single LED (OCU-440 UE420-X-T) purchased from OSA OPTO.

3.11.3. Characterization of the Products

(*R*)-2-phenylhexan-3-one (3a)

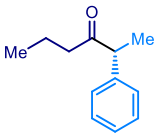

3a

Prepared according to the General Procedure 3 using butyric anhydride (16 μL, 0,1 mmol), 2,6-lutidine (12 μL, 0,1 mmol), $NiBr_2$ (2,2 mg, 10 mol%), ligand **L1** (4,0 mg, 12 mol%), the corresponding dihydropyridine (71 mg, 0,2 mmol) and THF (0.6 mL). Reaction time: 18 h. The crude material was purified by flash column chromatography

(hexane/dichlorometane 9:1) to give product **3a** (23 mg, 66% yield) as a pale-yellow oil that displayed spectroscopic data consistent with those reported previously.[36] The enantiomeric excess was determined by HPLC analysis on Daicel Chiralpack IC3 column, 98:2 hexane/isopropanol flow rate 1 mL/min, 20 ºC, 280 nm. τ_{minor} = 6.7 min, τ_{major} = 7.5 min (95% ee); $[\alpha]_D^{26}$ = -172.7 (c = 0.65, CH_2Cl_2, 95% ee).

^{1}H NMR (400 MHz, Chloroform-*d*) δ 7.36 – 7.29 (m, 2H), 7.28 – 7.24 (m, 1H), 7.24 – 7.17 (m, 2H), 3.74 (q, *J* = 7.0 Hz, 1H), 2.36 – 2.28 (t, *J* = 7.3 Hz 2H), 1.56 – 1.42 (m, 2H), 1.39 (d, *J* = 7.2 Hz, 3H), 0.79 (t, *J* = 7.4 Hz, 3H).

^{13}C NMR (101 MHz, Chloroform-*d*) δ 211.3, 141.1, 129.2, 128.2, 127.4, 53.3, 43.3, 17.8, 17.6, 13.9.

(*R*)-3-phenylheptan-4-one (37)

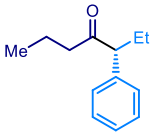

37

Prepared according to the General Procedure 3 using butyric anhydride (16 µL, 0,1 mmol), 2,6-lutidine (12 µL, 0,1 mmol), $NiBr_2$ (2,2 mg, 10 mol%), ligand **L1** (4,0 mg, 12 mol%), the corresponding dihydropyridine (71 mg, 0,2 mmol) and tetrahydrofuran (0.6 mL). Reaction time: 18h. The crude material was purified by flash column chromatography (hexane/dichlorometane 9:1) to give product **37** (19 mg, 51% yield) as a pale-yellow oil that displayed spectroscopic data consistent with those reported previously.[37] The enantiomeric excess was determined by HPLC analysis on Daicel Chiralpack IC3 column, 98:2 hexane/isopropanol flow rate 1 mL/min, 20 ºC, 215 nm. τ_{minor} = 6.0 min, τ_{major} = 6.4 min (90% ee); $[\alpha]_D^{26}$ = -31.6 (c = 0.2, CH_2Cl_2, 90% ee),

^{1}H NMR (400 MHz, Chloroform-*d*) δ 7.35 – 7.28 (m, 2H), 7.27 – 7.23 (m, 1H), 7.21 (m, 2H), 3.52 (t, *J* = 7.4 Hz, 1H), 2.37 – 2.29 (m, 2H), 2.13 – 1.98 (m, 1H), 1.70 (m, 1H), 1.57 – 1.41 (m, 2H), 0.80 (m, 6H).

^{13}C NMR (101 MHz, Chloroform-*d*) δ 211.0, 139.5, 129.1, 128.7, 127.4, 61.2, 44.2, 25.6, 17.5, 13.9, 12.5.

[36] Lou, S., Fu, G. C. "Nickel/Bis(oxazoline)-Catalyzed Asymmetric Kumada Reactions of Alkyl Electrophiles: Cross-Couplings of Racemic α-Bromoketones" *J. Am. Chem. Soc.* **2010**, *132*, 1264.

[37] Alsabeh, P. G., Stradiotto, M. "Addressing Challenges in Palladium-Catalyzed Cross-Couplings of Aryl Mesylates: Monoarylation of Ketones and Primary Alkyl Amines" *Angew. Chem. Int. Ed.* **2013**, *52*, 7242.

(*R*)-5-phenyloctan-4-one (38)

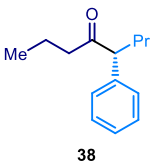

38

Prepared according to the General Procedure 3 using butyric anhydride (16 µL, 0,1 mmol), 2,6-lutidine (12 µL, 0,1 mmol), $NiBr_2$ (2,2 mg, 10 mol%), ligand **L1** (4,0 mg, 12 mol%), the corresponding dihydropyridine (77 mg, 0,2 mmol) and tetrahydrofuran (0.6 mL). Reaction time: 18h. The crude material was purified by flash column chromatography (hexane/dichlorometane 9:1) to give product **38** (20 mg, 48% yield) as a pale-yellow oil. The enantiomeric excess was determined by HPLC analysis on a Daicel Chiralpack IC3 column, 98:2 hexane/isopropanol flow rate 1 mL/min, 20 ºC, 230 nm. τ_{minor} = 5.6 min, τ_{major} = 6.3 min (92% ee); $[\alpha]_D^{26}$ = -100.7 (c = 0.25, CH_2Cl_2, 92 %ee).

^{1}H NMR (400 MHz, Chloroform-*d*) δ. 7.34 – 7.28 (m, 2H), 7.26 (m, 1H), 7.25 – 7.18 (m, 2H), 3.62 (t, *J* = 7.4 Hz, 1H), 2.37 – 2.28 (t, *J* = 7.6 Hz , 2H), 2.00 (m, 1H), 1.67 (, 1H), 1.54 – 1.39 (m, 2H), 1.25 – 1.10 (m, 2H), 0.88 (t, *J* = 7.3 Hz, 3H), 0.79 (t, *J* = 7.4 Hz, 3H).

^{13}C NMR (101 MHz, Chloroform-*d*) δ 211.0, 139.6, 129.1, 128.6, 127.4, 59.1, 44.2, 34.6, 21.0, 17.5, 14.3, 13.9.

HRMS (ESI) Exact mass calculated for $[M+H]^+$: 205.1514, found: 205.1582

(*R*)-5-phenylnonan-4-one (39)

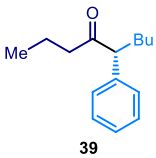

39

Prepared according to the General Procedure 3 using butyric anhydride (16 µL, 0,1 mmol), 2,6-lutidine (12 µL, 0,1 mmol), $NiBr_2$ (2,2 mg, 10 mol%), ligand **L1** (4,0 mg, 12 mol%), the corresponding dihydropyridine (80 mg, 0,2 mmol) and tetrahydrofuran (0.6 mL). Reaction time: 18h. The crude material was purified by flash column chromatography (hexane/dichlorometane 9:1) to give product **39** (18 mg, 42% yield) as a pale-yellow oil. The enantiomeric excess was determined by HPLC analysis on a Daicel Chiralpack IC3 column, 98:2 hexane/isopropanol flow rate 1 mL/min, 20ºC, 215 nm. τ_{minor} = 5.3 min, τ_{major} = 6.0 min (94% ee); $[\alpha]_D^{26}$ = -104.5 (c = 0.3, CH_2Cl_2, 94% ee).

^{1}H NMR (400 MHz, Chloroform-*d*) δ 7.34 – 7.28 (m, 2H), 7.27 – 7.23 (m, 1H), 7.23 – 7.17 (m, 2H), 3.60 (t, *J* = 7.4 Hz, 1H), 2.33 (td, *J* = 7.1, 0.9 Hz, 2H), 2.03 (m, 1H), 1.68 (m, 1H), 1.56 – 1.42 (m, 2H), 1.37 – 1.23 (m, 2H), 1.22 – 1.06 (m, 2H), 0.85 (t, *J* = 7.2 Hz, 3H), 0.79 (t, *J* = 7.4 Hz, 3H).

^{13}C NMR (101 MHz, Chloroform-*d*) δ 211.0, 139.7, 129.1, 128.6, 127.4, 59.4, 44.2, 32.2, 30.1, 23.0, 17.5, 14.3, 13.9.

HRMS (ESI) Exact mass calculated for $[M+Na]^+$: 241.1670, found: 241.1557

(*R*)-5-(naphthalen-2-yl)octan-4-one (40)

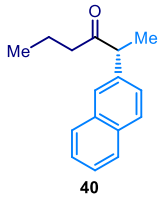

40

Prepared according to the General Procedure 3 using butyric anhydride (16 µL, 0,1 mmol), 2,6-lutidine (12 µL, 0,1 mmol), $NiBr_2$ (2,2 mg, 10 mol%), ligand **L1** (4,0 mg, 12 mol%), the corresponding dihydropyridine (82 mg, 0,2 mmol) and tetrahydrofuran (0.6 mL). Reaction time: 18h. The crude material was purified by flash column chromatography (hexane/dichlorometane 9:1) to give product **40** (19 mg, 42% yield) as a pale-yellow oil. The enantiomeric excess was determined by HPLC analysis on Daicel Chiralpack IC3 column, 98:2 hexane/isopropanol flow rate 1 mL/min, 20ºC, 230 nm. τ_{minor} = 9.4 min, τ_{major} = 10.3 min (84% ee); $[\alpha]_D^{26}$ = -154.9 (c = 0.5, CH_2Cl_2, 84% ee).

^{1}H NMR (400 MHz, Chloroform-*d*) δ. 7.86 – 7.78 (m, 3H), 7.71 – 7.66 (m, 1H), 7.52 – 7.43 (m, 2H), 7.33 (dd, *J* = 8.5, 1.8 Hz, 1H), 3.92 (q, *J* = 7.0 Hz, 1H), 2.36 (t, *J* = 7.3 Hz, 2H), 1.61 – 1.50 (m, 2H), 1.48 (d, *J* = 6.9 Hz, 4H), 0.79 (t, *J* = 7.4 Hz, 3H).

^{13}C NMR (101 MHz, Chloroform-*d*) δ 211.2, 138.6, 134.0, 132.9, 129.0, 128.0, 127.00, 126.6, 126.3, 126.2, 53.4, 43.4, 17.8, 17.6, 13.9.

(*R*)-2-(3-methoxyphenyl)hexan-3-one (41)

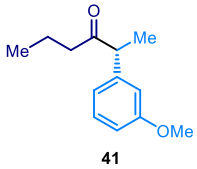

41

Prepared according to the General Procedure 3 using butyric anhydride (16 µL, 0,1 mmol), 2,6-lutidine (12 µL, 0,1 mmol), $NiBr_2$ (2,2 mg, 10 mol%), ligand **L1** (4,0 mg, 12 mol%), the corresponding dihydropyridine (77 mg, 0,2 mmol) and tetrahydrofuran (0.6 mL). Reaction time: 18h. The crude material was purified by flash column chromatography (hexane/dichlorometane 9:1) to give product **41** (16 mg, 39% yield) as a pale-yellow oil. The enantiomeric excess was determined by HPLC analysis on a Daicel Chiralpack IC3 chiral column, 98:2 hexane/isopropanol flow rate 1 mL/min, 20ºC, 230 nm. τ_{minor} = 12.4 min, τ_{major} = 13.9 min (91% ee); $[\alpha]_D^{26}$ = -115.60 (c = 0.5, CH_2Cl_2, 91% ee).

^{1}H NMR (400 MHz, Chloroform-*d*) δ 7.28 – 7.22 (m, 1H), 6.82 – 6.77 (m, 2H), 6.74 (m, 1H), 3.80 (s, 3H), 3.71 (q, *J* = 7.0 Hz, 1H), 2.40 – 2.26 (m, 2H), 1.55 – 1.44 (m, 2H), 1.37 (d, *J* = 6.9 Hz, 3H), 0.80 (t, *J* = 7.4 Hz, 3H).

^{13}C NMR (101 MHz, Chloroform-*d*) δ 211.1, 160.3, 142.7, 130.2, 120.6, 113.9, 112.7, 55.6, 53.3, 43.2, 17.7, 17.6, 13.9.

HRMS (ESI) Exact mass calculated for $[M+Na]^+$: 229.1306, found: 229.1202

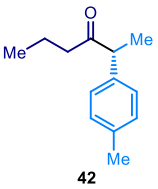

42

(*R*)-2-(p-tolyl)hexan-3-one (42)

Prepared according to the General Procedure 3 using butyric anhydride (16 µL, 0,1 mmol), 2,6-lutidine (12 µL, 0,1 mmol), $NiBr_2$ (2,2 mg, 10 mol%), ligand **L1** (4,0 mg, 12 mol%), the corresponding dihydropyridine (74 mg, 0,2 mmol) and tetrahydrofuran (0.6 mL). Reaction time: 18h. The crude material was purified by flash column chromatography (hexane/dichlorometane 9:1) to give product **42** (25 mg, 67% yield) as a paleyellow oil. The enantiomeric excess was determined by HPLC analysis on a Daicel Chiralpack IC3 column, 98:2 hexane/isopropanol flow rate 1 mL/min, 20ºC, 230 nm. τ_{minor} = 7.3 min, τ_{major} = 7.8 min (94% ee); $[\alpha]_D^{26}$ = -102.4 (c = 0.3, CH_2Cl_2, 94% ee).

^{1}H NMR (400 MHz, Chloroform-*d*) δ 7.17 – 7.11 (m, 2H), 7.09 (m, 2H), 3.70 (q, *J* = 7.0 Hz, 1H), 2.38 – 2.28 (m, 5H), 1.50 (m, 2H), 1.36 (d, *J* = 7.0 Hz, 3H), 0.80 (t, *J* = 7.4 Hz, 3H).

^{13}C NMR (101 MHz, Chloroform-*d*) δ 211.5, 138.1, 137.0, 129.9, 128.1, 52.9, 43.2, 21.4, 17.8, 17.6, 14.0.

HRMS (ESI) Exact mass calculated for $[M+Na]^+$: 213.1357, found: 213.1256.

(*R*)-2-(4-chlorophenyl)hexan-3-one (43)

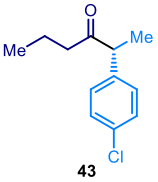

43

Prepared according to the General Procedure 3 using butyric anhydride (16 µL, 0,1 mmol), 2,6-lutidine (12 µL, 0,1 mmol), $NiBr_2$ (2,2 mg, 10 mol%), ligand **L1** (4,0 mg, 12 mol%), the corresponding dihydropyridine (78 mg, 0,2 mmol) and THF (0.6 mL). Reaction time: 18h. The crude material was purified by flash column chromatography (hexane/dichlorometane 9:1) to give product **43** (21 mg, 49% yield) as a pale-yellow oil. The enantiomeric excess was determined by HPLC analysis on a Daicel Chiralpack IC3 column ID3 chiral column, 100% hexane flow rate 1 mL/min, 20ºC, 230 nm. τ_{minor} = 22.2 min, τ_{major} = 23.7 min (93% ee); $[\alpha]_D^{26}$ = -112.3 (c = 0.5, CH_2Cl_2, 93% ee).

^{1}H NMR (400 MHz, Chloroform-*d*) δ 7.32 – 7.27 (m, 2H), 7.17 – 7.11 (m, 2H), 3.72 (q, *J* = 7.0 Hz, 1H), 2.32 (t, *J* = 7.3 Hz, 2H), 1.57 – 1.44 (m, 2H), 1.36 (d, *J* = 7.0 Hz, 3H), 0.80 (t, *J* = 7.4 Hz, 3H).

^{13}C NMR (101 MHz, Chloroform-*d*) δ 210.7, 139.5, 133.3, 129.5, 129.4, 52.6, 43.4, 17.8, 17.6, 13.9.

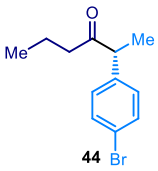

44

(*R*)-2-(4-bromophenyl)hexan-3-one (44)

Prepared according to the General Procedure 3 using butyric anhydride (16 µL, 0,1 mmol), 2,6-lutidine (12 µL, 0,1 mmol), $NiBr_2$ (2,2 mg, 10 mol%), ligand **L1** (4,0 mg, 12 mol%), the corresponding dihydropyridine (78 mg, 0,2 mmol) and tetrahydrofuran (0.6 mL). Reaction time: 18h. The crude material was purified by flash column chromatography (hexane/dichlorometane 9:1) to give product **44** (14 mg, 55% yield) as a pale-yellow oil. The enantiomeric excess was determined by HPLC analysis on a Daicel Chiralpack ID3 column, 100% hexane flow rate 1 mL/min, 20ºC, 230 nm. τ_{minor} = 20.9 min, τ_{major} = 21.9 min (90 % ee); $[\alpha]_D^{26}$ = -98.3 (c = 0.6, CH_2Cl_2, 90% ee),

^{1}H NMR (400 MHz, Chloroform-*d*) δ 7.48 – 7.42 (m, 2H), 7.12 – 7.06 (m, 2H), 3.71 (q, *J* = 7.0 Hz, 1H), 2.32 (t, *J* = 7.3 Hz, 2H), 1.54 – 1.44 (m, 2H), 1.36 (d, *J* = 7.0 Hz, 3H), 0.80 (t, *J* = 7.4 Hz, 3H).

^{13}C NMR (101 MHz, Chloroform-*d*) δ 210.6, 140.0, 132.3, 129.9, 121.4, 52.6, 43.4, 17.8, 17.6, 13.9.

(*R*)-2-phenylpentan-3-one (45)

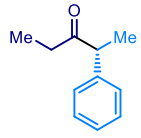

45

Prepared according to the General Procedure 3 using the corresponding anhydride (13 µL, 0,1 mmol), 2,6-lutidine (12 µL, 0,1 mmol), $NiBr_2$ (2,2 mg, 10 mol%), ligand **L1** (4,0 mg, 12 mol%), the corresponding dihydropyridine (72 mg, 0,2 mmol) and tetrahydrofuran (0.6 mL). Reaction time: 18h. The crude material was purified by flash column chromatography (hexane/dichlorometane 9:1) to give product **45** (11 mg, 66 % yield) as a pale-yellow oil. The enantiomeric excess was determined by HPLC analysis on a Daicel Chiralpack IC3 column, 98:02 hexane/isopropanol flow rate 1.0 mL/min, 20ºC. τ_{minor} = 7.7 min, τ_{major} = 8.6 min (93 % ee); $[\alpha]_D^{26}$ = -85 (c = 0.5, CH_2Cl_2, 93% ee).

^{1}H NMR (400 MHz, Chloroform-*d*) δ 7.36 – 7.29 (m, 2H), 7.28 – 7.18 (m, 3H), 3.76 (q, *J* = 7.0 Hz, 1H), 2.38 (dq, *J* = 8.6, 7.3 Hz, 2H), 1.39 (d, *J* = 6.9 Hz, 3H), 0.96 (t, *J* = 7.3 Hz, 3H).

^{13}C NMR (101 MHz, Chloroform-*d*) δ 211.9, 141.3, 129.2, 128.2, 127.4, 53.0, 34.6, 17.9, 8.3.

(*R*)-2-phenylnon-8-en-3-one (46)

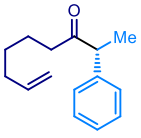

46

Prepared according to the General Procedure 3 using the corresponding anhydride (24 mg, 0,1 mmol), 2,6-lutidine (12 µL, 0,1 mmol), $NiBr_2$ (2,2 mg, 10 mol%), ligand **L1** (4,0 mg, 12 mol%), the corresponding dihydropyridine (72 mg, 0,2 mmol) and tetrahydrofuran (0.6 mL).

Reaction time: 18 h. The crude material was purified by flash column chromatography (hexane/dichlorometane 9:1) to give product **46** (13 mg, 58% yield) as a pale-yellow oil. The enantiomeric excess was determined by UPC^2 analysis using a AMY1 chiral column: after 1 min of 100% CO_2, gradient up to 60:40 CO_2/acetonitrile over 5 minutes, flow rate 2 mL/min. τ_{minor} = 2.0 min, τ_{major} = 2.10 min (92% ee); $[\alpha]_D^{26}$ = -128.4 (c = 0.75, CH_2Cl_2, 92% ee).

^{1}H NMR (400 MHz, Chloroform-*d*) δ 7.38 – 7.32 (m, 2H), 7.31 – 7.27 (m, 1H), 7.26 – 7.20 (m, 2H), 5.75 (ddt, *J* = 16.9, 10.2, 6.7 Hz, 1H), 5.05 – 4.80 (m, 2H), 3.77 (q, *J* = 7.0 Hz, 1H), 2.46 – 2.29 (m, 2H), 2.05 – 1.91 (m, 2H), 1.59 – 1.46 (m, 2H), 1.41 (d, *J* = 6.9 Hz, 3H), 1.34 – 1.20 (m, 2H)..

^{13}C NMR (101 MHz, Chloroform-*d*) δ 211.1, 141.1, 138.8, 129.2, 128.2, 127.4, 114.8, 53.3, 41.1, 33.8, 28.6, 23.6, 17.8.

HRMS (ESI) Exact mass calculated for $[M+Na]^+$: 239.1514, found: 239.1409

(*R*)-1,4-diphenylpentan-3-one (47)

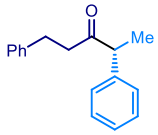

47

Prepared according to the General Procedure 3 using the corresponding anhydride (24 mg, 0,1 mmol), 2,6-lutidine (12 µL, 0,1 mmol), $NiBr_2$ (2,2 mg, 10 mol%), ligand **L1** (4,0 mg, 12 mol%), the corresponding dihydropyridine (72 mg, 0,2 mmol) and tetrahydrofuran (0.6 mL). Reaction time: 18 h. The crude material was purified by flash column chromatography (hexane/dichlorometane 9:1) to give product **47** (18 mg, 75% yield) as a pale-yellow oil. The enantiomeric excess was determined by UPC^2 analysis using a IE3 chiral column: after 1 min of 100% CO_2, gradient up to 60:40 CO_2/acetonitrile over 5 minutes, flow rate 2 mL/min. τ_{minor} = 3.5 min, τ_{major} = 3.7 min (90% ee); $[\alpha]_D^{26}$ = -407.4 (c = 0.2, CH_2Cl_2, 90% ee).

^{1}H NMR (400 MHz, Chloroform-*d*) δ 7.30 (m, 2H), 7.27 – 7.18 (m, 3H), 7.18 – 7.12 (m, 3H), 7.09 – 7.03 (m, 2H), 3.70 (q, *J* = 6.9 Hz, 1H), 2.92 – 2.70 (m, 2H), 2.70 – 2.57 (m, 2H), 1.37 (d, *J* = 6.9 Hz, 3H).

^{13}C NMR (101 MHz, Chloroform-*d*) δ 210.2, 141.4, 140.8, 129.3, 128.7, 128.6, 128.2, 127.5, 126.3, 53.5, 42.9, 30.3, 17.6.

(*R*)-1-(3-methoxyphenyl)-4-phenylpentan-3-one (48)

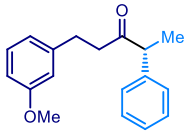

48

Prepared according to the General procedure 3 using the corresponding anhydride (34 mg, 0,1 mmol), 2,6-lutidine (12 µL, 0,1 mmol), $NiBr_2$ (2,2 mg, 10 mol%), ligand **L1** (4,0 mg, 12 mol%), the corresponding dihydropyridine (72 mg, 0,2 mmol) and tetrahydrofuran (0.6 mL). Reaction time: 18h. The crude material was purified by flash

column chromatography (hexane/dichlorometane 9:1) to give product **48** (19 mg, 71% yield) as a pale-yellow oil. The enantiomeric excess was determined by UPC^2 analysis using a IE3 chiral column: after 1 min of 100% CO_2, gradient up to 60:40 CO_2/acetonitrile over 5 minutes, flow rate 2 mL/min. τ_{minor} = 4.1 min, τ_{major} = 4.2 min (94% ee); $[\alpha]_D^{26}$ = -105.9 (c = 0.85, CH_2Cl_2, 94% ee).

^{1}H NMR (400 MHz, Chloroform-*d*) δ 7.36 – 7.30 (m, 2H), 7.30 – 7.24 (m, 1H), 7.21 – 7.13 (m, 2H), 6.73 (dd, *J* = 8.3, 2.6, 1H), 6.68 (d, *J* = 7.5, 1H), 6.64 (m, 1H), 3.78 (s, 3H), 3.74 (q, *J* = 7.0 Hz, 1H), 2.92 – 2.72 (m, 2H), 2.72 – 2.59 (m, 2H), 1.41 (d, *J* = 7.0 Hz, 3H).

^{13}C NMR (101 MHz, Chloroform-*d*) δ 210.2, 159.9, 143.0, 140.8, 129.7, 129.3, 128.2, 127.5, 121.0, 114.3, 111.7, 55.4, 53.5, 42.8, 30.3, 17.7.

HRMS (ESI) Exact mass calculated for [M+Na]+: 291.1463, found: 291.1351.

(*R*)-4-phenyl-1-(3,4,5-trimethoxyphenyl)pentan-3-one (49)

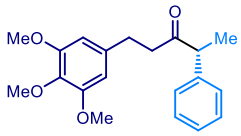

49

Prepared according to the General Procedure 3 using the corresponding anhydride (51 mg, 0,1 mmol), 2,6-lutidine (12 µL, 0,1 mmol), $NiBr_2$ (2,2 mg, 10 mol%), ligand **L1** (4,0 mg, 12 mol%), the corresponding dihydropyridine (72 mg, 0,2 mmol) and tetrahydrofuran (0.6 mL). Reaction time: 18h. The crude material was purified by flash column chromatography (hexane/ethyl acetate 9:1) to give the product **49** (22 mg, 67% yield) as a pale-yellow oil. The enantiomeric excess was determined by UPC^2 analysis using a IE3 chiral column: isocratic 89:11 CO_2/isopropanol over 9 minutes, flow rate 2 mL/min. τ_{minor} = 7.9 min, τ_{major} = 8.6 min (95% ee); $[\alpha]_D^{26}$ = -85.2 (c = 1.10, CH_2Cl_2, 95% ee).

^{1}H NMR (400 MHz, Chloroform-*d*) δ 7.34 – 7.20 (m, 3H), 7.17 – 7.10 (m, 2H), 6.26 (s, 2H), 3.80 (s, 3H), 3.78 (s, 6H), 3.71 (q, *J* = 6.9 Hz, 1H), 2.86 – 2.57 (m, 4H), 1.38 (d, *J* = 7.0 Hz, 3H)..

^{13}C NMR (101 MHz, Chloroform-*d*) δ 210.1, 153.4, 140.7, 137.1, 136.5, 129.2, 128.2, 127.5, 105.6, 61.1, 56.3, 53.8, 43.0, 30.7, 17.7.

(*R*)-7-phenyloctane-2,6-dione (50)

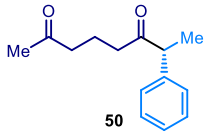

50

Prepared according to the General Procedure 3 using the corresponding anhydride (24 mg, 0,1 mmol), 2,6-lutidine (12 µL, 0,1 mmol), $NiBr_2$ (2,2 mg, 10 mol%), ligand **L1** (4,0 mg, 12 mol%), the corresponding dihydropyridine (72 mg, 0,2 mmol) and tetrahydrofuran (0.6 mL). Reaction time: 18h. The crude material was purified by flash column chromatography (hexane/dichlorometane 9:1) to give product **50** (15 mg, 67%

yield) as a pale-yellow oil. The enantiomeric excess was determined by UPC^2 analysis using a IE3 chiral column: isocratic 90:10 CO_2/acetonitrile over 9 minutes, flow rate 2 mL/min. τ_{minor} = 1.9 min, τ_{major} = 2.1 min (94% ee); $[\alpha]_D^{26}$ = -192.4 (c = 0.55, CH_2Cl_2, 94% ee).

^{1}H NMR (400 MHz, Chloroform-*d*) δ 7.35 – 7.30 (m, 2H), 7.28 – 7.23 (m, 1H), 7.22 – 7.17 (m, 2H), 3.74 (q, *J* = 7.0 Hz, 1H), 2.39 (t, *J* = 7.0 Hz, 2H), 2.36 – 2.22 (m, 2H), 2.03 (s, 3H), 1.76 (m, 2H), 1.38 (d, *J* = 7.0 Hz, 3H).

^{13}C NMR (101 MHz, Chloroform-*d*) δ 210.6, 208.7, 140.8, 129.3, 128.2, 127.5, 53.3, 42.7, 40.0, 30.1, 18.1, 17.6.

(*R*)-7-chloro-2-phenylheptan-3-one (51)

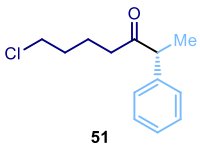

51

Prepared according to the General Procedure 3 using the corresponding anhydride (25 mg, 0,1 mmol), 2,6-lutidine (12 µL, 0,1 mmol), $NiBr_2$ (2,2 mg, 10 mol%), ligand **L1** (4,0 mg, 12 mol%), the corresponding dihydropyridine (72 mg, 0,2 mmol) and tetrahydrofuran (0.6 mL). Reaction time: 18h. The crude material was purified by flash column chromatography (hexane/dichlorometane 9:1) to give the product **51** (19 mg, 83% yield) as a pale-yellow oil. The enantiomeric excess was determined by UPC^2 analysis using a IE3 chiral column: after 1 min of 100% CO_2, gradient up to 60:40 CO_2/acetonitrile over 5 minutes, flow rate 2 mL/m. τ_{minor} = 2.0 min, τ_{major} = 2.2 min (88% ee); $[\alpha]_D^{26}$ = -88.8 (c = 1.2, CH_2Cl_2, 88% ee).

^{1}H NMR (400 MHz, Chloroform-*d*) δ 7.37 – 7.29 (m, 2H), 7.29 – 7.23 (m, 1H), 7.23 – 7.16 (m, 2H), 3.75 (q, *J* = 6.9 Hz, 1H), 3.41 (m, 2H), 2.49 – 2.27 (m, 2H), 1.73 – 1.54 (m, 4H), 1.39 (d, *J* = 7.0 Hz, 3H).

^{13}C NMR (101 MHz, Chloroform-*d*) δ 210.5, 140.9, 129.3, 128.2, 127.5, 53.4, 45.0, 40.2, 32.1, 21.4, 17.7.

(*S*)-2-(1H-indol-1-yl)hexan-3-one (3b)

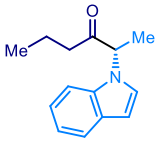

3b

Prepared according to the General Procedure 3 using butyric anhydride (16 µL, 0,1 mmol), 2,6-lutidine (12 µL, 0,1 mmol), $NiCl_2$ (1,3 mg, 10 mol%), ligand **L1** (4,0 mg, 12 mol%), the corresponding dihydropyridine (79 mg, 0,2 mmol), and tetrahydrofuran (0.6 mL). Reaction time: 48h. The crude material was purified by flash column chromatography (hexane/dichlorometane 9:1) to give product **3b** (12 mg, 56% yield) as a yellow oil. The enantiomeric excess was determined by UPC^2 analysis using a CEL1 chiral column: after 1 min of 100% CO_2, gradient up to 60:40 CO_2/acetonitrile over 5

minutes, flow rate 2 mL/min. τ_{minor} = 2.7 min, τ_{major} = 2.8 min (75% ee); $[\alpha]_D^{26}$ = -114.5(c = 0.5, CH_2Cl_2, 75% ee).

^{1}H NMR (400 MHz, Chloroform-*d*) δ 7.64 (dt, *J* = 7.9, 1.0 Hz, 1H), 7.26 – 7.18 (m, 2H), 7.15 – 7.10 (m, 2H), 6.59 (dd, *J* = 3.3, 0.8 Hz, 1H), 4.97 (q, *J* = 7.2 Hz, 1H), 2.22 – 2.04 (m, 2H), 1.69 (d, *J* = 7.2 Hz, 3H), 1.47 (h, *J* = 7.3 Hz, 2H), 0.74 (t, *J* = 7.4 Hz, 3H).

^{13}C NMR (101 MHz, Chloroform-*d*) δ 209.0, 136.3, 129.2, 125.5, 122.5, 121.6, 120.4, 109.5, 103.2, 60.3, 40.3, 17.1, 16.3, 13.9.

(*S*)-2-(5-fluoro-1H-indol-1-yl)hexan-3-one (52)

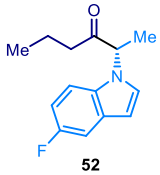

52

Prepared according to the General Procedure 3 using butyric anhydride (16 µL, 0,1 mmol), 2,6-lutidine (12 µL, 0,1 mmol), $NiCl_2$ (1,3 mg, 10 mol%), ligand **L1** (4,0 mg, 12 mol%), the corresponding dihydropyridine (83 mg, 0,2 mmol) and tetrahydrofuran (0.6 mL). Reaction time: 48h. The crude material was purified by flash column chromatography (hexane/dichlorometane 9:1) to give product **52** (10 mg, 43% yield) as a yellow oil. The enantiomeric excess was determined by UPC^2 analysis using a CEL1 chiral column: after 1 min of 100% CO_2, gradient up to 60:40 CO_2/acetonitrile over 5 minutes, flow rate 2 mL/min. τ_{minor} = 2.4 min, τ_{major} = 2.5 min (81% ee); $[\alpha]_D^{26}$ = -96.7 (c = 0.44, CH_2Cl_2, 81% ee).

^{1}H NMR (400 MHz, Chloroform-*d*) δ 7.29 (dd, *J* = 9.4, 2.5 Hz, 1H), 7.20 (d, *J* = 3.2 Hz, 1H), 7.15 (dd, *J* = 8.9, 4.2 Hz, 1H), 7.00 – 6.92 (td, 9.1, 2.5 Hz, 1H), 6.56 (dd, *J* = 3.2, 0.8 Hz, 1H), 4.94 (q, *J* = 7.2 Hz, 1H), 2.24 – 2.03 (m, 2H), 1.70 (d, *J* = 7.2 Hz, 3H), 1.49 (sextet, *J* = 7.3 Hz, 2H), 0.76 (t, *J* = 7.4 Hz, 3H).

^{13}C NMR (101 MHz, Chloroform-*d*) δ 208.7, 158.4 (d, $^1J_{CF}$ = 235.0 Hz), 133.0, 129.5 (d, $^3J_{CF}$ = 10.1 Hz), 127.1, 110.9 (d, $^2J_{CF}$ = 26.4 Hz), 110.1 (d, $^3J_{CF}$ = 9.7 Hz), 106.4 (d, $^2J_{CF}$ = 23.4 Hz), 103.2 (d, long range *J* = 4.7 Hz), 60.7, 40.2, 17.1, 16.3, 13.9.

^{19}F NMR (376 MHz, Chloroform-*d*) δ -124.6.

(*S*)-2-(5-chloro-1H-indol-1-yl)hexan-3-one (53)

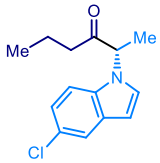

53

Prepared according to the General Procedure 3 using butyric anhydride (16 µL, 0,1 mmol), 2,6-lutidine (12 µL, 0,1 mmol), $NiCl_2$ (1,3 mg, 10 mol%), ligand **L1** (4,0 mg, 12 mol%), the corresponding dihydropyridine (86 mg, 0,2 mmol) and tetrahydrofuran (0.6 mL). Reaction time: 48h. The crude material was purified by flash column chromatography (hexane/dichlorometane 9:1) to give product **53** (16 mg, 64% yield) as a yellow oil. The enantiomeric excess was determined by UPC^2 analysis using a CEL1 chiral column: after 1 min of 100% CO_2, gradient up to 60:40 CO_2/acetonitrile over 5

minutes, flow rate 2 mL/min. τ_{minor} = 2.70 min, τ_{major} = 2.9 min (78% ee); $[\alpha]_D^{26}$ = -74.7 (c = 0.91, CH_2Cl_2, 78% ee).

^{1}H NMR (300 MHz, Chloroform-*d*) δ 7.61 (m, 1H), 7.20 – 7.14 (m, 3H), 6.54 (d, *J* = 3.3 Hz, 1H), 4.94 (q, *J* = 7.2 Hz, 1H), 2.25 – 2.01 (m, 2H), 1.70 (d, *J* = 7.2 Hz, 3H), 1.48 (sextet, *J* =7.4 Hz, 2H), 0.76 (t, *J* = 7.4 Hz, 3H).
^{13}C NMR (101 MHz, Chloroform-*d*) δ 208.4, 134.7, 130.2, 126.9, 126.1, 122.8, 121.0, 110.5, 102.9, 60.5, 40.3, 17.1, 16.3, 13.8.
HRMS (ESI) Exact mass calculated for $[M+Na]^+$: 272.0920, found: 272.0813.

(*S*)-2-(3-methyl-1H-indol-1-yl)hexan-3-one (54)

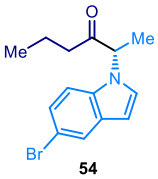

54

Prepared according to the General Procedure 3 using butyric anhydride (16 µL, 0,1 mmol), 2,6-lutidine (12 µL, 0,1 mmol), $NiCl_2$ (1,3 mg, 10 mol%), ligand **L1** (4,0 mg, 12 mol%), the corresponding dihydropyridine (95 mg, 0,2 mmol) and tetrahydrofuran (0.6 mL). Reaction time: 48h. The crude material was purified by flash column chromatography (hexane/dichlorometane 9:1) to give product **54** (13 mg, 44 % yield) as a pale-yellow oil. The enantiomeric excess was determined by UPC^2 analysis using a CEL1 chiral column: after 1 min of 100% CO_2, gradient up to 60:40 CO_2/acetonitrile over 5 minutes, flow rate 2 mL/min. τ_{minor} = 2.9 min, τ_{major} = 3.2 min (78 % ee); $[\alpha]_D^{26}$ = -79.8 (c = 0.6, CH_2Cl_2, 78% ee).
^{1}H NMR (400 MHz, Chloroform-*d*) 7.78 (d, *J* = 1.9 Hz, 1H), 7.33 – 7.24 (m, 1H), 7.19 – 7.08 (m, 2H), 6.54 (dd, *J* = 3.4, 0.8 Hz, 1H), 4.94 (q, *J* = 7.2 Hz, 1H), 2.23 – 2.04 (m, 2H), 1.70 (d, *J* = 7.2 Hz, 3H), 1.49 (h, *J* = 7.3 Hz, 2H), 0.76 (t, *J* = 7.4 Hz, 3H).
^{13}C NMR (101 MHz, Chloroform-*d*) δ 208.4, 135.0, 130.9, 126.7, 125.3, 124.1, 113.7, 110.9, 102.8, 60.5, 40.3, 17.1, 16.3, 13.9.

(*S*)-2-(1,2,3,4-tetrahydro-9H-carbazol-9-yl)hexan-3-one (55)

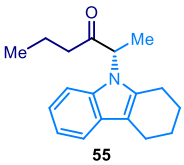

55

Prepared according to the General Procedure 3 using butyric anhydride (16 µL, 0,1 mmol), 2,6-lutidine (12 µL, 0,1 mmol), $NiCl_2$ (1,3 mg, 10 mol%), ligand **L1** (4,0 mg, 12 mol%), the corresponding dihydropyridine (90 mg, 0,2 mmol) and tetrahydrofuran (0.6 mL). Reaction time: 48h. The crude material was purified by flash column chromatography (hexane/dichlorometane 9:1) to give product **55** (23 mg, 85 % yield) as a pale-yellow oil. The enantiomeric excess was determined by HPLC analysis on a Daicel Chiralpack IC3 column, 98:02 hexane/isopropanol flow rate 1.3 mL/min, 20ºC. τ_{minor} = 4.90 min, τ_{major} = 5.3 min (46% ee); $[\alpha]_D^{26}$ = -47.9 (c = 0.7, CH_2Cl_2, 40% ee).

^{1}H NMR (400 MHz, Chloroform-*d*) δ 7.54 – 7.45 (m, 1H), 7.17 – 7.03 (m, 3H), 4.81 (q, *J* = 7.0 Hz, 1H), 2.84 – 2.56 (m, 4H), 2.24 – 2.04 (m, 2H), 2.03 – 1.80 (m, 4H), 1.60 (d, *J* = 7.1 Hz, 3H), 1.55 – 1.42 (m, 2H), 0.81 – 0.74 (t, *J* = 7.4 Hz, 3H)
^{13}C NMR (101 MHz, Chloroform-*d*) δ 209.3, 135.6, 135.1, 128.5, 121.5, 119.6, 118.4, 111.4, 109.7, 58.7, 41.1, 23.7, 23.3, 23.1, 21.4, 17.3, 15.0, 13.94.
HRMS (ESI) Exact mass calculated for $[M+Na]^+$: 292.1779, found: 292.1674.

(*S*)-2-(9H-carbazol-9-yl)hexan-3-one (56)

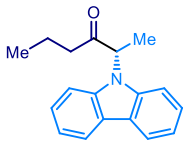

56

Prepared according to the General Procedure 3 using butyric anhydride (16 µL, 0,1 mmol), 2,6-lutidine (12 µL, 0,1 mmol), $NiCl_2$ (1,3 mg, 10 mol%), ligand **L1** (4,0 mg, 12 mol%), the corresponding dihydropyridine (89 mg, 0,2 mmol) and tetrahydrofuran (0.6 mL). Reaction time: 48h. The crude material was purified by flash column chromatography (hexane/dichlorometane 9:1) to give product **56** (17 mg, 64 % yield) as a pale-yellow oil. The enantiomeric excess was determined by UPC^2 analysis using a CEL1 chiral column: after 1 min of 100% CO_2, gradient up to 60:40 CO_2/acetonitrile over 5 minutes, flow rate 2 mL/min. τ_{minor} = 3.9 min, τ_{major} = 4.0 min (47 % ee); $[\alpha]_D^{26}$ = -74.2 (c = 0.7, CH_2Cl_2, 47% ee).
^{1}H NMR (300 MHz, Chloroform-*d*) δ 8.17 – 8.09 (m, 2H), 7.45 (ddd, *J* = 8.3, 7.1, 1.2 Hz, 2H), 7.32 – 7.23 (m, 4H), 5.18 (q, *J* = 7.0 Hz, 1H), 2.32 – 2.02 (m, 2H), 1.68 (d, *J* = 7.0 Hz, 3H), 1.55 – 1.39 (m, 2H), 0.70 (t, *J* = 7.4 Hz, 3H).
^{13}C NMR (101 MHz, Chloroform-*d*) δ 209.3, 139.9, 126.4, 123.9, 120.96, 120.0, 109.3, 58.7, 41.2, 17.4, 13.9, 13.7.
HRMS (ESI) Exact mass calculated for $[M+H]^+$: 266.1466, found: 266.1551.

(*S*)-7-chloro-2-(1H-indol-1-yl)heptan-3-one (57)

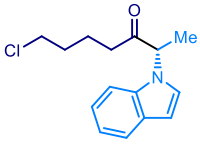

57

Prepared according to the General procedure 3 using the corresponding anhydride (25 mg, 0,1 mmol), 2,6-lutidine (12 µL, 0,1 mmol), $NiCl_2$ (1,3 mg, 10 mol%), ligand **L1** (4,0 mg, 12 mol%), the corresponding dihydropyridine (79 mg, 0,2 mmol) and tetrahydrofuran (0.6 mL). Reaction time: 48h. The crude material was purified by flash column chromatography (hexane/dichlorometane 9:1) to give product **57** (13 mg, 50% yield) as a pale-yellow oil. The enantiomeric excess was determined by UPC^2 analysis using a CEL1 chiral column: after 1 min of 100% CO_2, gradient up to 60:40 CO_2/acetonitrile over 5 minutes, flow rate 2 mL/min. $\tau_{minor}r$ = 3.2 min, τ_{major} = 3.4 min (73% ee); $[\alpha]_D^{26}$ = -59.5 (c = 0.65, CH_2Cl_2, 73% ee).

^{1}H NMR (400 MHz, Chloroform-*d*) δ 7.65 (dt, *J* = 7.8, 1.0 Hz, 1H), 7.24 – 7.18 (m, 2H), 7.18 – 7.10 (m, 2H), 6.60 (d, *J* = 3.2, 1H), 4.98 (q, *J* = 7.2 Hz, 1H), 3.40 – 3.32 (m, 2H), 2.25 – 2.08 (m, 2H), 1.70 (d, *J* = 7.2 Hz, 3H), 1.64-1.50 (m, 4H).
^{13}C NMR (101 MHz, Chloroform-*d*) δ 208.5, 136.3, 129.2, 125.4, 122.6, 121.7, 120.5, 109.4, 103.5, 60.3, 44.8, 37.3, 31.9, 21.0, 16.2.

(*S*)-6-(1H-indol-1-yl)-1-phenylheptane-1,5-dione (58)

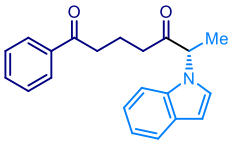

58

Prepared according to the General Procedure 3 using the corresponding anhydride (25 mg, 0,1 mmol), 2,6-lutidine (12 µL, 0,1 mmol), $NiCl_2$ (1,3 mg, 10 mol%), ligand **L1** (4,0 mg, 12 mol%), the corresponding dihydropyridine (79 mg, 0,2 mmol) and tetrahydrofuran (0.6 mL). Reaction time: 48h. The crude material was purified by flash column chromatography (hexane/dichlorometane 9:1) to give product **58** (15 mg, 47% yield) as a pale-yellow oil. The enantiomeric excess was determined by UPC^2 analysis using a CEL1 chiral column: after 1 min of 100% CO_2, gradient up to 60:40 CO_2/acetonitrile over 5 minutes, flow rate 2 mL/min. τ_{minor} = 4.4 min, τ_{major} = 4.8 min (79% ee); $[\alpha]_D^{26}$ = -58.4 (c = 0.75, CH_2Cl_2, 79% ee).
^{1}H NMR (400 MHz, Chloroform-*d*) δ 7.85 – 7.76 (m, 2H), 7.62 (dt, *J* = 7.8, 1.0 Hz, 1H), 7.55 – 7.49 (m, 1H), 7.44 – 7.36 (m, 2H), 7.25 (m, 1H), 7.19 (ddd, *J* = 8.2, 6.8, 1.3 Hz, 1H), 7.14 (d, *J* = 3.3 Hz, 1H), 7.11 (ddd, *J* = 7.9, 6.8, 1.2 Hz, 1H), 6.57 (dd, *J* = 3.3, 0.9 Hz, 1H), 5.00 (q, *J* = 7.2 Hz, 1H), 2.76 (td, *J* = 7.0, 1.9 Hz, 2H), 2.28 (m, 2H), 1.89 (p, *J* = 7.0 Hz, 2H), 1.71 (d, *J* = 7.2 Hz, 3H).
^{13}C NMR (101 MHz, Chloroform-*d*) δ 208.6, 199.8, 137.0, 136.3, 133.4, 129.2, 128.9, 128.3, 125.5, 122.5, 121.7, 120.4, 109.5, 103.4, 60.4, 37.5, 37.4, 18.2, 16.2.

(*S*)-2-(1H-indol-1-yl)-6-phenylhexan-3-one (59)

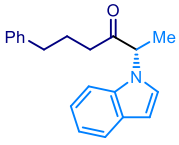

59

Prepared according to the General Procedure 3 using the corresponding anhydride (25 mg, 0,1 mmol), 2,6-lutidine (12 µL, 0,1 mmol), $NiCl_2$ (1,3 mg, 10 mol%), ligand **L1** (4,0 mg, 12 mol%), the corresponding dihydropyridine (79 mg, 0,2 mmol) and tetrahydrofuran (0.6 mL). Reaction time: 48h. The crude material was purified by flash column chromatography (hexane/dichlorometane 9:1) to give product **59** (14 mg, 48% yield) as a pale-yellow oil. The enantiomeric excess was determined by UPC^2 analysis using a CEL1 chiral column: after 1 min of 100% CO_2, gradient up to 60:40 CO_2/acetonitrile over 5 minutes, flow rate 2 mL/min. τ_{minor}= 3.9 min, τ_{major} = 4.1 min (80% ee); $[\alpha]_D^{26}$ = -53.9 (c = 0.7, CH_2Cl_2, 80% ee).

^{1}H NMR (400 MHz, Chloroform-*d*) δ 7.67 (dt, *J* = 7.8, 1.1 Hz, 1H), 7.25 – 7.19 (m, 4H), 7.18 – 7.11 (m, 3H), 7.03 – 6.98 (m, 2H), 6.60 (d, *J* = 3.3 Hz, 1H), 4.96 (q, *J* = 7.2 Hz, 1H), 2.43 (tt, *J* = 13.8, 6.8 Hz, 2H), 2.28 – 2.10 (m, 2H), 1.79 (p, *J* = 7.4 Hz, 2H), 1.69 (d, *J* = 7.2 Hz, 3H).
^{13}C NMR (101 MHz, Chloroform-*d*) δ 208.7, 141.7, 136.4, 129.2, 128.7, 126.2, 125.4, 122.5, 121.6, 120.4, 109.5, 103.3, 60.3, 37.6, 35.1, 25.1, 16.3.

(*S*)-7-(1H-indol-1-yl)octane-2,6-dione (60)

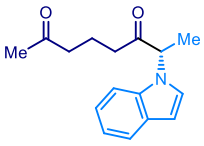

60

Prepared according to the General Procedure 3 using the corresponding anhydride (25 mg, 0,1 mmol), 2,6-lutidine (12 µL, 0,1 mmol), $NiCl_2$ (1,3 mg, 10 mol%), ligand **L1** (4,0 mg, 12 mol%), the corresponding dihydropyridine (79 mg, 0,2 mmol) and tetrahydrofuran (0.6 mL). Reaction time: 48h. The crude material was purified by flash column chromatography (hexane/dichlorometane 9:1) to give product **60** (16 mg, 61% yield) as a pale-yellow oil. The enantiomeric excess was determined by UPC[2] analysis using a CEL1 chiral column: after 1 min of 100% CO_2, gradient up to 60:40 CO_2/acetonitrile over 5 minutes, flow rate 2 mL/min. τ_{minor}= 3.40 min, τ_{major} = 3.5 min (75% ee); $[\alpha]_D^{26}$ = -51.9 (c = 0.8, CH_2Cl_2, 75% ee).
^{1}H NMR (400 MHz, Chloroform-*d*) δ 7.62 (dt, *J* = 7.8, 1.0 Hz, 1H), 7.24 – 7.16 (m, 2H), 7.14 – 7.07 (m, 2H), 6.57 (dd, *J* = 3.3, 0.7 Hz, 1H), 4.96 (q, *J* = 7.2 Hz, 1H), 2.22 (td, *J* = 7.0, 3.1 Hz, 2H), 2.16 (q, *J* = 6.9 Hz, 2H), 1.96 (s, 3H), 1.73-1.64 (app m: q, *J* = 7.1 Hz, 2H; d, *J* = 7.2 Hz , 3H).
^{13}C NMR (101 MHz, Chloroform-*d*) δ 208.5, 208.4, 136.3, 129.2, 125.5, 122.5, 121.7, 120.5, 109.5, 103.4, 60.3, 42.4, 37.2, 30.0, 17.7, 16.2.

(*S*)-4-(1H-indol-1-yl)-1-phenylpentan-3-one (61)

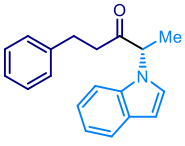

61

Prepared according to the General Procedure 3 using the corresponding anhydride (25 mg, 0,1 mmol), 2,6-lutidine (12 µL, 0,1 mmol), $NiCl_2$ (1,3 mg, 10 mol%), ligand **L1** (4,0 mg, 12 mol%), the corresponding dihydropyridine (79 mg, 0,2 mmol) and tetrahydrofuran (0.6 mL). Reaction time: 48h. The crude material was purified by flash column chromatography (hexane/dichlorometane 9:1) to give product **61** (14 mg, 51% yield) as a pale-yellow oil. The enantiomeric excess was determined by HPLC analysis on a Daicel Chiralpack IC3 column, 98:02 hexane/isopropanol flow rate 1.3 mL/min, 20ºC. τ_{minor} = 11.4 min, τ_{major} = 12.8 min (80% ee); $[\alpha]_D^{26}$ = -55.5 (c = 0.7, CH_2Cl_2, 80% ee).

^{1}H NMR (400 MHz, Chloroform-*d*) δ 7.65 (dt, *J* = 7.7, 1.0 Hz, 1H), 7.24 – 7.11 (m, 6H), 7.08 (d, *J* = 3.3 Hz, 1H), 7.03 – 6.98 (m, 2H), 6.59 (dd, *J* = 3.3, 0.7 Hz, 1H), 4.93 (q, *J* = 7.2 Hz, 1H), 2.81 – 2.75 (t, *J* = 7.9 Hz, 2H), 2.58 – 2.39 (m, 2H), 1.66 (d, *J* = 7.2 Hz, 3H).
^{13}C NMR (101 MHz, Chloroform-*d*) δ 208.2, 140.9, 136.3, 129.2, 128.8, 128.6, 126.5, 125.4, 122.5, 121.6, 120.4, 109.4, 103.4, 60.5, 40.0, 29.9, 16.1.

(*S*)-4-(1H-indol-1-yl)-1-(3-methoxyphenyl)pentan-3-one (62)

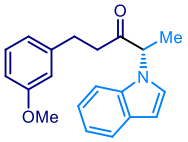

62

Prepared according to the General Procedure 3 using the corresponding anhydride (25 mg, 0,1 mmol), 2,6-lutidine (12 µL, 0,1 mmol), $NiCl_2$ (1,3 mg, 10 mol%), ligand **L1** (4,0 mg, 12 mol%), the corresponding dihydropyridine (79 mg, 0,2 mmol) and tetrahydrofuran (0.6 mL). Reaction time: 48h. The crude material was purified by flash column chromatography (hexane/dichlorometane 9:1) to give product **62** (15 mg, 49% yield) as a pale-yellow oil. The enantiomeric excess was determined by HPLC analysis on a Daicel Chiralpack IC3 column, 98:02 hexane/isopropanol flow rate 1.3 mL/min, 20ºC. τ_{minor} = 16.8 min, τ_{major} = 18.0 min (82% ee); $[\alpha]_D^{26}$ = -49.77 (c = 0.75, CH_2Cl_2, 82% ee).
^{1}H NMR (400 MHz, Chloroform-*d*) δ 7.67 (dt, *J* = 7.8, 1.0 Hz, 1H), 7.27 – 7.19 (m, 2H), 7.19 – 7.09 (m, 3H), 6.72 (ddd, *J* = 8.3, 2.6, 1.0 Hz, 1H), 6.65 – 6.59 (m, 2H), 6.58 – 6.54 (m, 1H), 4.95 (q, *J* = 7.2 Hz, 1H), 3.75 (s, 3H), 2.77 (td, *J* = 7.2, 6.6, 1.7 Hz, 2H), 2.60 – 2.42 (m, 2H), 1.69 (d, *J* = 7.2 Hz, 3H).
^{13}C NMR (101 MHz, Chloroform-*d*) δ 208.2, 159.9, 142.4, 136.3, 129.7, 129.2, 125.4, 122.5, 121.6, 121.0, 120.4, 114.3, 111.9, 109.4, 103.4, 60.5, 55.4, 40.0, 30.0, 16.1.

3.11.4 Assignment of Absolute Configuration

(*R*)-2-phenylpentan-3-one (45)

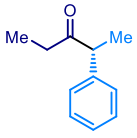

45

$[\alpha]_D^{26}$ = -85 (c = 0.5, CH_2Cl_2, 93% ee), Lit. for *R* isomer: $[\alpha]_D^{26}$ = -76 (c = 1.2, $CHCl_3$, for 93% ee,);[38] $[\alpha]_D^{21}$ = -42 (c = 1.0, $CHCl_3$, for 73% ee, R isomer);[36] $[\alpha]_D^{25}$ = -225.9 (c = 0.57, $CHCl_3$, for 91% ee).[11]

The absolute configuration of the other cross-coupling products was assigned by analogy, considering a uniform mechanism of stereoinduction.

[38] Rodríguez, C., de Gonzalo, G., Fraaije, M. W., Gotor, V. "Enzymatic Kinetic Resolution of Racemic Ketones Catalyzed by Baeyer-Villiger Monooxygenases" *Tetrahedron: Asymmetry* **2007**, *18*, 1338.

3.11.5 Evaluation of the Excited State Potential of 1a and 1c

Using the data collected from the absorption spectra studies and the cyclic voltammetry (Paragraph 3.5.1) of the 4-alkyl-1,4-dihydropyridines **1a** and **1b**, we could estimate the redox potential of the excited compounds (**1***) employing the following Equation 1:[39]

$$E(\mathbf{1}^{\cdot+}/\mathbf{1}^{*}) = E(\mathbf{1}^{\cdot+}/\mathbf{1}) - E_{0\text{-}0}(\mathbf{1}^{*}/\mathbf{1}) \quad [\text{Eq. 3.1}]$$

DHP **1a** - Equation 1 was applied. Since the electrochemical oxidation of the DHP **1a** is irreversible (Figure 3.3), the irreversible peak potential E_p^{Anode} was used for E(**1a** $^{\cdot+}$/**1a**). $E_{0\text{-}0}$(**1a***/**1a**), which is the excited state energy of the 4-alkyl-1,4-dihydropyridine **1a**, was estimated spectroscopically from the position of the long wavelength tail of the absorption spectrum recorded in acetonitrile (420 nm, Figure 3.1), the same solvent used for the electrochemical analysis.

For the DHP **1a**, the E_p^{Anode}, which provides the E(**1a**$^{\cdot+}$/**1a**), is +1.3 V (Figure 3.3), while the position of the long wavelength tail of the absorption spectrum corresponds to *420 nm* (Figure 3.1), which translates into an $E_{0\text{-}0}$(**1a***/**1a**$^{\cdot+}$) of 2.96 eV.

$$E(\mathbf{1a}^{*}/\mathbf{1a}^{\cdot+}) = 1.3 - 2.96 = \mathbf{-\ 1.65\ V}\ (\text{vs Ag/AgCl})$$

DHP **1b -** Equation 1 was applied. Since the electrochemical oxidation of the DHP **1b** is irreversible (Figure 3.4), the irreversible peak potential E_p^{Anode} was used for E(**1b** $^{\cdot+}$/**1b**). $E_{0\text{-}0}$(**1b***/**1b**), which is the excited state energy of **1b** was estimated spectroscopically from the position of the long wavelength tail of the absorption spectrum recorded in acetonitrile (418 nm, Figure 3.2), the same solvent used for the electrochemical analysis.

For the DHP **1b**, the E_p^{Anode}, which provides the E(**1b**$^{\cdot+}$/**1b**), is + 1.3 V (Figure 3.4), while the position of the long wavelength tail of the absorption spectrum corresponds to 420 nm (Figures 3.2), which translates into an $E_{0\text{-}0}$(**1b***/**1b**$^{\cdot+}$) of 2.96 eV.

$$E(\mathbf{1b}^{*}/\mathbf{1b}^{\cdot+}) = 1.3 - 2.96 = \mathbf{-\ 1.66V}\ (\text{vs Ag/AgCl})$$

[39] Kavarnos, G. J. "Fundamentals of Photoinduced Electron Transfer" VCH Publishers, 1993.

3.11.6 Characterization of Selected Compounds

3.11.6.1 UV-vis Absorption Spectra of 79, 80 and 56

A Solution of DHP **79** ([**79**] = 3 mM in dry CH_3CN) was introduced into a 1 cm path length quartz cuvette equipped with a Teflon® septum. The solution was analyzed using a Shimadzu 2401PC UV-Vis spectrophotometer.

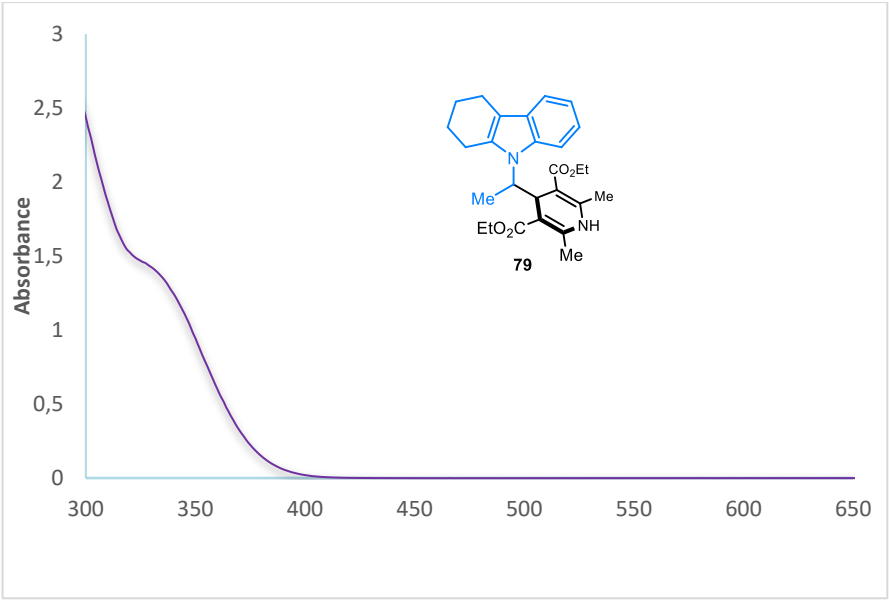

Figure 3.9. Absorption spectra of diethyl 2,6-dimethyl-4-(1-(1,2,3,4-tetrahydro-9H-carbazol-9-yl)ethyl)-1,4-dihydropyridine-3,5-dicarboxylate **79** ([**79**] = 3 mM in CH_3CN): λ_{max} = 294 nm. The tail wavelength of absorption was considered at 413 nm.

A Solution of DHP **80** ([**80**] = 3 mM in dry CH_3CN) was introduced into a 1 cm path length quartz cuvette equipped with a Teflon® septum. The solution was analyzed using a Shimadzu 2401PC UV-Vis spectrophotometer.

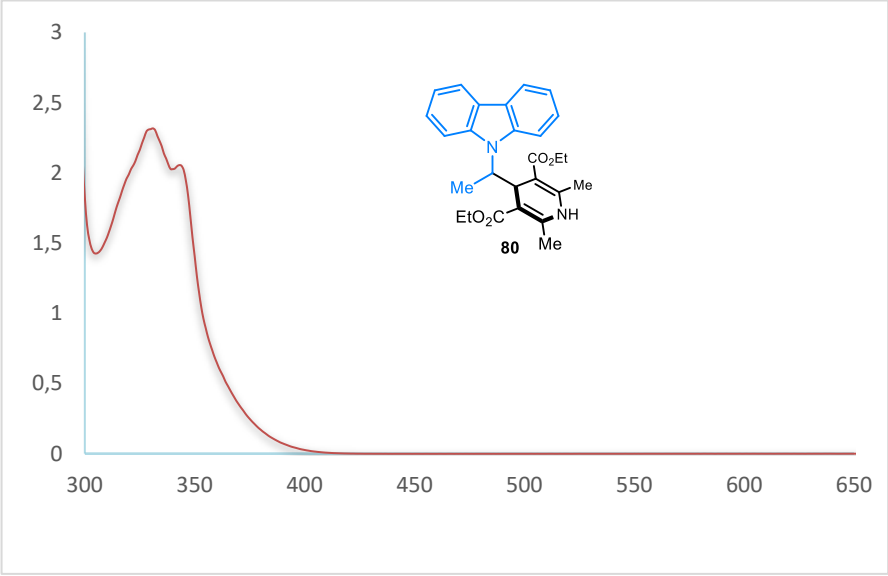

Figure 3.10. Absorption spectra of diethyl 4-(1-(9H-carbazol-9-yl)ethyl)-2,6-dimethyl-1,4-dihydropyridine-3,5-dicarboxylate **80** ([**80**] = 3 mM in CH_3CN): λ_{max} = 329 nm. The tail wavelength of absorption was considered at 410 nm.

A Solution of product **56** ([**56**] = 3 mM in dry CH_3CN) was introduced into a 1 cm path length quartz cuvette equipped with a Teflon® septum. The solution was analyzed using a Shimadzu 2401PC UV-Vis spectrophotometer.

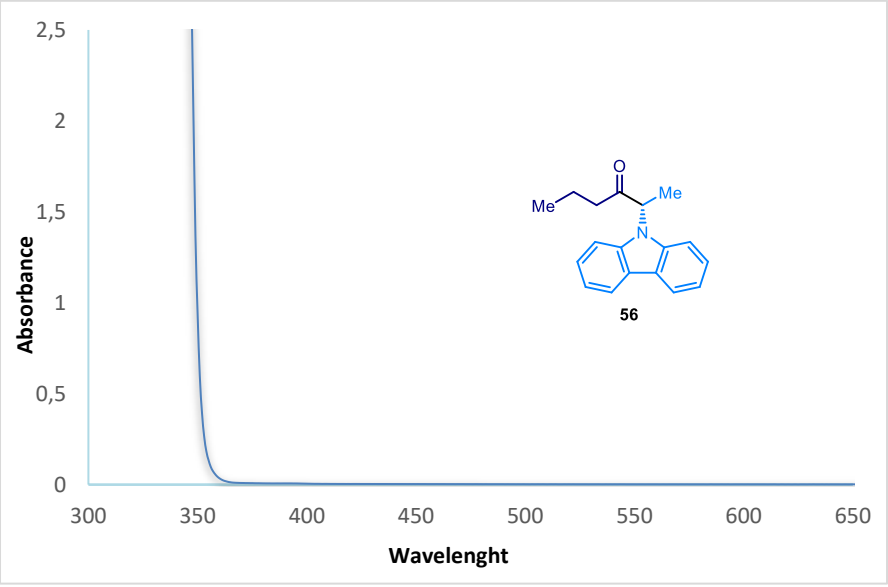

Figure 3.11. Absorption spectra of (S)-2-(9H-carbazol-9-yl)hexan-3-one **56** ([**56**] = 3 mM in CH_3CN): The tail wavelength of absorption was considered at 360 nm.

Comparison of the absorption spectra of substrates**, 1a**, **1b, 79, 80** and product **56**.

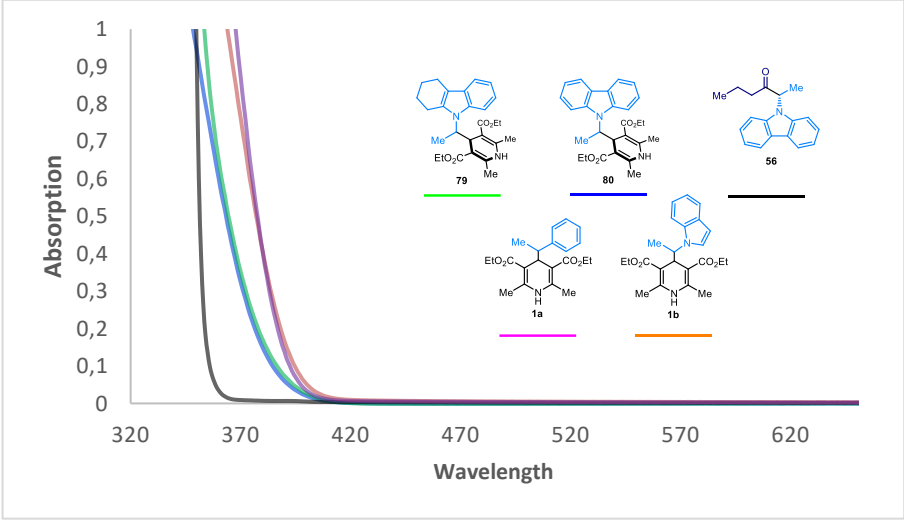

Figure 3.12. Combined absorption spectra of **1a**, **1b**, **79**, **80** and **56**.

3.11.6.2 Cyclic Voltammetry Study of 79, 80 and 56

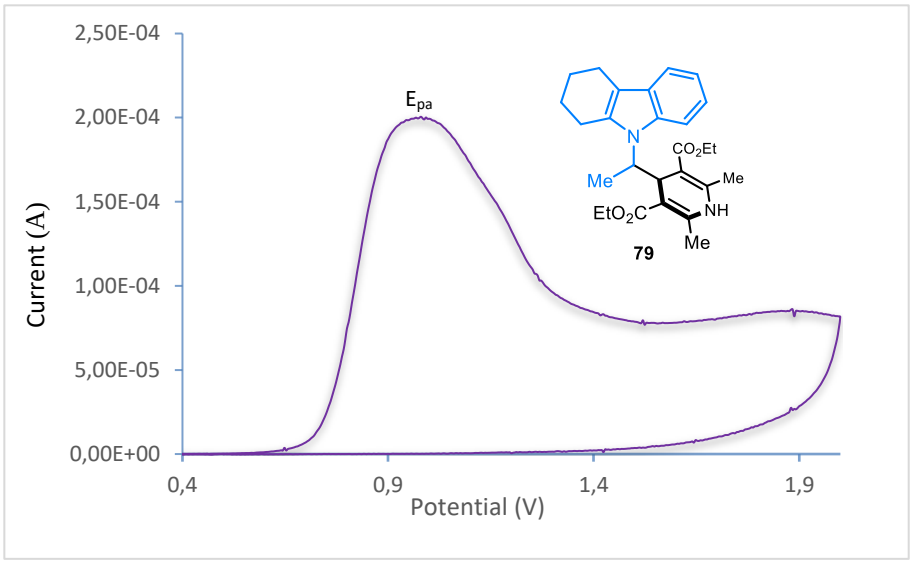

Figure 3.13. Cyclic voltammogram of **79** [0.02 M] in [0.1 M] $TBAPF_6$ in CH_3CN. Sweep rate: 30 mV/s. Pt electrode working electrode, Ag/AgCl (NaCl saturated) reference electrode, Pt wire auxiliary electrode. Irreversible oxidation. $E_p^A = E_{ox}$ (**79**$^{\cdot+}$/**79**) = +1.0 V; E_p^A is the anodic peak potential, while E_{ox} value describes the electrochemical properties of **79**.

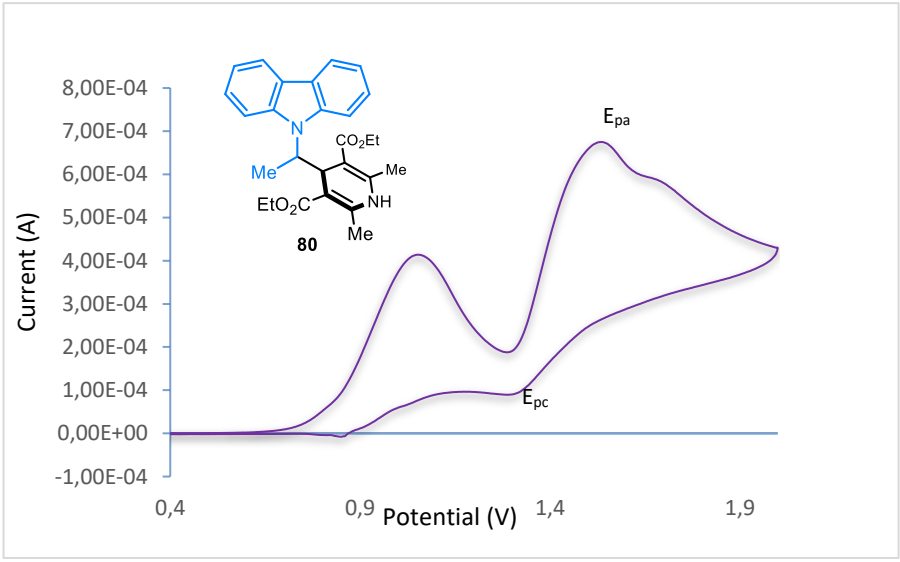

Figure 3.14. Cyclic voltammogram of **79** [0.02 M] in [0.1 M] $TBAPF_6$ in CH_3CN. Sweep rate: 200 mV/s. Pt electrode working electrode, Ag/AgCl (NaCl saturated) reference electrode, Pt wire auxiliary

electrode. Irreversible oxidation. $E_p^{ox} = E_{pa} = +1.53$ V; $E_p^{red} = E_{pc} = +1.31$ V; E_{pa} is the anodic peak potential, while and E_{pc} is the cathodic peak potential. E_p^{ox} and E_p^{red} values describe the electrochemical properties of **79**.

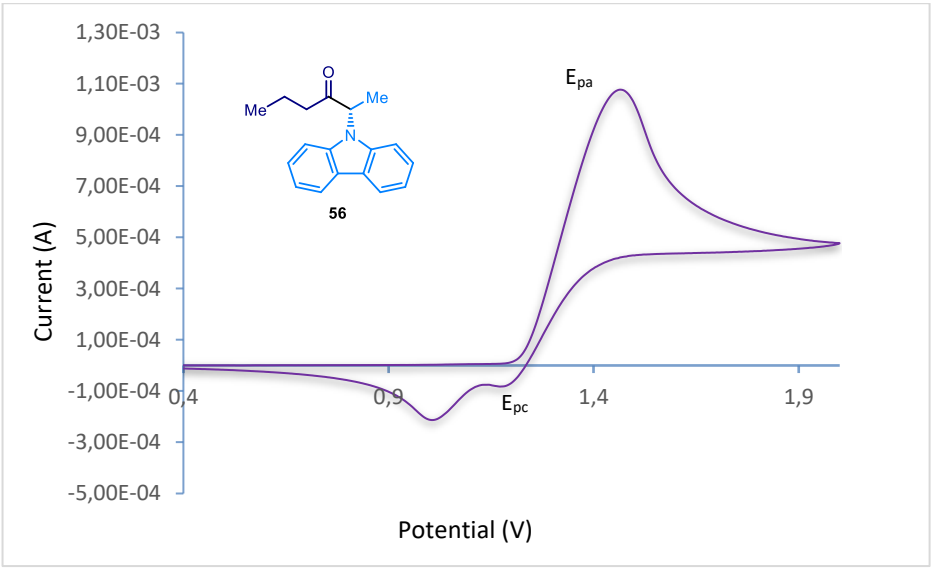

Figure 3.15. Cyclic voltammogram of **56** [0.02 M] in [0.1 M] $TBAPF_6$ in CH_3CN. Sweep rate: 200 mV/s. Pt electrode working electrode, Ag/AgCl (NaCl saturated) reference electrode, Pt wire auxiliary electrode. Irreversible oxidation. $E_p^{ox} = E_{pa} = +1.46$ V; $E_p^{red} = E_{pc} = +1.20$ V; E_{pa} is the anodic peak potential, while and E_{pc} is the cathodic peak potential. E_p^{ox} and E_p^{red} values describe the electrochemical properties of **56**.

Chapter IV

Catalytic Asymmetric C-C Cross-Couplings Enabled by Photoexcitation of an Allyl-Iridium Complex

Target

Developing an asymmetric C(sp^3)-C(sp^3) radical cross-coupling between allylic alcohols **1** and readely available radical precursors based on the photoexcitation of an allyl-iridium complex **I**.

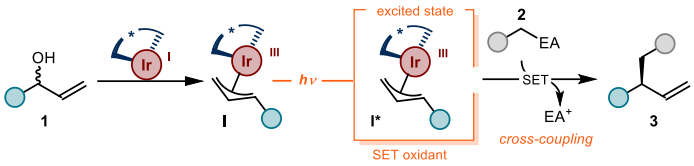

Tools

Exploiting the oxidative power of an excited chiral iridium-π-allylic complex to activate, via single-electron transfer, 4-alkyl-1,4-dihydropyridine radical precursors.[1]

4.1 Introduction

Chiral (η^3-allyl)iridium(III) organometallic complexes, generated upon oxidative addition of an Ir(I) catalyst with an activated allylic substrate, have been widely used to catalyze the synthesis of enantioenriched chiral molecules (Scheme 4.1a). In 2007, a major advance in this area was reported by Carreira, who introduced a new hybrid phosphoroamidite-olefin ligand (*S*)-**L1** (Scheme 4.1b, left). The resultant chiral (η^3-allyl) iridium(III) complex **I** (Scheme 4.1, bottom-right)[2] is widely recognized as a privileged organometallic intermediate to catalyze enantioselective allylic substitution reactions.[3] The marked electrophilicity of complex **I** enabled the addition of a large variety of

[1] The project discussed in this Chapter has been conducted in collaboration with Dr Giacomo E. M. Crisenza, Adriana Faraone, and Dr Daniele Mazzarella. Part of the work has been published in: Crisenza, G. E. M., Faraone, A., Gandolfo, E., Mazzarella, D., Melchiorre, P. "Catalytic asymmetric C–C cross-couplings enabled by photoexcitation" *Nat. Chem.* **2021**, *13*, 575-581-

[2] Defieber, C., Ariger, M. A., Moriel, P., Carreira, E. M. "Iridium-Catalyzed Synthesis of Primary Allylic Amines from Allylic Alcohols: Sulfamic Acid as Ammonia Equivalent" *Angew. Chem. Int. Ed.* **2007**, *46*, 3139.

[3] Rössler, S. L., Petrone, D. A., Carreira, E. M. "Iridium-Catalyzed Asymmetric Synthesis of Functionally Rich Molecules Enabled by (Phosphoramidite, Olefin) Ligands" *Acc. Chem. Res.* **2019**, *52*, 2657.

nucleophiles to easily accessible racemic branched allylic alcohols **4** in high stereocontrol and exquisite branched selectivity.

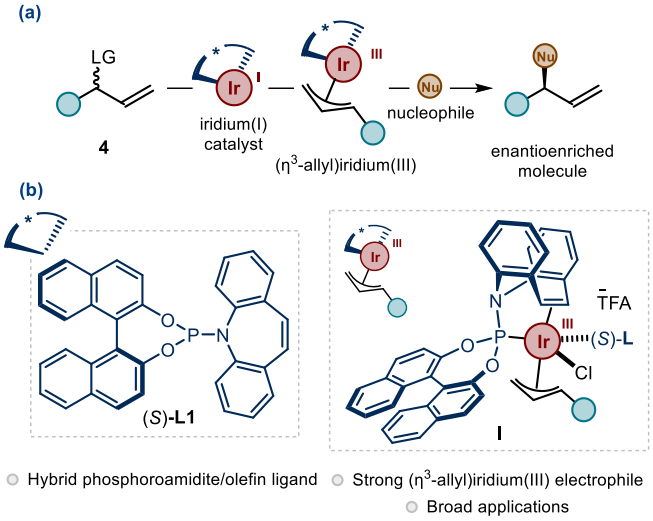

Scheme 4.1: a) General scheme for Ir-catalyzed allylations; b) hybrid phosphoroamidite-olefin ligand and the corresponding (η^3-allyl)iridium(III) complex.

In the realm of asymmetric catalysis, it has been recently demonstrated that photoexcitation could open up new opportunities for catalytic activation that go beyond the established ground-state reactivity. For example, our group has demonstrated that direct excitation of certain chiral organocatalytic intermediates,[4] with an established ground-state reactivity, unlocks novel catalytic functions which enable otherwise unachievable transformations. We showed that chiral iminium ions **II** (Scheme 4.2a),[5] generated upon condensation of a chiral secondary amine catalyst with enals, become upon light excitation strong oxidants (**II***), which are capable to engage in a single-electron transfer (SET) with the non-nucleophilic substrate **2**, adorned with suitable redox-active moieties. This SET event leads to the formation of alkyl radicals **III** and the concomitant reduction of chiral intermediates **II**, which can undergo stereoselective radical coupling to provide the chiral β-alkylated products **5**. Importantly, such β-alkylation of enals cannot be achieved within the ground-state domain via polar reactivity and can only be accomplished by this photo-driven radical-based protocol.

[4] Silvi, M., Melchiorre, P. "Enhancing the Potential of Enantioselective Organocatalysis with Light", *Nature* **2018**, *554*, 41.
[5] Silvi, M.; Verrier, C.; Rey, Y. P.; Buzzetti, L; Melchiorre, P. "Visible-light Excitation of Iminium Ions Enables the Enantioselective Catalytic β-Alkylation of Enals" *Nat. Chem.*, **2017**, *9*, 868.

Inspired by this work, we recently wonder if we could translate this photochemical strategy from organocatalysis into organometallic catalysis. We envisioned some similarities between the chiral iminium ion **II** and the chiral (η^3-allyl) iridium(III) complex **I** (Scheme 4.2b): both intermediates are strongly electrophilic in the ground state and display an intense coloration, which reveals their ability to absorb light in the visible region. In analogy to the photochemistry of the iminium ion **II**, we surmised that photoexcitation of the electrophilic iridium complex **I** would provide the oxidizing transient species **I*** able to activate, via SET, a suitable radical precursor **2**. Such event would lead to the formation of radical **III** and concomitant reduction of the Ir(III) complex **I**. Stereoselective trapping of radical **III** followed by reductive elimination would then deliver the enantioenriched chiral product **3** (Scheme 4.2b).

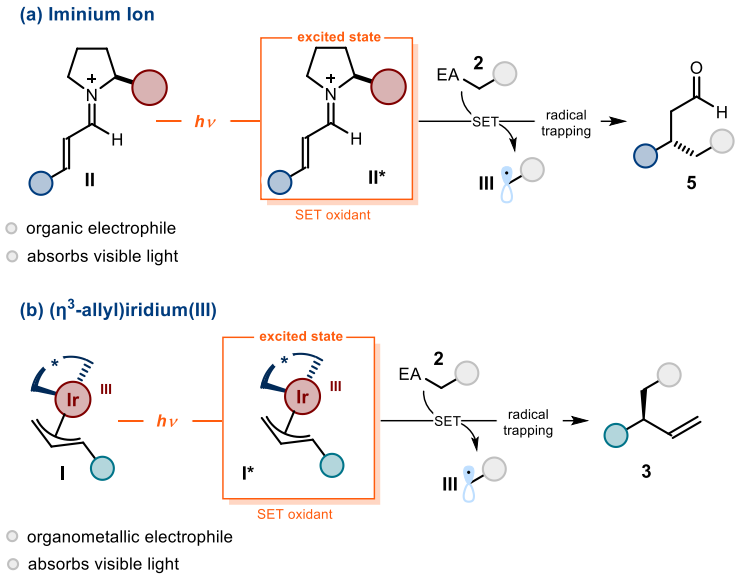

Scheme 4.2: a) Light-excitation of electron-poor iminium ions **II** provides an oxidizing excited state that engages in SET oxidation of radical precursors; b) light-excitation of the electron-poor (η^3-allyl)iridium(III) **I** complex may provide an oxidizing excited state.

This chapter documents how this design blueprint was translated to experimental reality. Specifically, we demonstrated that visible light excitation could override the established reactivity of the chiral organometallic complex **I**, unlocking novel reaction manifolds which enabled mechanistically unrelated radical-based pathways. This unconventional reactivity was harnessed to develop a difficult-to-realize enantioselective alkyl-alkyl cross-coupling. The protocol uses readily available, non-nucleophilic radical sources and proceeds under blue light irradiation at ambient temperature. We also conducted

mechanistic experiments that provided important insights on the photochemical role played by the organoiridum complex **I**.

4.2 Direct Photoexcitation of Chiral Organometallic Catalysts

The reborn interest in photochemistry brought a new perspective in asymmetric catalysis, expanding the mechanisms of catalytic activation beyond the conventional ground-state reactivity.[6] (Scheme 4.3). Major advances in asymmetric catalysis have traditionally been spurred by the identification of a few generic catalytic modes of substrate activation and stereochemical induction. The power of a mode of catalytic reactivity is that the intermediate formed upon activation of the substrate by the chiral catalyst can participate in many reaction types with consistently high stereoselectivity.[7] An intrinsic limit of this approach is that it allows the design of new but mechanistically related enantioselective processes. Recent studies have shown that light excitation can bring up novel reactivities from classical chiral catalytic intermediates, commonly employed in the thermal domain.

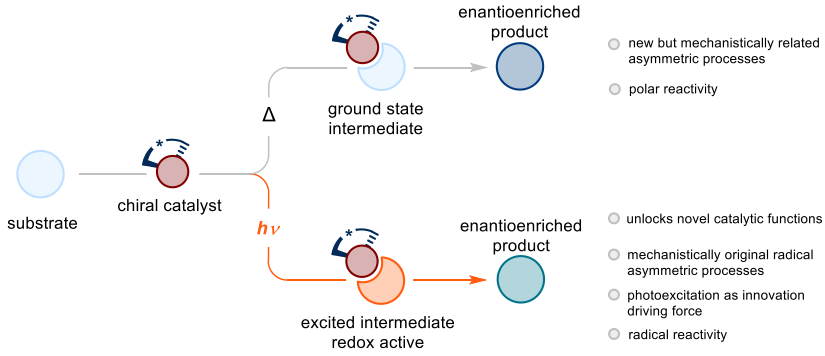

Scheme 4.3: Formation of a chiral reactive intermediate by catalyst activation followed by its participation in thermal or photochemical processes.

The direct excitation approach was mainly exploited within the fields of asymmetric organocatalysis (e.g. using iminium ion **II** intermediates),[4,5] biocatalysis (ene-reductase enzyme (ERED) as catalyst, upon photoexcitation of co-factor **IV**)[8] and Lewis-acid catalysis (complex **V** as catalyst)[9] to unlock novel catalytic functions and trigger photochemical asymmetric radical processes (Scheme 4.4).

---

[6] Meggers, E. "Asymmetric catalysis activated by visible light" *Chem. Commun* **2015**, *51*, 3290.
[7] Walsh, P. J., Kozlowski, M. C. "*Fundamental of Asymmetric Catalysis*" University Science Books, 2009.
[8] Sandoval, B. A., Hyster, T. K. "Emerging Strategies for Expanding the Toolbox of Enzymes in Biocatalysis" *Curr. Opin. Chem. Biol.* **2020**, *55*, 45.
[9]Selected examples: a)Brimioulle, R., Bach, T. "Enantioselective Lewis Acid Catalysis of Intramolecular Enone [2+2] Photocycloaddition Reactions" *Science* **2013**, *342,* 840; b)Huo, H., Shen, X., Wang, C., Zhang, L., Röse, P., Chen, L.-A., Harms, K., Marsch, M., Hilt, G., Meggers, E., "Asymmetric

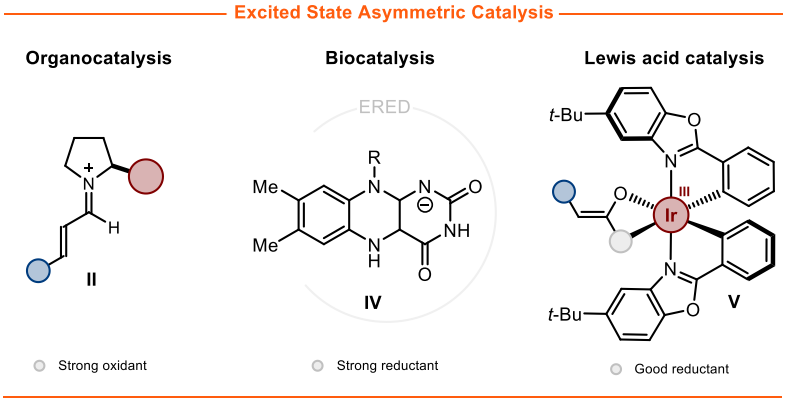

Scheme 4.4: Selected examples of catalytic asymmetric tools empowered by light-excitation; ERED, ene-reductase enzyme.

Within the field of organometallic catalysis, this photochemical strategy was mainly exploited[10] in non-asymmetric transformations. Specifically, photoexcitation of organometallic intermediates served to easily generate radicals or to facilitate elementary steps (e.g. oxidative addition and reductive elimination) that would be challenging under thermal conditions.[11] In contrast, the application of direct excitation in asymmetric organometallic catalysis has experienced far less development.

In 2016, Peters and Fu[12] reported the first example where a single (earth-abundant) metal complex conveys photochemical activation of substrates but also directs the enantioselective formation of bonds. This protocol served to develop a radical-based,

Photoredox Transition-Metal Catalysis Activated by Visible Light" *Nature* **2014**, *515*, 100; c)Skubi, K. L., Kidd, J. B., Jung, H., Guzei, I. A., Baik, M. H., Yoon, T. P. "Enantioselective Excited-State Photoreactions Controlled by a Chiral Hydrogen-Bonding Iridium Sensitizer" *J. Am. Chem. Soc.* **2017**, *139*, 17186; d) Li, Y., Zhou, K., Wen, Z., Cao, S., Shen, X., Lei, M., Gong, L. "Copper(II)-Catalyzed Asymmetric Photoredox Reactions: Enantioselective Alkylation of Imines Driven by Visible Light" *J. Am. Chem. Soc.* **2018**, *140,* 15850.

[10] For reviews on the topic, see: a) Cheng, W-M., Shang, R. "Transition Metal-Catalyzed Organic Reactions Under Visible Light: Recent Developments and Future Perspectives" *ACS Catal.* **2020**, *10*, 9170; b) Lunic, D., Bergamaschi, E., Teskey, C. J. "Using Light to Modify Selectivity of Transition Metal Catalysed Transformations" *Angew. Chem. Int. Ed.* DOI: 10.1002/anie.202105043; c) Wenger, O. S. "Photoactive Complexes with Earth-Abundant Metals" *J. Am. Chem. Soc.* **2018**, *140*, 13522; d) Parasram, P., Gevorgyan, V. "Visible Light-Induced Transition Metal-Catalyzed Transformations: Beyond Conventional Photosensitizers" *Chem. Soc. Rev.* **2017**, *46*, 6227; e) Hossain, A., Bhattacharyya, A., Reiser, O. "Copper's Rapid Ascent in Visible-Light Photoredox Catalysis" *Science* **2019**, *364,* eaav9713.

[11] For a recent example see: Torres, G. M., Liu, Y., Arndtsen, B. A. "A Dual Light-Driven Palladium Catalyst: Breaking the Barriers in Carbonylation Reactions" *Science* **2020**, *368*, 318.

[12] Kainz, Q. M., Matier, C. D., Bartoszewicz, A., Zultanski, S. L., Peters, J. C., Fu, G. C. "Asymmetric copper-catalyzed C-N cross-couplings induced by visible light" *Science* **2016**, *351*, 681.

copper-catalyzed enantioselective cross-coupling to forge carbon-nitrogen bonds (Scheme 4.5). The method used a tailored chiral copper (I)-amido complex **VII**, which had no previous applications in the polar enantioselective catalysis, to trigger radical reactivity and ensure stereocontrol. The catalytic cycle begins with the coordination of carbazole derivative **7** to the copper-phospine complex **VI** leading to the electron-rich intermediate **VII**. Blue-light excitation of this intermediate generates **VII***, which possesses enhanced reducing properties. SET from the excited complex **VII*** to the electron-poor alkyl chlorides **6** generates the radical couple **VIII** and **IX**, which can recombine, via either an *inner*- or *outer*-sphere event, to deliver the chiral product **8** in a stereocontrolled fashion.

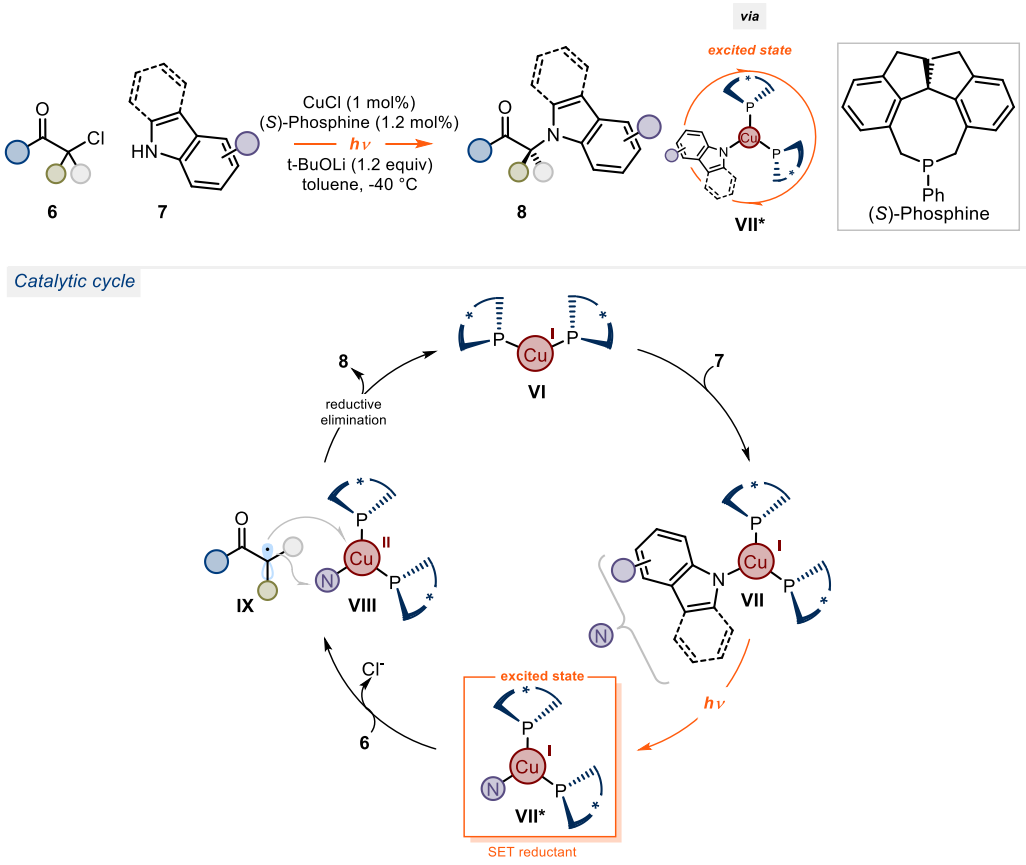

Scheme 4.5: First example of transition-metal asymmetric catalysis driven by direct photoexcitation of an organometallic intermediate.

Zhang recently expanded this concept to include chiral organocopper complexes enabling enantioselective cross-couplings reactions.[13] The authors used modified chiral bis-oxazoline (Box) ligands, which enhanced the photoreducing capability of the corresponding copper-complex X**II**, to trigger radical reactivity upon excitation and impart stereocontrol (Scheme 4.6). In the reported enantioselective dual carbo-functionalization of alkenes, the photoactive chiral organocopper intermediate **XII** was formed in situ by coordination of acetylide **XI** to the catalytic complex **X**. Upon light excitation of **XII**, SET reduction of the electron poor alkyl iodide **11** delivers the Cu(II) species **XIV** and the radical intermediate **XIII**, which is trapped by styrene **9**.

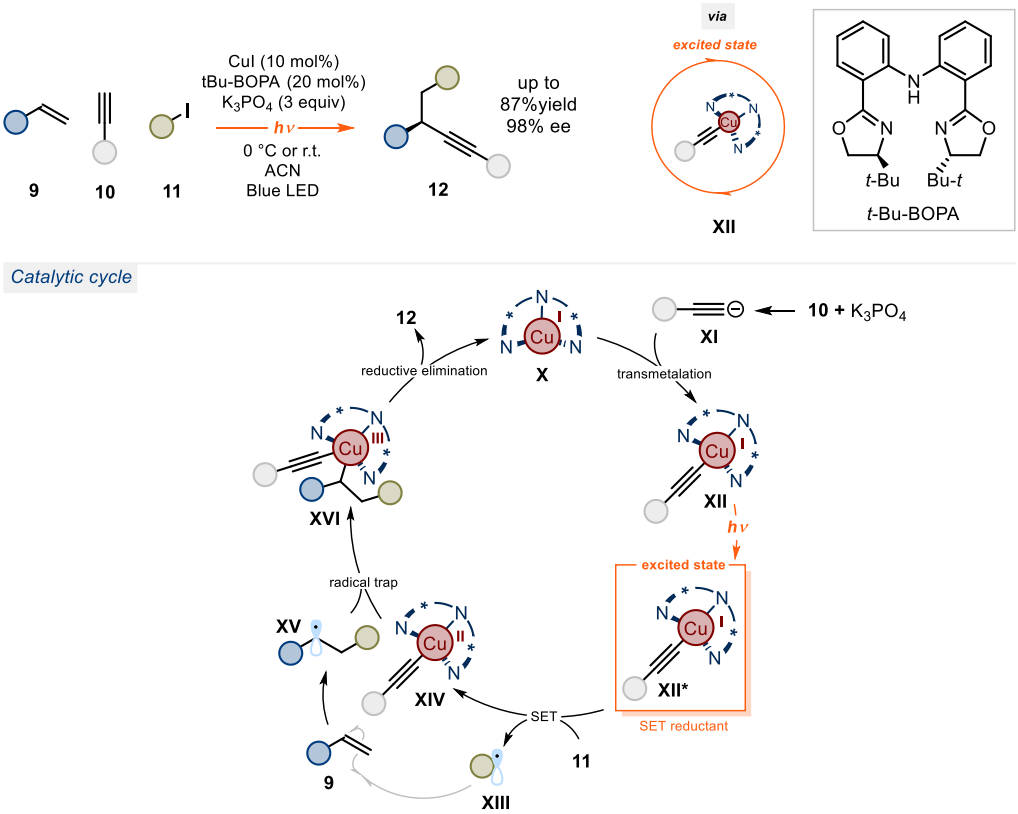

Scheme 4.6: Direct photoexcitation of chiral organometallic complexes **XIII** for the enantioselective carbo-difunctionalization of olefins.

[13] Zhang, Y., Sun, Y., Chen, B., Xu, M., Li, C., Zhang, D., Zhang , G. "Copper-Catalyzed Photoinduced Enantioselective Dual Carbofunctionalization of Alkenes" *Org. Lett.* **2020**, *22*, 1490.

The resulting benzyl radical **XV** reacts with Cu(II) intermediate **XIV** to deliver the Cu(III) complex **XVI**. Reductive elimination furnishes product **12** along with the Cu(I) catalyst **X**, thus closing the catalytic cycle (Scheme 4.6). This strategy was also applied to promote a photochemical asymmetric alkylation of azoles.[14]

We recently wondered if, upon light excitation, the (η^3-allyl)iridium(III) complex **I**, which has an established electrophilic profile in the ground state, could divert its reactivity to unlock mechanistic novel reaction pathways unattainable in the polar domain. In the following paragraph, the reader will be provided with some background on the rich polar, ground-state chemistry of the (η^3-allyl)iridium(III) complex **I**.

4.3 Iridium Catalyzed Asymmetric Allylations

Metal-catalyzed asymmetric allylations (AAs) were conceived and mainly developed using palladium as the metal of choice.[15] Only in 1997 Helmchen reported the first iridium-catalyzed asymmetric allylation, featuring protected linear allylic alcohols **13** and sodium-malonates (brown circle in Scheme 4.7) to access enantioenriched products **14** with exquisite branched selectivity. A chiral phosphinooxazoline (Phox) ligand secured the stereocontrol of the reaction (Scheme 4.7).[16]

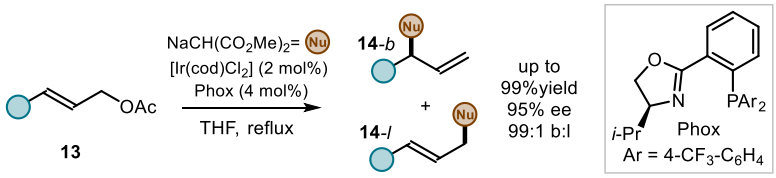

Scheme 4.7: First Iridium Catalyzed Asymmetric Allylic Alkylation.

Since this first report, the unique reactivity offered by iridium found broad synthetic applications supplementing the traditional palladium-catalyzed variants, which typically afford linear products.[17] A major contribution in this area was reported, in 2007, by the

[14] Li, C., Chen, B., Ma, X., Mo, X., Zhang, G. "Light-Promoted Copper-Catalyzed Enantioselective Alkylation of Azoles" *Angew. Chem. Int. Ed.* **2021**, *60*, 2130.
[15] Van Vranken, D. L., Trost, B. "Asymmetric Transition Metal-Catalyzed Allylic Alkylations" *Chem. Rev.* **1996**, *96*, 395.
[16] Jannssen, J. P., Helmchen, G. "First Enantioselective Alkylations of Monosubstituted Allylic Acetates Catalyzed by Chiral Iridium Complexes" *Tetrahedron Lett.* **1997**, *38,* 8025.
[17]a)Qu, J., Helmchen, G. "Applications of Iridium-Catalyzed Asymmetric Allylic Substitution Reactions in Target-Oriented Synthesis" *Acc. Chem. Res.* **2017***, 50*, 2539. b) Tosatti, P., Nelson, A., Mardsen, S. P. "Recent Advances and Applications of Iridium-Catalysed Asymmetric Allylic Substitution" Org. *Biomol. Chem.* **2012***, 10*, 3147; c) Dahnz, A., Dubon, P., Schelwies, M., Weihofen, R., Helmchen, G. "Iridium-catalysed asymmetric allylic substitutions" *Chem. Commun.* **2007**, *7*, 675.

group of Carreira[18] with the development of a new class of hybrid phosphoroamidites-olefin ligands (*S*)-**L1** (Scheme 4.8 bottom-left). The introduction of this ligand also set the stage for the establishment of a novel allylation approach, defined as type II.[19] Type II allylations occur in presence of Lewis or Brønsted acid activation of the allylic substrate, starting from readily available branched unprotected allylic alcohols **1** (Scheme 4.8 top). Moreover, the η^3-allyliridium complexes generated under these conditions are very powerful electrophiles. The presence of an olefin as second binding site within the ligand secures the stability of the corresponding η^3-allyl metal complex under acidic conditions.

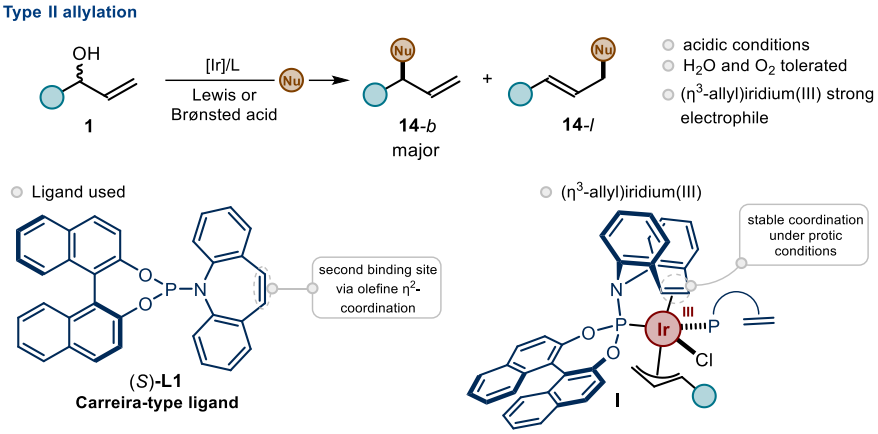

Scheme 4.8: Characteristics of type II allylations.

In contrast, type I allylations are conducted under basic conditions using protected linear alcohols **15** and are generally more sensitive towards oxygen or water (Scheme 4.9). In this case, the Feringa-type phosphoroamidite ligands are employed. The corresponding η^3-allyliridium complex **XVII** holds the second binding site through a carbon-iridium bond, formed upon C-H activation/carbometallation. In such bond the carbon donates electron density to the Ir(III) center making the corresponding η^3-allyliridium complex less electrophilic and prone to protodemetalation.

[18] Defieber, C., Ariger, M. A., Moriel, P., Carreira, E. M. "Iridium-Catalyzed Synthesis of Primary Allylic Amines from Allylic Alcohols: Sulfamic Acid as Ammonia Equivalent" *Angew. Chem. Int. Ed.* **2007**, *46*, 3139.

[19] Such useful classification, although not widely adopted, has been initially drawn by Helmchen in: Qu, J., Helmchen, G. "Applications of Iridium-Catalyzed Asymmetric Allylic Substitution Reactions in Target-Oriented Synthesis" *Acc. Chem. Res.* **2017**, *50*, 2539.

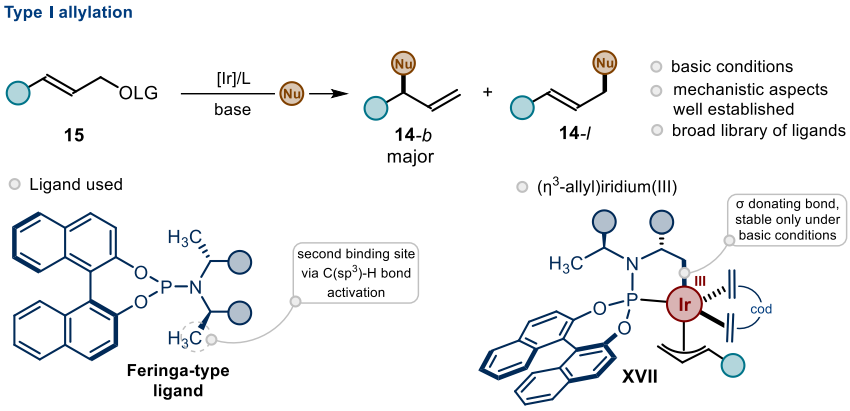

Scheme 4.9: Characteristics of type I allylations. cod, cyclooctadiene.

Mechanistic studies from the Carreira's group have shed light on several key structural features of complex catalyst **I**, explaining the marked electrophilicity of this intermediate.[20] Specifically, it was found that the metal center in complex **I** (Scheme 4.10, center) coordinates two different molecules of ligand; the first one in a bidentate fashion, by phosphorous and the olefin moiety, whereas the second in a monodentate fashion, by the sole phosphorus. The coordination of these three π-acidic sites is responsible for the enhanced electrophilicity of the metal. In fact, the iridium center cedes electron density via back-donation from its *d* orbitals to the σ* orbitals on the P-O or P-N bonds (Scheme 4.10, left) and to the π^* orbitals of the olefin (Scheme 4.10, right).[21]

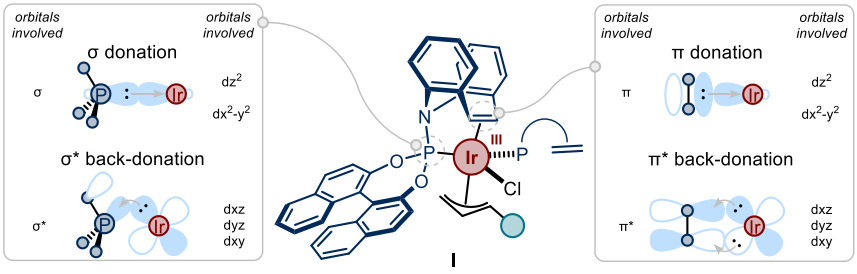

Scheme 4.10: Contribution of the ligand coordination to the iridium (η^3-allyl) complex electrophilicity.

[20] Rössler, S. L.; Krautwald, S.; Carreira, E. M. "Study of Intermediates in Iridium-(Phosphoramidite, Olefin)-Catalyzed Enantioselective Allylic Substitution" *J. Am. Chem. Soc.* **2017**, *139*, 3603.
[21] Defieber, C., Hansjörg Grützmacher, Carreira, E. M. "Chiral Olefins as Steering Ligands in Asymmetric Catalysis" *Angew. Chem. Int. Ed.* **2008**, *47*, 4482.

Overall, these findings helped to draw a general catalytic cycle (Scheme 4.11), which starts with the in situ formation of intermediate **XVIII**, upon coordination of substrate **1** in a η^2-fashion to the chiral Ir(I) complex. Acid promoted oxidative addition leads to the formation of the active (η^3-allyl)iridium(III) **I** complex, in equilibrium between the *endo-exo* isomers, which upon stereocontrolled nucleophilic attack delivers intermediate **XIX**. Detachment of the enantioenriched product **14-b** regenerates the catalyst.[22]

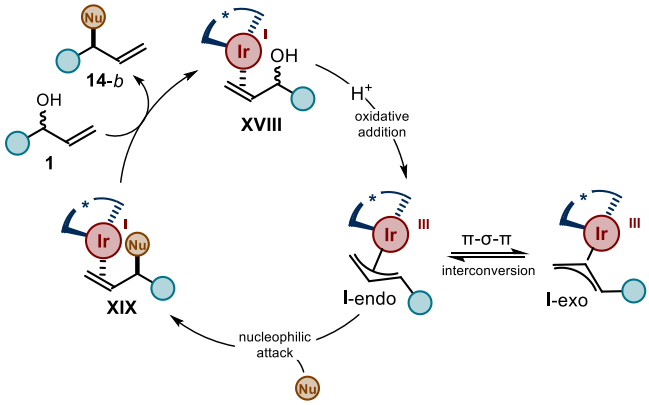

Scheme 4.11: General mechanistic cycle for type II asymmetric allylations.

After the initial report in 2007,[3] the Carreira's group largely shaped this area developing a series of enantio- and diastereoselective allylations. These protocols were also oriented towards the synthesis of complex natural scaffolds[23] and exploited a wide array of nucleophiles. For example, simple olefins **16**, which do not participate in type I allylations and are generally considered very weak nucleophiles, could instead engage in allylation substitutions under type II conditions (Scheme 4.12).[24]

---

[22] Rössler, S. L., Petrone, D. A., Carreira, E. M. "Iridium-Catalyzed Asymmetric Synthesis of Functionally Rich Molecules Enabled by (Phosphoramidite, Olefin) Ligands" *Acc. Chem. Res.* **2019**, *52*, 2657.

[23] a) Schafroth, M. A.; Zuccarello, G.; Krautwald, S.; Sarlah, D.; Carreira, E. M. "Stereodivergent Total Synthesis of Δ9 -Tetrahydrocannabinols" *Angew. Chem., Int. Ed.* **2014**, *53*, 13898; b) Schafroth, M. A.; Sarlah, D.; Krautwald, S.; Carreira, E. M. "Iridium-Catalyzed Enantioselective Polyene Cyclization" *J. Am. Chem. Soc.* **2012**, *134*, 20276; c) Hamilton, J. Y.; Hauser, N.; Sarlah, D.; Carreira, E. M. "Iridium Catalyzed Enantioselective Allyl−Allylsilane Cross-Coupling" *Angew. Chem., Int. Ed.* **2014**, *53*, 10759; d) Rössler, S. L.; Schreib, B. S.; Ginterseder, M.; Hamilton, J. Y.; Carreira, E. M. "Total Synthesis and Stereochemical Assignment of (+)-Broussonetine H" *Org. Lett.* **2017**, *19*, 5533; e) Hamilton, J. Y.; Rössler, S. L.; Carreira, E. M. "Enantio- and Diastereoselective Spiroketalization Catalyzed by Chiral Iridium Complex" *J. Am. Chem. Soc.* **2017**, *139*, 8082.

[24] Hamilton, J. Y., Sarlah, D.; Carreira, E. M. "Iridium-Catalyzed Enantioselective Allyl−Alkene Coupling" *J. Am. Chem. Soc.* **2014**, *136*, 3006.

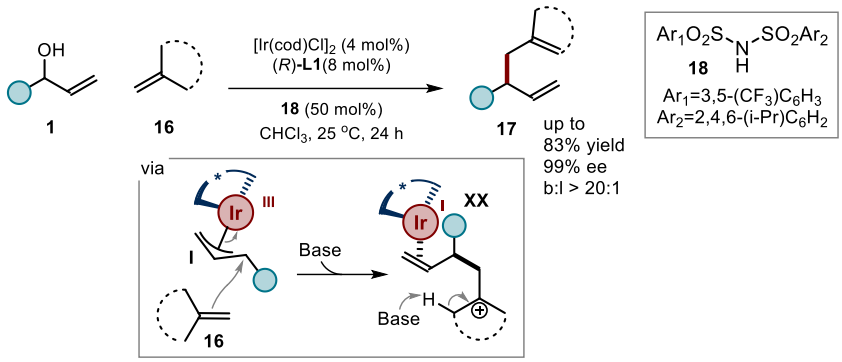

Scheme 4.12: Employment of olefins **16** in type II allylations as weak nucleophiles.

4.4 Target of the Project

The aim of this project is to show that, by light excitation, it is possible to override the ground-state features of the organoiridium complex **I** developed by Carreira and unlocking novel catalytic functions to drive mechanistically original asymmetric radical processes (Scheme 4.13).

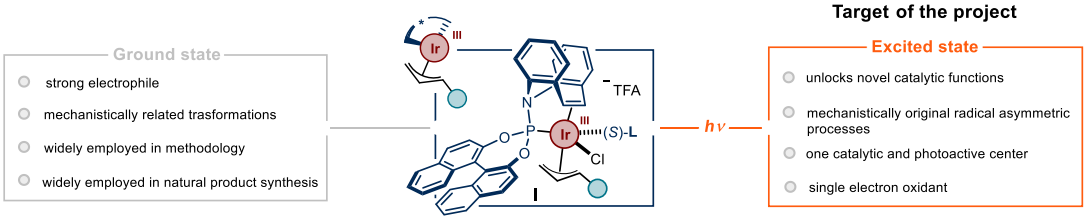

Scheme 4.13: Target of the project.

We anticipated that this strategy would allow the formation of radical intermediates under mild conditions, which then could be exploited in stereocontrolled carbon-carbon bond forming processes. If successful, this approach would represent the first example where a known chiral organometallic intermediate, upon light excitation, unlocks unique reaction manifolds unattainable under thermal domain.

4.5 Design Plan

We sought to exploit the novel catalytic functions acquired by the photoexcitation of chiral (η^3-allyl) iridium(III) complex **I** to develop a photo-driven enantioselective radical alkyl-alkyl cross-coupling (Scheme 4.14).

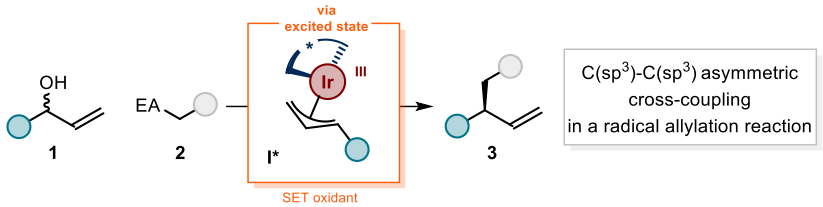

Scheme 4.14: Enantioselective alkyl-alkyl cross-coupling via a radical allylation reaction.

To date, within the emerging field of metallaphotoredox catalysis, only few studies were dedicated to the development of an asymmetric radical allylic alkylation protocol.[25] Specifically, the group of Yu[26] exploited the excited-state properties of the iridium photocatalyst **22** to activate the dihydropyridine radical precursors **19** and modulate the oxidation state of a palladium chiral complex (Scheme 4.15). The catalytic cycle starts with the oxidative addition of Pd(0) catalyst **XXII** with substrate **20** forming the chiral (η^3-allyl)palladium(II) complex **XXIII**. This electrophilic Pd(II) complex intercepts the stabilized radical **XXI**, generated upon SET oxidation of the dihydropyridine **19** by the excited photocatalyst **22***. The emerging Pd(III) intermediate **XXIV** undergoes reductive elimination delivering the chiral branched product **21** in excellent yields and ee. The Pd (0) active catalyst is regenerated by an SET event from the reduced photocatalyst **22**$^{\bullet-}$. This methodology still required an external photocatalyst to unlock radical reactivity and modulate the oxidation state of the palladium catalyst.

[25] Zhang, M-M., Wang, Y-N,. Lu, L-Q., Xiao, W-J. "Light Up the Transition Metal-Catalyzed Single-Electron Allylation" *Trends Chem.* **2020**, 2, 764. For a recent report see: Xue, S., Limburg, B., Ghorai, D., Benet-Buchholz, J., Kleij A. W. "Asymmetric Synthesis of Homoallylic Alcohols Featuring Vicinal Tetrasubstituted Carbon Centers via Dual Pd/Photoredox Catalysis" Org. Lett. 2021, 23, 4447.

[26] Zhang, H-H., Zhao, J.-J., Yu, S. "Enantioselective Allylic Alkylation with 4-Alkyl-1,4-dihydropyridines Enabled by Photoredox/Palladium Cocatalysis" *J. Am. Chem. Soc.* **2018**, *140*, 16914.

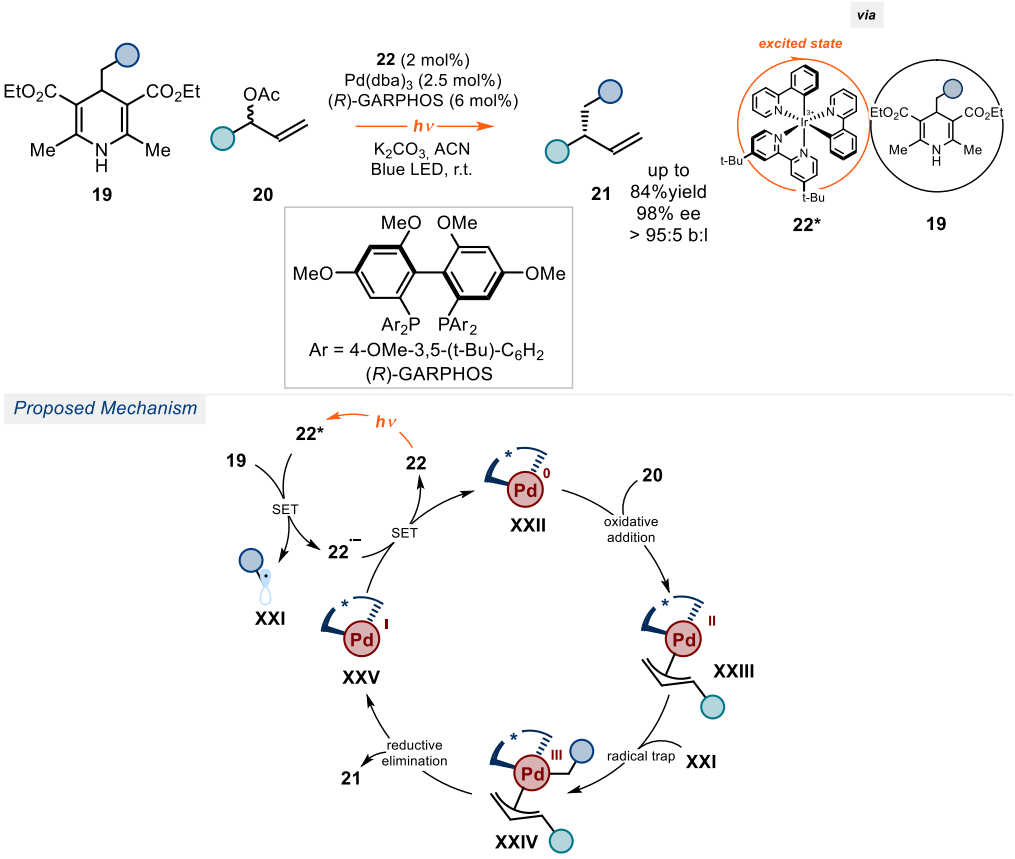

Scheme 4.15: Pd-catalyzed asymmetric radical alkyl allylation via photoredox catalysis.

4.5.1 Synthesis and Photophysical/Electrochemical Characterization of the Chiral (η^3-allyl)iridium(III) Complex

At the onset of our studies, we synthetized the chiral (η^3-allyl) iridium(III) complex **I** according to a reported procedure[20] by mixing the chiral phosphoroamidite-olefin ligand (*S*)-**L1**, $[Ir(cod)Cl]_2$, and racemic 1-phenylprop-2-en-1-ol **1a** in the presence of trifluoromethanesulfonic acid in chloroform at room temperature (Scheme 4.16). The isolated complex **I** presented an intense orange coloration, which indicates its ability to absorb visible-light radiation (400-800 nm).

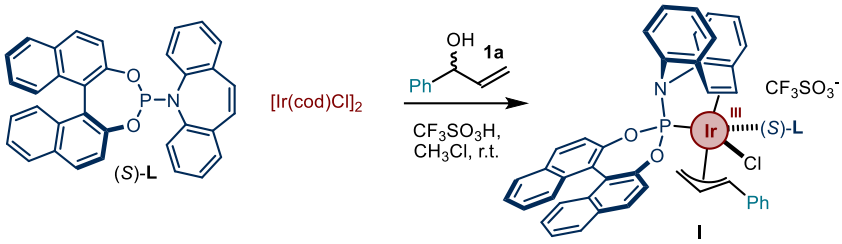

Scheme 4.16: Synthetic route to complex **I**.

In analogy to our previous studies with iminium ions,[5] we wondered if this colored electron-poor chiral (η^3-allyl)iridium(III) complex **I**, upon visible-light excitation, could divert its ground-state polar reactivity and trigger an SET with a suitable alkyl radical precursor **2** (Scheme 4.17). Such SET event would lead to the reduction of the iridium center **I** and the concurrent release of an alkyl radical **III** from the activated precursor **2**. At this point, the fleeting (η^3-allyl)iridium(II) complex **XXVI** intercepts the radical intermediate **III**, in an outer- or inner-sphere manifold, yielding the desired chiral product **3**.

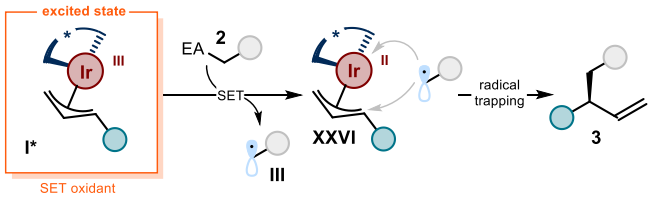

Scheme 4.17: Our initial design plan.

To support our hypothesis, we initially estimated the excited-state potential of **II** using the Rehm-Weller formalism, which requires the characterization of complex **II** via spectroscopic and electrochemical analysis. [27]

UV-vis spectroscopic analysis confirmed our initial observation, indicating that complex **II** absorbs light until 480 nm in a concentration range between 0.28 to 1.6 mM. We also estimated the molar extinction coefficient (ε) at 460 nm to be 930 $M^{-1}cm^{-1}$, thus indicating the marked ability of **II** to absorb blue light (450-460 nm). We identified the position of the long wavelength tail λ_{tail} at 480 nm, which determines the excited-state energy E_{00} of **II** to be of 2.58 eV (Figure 4.1).

[27] Buzzetti, L., Crisenza, G. E. M., Melchiorre, P. "Mechanistic Studies in Photocatalysis" *Angew. Chem. Int. Ed.* **2019**, *58*, 3730.

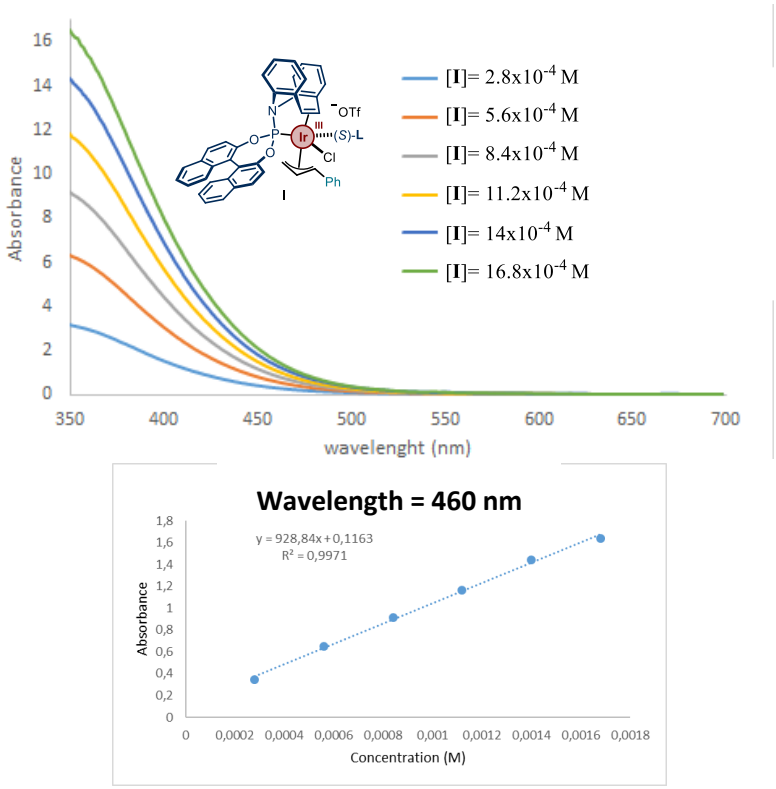

Figure 4.1. UV-vis absorption spectra in a 0.1 cm path length quartz cuvette of the pre-formed complex **I** and Lambert-beer linear correlation between absorbance and concentration at 460 nm.

We then focused on the electrochemical characterization of complex **I**. Using differential pulse voltammetry (DPV),[28] we measured the ground-state redox properties of complex **I** revealing an irreversible reduction peak with E (**Ir**(III)/**Ir**(II)) = -1.34 V vs Ag/Ag^+ in CH_2Cl_2 (Figure 4.2).

[28] We thank Prof. A. Llobet and Dr. J. Holub for assistance with differential pulse voltammetry.

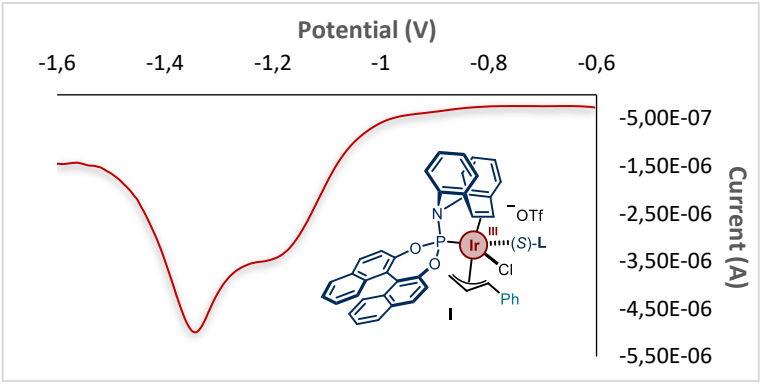

Figure 4.2: Differential pulse voltammogram for the pre-formed complex **I** [0.005M] in [0.1 M] $TBAPF_6$ in CH_2Cl_2. Initial E: -0.6 V; final E: -1.6 V; amplitude: 0.05 V; pulse width: 0.05 sec; sample width: 0.017 sec; pulse period: 0.5 sec; quiet time: 2 sec. Glassy carbon electrode working electrode, $Ag/AgNO_3$ (in Et_2O) reference electrode, Pt wire auxiliary electrode.

Based on the spectroscopic and electrochemical measurements and applying the Rehm-Weller formalism,[29] we estimated the excited-state redox potential of the (η^3-allyl)iridium(III) complex **I** to be E* (**Ir-1**(III)*/**Ir-1**(II)) = +1.24 V.

This redox value confirmed that photoexcitation might diverts the electrophilic nature of complex **II**, turning it into a good SET oxidant.

4.6 The Choice of the Radical Precursor

After establishing the excited-state potential of the organoiridium complex **I**, we focused on the choice of a suitable alkyl radical source. An appropriate radical precursor should meet two main requirements: *i*) it should be prone to activation via SET oxidation from the excited complex **I**; *ii*) upon SET, it should undergo a facile fragmentation with consequent generation of an alkyl radical. Based on our previous works,[5,30] we selected the carbazole silane **2a** as the redox partner, since it holds both the requirements. In fact, the redox potential of **2a** (E (**2a**$^{\cdot+}$/**2a**) = +1.13 V vs Ag/Ag^+ in CH_3CN) is within the estimated redox window for the excited complex **I**, thus implying an exergonic SET transfer oxidation (Figure 4.3). In addition, the presence of an electron-auxiliary moiety, such as the trimethylsilyl group, which can easily fragment upon SET oxidation,

[29] Rehm, D., Weller, A., "Kinetics of Fluorescence Quenching by Electron and H-Atom Transfer" *Isr. J. Chem.* **1970**, *8*, 259.
[30] Cao, Z-Y., Ghosh, T., Melchiorre, P. "Enantioselective radical conjugate additions driven by a photoactive intramolecular iminium-ion-based EDA complex" *Nat Comm* **2018**, *9*, 3274.

facilitates the generation of radicals by hampering back-electron transfer (BET).[31] We also sought the synthetical advantage of using substrate **2a** bearing a carbazole moiety, since it would enable the installation of this biologically relevant scaffold in a stereocontrolled fashion within the final product.[32]

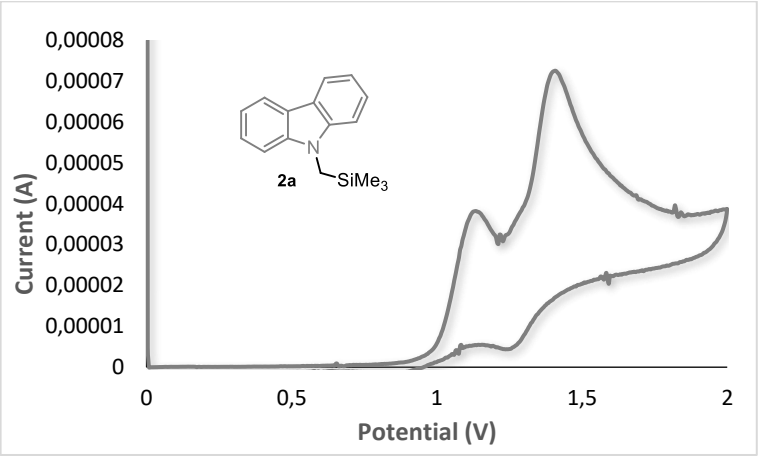

Figure 4.3: Cyclic voltammogram for silane **2a** [0.001 M] in [0.1 M] $TBAPF_6$ in CH_3CN. Sweep rate: 100 mV/s. Glassy carbon working electrode, Ag/AgCl (KCl saturated) reference electrode, Pt wire auxiliary electrode.

4.7 Preliminary Results and Optimization Studies

We tested the feasibility of our hypothesis (Table 4.1) by reacting substrates **1a** and **2a** in the presence of 5 mol% of $[Ir(cod)Cl]_2$, 11 mol% of (*S*)-**L1** and 1 equivalent of trifluoroacetic acid (TFA). The reaction was conducted for 12 hours at ambient temperature and under illumination by a blue-light-emitting diode (LED, λ_{max} = 460 nm). Pleasingly, the target chiral product **3a** was formed in 58% yield, 86% enantiomeric excess (ee), and complete branch selectivity (Entry 1). Control experiments revealed that the reactivity was completely inhibited in the dark, even when heating the mixture at 60 °C, indicating that the light is essential for the process (Entry 2). We also tested other electron auxiliary (EA) groups having a lower redox potential than silane **2a**. Substrate **2b**, bearing a potassium trifluoroborate redox handle (E (**2b**$^{\bullet+}$/**2b**) = +0.98 V vs Ag/Ag^+ in CH_3CN), led to product **3a** with a lower yield and enantiomeric excess (entry 4),

[31] Yoshida, J.-I., Kataoka, K., Horcajada, R., Nagaki, A. "Modern Strategies in Electroorganic Synthesis" *Chem. Rev.* **2008**, *108*, 2265.
[32] Bashir, M., Bano, A., Ijaz, A. S., Chaudhary, B. A. "Recent Developments and Biological Activities of N-Substituted Carbazole Derivatives: A Review" *Molecules* **2015**, *20*, 13496.

whereas the use of 1,4-dihydropyridine derivative **2c** (E (**2c**$^{\cdot+}$/**2c**) = +0.96 V vs Ag/Ag^{+} in CH_3CN) secured a better yield and enantiomeric excess (entry 5).

Table 4.1: Initial screening of radical precursors and control experiments.

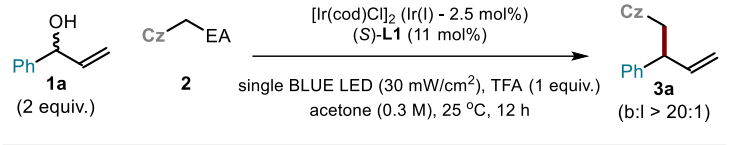

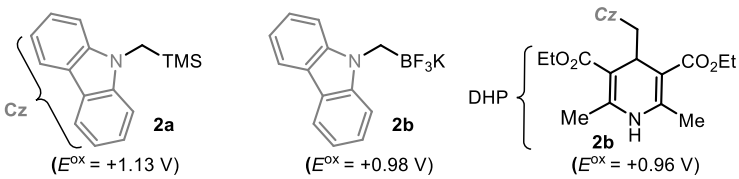

entry	deviation	yield (%)[a]	ee(%)
1	**2a**	58	86
2	Dark, 60 °C	0[b]	-
4	**2b**	44	82
5	**2c**	81	88

Reaction performed on a 0.1 mmol scale in acetone (0.3 M) under illumination by a single high-power (HP) LED (λ_{max} = 460 nm) for 12 hours [a] Yield of isolated **3a**. [b] Complete recovery of **2a** after the reaction. EA, electron auxiliary.

Because of the known photoactivity of 1,4-dihydripyridines (see Chapter 2 and 3 of this thesis), we conducted a UV-Vis analysis of substrate **2c** and complex **I**, mirroring the reaction concentration, in order to determine which species displays the higher absorption coefficient at 460 nm (Figure 4.4).

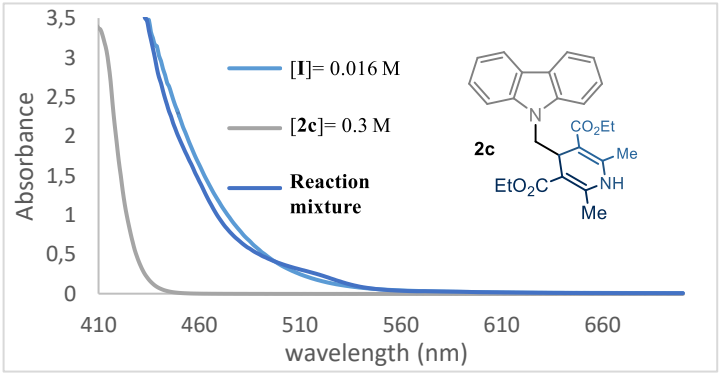

Figure 4.4: UV-vis absorption spectra of 1,4-dihydropyridine **2c** (0.3 M), the in situ formed complex **I** (0.016M), and the reaction mixture in degassed acetone.

The spectroscopic profile of substrate **2c** (concentration 0.3 M) shows a non-negligible absorption at 460 nm. However, the molar absorptivity of complex **I** (concentration ~ 0.015-16 M) in the same spectral region was far higher, presenting a tail absorption up to 560 nm. This experiment highlighted that complex **I** is the main chromophore in the reaction (Figure 4.4). A further support to this notion came from the use of green light (525 nm), an excitation wavelength which could only be absorbed by the Ir(III)-π-allylic complex **I**. The reaction with green light proceeded smoothly leading to product **3a** in 57% yield and 85% ee (Scheme 4.18).

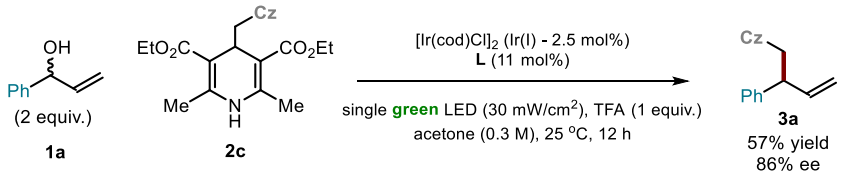

Scheme 4.18: Reactivity promoted by green light.

We then continued the reaction optimization using substrate **2c** (Table 4.2). Screening the equivalent of alcohol **1a**, we found the optimal amount to be 2 equivalents (entries 1-3). Acid promoter **24**, previously employed in type II allylations,[24] did not improve the reactivity (Entry 4). We also tested the pre-formed complex **I**, confirming its catalytic competence yielding product **3a** with only a modest drop in yield (entry 5). The reaction was also scaled up to 1 mmol, using the opposite enantiomer of the ligand (*R*)-**L**, obtaining product *ent*-**3a** with a modest drop in yield and same (but opposite in sign) level of stereocontrol (Entry 6). Finally, a control reaction with the exclusion of light, heating at 60 °C, completely suppressed the reactivity (Entry 7).

Table 4.2: Screening of the different parameters using **2c** as radical precursor.

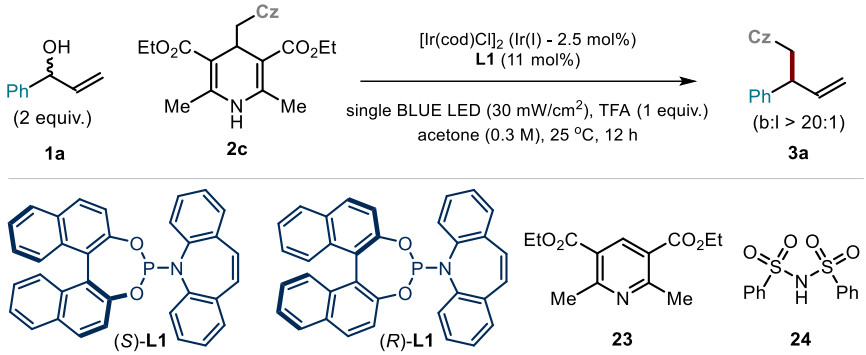

entry	deviation	yield (%)[a]	ee(%)
1	none	81	88
2	**1a** (100 mol%)	44	82
3	**1a** (300 mol%)	66	88
4	**24** as acid promoter	57[b, c]	n.d.
5	Complex II (preformed)	75	88
6	**2c** (1 mmol), (*R*)-**L**	68	(-)88
7	dark, 60 °C	0[d]	-

Reaction performed on a 0.1 mmol scale in acetone (0.3 M) using under illumination by a single high-power (HP) LED (λ_{max} = 460 nm) for 12 hours [a] Yield of the isolated **3a**.[b] Yield determined by ^{1}H-NMR. [c] 57% of pyridine byproduct **23** formed. [d] 25% of pyridine byproduct **24** formed.

4.8 Scope of the Method

With the best conditions in hand (Table 4.2, entry 1), we tested the generality of the photochemical asymmetric cross-coupling. First, we evaluated different 1,4-dihydropyridine radical precursors in combination with alcohol **1a** (Figure 4.5). A carbazole moiety bearing different functional groups, including alkyl (**25**), halogen (**26**, **27**, **29**, **30**, **31**) and boron (**28**), could be installed in the products in good to high yields and ee. The use of α-amino radical precursors enabled the stereoselective installation of *N*-heterocyclic fragments of pharmaceutical interest, such as an indole (**32**), an oxindole (**33**), a 3,4-dihydroquinolone (**34**), and a quinolone (**35**) moiety. In addition, the natural occurring tryptamine unit (**36**) and *aripiprazole* scaffold (**37**) were included in the final products. The use of a chiral substrate adorned with the *efavirenz* core, a drug used in the HIV/AIDS treatment, participated in the coupling process affording the product as a single diastereoisomer (**38**). Swapping the ligand enantiomer afforded the opposite diastereomer, indicating that the catalyst controls the stereoselectivity of the process (**39**).

Carbamates, including a derivative of the insecticide *carbaryl*, also participated in the reaction, leading to products **40** and **41**. One limitation of the methodology is that a 4-benzyl-DHPs derivative did not participate in the cross-coupling protocol.

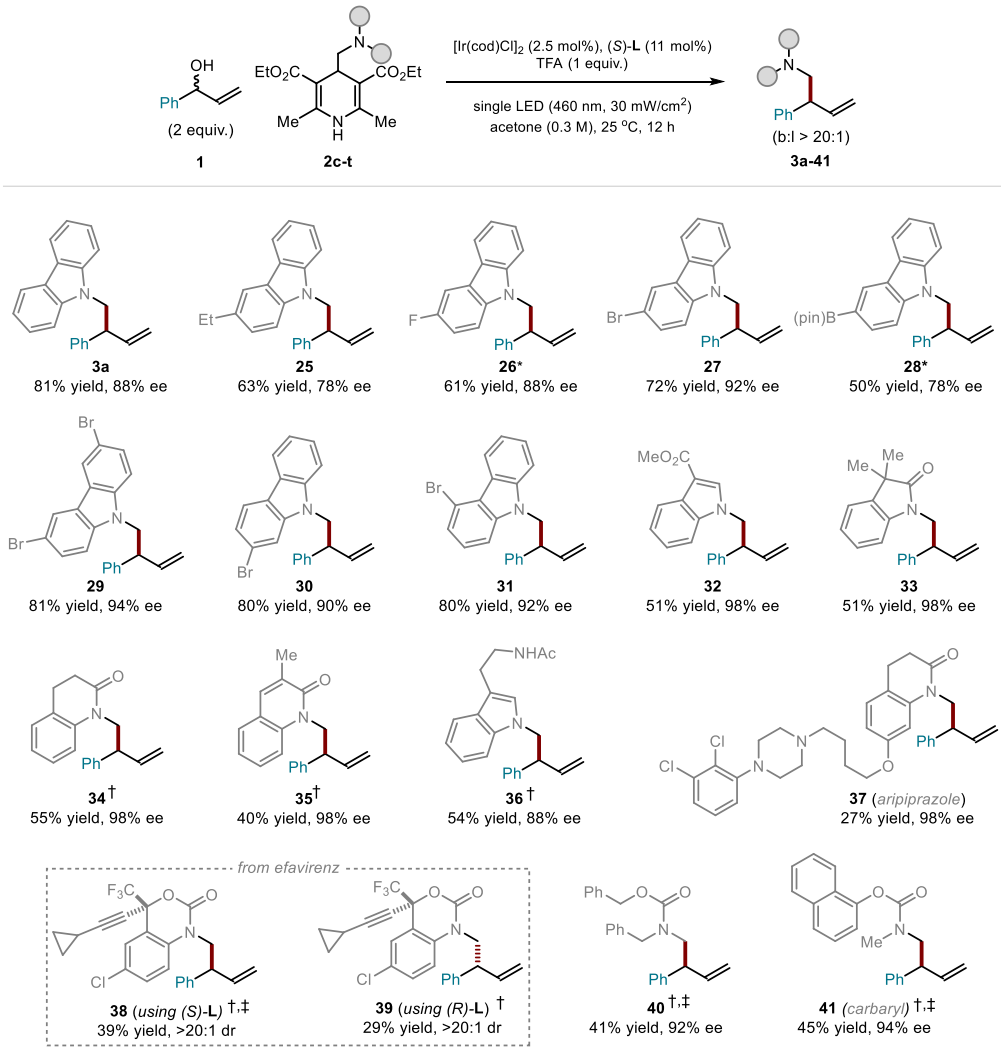

Figure 4.5: Survey of the radical precursors that can participate in the reaction. Reaction performed on a 0.1 mmol scale using 2 equiv. of allylic alcohol. Yields and enantiomeric excesses of the isolated products are indicated below each entry (average of two runs per substrate). * Using the trimethylsilane radical precursor **2a**; † Performed in $CHCl_3$; ‡ using the pre-formed complex **I** as the catalyst (5 mol%). cod, cyclooctadiene; TFA, trifluoroacetic acid; B(pin), pinacol borane; Ac, acetyl.

We then tested aromatic allylic alcohol precursors **1** adorned with a broad range of functional groups at their phenyl ring in combination with 1,4-dihydropyridine **2c** (Figure 4.6).

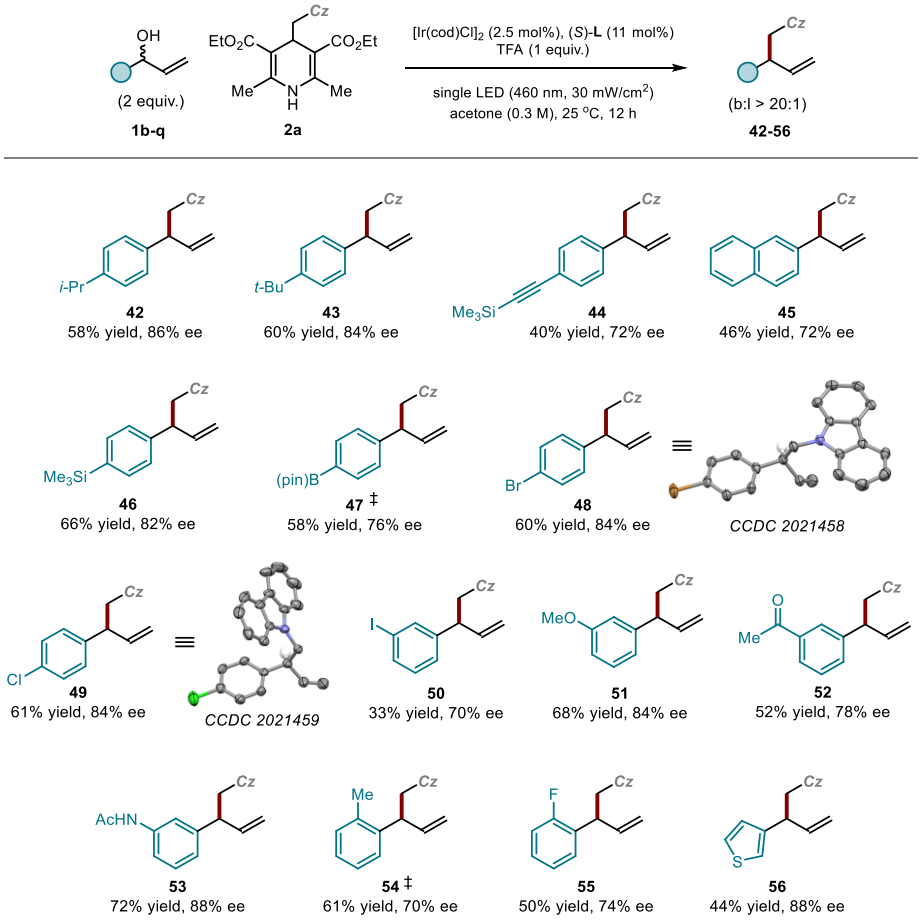

Figure 4.6: Survey of the alcohol precursors that can participate in the reaction. Reaction performed on a 0.1 mmol scale using 2 equiv. of allylic alcohol. Yields and enantiomeric excesses of the isolated products are indicated below each entry (average of two runs per substrate). ‡Using the pre-formed complex **I** as the catalyst (5 mol%). Cod, cyclooctadiene; TFA, trifluoroacetic acid; Cz, carbazole; BPin, pinacol borane; Ac, acetyl.

The protocol tolerates *para*-substituted phenyl rings bearing alkyl moieties (**42** and **43**), extended aromatic rings (**45**), and synthetic handles useful for further modifications, including alkynyl- (**44**), silyl (**46**), boron- (**47**), and halogens (**48**, **49**), yielding the desired products in good yield and high ee. Crystals from products **48** and **49** were suitable for X-ray crystallographic analysis, which unambiguously established their absolute

configurations. Substituents at *meta*-position of the aryl moiety, including halogen- (**50**), alkoxy (**51**), keto and amino-groups (**52** and **53**), were also tolerated. Introduction of *ortho*-substituents slightly affected the enantioselectivity of the reaction (**54** and **55**). We also tested the reactivity of the heteroaromatic thienyl-containing alcohol, which afforded the desired product in good yield and high ee (**56**).

4.9 Limitations of the Methodology

Figure 4.7 shows a series of radical precursors that failed to afford the desired products. One limitation of the methodology is the scarce or absent reactivity of secondary radicals (**57**, **60**, **67**, **68,** **72** and **73**).

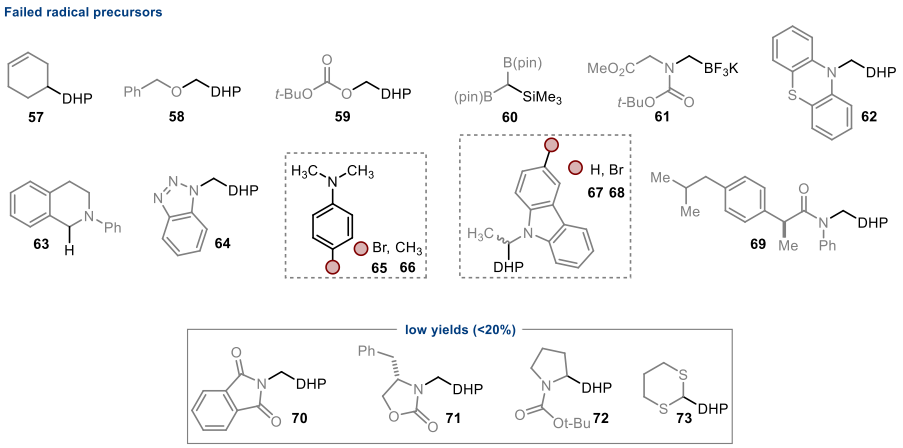

Figure 4.7: Failed and low-yielding radical precursors for the asymmetric photochemical Ir-catalyzed alkyl-alkyl cross-coupling.

Another radical precursor that failed under the reaction conditions was the simple 4-benzyl-1,4-dihydropyridine **74**. Also exposing the reaction mixture to purple-light irradiation (405 nm),[33] we could not obtain any improvement compared to the model

[33] Excitation of substrate **77** under purple light irradiation can generate benzyl radicals, see: Buzzetti, L., Prieto, A., Raha Roy, S., Melchiorre, P. "Radical-Based C−C Bond-Forming Processes Enabled by the Photoexcitation of 4-Alkyl-1,4-dihydropyridines" *Angew. Chem. Int. Ed.* **2017**, *56*, 15039.

conditions (460 nm). Full degradation of substrate **74** to by-products **23** and **76** (Scheme 4.19) was observed.

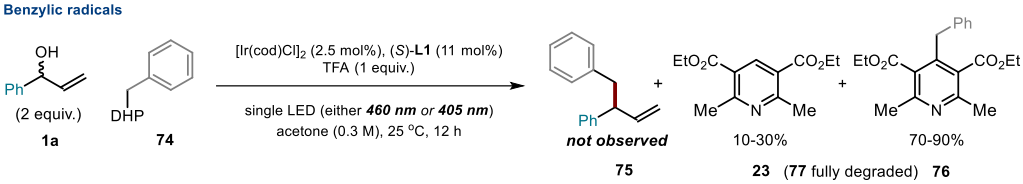

Scheme 4.19: Testing the reactivity of DHP **74** under different irradiation wavelength.

For the allylic alcohols, substrates bearing an alkyl substituent (**77**, **78**) or substituents on the olefin moiety (**79**, **80**) remained completely unreacted (Figure 4.8).

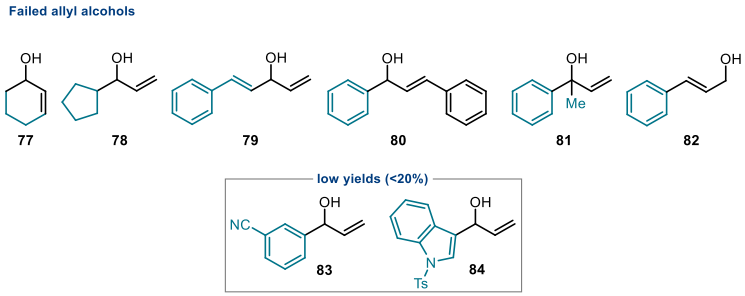

Figure 4.8: Failed and low-yielding allylic alcohols for the asymmetric photochemical Ir-catalyzed alkyl-alkyl cross-coupling.

4.10 Mechanistic Studies

In order to glean insights into the reaction mechanism, we examined one by one the key steps of this photochemical cross-coupling process. Gathering those information together we could draw a final mechanistic scenario.

Note: The following discussion will concern topics relative to luminescence and Stern-Volmer quenching studies. Therefore, the ensuing paragraph aims to provide the reader with a general overview on the phenomenon of luminescence and Stern-Volmer quenching studies.

4.10.1 Luminescence: General Principles and Stern-Volmer Quenching Studies

Luminescence is the spontaneous emission of light by a molecule in its excited state. This phenomenon originates from the intramolecular deactivation of an excited-state molecule and occurs with a specific lifetime (τ^0). From an experimental point of view, the luminescence is recorded as a spectrum of emission and can be considered the fingerprint of a molecule in its excited state (Scheme 4.20, left). Therefore, the analysis of an emission profile and its variation can give important insights related to the reaction mechanism. The rate of luminescence deactivation can be affected by a variety of processes called *quenching processes*, which can cause a decrease of the emission intensity and a shorter lifetime (τ) (Scheme 4.20, right).[34] The study of these processes takes the name of *quenching studies*.

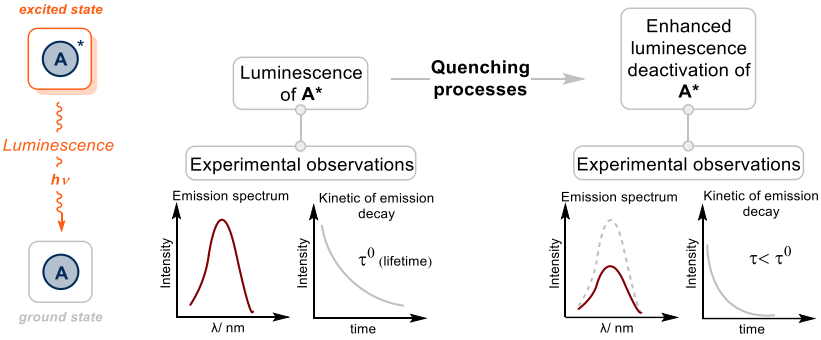

Scheme 4.20: Luminescence and quenching processes.

Among the different quenching processes possible, the only relevant one to this discussion is the *collisional quenching*, which takes place when an excited-state molecule **A*** interacts with another entity **B** (in its ground state) either via electron-transfer or energy-transfer (Scheme 4.21, top). Importantly, Stern-Volmer analysis does not inform about the nature of the collisional quenching, therefore we cannot distinguish if an electron-transfer or energy-transfer is taking place.

[34] a) Balzani, V., Ceroni, P., Juris, A. "Photochemistry and Photophysics: Concept, Research and Applications", Weinheim, Wiley-VCH, 2014; b) Turro, N. J., Ramamurthy, V., Scaiano, J. C. "Principles of Molecular Photochemistry: An Introduction", University Science Books, 2009.

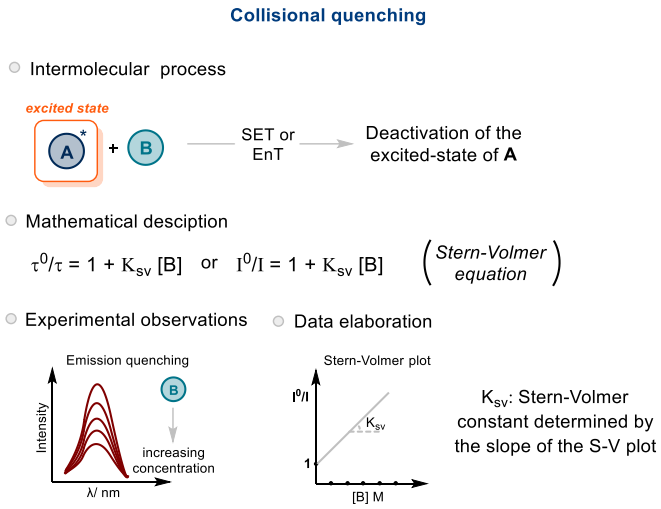

Scheme 4.21: Collisional quenching and Stern-Volmer studies.

Collisional quenching is described by the Stern-Volmer equation (Eq. 4.1). This is derived by the lifetimes ratio (τ^0/τ) of two competitive processes; the first one is the intramolecular deactivation of **A***, via luminescence, to which corresponds τ^0. The second one is the intermolecular deactivation of **A***, due to the interaction with **B**, that provides τ.

From this ratio, one can obtain the Stern-Volmer Equation:

$$\frac{\tau^0}{\tau} = 1 + \tau^0 k_q[\boldsymbol{B}] \qquad \text{Eq. 4.1}$$

In equation 4.1, the product $\tau^0 k_q$ is defined as Stern-Volmer constant K_{SV}. Therefore, the Stern-Volmer equation can be reformulated as in Equation 4.2:

$$\frac{\tau^0}{\tau} = 1 + K_{SV}[\mathbf{B}] \qquad \text{Eq. 4.2}$$

Under certain experimental conditions,[35] equation 4.2 can be written also as ratio of the emission intensity of **A*** in absence (I^0) and in presence (I) of increasing concentration of the quencher **B**.

[35] The necessary conditions are the following: i) keeping the same spectrofluorimeter settings for each measurement after the addition of the quencher; ii) the quencher must not absorb under the excitation and emission wavelengths; iii) the concentration of the fluorophore **A** should be chosen in order to have an absorbance around 0.1-0.3 at the excitation wavelength; iv) if the quencher is a charged species, the ionic strength of the solution has to be keep constant; for further details, see: reference 34.

$$\frac{I^0}{I} = 1 + K_{SV}[B] \qquad \text{Eq. 4.3}$$

This new expression enables a simplified experimental analysis of the quenching rate. In the current discussion, we used Equation 4.3 to assess if the photoexcited (η^3-allyl)iridium(III) complex **I** undergoes quenching by substrate **2a**.

4.10.2 Application of the Stern-Volmer Quenching Studies

According to what discussed in the previous paragraph, we used Stern-Volmer quenching analysis to evaluate if the excited complex **I** interacts with the radical precursor trimethylsilyl carbazole **2a**,[36] which would act as a quencher. We recorded the emission spectrum of complex **I** since the prerogative starting point for any quenching experiment is the emissivity of the chromophore under study. Complex **I**, upon excitation with monochromatic light set at 480 nm, produced an intense emission centered at 535 nm (Figure 4.9).

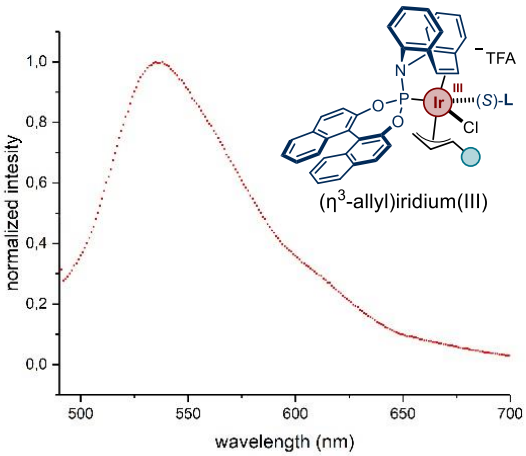

Figure 4.9 Normalized emission spectrum of the preformed (η^3-allyl)iridium(III) complex **I** (excitation wavelength at 480 nm), maximum peak at 535 nm.

A series of Stern-Volmer quenching experiments on such emission indicated a pronounced quenching by progressive addition of a solution containing trimethylsilyl carbazole **2a** ([**2a**]>>[**I**]) (Figure 4.8 top). By means of the Stern-Volmer plot (Eq. 4.3), we found a linear correlation between the concentration of the quencher **2a** and the ratio

[36] **2a** was a competent substrate for the photochemical radical cross-coupling, see Table 4.1 for details.

of I^0/I. From the slope of the line, we could estimate the Stern-Volmer constant to be 137 M^{-1} (Figure 4.10, bottom).

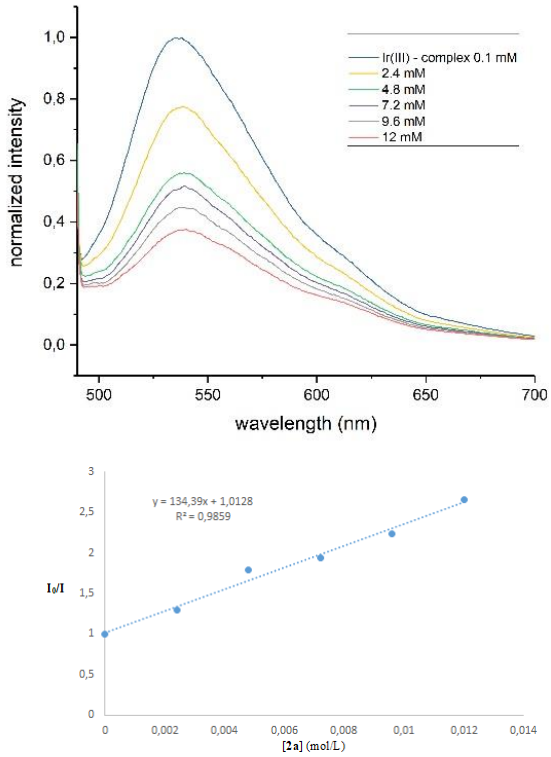

Figure 4.10: Quenching of the complex **I** emission (0.1 mM in $CHCl_3$) in the presence of increasing amounts of silane **2a** (above) and the corresponding Stern-Volmer quenching plot (below).

Applying the correction factor, coming from UV-vis analysis of the sample at each addition of the quencher, we estimated a final K_{sv} of 102 M^{-1}. The correction factor accounts for different experimental aspects, including: i) sample dilution, ii) minimal degradation of complex **I** because of its participation in the cross-coupling or its eventual photo-instability. From the aforementioned UV-vis analysis, we could also assess that no pre-association of complex **I** and quencher **2a** was taking place since no new absorption bands were observed (Figure 4.11). Overall, this finding confirmed the interaction of the excited-state complex **I** with substrate **2a**, which is consistent with our mechanistic hypothesis that substrate **2a** can be activated by the excited complex **I**.

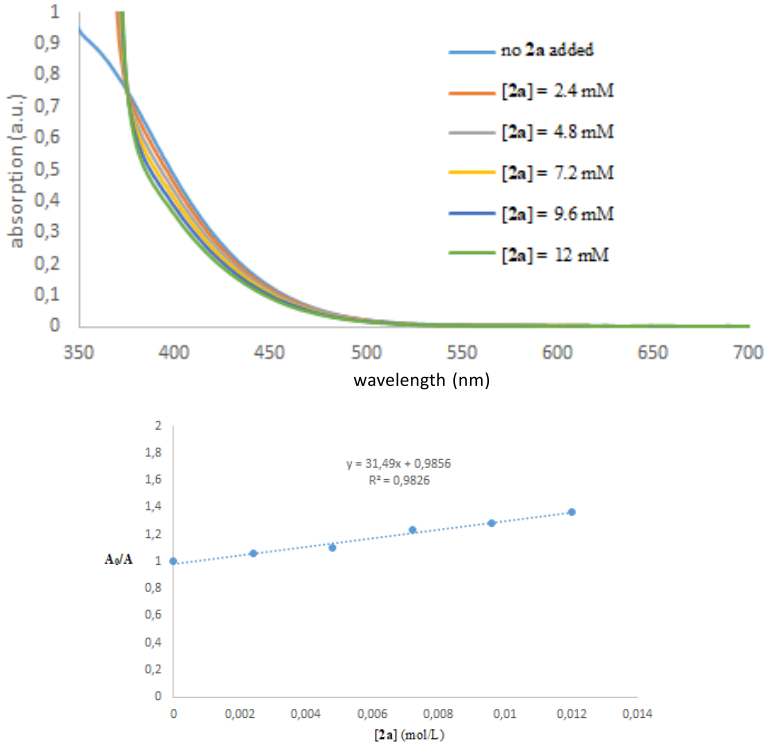

Figure 4.11: Absorption spectra of **I** with increasing amounts of quencher **2a**. No spectral variation are observed (above). Slight decrease in absorption of **I** during the quenching experiment (below).

4.10.3 Generation of Radicals

One crucial aspect of our proposed mechanism is the ability of (η^3-allyl)iridium(III) complex **I** to generate, upon photoexcitation, radicals via SET oxidation of substrates **2**. To prove this pathway, we tested the ability of complex **I** (5 mol%) to promote the formation of radical **XXVII** from dihydropyridine **2c**, which then undergoes addition to ally sulfone **85**, serving as radical trap (Scheme 4.22). Since the iridium complex is present only in catalytic amount, the reaction needs tris(4-bromophenyl)amine (TBPA) as redox mediator (E (TBPA$^{\bullet+}$/TBPA) = +1.05 V) in order to sustain the reactivity.[37] After 12 hours of irradiation, the desired allylation product **86** was obtain in good yields, thus giving an indication of the ability of photoexcited complex **I** to promote the formation of radical **XXVII**.

[37] Herath, A. C., Becker, J. Y. "Kinetics of Redox Mediator Tris(4-Bromophenyl) Amine in Acetonitrile and Ionic Liquid [Bmim][PF6]: Oxidation of Benzyl and Cyclohexyl Alcohols" *J. Electroanal. Chem.* **2008** *619–620*, 98.

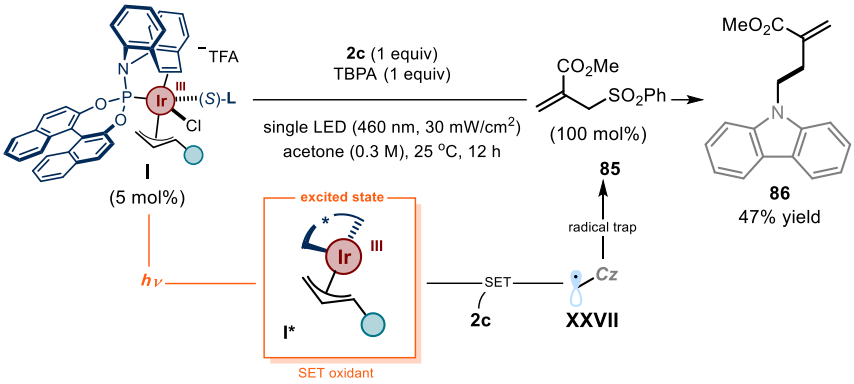

Scheme 4.22: Proving the formation of radicals that trigger a desulfonylative allylation process.

In addition, we performed the model photochemical reaction with substrate **2c** and alcohol **1a** in the presence of (2,2,6,6-tetramethylpiperidin-1-yl)oxidanyl (TEMPO) as radical scavenger, obtaining the TEMPO-adduct **87** in good yield (Scheme 4.23). This result further supports the formation of open-shell intermediates under the reaction conditions.

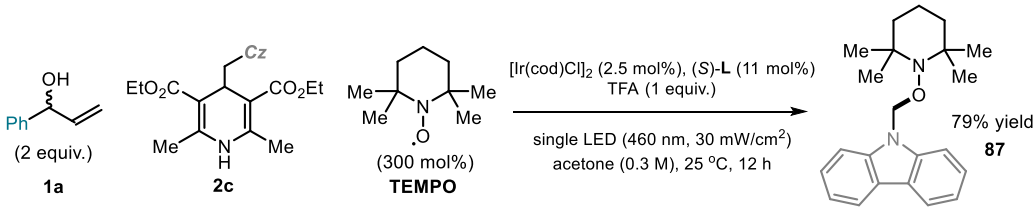

Scheme 4.23: Trapping the radical α-amino radicals with TEMPO.

4.10.4 Evaluating a Radical Chain Propagation Mechanism

We then evaluated the possibility that a radical chain propagation mechanism could be operative. In this scenario, radical **XXVII**, generated upon SET oxidation of substrate **2c**, would attack a ground state Ir(III)-allyl intermediate **I**, delivering product **3** and a fleeting Ir(II) complex **XXVIII** (Scheme 4.29). This latter would start a chain propagation event oxidizing a second molecule of **2c**, affording the Ir(I) pre-catalyst **XXIX** that, after oxidative addition with the allylic alcohol substrate **2**, regenerates complex **I**. The SET event between **XXIX** and substrate **2** would be needed to feed a self-propagation radical process where the photoactivity of complex **I** would solely serve as an initiation.

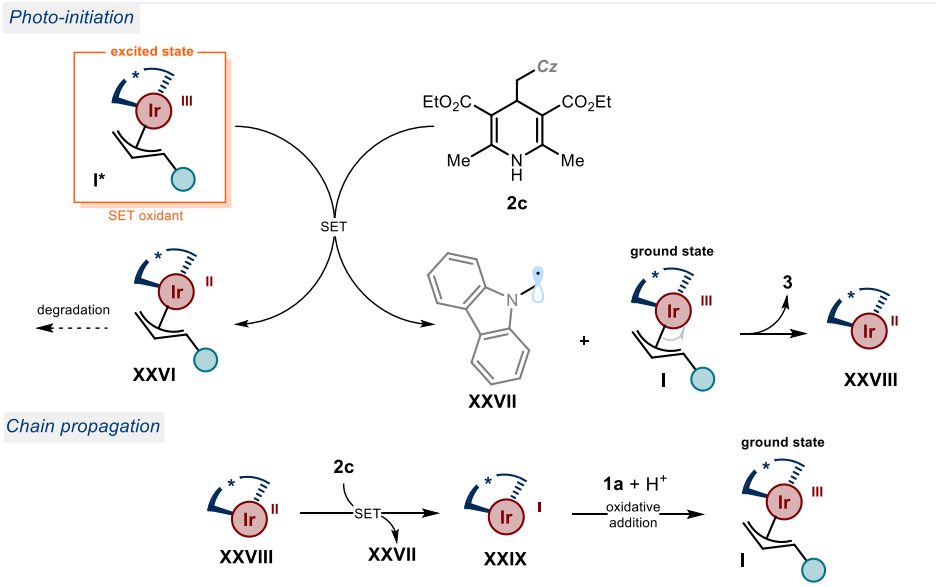

Scheme 4.24: Possible radical chain mechanism.

To evaluate the feasibility of this chain mechanism, we designed an experiment in which the radicals were generated in the absence of light, so to verify if a radical addition to the ground-state electrophilic Ir(III)-π-allyl complex **I** could be the key C-C bond forming step. Specifically, we found that a combination of cerium ammonium nitrate (CAN), which could act as an SET oxidant (E(Ce(IV)/Ce(III) = +0.96 V) instead of complex **I**, and TBPA, which served as a redox mediator, was suitable to generate radicals from substrate **2c** in the dark. In fact, this protocol was used to replicate the results of the radical desulfonylative allylation depicted in Scheme 4.22 (see results in Scheme 4.25). Overall, these thermal conditions provided a way to generate radicals from **2c** (a competent substrate in our cross-coupling protocol) in the absence of light.

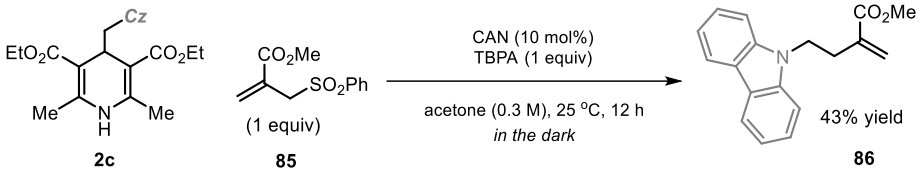

Scheme 4.25: Generating radicals in the absence of light via a CAN/TBPA combination.

We then used the CAN/TBPA system in the model reaction to mimic the radical initiation step in the absence of light (Scheme 4.26). Product **3a** was obtained only in traces,

indicating that, even if radical **XXVII** might add on the ground-state iridium complex **I**, the emerging Ir(II) intermediate **XXVIII** cannot sustain a radical chain propagation.

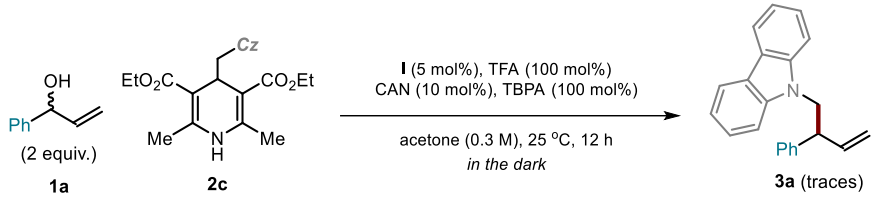

Scheme 4.26: Evaluating a possible radical chain propagation mechanism.

To prove the compatibility of the CAN/TBPA combination with complex **I**, we repeated the same reaction depicted in Scheme 4.26, but this time under blue light irradiation. Product **3a** was obtained in similar yields and ee as the model rection, confirming once again that light is essential for the process (Scheme 4.27).

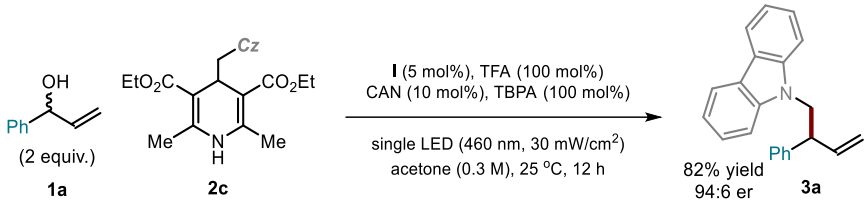

Scheme 4.27: Verifying the compatibility of **I** and CAN/TBPA. These additives do not affect the catalyst performance under light irradiation.

Finally, we conducted quantum yield measurements of the Ir-catalyzed photochemical coupling reaction between **1a** and both silane substrates **2a** and **2c**. The overall quantum yield (Φ) of a photochemical reaction gives an important indication on whether a radical chain mechanism is operational. For a given photochemical reaction, the corresponding Φ is a dimensionless value, which expresses the number of molecules produced per photon absorbed by the chromophore and it is described by Eq. 4.4:

$$\Phi = \frac{mol\ of\ product\ formed}{mol\ of\ photons\ absorbed} \qquad \text{Eq. 4.4}$$

A $\Phi > 1$ indicates that a radical chain mechanism is taking place, since per each photon absorbed by the reaction, more than one molecule of product is formed. Thus, light only initiate a self-propagating radical mechanism, which continues in the dark. Conversely, for $\Phi < 1$ *it is likely* that a radical chain is not taking place. In our case, the quantum yields

measured for the reactions with substrates **2a** and **2c** were both below 1, respectively (Φ = 0.13 and 0.8, respectively) indicating that a radical chain mechanism is unlikely.

Collectively, the mechanistic results discussed in this section indicate that a radical-chain process triggered by the radical addition to the ground-state complex **I** is highly unlikely.

4.10.5 Origin of the Stereoselectivity

With the aim to prove the origin of the stereoselectivity, we performed two reactions employing the enantiopure allylic alcohol (*S*)-**1a** in the presence of both enantiomers of the chiral ligand **L1** (Scheme 4.28). In either cases, the cross-coupling product **3a** was obtained in comparable yield but with opposite absolute configuration. These experiments suggested that any stereochemical information present in the alcohol substrate (*S*)-**1a** is erased upon oxidative addition with the allyl-iridium(III) complex **I**, and the absolute configuration of the product is dictated solely by the chiral ligand.

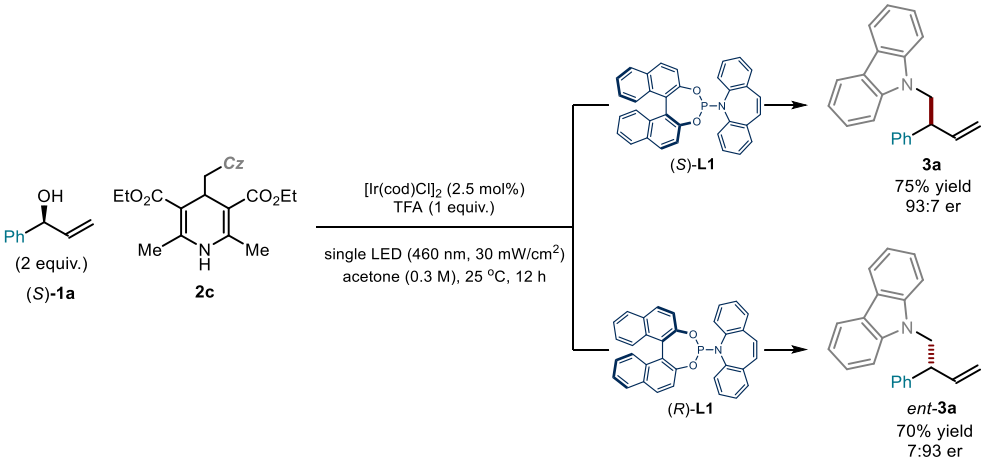

Scheme 4.28: Investigating the origin of stereoselectivity.

4.10.6 Proposed Mechanism

The gather of the mechanistic information showed in the previous paragraph supports the catalytic cycle depicted in Scheme 4.29. The process starts with the formation of the (η^3-allyl)iridium(III) complex **I** by acid promoted oxidative addition of the Ir(I) catalyst **XXIX**, generated from $[Ir(cod)Cl]_2$ and two equivalents of ligand **L**, to allylic alcohol **1**. Upon blue light excitation, the Ir(III) complex **I*** reveals its oxidizing properties, activating the radical precursor **2** via SET oxidation. This redox step switches on a unique reaction pattern, since it triggers the simultaneous formation of radical **XXXI**, upon

fragmentation of the radical cation **XXX**, and of the iridium(II) center **XXVI**. The latter fleeting intermediate then intercepts **XXXI** via radical-metal crossover to afford a more stable iridium(III) complex **XXXII**. A regio- and stereo-determining reductive elimination eventually forges the C(sp^3)-C(sp^3) bond within product **3** while restoring the active Ir(I)-catalyst **I**.

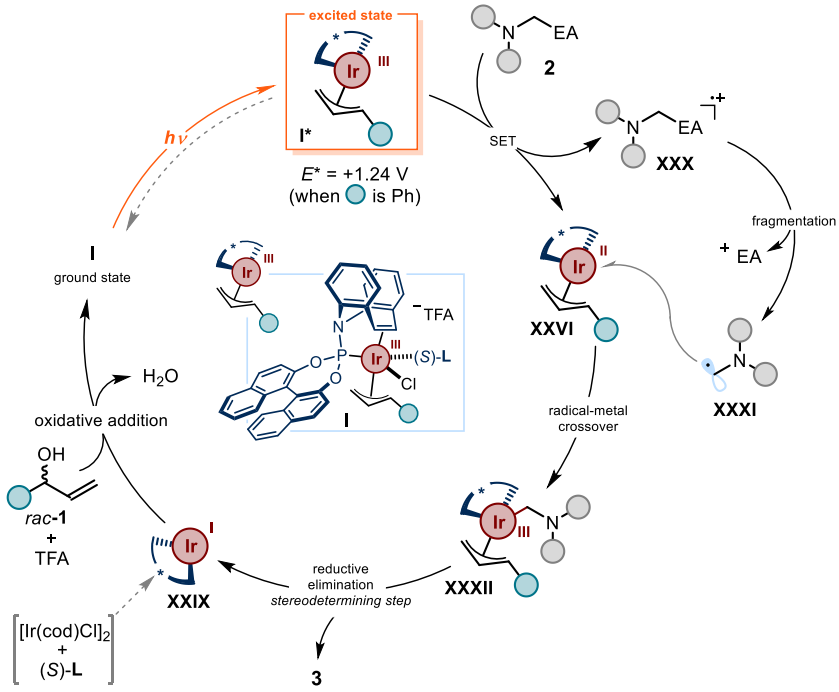

Scheme 4.29: Proposed catalytic cycle.

4.11 Conclusion

Our studies demonstrated that chiral organometallic intermediates with an established thermal reactivity can be repurposed to mediate mechanistically different enantioselective processes using simple light excitation. In particular, we found that the (η^3-allyl)iridium(III) complex **I**, which is a known electrophilic intermediate in polar asymmetric allylation, when excited with weak blue light can reveal oxidizing properties. We exploited this feature to generate α-amino radicals via SET activation of non-nucleophilic radical precursors, which would not react under thermal conditions. In addition, this photochemical strategy generates an elusive transition metal species (**XXVI**), whose reactivity triggers a difficult-to-realize enantioselective alkyl-alkyl cross

coupling process. The reaction is operationally simple, tolerates different functional groups and is amenable to the stereocontrolled introduction of biological relevant molecules and drugs in the final products. Lastly, the effectiveness of this methodology expanded the limited repertoire of asymmetric catalytic tools empowered by light excitation, serving as blueprint to further studies on the photochemistry of chiral organometallic intermediates.

4.12 Experimental Section

General Information. The ^{1}H NMR, ^{13}C NMR spectra and UPC[2] traces are available in the literature[1] and are not reported in the present thesis.

The NMR spectra were recorded at 300 MHz, 400 MHz and 500 MHz for ^{1}H, at 75 MHz, 101 MHz and 125 MHz for ^{13}C, at 376 MHz for ^{19}F and at 162 and 202 MHz for ^{31}P. The chemical shifts (δ) for ^{1}H and ^{13}C are given in ppm relative to residual signals of the solvents ($CHCl_3$ @ 7.26 ppm ^{1}H NMR, 77.16 ppm ^{13}C NMR; DMSO @ 2.54 ppm ^{1}H NMR, 40.45 ppm ^{13}C NMR). Coupling constants (*J*) are given in Hz, and are quoted to the nearest 0.5 Hz. The following abbreviations are used to indicate the multiplicity: s, singlet; d, doublet; t, triplet; q, quartet; sext, sextet; hept, heptuplet; m, multiplet. Additionally, signals can be described as broad (br) and apparent (app).

High-resolution mass spectra (HRMS) were obtained from the ICIQ High Resolution Mass Spectrometry Unit on MicroTOF Focus and Maxis Impact (Bruker Daltonics) with electrospray ionization. Optical rotations were measured on a Polarimeter Jasco P-1030 and are reported as follows: $[\alpha]_D^T$ (c in g per 100 mL, solvent).

UV-vis measurements were carried out on a UV-Vis cary60-TR0 spectrophotometer equipped with photomultiplier detector, double beam optics and D2 and W light sources. Emission spectra were recorded on a Fluorolog Horiba Jobin Yvon spectrofluorimeter, equipped with a photomultiplier detector, a double monochromator, and a 350W xenon light source.

Cyclic voltammetry studies were carried out on a Princeton Applied Research PARSTAT 2273 potentiostat offering compliance voltage up to ± 100 V (available at the counter electrode), ± 10 V scan range and ± 2 A current range. Cyclic voltammetry and differential pulse voltammetry (DPV) analyses, performed on air-sensitive compounds, were obtained using a CH Instruments CHI660C electrochemical workstation installed inside a glovebox, in order to secure measurements under inert atmosphere. The latter experimental set-up was courtesy of the Llobet group at ICIQ.

The authors are indebted to the team of the Research Support Area at ICIQ.

General Procedures. All reactions were set up under an argon atmosphere in oven-dried glassware using standard Schlenk techniques, unless otherwise stated. Synthesis and HPLC grade solvents were used as purchased. Anhydrous solvents were taken from a commercial SPS solvent dispenser. Chromatographic purification of products was accomplished using force-flow chromatography (FC) on silica gel (35-70 mesh). When required, neutralization of silica gel was accomplished adding 3-4 mL of triethylamine

per 150 g of silica powder. For thin layer chromatography (TLC) analyses throughout this work, Merck precoated TLC plates (silica gel 60 GF_{254}, 0.25 mm) were employed. UV light was used as the visualizing agent, and either an ethanol solution of phosphomolybdic acid or basic aqueous potassium permanganate ($KMnO_4$), and heat served as developing agents. Organic solutions were concentrated under reduced pressure on a Büchi rotary evaporator (in vacuo at 40 ºC, ~5 mbar).

Determination of Enantiomeric Purity: HPLC analyses on chiral stationary phase were performed on an Agilent 1200 series HPLC, using a Daicel Chiralpak IC-3 column. UPC^2 analyses on chiral stationary phases were performed on a Waters ACQUITY® UPC^2 instrument, using either Daicel Chiralpak IB-3 and IG-3 columns, or a CHIRALCEL® OJ-3 chiral column. For each compound, the exact conditions for the analysis are specified within the characterization section (*Section E*). HPLC/UPC^2 traces were compared to racemic samples prepared by running the reactions under the conditions specified in *Section E* of the Supplementary Information.

Materials: Commercial grade reagents and solvents were purchased at the highest commercial quality from Sigma Aldrich, Fluka, Acros Organics, Fluorochem or Alfa Aesar and used as received, unless otherwise stated. The $[Ir(cod)Cl]_2$ dimer precatalyst was purchased from Strem Chemicals. Both the iridium catalyst and the chiral ligands were stored at -20 ºC, and in the dark, prior to use. Allylic alcohol **1a**, also in its enantiopure form, is commercially available and has been purchased from Sigma Aldrich.

4.12.1 General Procedure for the Asymmetric Photochemical Ir-Catalyzed Cross-Coupling

GP1 – General Procedure

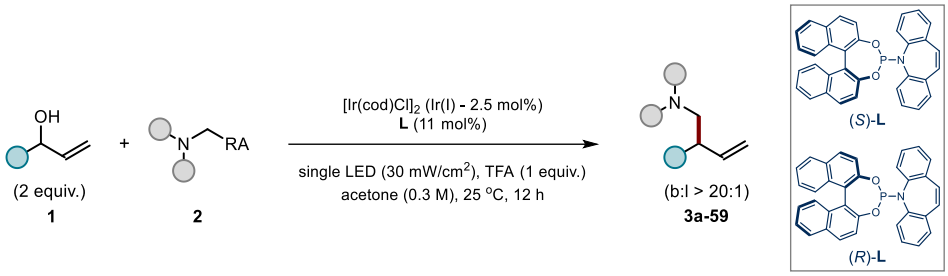

Scheme 4.30: General procedure for the enantioselective transformation.

A screw-capped vial, fitted with a rubber septum, was charged with $[Ir(cod)Cl]_2$ (1.7 mg, 2.50 μmol, 2.5 mol%), the appropriate enantiomer of chiral ligand **L** (5.6 mg, 11.0 μmol, 11 mol%) and anhydrous, argon-purged reaction solvent (300 μL), under an argon atmosphere. The resulting solution was vigorously stirred for 15 minutes and then transferred to a Schlenk tube containing the allylic alcohol **1** (200 μmol, 2 equiv.) and the radical precursor **2** (100 μmol, 1 equiv.), affording a yellow solution. TFA (7.7 μL, 100 μmol, 1 equiv.) was added to this solution and the Schlenk tube was sealed with a screw-cap. The vessel was placed into a 3D-printed plastic support mounted on an aluminum block fitted with a 460 nm high-power single LED (λ = 460 nm, irradiance = 30 mW/cm^2 as controlled by an external power supply; a detailed representation of the set-up is depicted in Figure 4.12). This set-up secured a reliable irradiation while keeping a constant distance of 1 cm between the bottom of the reaction vessel and the light source. The reaction was stirred under visible light irradiation at ambient temperature for 12 hours, prior to removal of the solvent under reduced pressure. Purification of the crude mixture by flash column chromatography on silica gel gave the corresponding products **3-56** in the stated yield and enantiomeric purity. All of the obtained cross-coupling products were previously unknown.

N.B. When pre-formed complex **I** was used as the catalyst, a solution of the latter (7.6 mg, 5 mol%) in 300 μL of the appropriate solvent was directly charged into the reaction vessel, containing **1** and **2**.

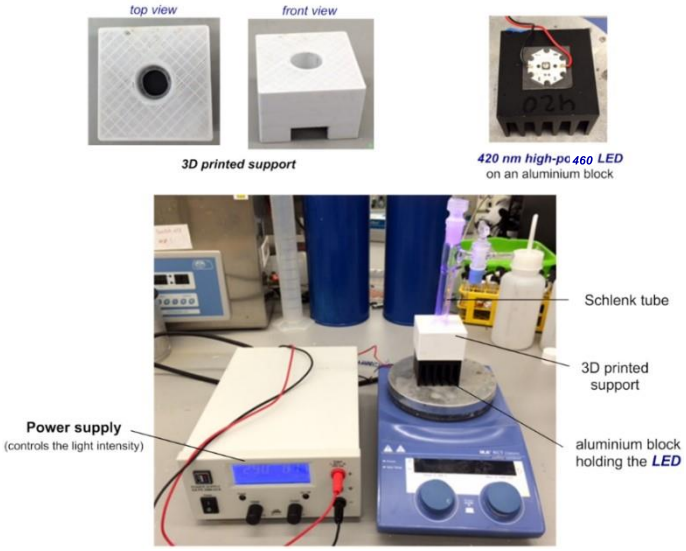

Figure 4.12: Detailed set-up and illumination system. The light source for illuminating the reaction vessel consisted in a 460 nm high-power single LED (LZ1-00DB00) purchased from OSA OPTO**.**

Synthesis of Racemic Coupling Products

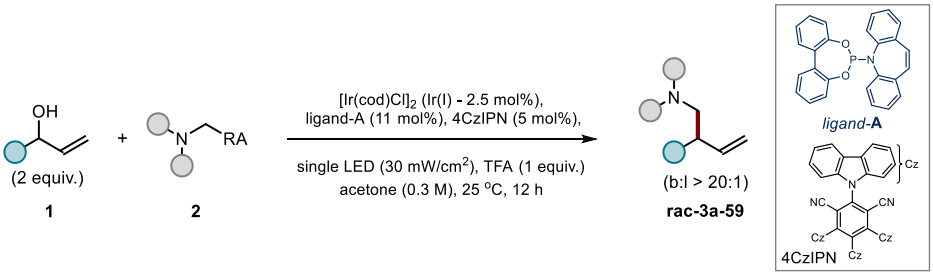

Scheme 4.31: General procedure for the racemic transformation.

The synthesis of the racemic products **3-59**, needed for enantiomeric ratio determination, was initially attempted performing protocol **GP1** in the presence of 11 mol% of an equimolar mixture of ligands (*S*)-**L1** and (*R*)-**L1**. However, the resulting racemic (η^3-allyl)iridium(III) **I** complex was insoluble in the reaction solvents, thwarting the efficiency of the photochemical method. To overcome this issue, a different procedure was developed (depicted in Scheme S4.2): the reaction was carried out in the presence of ligand **A** and photocatalyst 1,2,3,5-tetrakis(carbazol-9-yl)-4,6-dicyanobenzene (4CzIPN), both of which were synthesized according to reported procedures.[18,38] In all

[38] Luo, J., Zhang, J. "Donor–acceptor Fluorophores for Visible-light-promoted Organic Synthesis: Photoredox/Ni Dual Catalytic C(sp3)–C(sp2) Cross-coupling" *ACS Catal.* **2016**, *6*, 873.

case, this protocol delivered the corresponding racemic products with decreased chemical yield compared to our asymmetric photochemical method (**GP1**).

4.12.2 Characterization Data of Products 3a-41

(*S*)-9-(2-phenylbut-3-en-1-yl)-9*H*-carbazole (3a)

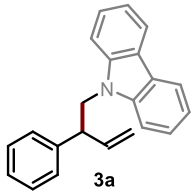

3a

Prepared according to the general procedure using $[Ir(cod)Cl]_2$/(*S*)-**L1** as the catalytic system, diethyl 4-((9*H*-carbazol-9-yl)methyl)-2,6-dimethyl-1,4-dihydropyridine-3,5-dicarboxylate **2c** (43.3 mg, 100 µmol) and 1-phenylprop-2-en-1-ol **1a** (26.0 µL, 200 µmol) as the substrates, and performing the reaction in acetone. The crude mixture was purified by flash column chromatography (isocratic 5% PhMe in hexane) to afford product **3a** (24.0 mg, 80% yield, 94:6 er) as a colorless oil. The enantiomeric ratio was determined by UPC^2 analysis on a Daicel Chiralpak IB-3 column: gradient CO_2/CH_3CN from 100% CO_2 to 60:40 over 4 minutes, curve 6, flow rate 2 mL/min, λ = 260 nm: τ_{major} = 4.1 min, τ_{minor} = 4.3 min; $[\alpha]_D^{26}$ = +2.0 (c = 1.00, CH_2Cl_2, 94:6 er).

^{1}H NMR (500 MHz, $CDCl_3$): δ 8.06 (dt, *J* = 7.5, 1.0 Hz, 2H), 7.38 (ddd, *J* = 8.5, 7.0, 1.0 Hz, 2H), 7.27 – 7.21 (m, 4H), 7.22 – 7.14 (m, 5H), 6.13 (ddd, *J* = 17.0, 10.5, 7.5 Hz, 1H), 5.01 (dt, *J* = 10.5, 1.0 Hz, 1H), 4.95 (dt, *J* = 17.0, 1.5 Hz, 1H), 4.61 (dd, *J* = 14.5, 8.0 Hz, 1H), 4.48 (dd, *J* = 14.5, 7.0 Hz, 1H), 4.02 (app q, *J* = 7.5 Hz, 1H).

^{13}C NMR (126 MHz, $CDCl_3$): δ 141.4, 140.7, 138.4, 128.8, 127.9, 127.2, 125.6, 123.0, 120.4, 119.0, 117.0, 109.1, 49.4, 49.1.

HRMS (ESI) Exact mass calculated for $C_{22}H_{20}N$ $[M+H]^+$: 298.1590, found: 298.1592.

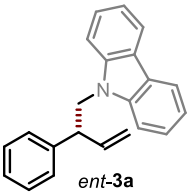

ent-**3a**

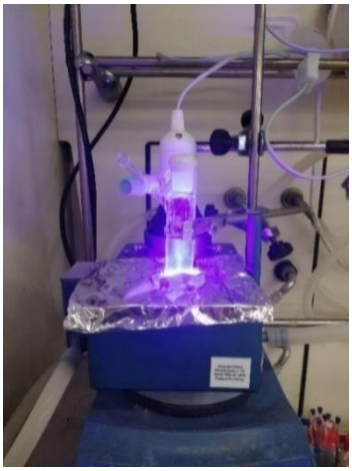

1 mmol scale reaction: A screw-capped vial, fitted with a rubber septum, was charged with $[Ir(cod)Cl]_2$ (17.0 mg, 25.0 µmol), chiral ligand (*R*)-**L1** (56.0 mg, 110.0 µmol) and anhydrous, argon-sparged acetone (3 mL), under an argon atmosphere. The resulting solution was vigorously stirred for 15 minutes and, then, transferred to a 20 mL Schlenk tube containing 1,4-dihydropyridine **2c** (1.00 mmol) and allylic alcohol **1a** (2.00 mmol), affording a yellow solution. TFA (78.0 µL, 1.00 mmol) was added to this solution and the vial was sealed with a glass stopper. The vessel was placed into a HepatoChem PhotoRedox TC photoreactor, fitted with an EvoluChem™ lamp (λ = 450-455 nm), and connected to a programmable chiller, securing the temperature to be kept at 25 ºC (see pictures on the right). The reaction was stirred under visible light irradiation for 18 hours, prior to removal of the solvent under reduced pressure. Purification of the crude mixture by flash column chromatography on silica gel (isocratic 5% PhMe in hexane) afforded product *ent*-**3a** (200 mg, 68% yield, 6:94 er) as a colorless oil. The enantiomeric ratio was determined by UPC[2] analysis on a Daicel Chiralpak IB-3 column: gradient CO_2/CH_3CN from 100% CO_2 to 60:40 over 9 minutes, curve 6, flow rate 2 mL/min, λ = 260 nm: τ_{minor} = 4.1 min, τ_{major} = 4.3 min. ; $[\alpha]_D^{26}$ = -6.9 (c = 0.23, CH_2Cl_2, 6:94 er). The spectra obtained for compound *ent*-**3a** were identical to those obtained for its enantiomer **3a**.

(*S*)-3-ethyl-9-(2-phenylbut-3-en-1-yl)-9*H*-carbazole (25)

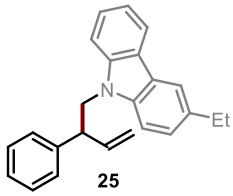

25

Prepared according to the general procedure, using $[Ir(cod)Cl]_2$/(*S*)-**L1** as the catalytic system, diethyl 4-((3-ethyl-9*H*-carbazol-9-yl)methyl)-2,6-dimethyl-1,4-dihydropyridine-3,5-dicarboxylate **2d** (46.0 mg, 100 µmol) and 1-phenylprop-2-en-1-ol **1a** (26.0 µL, 200 µmol) as the substrates, and performing the reaction in acetone. The crude mixture was purified by flash column chromatography (isocratic 5% PhMe in hexane) to afford product **25** (20.5 mg, 63% yield, 89:11 er) as a pale yellow oil. The enantiomeric ratio was determined by UPC[2] analysis on a Daicel Chiralpak IB-3 column: gradient CO_2/CH_3CN from 100% CO_2 to 60:40 over 4 minutes, curve 6, flow rate 2 mL/min, λ =

260 nm: τ_{major} = 5.0 min, τ_{minor} = 5.4 min; $[\alpha]_D^{26}$ = +0.9 (c = 0.22, $CHCl_3$, 89:11 er). The absolute configuration for the title compound was assigned in comparison to compounds **48** and **49**.

^{1}H NMR (400 MHz, $CDCl_3$): δ 8.08 (dt, *J* = 7.5, 1.0 Hz, 1H), 7.93 (t, *J* = 1.0 Hz, 1H), 7.40 (ddd, *J* = 8.5, 7.0, 1.0 Hz, 1H), 7.36 – 7.17 (m, 9H), 6.18 (ddd, *J* = 17.5, 10.5, 7.5 Hz, 1H), 5.06 (dt, *J* = 10.5, 1.0 Hz, 1H), 4.99 (dt, *J* = 17.5, 1.0 Hz, 1H), 4.64 (dd, *J* = 14.5, 8.0 Hz, 1H), 4.51 (dd, *J* = 14.5, 6.5 Hz, 1H), 4.07 (q, *J* = 7.5 Hz, 1H), 2.87 (q, *J* = 7.5 Hz, 2H), 1.38 (t, *J* = 7.5 Hz, 3H).

^{13}C NMR (101 MHz, $CDCl_3$): δ 141.5, 141.0, 139.2, 138.5, 135.0, 128.8, 127.9, 127.1, 126.0, 125.4, 123.1, 122.9, 120.2, 119.1, 118.7, 117.0, 109.0, 108.8, 49.5, 49.2, 29.0, 16.6.

HRMS (ESI) Exact mass calculated for $C_{24}H_{23}N$ $[M+H]^+$: 326.1903, found: 326.1903.

(*S*)-3-fluoro-9-(2-phenylbut-3-en-1-yl)-9*H*-carbazole (26)

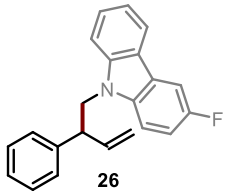

26

Prepared according to the general procedure, using $[Ir(cod)Cl]_2$/(*S*)-**L1** as the catalytic system, 3-fluoro-9-((trimethylsilyl)methyl)-9*H*-carbazole **2e** (27.0 mg, 100 µmol) and 1-phenylprop-2-en-1-ol **1a** (26.0 µL, 200 µmol) as the substrates, and performing the reaction in acetone. The crude mixture was purified by flash column chromatography (isocratic 5% PhMe in hexane) to afford product **26** (19.5 mg, 61% yield, 94:6 er) as a colorless wax. The enantiomeric ratio was determined by UPC^2 analysis on a Daicel Chiralpak IB-3 column: gradient CO_2/CH_3CN from 100% CO_2 to 60:40 over 4 minutes, curve 6, flow rate 2 mL/min, λ = 260 nm: τ_{major} = 3.4 min, τ_{minor} = 3.5 min; $[\alpha]_D^{26}$ = -13.3 (c = 0.21, $CHCl_3$, 94:6 er). The absolute configuration for the title compound was assigned in comparison to compounds **48** and **49.**

^{1}H NMR (400 MHz, $CDCl_3$): δ 8.01 (d, *J* = 8.0 Hz, 1H), 7.74 – 7.67 (m, 1H), 7.42 (ddd, *J* = 8.5, 7.0, 1.0 Hz, 1H), 7.30 – 7.05 (m, 9H), 6.15 (ddd, *J* = 17.5, 10.5, 7.5 Hz, 1H), 5.06 (dd, J = 10.5, 1.0 Hz, 1H), 5.00 (dt, J = 17.0, 1.0 Hz, 1H), 4.61 (dd, *J* = 14.5, 8.0 Hz, 1H), 4.48 (dd, *J* = 14.5, 7.0 Hz, 1H), 4.00 (q, *J* = 7.5 Hz, 1H).

^{13}C NMR (101 MHz, $CDCl_3$): δ δ 157.3 (d, $^1J_{C\text{-}F}$ = 235.2 Hz), 141.5, 141.2, 138.3, 137.1, 128.8, 127.9, 127.2, 126.2, 123.3 (d, $^3J_{C\text{-}F}$ = 9.4 Hz), 122.5 (d, *J* = 4.1 Hz), 120.6, 119.0, 117.1, 113.3 (d, $^2J_{C\text{-}F}$ = 25.5 Hz), 109.6 (d, $^3J_{C\text{-}F}$ = 9.0 Hz), 109.3, 106.0 (d, $^2J_{C\text{-}F}$ = 23.7 Hz), 49.4, 49.3.

^{19}F NMR (376 MHz, $CDCl_3$) δ -125.39 – -125.47 (m, 1F).

HRMS (ESI) Exact mass calculated for $C_{22}H_{18}FN$ $[M+H]^+$: 316.1496, found: 316.1494.

(*S*)-3-bromo-9-(2-phenylbut-3-en-1-yl)-9*H*-carbazole (27)

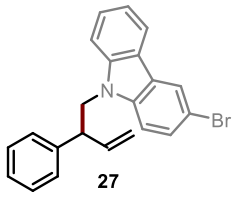

27

Prepared according to the general procedure, using $[Ir(cod)Cl]_2$/(*S*)-**L1** as the catalytic system, diethyl 4-((3-bromo-9*H*-carbazol-9-yl)methyl)-2,6-dimethyl-1,4-dihydropyridine-3,5-dicarboxylate **2f** (51.0 mg, 100 µmol) and 1-phenylprop-2-en-1-ol **1a** (26.0 µL, 200 µmol) as the substrates, and performing the reaction in acetone. The crude mixture was purified by flash column chromatography (isocratic 5% PhMe in hexane) to afford product **27** (27.5 mg, 72% yield, 96:4 er) as a colorless wax. The enantiomeric ratio was determined by UPC^2 analysis on a Daicel Chiralpak IB-3 column: gradient CO_2/CH_3CN from 100% CO_2 to 60:40 over 9 minutes, curve 6, flow rate 2 mL/min, λ = 260 nm: τ_{major} = 4.9 min, τ_{minor} = 5.1 min; $[\alpha]_D^{26}$ = -6.8 (c = 0.31, $CHCl_3$, 96:4 er). The absolute configuration for the title compound was assigned in comparison to compounds **48** and **49**.

^{1}H NMR (400 MHz, $CDCl_3$): δ 8.19 (d, *J* = 2.0 Hz, 1H), 8.04 (dt, *J* = 8.0, 1.0 Hz, 1H), 7.51 – 7.41 (m, 2H), 7.34 – 7.21 (m, 5H), 7.20 – 7.14 (m, 2H), 7.11 (d, *J* = 8.5 Hz, 1H), 6.13 (ddd, *J* = 17.0, 10.5, 7.5 Hz, 1H), 5.09 (dt, *J* = 10.5, 1.0 Hz, 1H), 5.02 (dt, *J* = 17.0, 1.0 Hz, 1H), 4.63 (dd, *J* = 14.5, 8.0 Hz, 1H), 4.50 (dd, *J* = 14.5, 7.0 Hz, 1H), 4.02 (q, *J* = 7.5 Hz, 1H).

^{13}C NMR (101 MHz, $CDCl_3$): δ 141.1, 140.9, 139.3, 138.2, 128.9, 128.2, 127.8, 127.3, 126.4, 124.6, 123.1, 122.0, 120.6, 119.5, 117.2, 111.8, 110.5, 109.3, 49.3, 49.2.

HRMS (ESI) Exact mass calculated for $C_{22}H_{18}BrN$ $[M+H]^+$: 376.0695, found: 376.0679.

(*S*)- 9-(2-phenylbut-3-en-1-yl)-3-(4,4,5,5-tetramethyl-1,3,2-dioxaborolan-2-yl)-9*H*-carbazole (28)

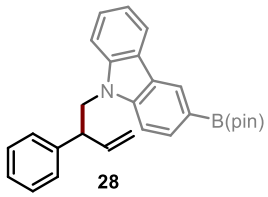

28

Prepared according to the general procedure, using $[Ir(cod)Cl]_2$/(*S*)-**L1** as the catalytic system, 3-(4,4,5,5-tetramethyl-1,3,2-dioxaborolan-2-yl)-9-((trimethylsilyl)methyl)-9*H*-carbazole **2g** (38.0 mg, 100 µmol) and 1-phenylprop-2-en-1-ol **1a** (26.0 µL, 200 µmol) as the substrates, and performing the reaction in acetone. The crude mixture was purified by flash column chromatography (isocratic 5% PhMe in hexane) to afford product **28** (21.0 mg, 50% yield, 89:11 er) as an off-white wax. The enantiomeric

ratio was determined by UPC^2 analysis on a Daicel Chiralpak IB-3 column: gradient CO_2/CH_3CN from 100% CO_2 to 60:40 over 4 minutes, curve 6, flow rate 2 mL/min, λ = 260 nm: τ_{major} = 3.8 min, τ_{minor} = 4.00 min; $[\alpha]_D^{26}$ = -11.5 (c = 0.23, $CHCl_3$, 89:11 er). The absolute configuration for the title compound was assigned in comparison to compounds **48** and **49**.

^{1}H NMR (400 MHz $CDCl_3$): δ 8.57 (t, *J* = 1.0 Hz, 1H), 8.12 – 8.09 (m, 1H), 7.85 (dd, *J* = 8.0, 1.0 Hz, 1H), 7.39 (ddd, *J* = 8.5, 7.0, 1.0 Hz, 1H), 7.29 – 7.17 (m, 8H), 6.13 (ddd, *J* = 17.0, 10.5, 7.5 Hz, 1H), 5.01 (dt, *J* = 10.5, 1.0 Hz, 1H), 4.94 (dt, *J* = 17.0, 1.0 Hz, 1H), 4.51 (dd, *J* = 14.5, 7.0 Hz, 1H), 6.13 (ddd, *J* = 17.0, 10.5, 7.5 Hz, 1H), 4.03 (q, *J* = 7.5 Hz, 1H), 1.40 (s, 12H).

^{13}C NMR (101 MHz, $CDCl_3$): δ δ 142.8, 141.2, 140.7, 138.3, 132.2, 128.9, 128.8, 128.8, 127.9, 127.8, 127.7, 127.2, 125.7, 123.2, 122.7, 120.6, 119.4, 117.1, 109.1, 108.5, 83.7, 49.3, 49.0, 25.1, 25.1.

HRMS (ESI) Exact mass calculated for $C_{28}H_{30}BNO_2$ $[M+H]^+$: 423.2479, found: 423.2471.

(*S*)-3,6-dibromo-9-(2-phenylbut-3-en-1-yl)-9*H*-carbazole (29)

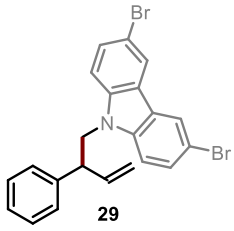

29

Prepared according to the general procedure, using $[Ir(cod)Cl]_2$/(*S*)-**L1** as the catalytic system, diethyl 4-((3,6-dibromo-9*H*-carbazol-9-yl)methyl)-2,6-dimethyl-1,4-dihydropyridine-3,5-dicarboxylate **2h** (59.0 mg, 100 µmol) and 1-phenylprop-2-en-1-ol **1a** (26.0 µL, 200 µmol) as the substrates, and performing the reaction in acetone. The crude mixture was purified by flash column chromatography (isocratic 5% PhMe in hexane) to afford product **29** (37.0 mg, 81% yield, 97:3 er) as a colorless wax. The enantiomeric ratio was determined by UPC^2 analysis on a Daicel Chiralpak IB-3 column: gradient CO_2/CH_3CN from 100% CO_2 to 60:40 over 4 minutes, curve 6, flow rate 2 mL/min, λ = 260 nm: τ_{major} = 4.3 min, τ_{minor} = 4.2 min; $[\alpha]_D^{26}$ = -30.4 (c = 0.41, $CHCl_3$, 97:3 er). The absolute configuration for the title compound was assigned in comparison to compounds **48** and **49**.

^{1}H NMR (400 MHz, $CDCl_3$): δ 8.10 (d, *J* = 2.0 Hz, 2H), 7.49 (dd, *J* = 8.5, 2.0 Hz, 2H), 7.35 – 7.18 (m, 4H), 7.16 – 7.05 (m, 3H), 6.13 (ddd, *J* = 17.0, 10.5, 7.5 Hz, 1H), 5.09 (dt, *J* = 10.5, 1.0 Hz, 1H), 5.03 (dt, *J* = 17.0, 1.5 Hz, 1H), 4.57 (dd, *J* = 14.5, 7.5 Hz, 1H), 4.43 (dd, *J* = 14.5, 7.5 Hz, 1H), 3.95 (q, *J* = 7.5 Hz, 1H).

^{13}C NMR (101 MHz, $CDCl_3$): δ 140.8, 139.5, 137.9, 129.2, 129.0, 128.9, 128.4, 127.8, 127.4, 125.4, 123.5, 123.3, 117.3, 112.2, 110.8, 49.3, 49.2.

HRMS (ESI) Exact mass calculated for $C_{22}H_{17}Br_2N$ $[M+H]^+$: 453.9801, found: 453.9801.

(*S*)-2-bromo-9-(2-phenylbut-3-en-1-yl)-9*H*-carbazole (30)

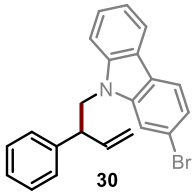

30

Prepared according to the general procedure, using $[Ir(cod)Cl]_2$/(*S*)-**L1** as the catalytic system, diethyl 4-((2-bromo-9*H*-carbazol-9-yl)methyl)-2,6-dimethyl-1,4-dihydro pyridine-3,5-dicarboxylate **2i** (51.0 mg, 100 µmol) and 1-phenylprop-2-en-1-ol **1a** (26.0 µL, 200 µmol) as the substrates, and performing the reaction in acetone. The crude mixture was purified by flash column chromatography (isocratic 5% PhMe in hexane) to afford product **30** (30.0 mg, 80% yield, 95:5 er) as a colorless wax. The enantiomeric ratio was determined by UPC^2 analysis on a Daicel Chiralpak IB-3 column: gradient CO_2/CH_3CN from 100% CO_2 to 60:40 over 4 minutes, curve 6, flow rate 2 mL/min, λ = 260 nm: τ_{major} = 5.0 min, τ_{minor} = 4.6 min; $[\alpha]_D^{26}$ = +12.5 (c = 0.34, $CHCl_3$, 95:5 er). The absolute configuration for the title compound was assigned in comparison to compounds **48** and **49**.

^{1}H NMR (400 MHz, $CDCl_3$): δ 8.05 (d, *J* = 8.0 Hz, 1H), 7.91 (d, *J* = 8.0 Hz, 1H), 7.45 (ddd, *J* = 8.5, 7.0, 1.0 Hz, 1H), 7.35 – 7.21 (m, 7H), 7.22 – 7.13 (m, 2H), 6.16 (ddd, *J* = 17.0, 10.5, 7.5 Hz, 1H), 5.11 (dt, *J* = 10.5, 1.0 Hz, 1H), 5.04 (dt, *J* = 17.0, 1.0 Hz, 1H), 4.61 (dd, *J* = 14.5, 7.5 Hz, 1H), 4.47 (dd, *J* = 14.5, 7.5 Hz, 1H), 4.01 (q, *J* = 7.5 Hz, 1H).

^{13}C NMR (101 MHz, $CDCl_3$): δ 141.5, 141.1, 140.8, 138.1, 128.9, 127.9, 127.4, 126.1, 122.5, 122.1, 121.8, 121.4, 120.4, 119.6, 119.2, 117.2, 112.2, 109.3, 49.2.

HRMS (ESI) Exact mass calculated for $C_{22}H_{18}BrN$ $[M+H]^+$: 398.0515, found: 398.0502.

(*S*)-4-bromo-9-(2-phenylbut-3-en-1-yl)-9*H*-carbazole (31)

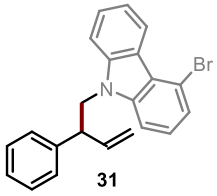

31

Prepared according to the general procedure, using $[Ir(cod)Cl]_2$/(*S*)-**L1** as the catalytic system, diethyl 4-((4-bromo-9*H*-carbazol-9-yl)methyl)-2,6-dimethyl-1,4-dihydropyridine-3,5-dicarboxylate **2j** (51.0 mg, 100 µmol) and 1-phenylprop-2-en-1-ol **1a** (26.0 µL, 200 µmol) as the substrates, and performing the reaction in acetone. The crude mixture was purified by flash column chromatography (isocratic 5% PhMe in hexane) to afford product **31** (30.0 mg, 80% yield, 96:4 er) as a colorless wax. The enantiomeric ratio was determined by UPC^2 analysis on a Daicel Chiralpak IG-3 column: gradient CO_2/CH_3CN from 100% CO_2 to

60:40 over 4 minutes, curve 6, flow rate 2 mL/min, λ = 260 nm: τ_{major} = 3.3 min, τ_{minor} = 3.2 min; $[\alpha]_D^{26}$ = -17.5 (c = 0.33, $CHCl_3$, 96:4 er). The absolute configuration for the title compound was assigned in comparison to compounds **48** and **49**.

^{1}H NMR (400 MHz, $CDCl_3$): δ 8.85 – 8.77 (m, 1H), 7.50 (ddd, *J* = 8.5, 6.5, 1.0 Hz, 1H), 7.40 (dd, *J* = 6.5, 2.0 Hz, 1H), 7.35 – 7.15 (m, 9H), 6.24 – 6.10 (m, 1H), 5.08 (dt, *J* = 10.5, 1.0 Hz, 1H), 5.02 (dt, *J* = 17.0, 1.0 Hz, 1H), 4.65 (dd, *J* = 14.5, 8.0 Hz, 1H), 4.52 (dd, *J* = 14.5, 7.0 Hz, 1H), 4.04 (q, *J* = 7.5 Hz, 1H).

^{13}C NMR (101 MHz, $CDCl_3$): δ 141.8, 141.1, 140.8, 138.1, 128.9, 127.9, 127.3, 126.3, 126.0, 123.2, 122.8, 122.6, 121.6, 119.2, 117.2, 116.8, 108.9, 108.0, 49.2, 49.1.

HRMS (ESI) Exact mass calculated for $C_{22}H_{18}BrN$ $[M+H]^+$: 376.0695, found: 376.0688.

methyl (*S*)-1-(2-phenylbut-3-en-1-yl)-1*H*-indole-3-carboxylate (32)

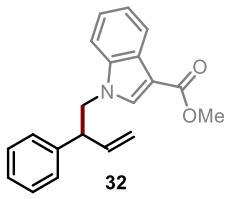

32

Prepared according to the general procedure, using $[Ir(cod)Cl]_2$/(*S*)-**L1** as the catalytic system, diethyl 4-((3-(methoxycarbonyl)-1*H*-indol-1-yl)methyl)-2,6-dimethyl-1,4-dihydropyridine-3,5-dicarboxylate **2k** (44.0 mg, 100 µmol) and 1-phenylprop-2-en-1-ol **1a** (26.0 µL, 200 µmol) as the substrates, and performing the reaction in acetone. The crude mixture was purified by flash column chromatography (gradient from hexane to 5% EtOAc in hexane) to afford product **32** (16.0 mg, 52% yield, 99:1 er) as a colorless wax. The enantiomeric ratio was determined by HPLC analysis on a Daicel Chiralpak IC-3 column: isocratic hexane/*i*-PrOH 95:5, flow rate 1 mL/min, λ = 230 nm: τ_{major} = 31.4 min, τ_{minor} = 36.8 min; $[\alpha]_D^{26}$ = -12.7 (c = 0.18, $CHCl_3$, 99:1 er). The absolute configuration for the title compound was assigned in comparison to compounds **48** and **49**.

^{1}H NMR (400 MHz, $CDCl_3$): δ 8.19 – 8.12 (m, 1H), 7.57 (s, 1H), 7.39 – 7.22 (m, 6H), 7.17 – 7.10 (m, 2H), 6.06 (ddd, *J* = 17.0, 10.5, 7.5 Hz, 1H), 5.13 (dt, *J* = 10.5, 1.0 Hz, 1H), 5.00 (dt, *J* = 17.0, 1.0 Hz, 1H), 4.40 (qd, *J* = 14.0, 7.5 Hz, 2H), 3.94 – 3.84 (m, 4H).

^{13}C NMR (101 MHz, $CDCl_3$): δ 165.6, 140.4, 137.6, 136.6, 135.0, 129.1, 127.7, 127.5, 126.8, 122.8, 122.0, 121.9, 117.7, 110.1, 107.0, 52.4, 51.1, 50.0.

HRMS (ESI) Exact mass calculated for $C_{20}H_{19}NaNO_2$ $[M+Na]^+$: 328.1308, found: 328.1306.

(*S*)- 3,3-dimethyl-1-(2-phenylbut-3-en-1-yl)indolin-2-one (33)

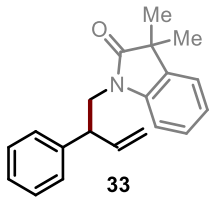

33

Prepared according to the general procedure, using [Ir(cod)Cl]$_2$/(*S*)-**L1** as the catalytic system, diethyl 4-((3,3-dimethyl-2-oxoindolin-1-yl)methyl)-2,6-dimethyl-1,4-dihydropyridine-3,5-dicarboxylate **2l** (42.7 mg, 100 µmol) and 1-phenylprop-2-en-1-ol **1a** (26.0 µL, 200 µmol) as the substrates, and performing the reaction in acetone. The crude mixture was purified by flash column chromatography (isocratic 5% EtOAc in hexane) to afford product **33** (15.0 mg, 51% yield, 99:1 er) as a colorless oil. The enantiomeric ratio was determined by HPLC analysis on a Daicel Chiralpak IC-3 column: isocratic hexane/*i*-PrOH 90:10, flow rate 1 mL/min, λ = 254 nm: τ_{major} = 8.2 min, τ_{minor} = 8.7 min; $[\alpha]_D^{26}$ = +2.5 (c = 0.59, $CHCl_3$, 99:1 er). The absolute configuration for the title compound was assigned in comparison to compounds **48** and **49**.

^{1}H NMR (400 MHz, $CDCl_3$): δ 7.35 – 7.14 (m, 7H), 7.04 (td, *J* = 7.5, 1.0 Hz, 1H), 6.87 (d, *J* = 8.0 Hz, 1H), 6.15 – 5.99 (m, 1H), 5.11 – 4.98 (m, 2H), 4.15 – 4.02 (m, 1H), 3.97 – 3.82 (m, 2H), 1.32 (s, 3H), 1.20 (s, 3H).

^{13}C NMR (101 MHz, $CDCl_3$): δ 181.4, 141.9, 140.8, 138.5, 136.0, 128.8, 128.0, 127.6, 127.2, 122.5, 122.4, 116.8, 108.5, 47.9, 44.4, 44.1, 24.6, 24.4.

HRMS (ESI) Exact mass calculated for $C_{20}H_{22}NO$ $[M+H]^+$: 292.1696, found: 292.1706.

(*S*)- 1-(2-phenylbut-3-en-1-yl)-3,4-dihydroquinolin-2(1*H*)-one (34)

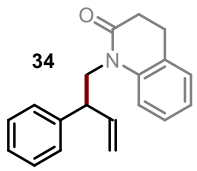

34

Prepared according to the general procedure, using [Ir(cod)Cl]$_2$/(*S*)-**L1** as the catalytic system, diethyl 2,6-dimethyl-4-((2-oxo-3,4-dihydroquinolin-1(2*H*)-yl)methyl)-1,4-dihydropyridine-3,5-dicarboxylate **2m** (41.2 mg, 100 µmol) and 1-phenylprop-2-en-1-ol **1a** (26.0 µL, 200 µmol) as the substrates, and performing the reaction in $CHCl_3$. The crude mixture was purified by flash column chromatography (isocratic 5% EtOAc in hexane) to afford product **34** (15.3 mg, 55% yield, 99:1 er) as an off-white wax. The enantiomeric ratio was determined by UPC^2 analysis on a CHIRALCEL® OJ-3 column: gradient CO_2/EtOH from 100% CO_2 to 60:40 over 4 minutes, curve 6, flow rate 2 mL/min, λ = 260 nm: τ_{major} = 2.8 min, τ_{minor} = 3.1 min; $[\alpha]_D^{26}$ = +53.0 (c = 0.12, CH_2Cl_2, 99:1 er). The absolute configuration for the title compound was assigned in comparison to compounds **48** and **49**.

^{1}H NMR (500 MHz, $CDCl_3$): δ 7.30 – 7.22 (m, 3H), 7.22 – 7.15 (m, 3H), 7.13 (dd, *J* = 7.5, 1.5 Hz, 1H), 7.05 – 6.98 (m, 2H), 6.02 (ddd, *J* = 17.0, 10.0, 8.0 Hz, 1H), 5.03 (d, *J* =

10.0 Hz, 1H), 4.94 (d, *J* = 17.0 Hz, 1H), 4.53 – 4.41 (m, 1H), 4.22 – 4.11 (m, 1H), 3.70 (q, *J* = 8.0 Hz, 1H), 2.79 – 2.69 (m, 1H), 2.63 – 2.45 (m, 3H).

^{13}C NMR (126 MHz, $CDCl_3$): δ 170.6, 141.1, 139.2, 138.8, 128.7, 128.1, 127.9, 127.7, 127.4, 127.0, 123.0, 116.3, 115.6, 47.7, 45.0, 32.2, 25.4.

HRMS (ESI) Exact mass calculated for $C_{19}H_{19}NNaO$ $[M+Na]^+$: 300.1359, found: 300.1359.

(*S*)-3-methyl-1-(2-phenylbut-3-en-1-yl)quinolin-2(1*H*)-one (35)

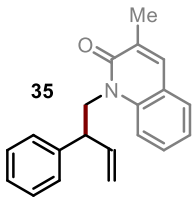

35

Prepared according to the general procedure, using $[Ir(cod)Cl]_2$/(*S*)-**L1** as the catalytic system, diethyl 2,6-dimethyl-4-((3-methyl-2-oxoquinolin-1(2H)-yl)methyl)-1,4-di hydropyridine-3,5-dicarboxylate **2n** (42.4 mg, 100 µmol) and 1-phenylprop-2-en-1-ol **1a** (26.0 µL, 200 µmol) as the substrates, and performing the reaction in $CHCl_3$. The crude mixture was purified by flash column chromatography (isocratic 2% EtOAc in CH_2Cl_2) to afford product **35** (11.7 mg, 40% yield, 99:1 er) as an off-white wax. The enantiomeric ratio was determined by HPLC analysis on a Daicel Chiralpak IC-3 column: isocratic hexane/*i*-PrOH 95:5, flow rate 1 mL/min, λ = 230 nm: τ_{major} = 44.2 min, τ_{minor} = 38.0 min; $[\alpha]_D^{26}$ = +40.4 (c = 0.07, CH_2Cl_2, 99:1 er). The absolute configuration for the title compound was assigned in comparison to **48** and **49**.

^{1}H NMR (500 MHz, $CDCl_3$): δ 7.52 (s, 1H), 7.51 – 7.43 (m, 2H), 7.36 – 7.29 (m, 5H), 7.28 – 7.22 (m, 1H), 7.18 (ddd, *J* = 7.5, 7.5, 1.0 Hz, 1H), 6.15 (ddd, *J* = 17.0, 10.0, 8.5 Hz, 1H), 5.06 – 4.97 (m, 1H), 4.95 (ddd, *J* = 10.0, 1.5, 1.0 Hz, 1H), 4.84 (ddd, *J* = 17.0, 1.5, 1.0 Hz, 1H), 4.39 – 4.26 (m, 1H), 3.93 (td, *J* = 9.5, 6.0 Hz, 1H), 2.24 (d, *J* = 1.5 Hz, 3H).

^{13}C NMR (126 MHz, $CDCl_3$): δ 163.1, 141.4, 138.6, 138.5, 135.9, 130.1, 129.2, 128.9, 128.2, 127.9, 127.1, 121.9, 121.1, 116.5, 114.3, 48.7, 47.0, 17.8.

HRMS (ESI) Exact mass calculated for $C_{20}H_{19}NNaO$ $[M+Na]^+$: 312.1359, found: 312.1346.

(S)-N-(2-(1-(2-phenylbut-3-en-1-yl)-1H-indol-3-yl)ethyl)acetamide (36)

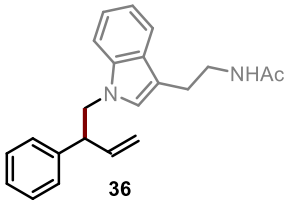

36

Prepared according to the general procedure, using $[Ir(cod)Cl]_2$/(*S*)-**L1** as the catalytic system, diethyl 4-((3-(2-acetamidoethyl)-1H-indol-1-yl)methyl)-2,6-dimethyl-1,4-dihydropyridine-3,5-dicarboxylate **2o** (47.0 mg, 100 µmol) and 1-phenylprop-2-en-1-ol **1a** (26.0 µL, 200 µmol) as the substrates, and performing the reaction in chloroform, reaction time 4h. The crude mixture was purified by flash column chromatography (gradient from hexane:EtOAc 50% to 80% EtOAc in hexane) to afford product **36** (19.5 mg, 58% yield, 94:6 er) as a yellow wax. The enantiomeric ratio was determined by UPC^2 analysis on a Daicel Chiralpak IB-3 column: isocratic CO_2/MeOH 10% MeOH, curve 6, flow rate 2 mL/min, λ = 220 nm: τ_{minor} = 7.7 min, τ_{major} = 8.2 min;$[\alpha]_D^{26}$ = -49.3 (c = 0.9, $CHCl_3$, 94:6 er). The absolute configuration for the title compound was assigned in comparison to compounds **48** and **49**.

^{1}H NMR (400 MHz, $CDCl_3$) δ 7.58 (dt, *J* = 7.9, 1.0 Hz, 1H), 7.40 – 7.21 (m, 5H), 7.17 – 7.09 (m, 3H), 6.65 (s, 1H), 6.10 (ddd, *J* = 17.2, 10.4, 7.5 Hz, 1H), 5.48 – 5.36 (bs, 1H), 5.14 (dt, *J* = 10.4, 1.2 Hz, 1H), 5.06 (dt, *J* = 17.2, 1.3 Hz, 1H), 4.44 (dd, *J* = 14.2, 7.5 Hz, 1H), 4.32 (dd, *J* = 14.2, 7.5 Hz, 1H), 3.89 (q, *J* = 7.5 Hz, 1H), 3.51 (q, *J* = 6.4 Hz, 2H), 2.94 – 2.82 (m, 2H), 1.91 (s, 3H).

^{13}C NMR (101 MHz, $CDCl_3$) δ 169.98, 141.11, 138.37, 136.37, 128.69, 127.99, 127.76, 127.09, 126.38, 121.75, 119.06, 118.91, 116.81, 111.18, 109.55, 51.74, 50.15, 39.85, 25.00, 23.38.

HRMS (ESI) Exact mass calculated for $C_{22}H_{24}N_2O$ $[M+Na]^+$: 355.1888, found: 355.1781.

(S)-7-(4-(4-(2,3-dichlorophenyl)piperazin-1-yl)butoxy)-1-(2-phenylbut-3-en-1-yl)-3,4-dihydroquinolin-2(1H)-one (37)

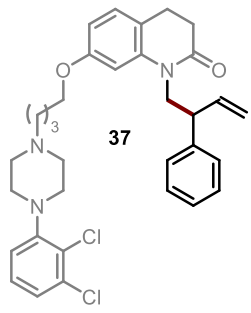

37

Prepared according to the general procedure, using $[Ir(cod)Cl]_2$/(*S*)-**L1** as the catalytic system, diethyl 4-((7-(4-(4-(2,3-dichlorophenyl)piperazin-1-yl)butoxy)-2-oxo-3,4-dihydroquinolin-1(2H)-yl)methyl)-2,6-dimethyl-1,4-dihydropyridine-3,5-dicarboxylate **2p** (71.4 mg, 100 µmol) and 1-phenylprop-2-en-1-ol **1a** (26.0 µL, 200 µmol) as the substrates, trifluoroacetic acid (23.1 µL, 300 µmol), and performing the reaction in acetone or $CHCl_3$. The crude

mixture was purified by flash column chromatography (isocratic 50% EtOAc in hexane) to afford product **37** (16.0 mg, 27% yield, 99:1 er) as a yellow oil. The enantiomeric ratio was determined by HPLC analysis on a Daicel Chiralpak IC-3 column: isocratic hexane/*i*-PrOH 90:10, flow rate 1.2 mL/min, λ = 225 nm: τ_{major} = 41.5 min, τ_{minor} = 43.9 min; $[\alpha]_D^{26}$ = +9.2 (c = 0.61, $CHCl_3$, 98:2 er). The absolute configuration for the title compound was assigned in comparison to compounds **48** and **49**.

^{1}H NMR (400 MHz, $CDCl_3$, *isolated as a 5:1 mixture of rotamers* A *and* B): δ 7.47 – 7.10 (m, 7H, A + 7H, B), 7.02 (d, *J* = 8.0 Hz, 1H, A), 6.99 – 6.91 (m, 1H, A + 2H, B). 6.77 (dd, *J* = 8.5, 2.0 Hz, 1H, B), 6.72 (d, *J* = 2.0 Hz, 1H, B), 6.60 (d, *J* = 2.5 Hz, 1H, A), 6.54 (dd, *J* = 8.0, 2.5 Hz, 1H, A), 6.16 (ddd, *J* = 17.0, 10.0, 8.0 Hz, 1H, B), 6.03 (ddd, *J* = 17.0, 10.0, 8.0 Hz, 1H, A), 5.10 – 4.91 (m, 2H, A), 5.02 – 4.81 (m, 3H, B), 4.52 – 4.35 (m, 1H, A), 4.29 – 4.07 (m, 1H, A + 1H, B), 4.04 (t, *J* = 6.0 Hz, 2H, B), 3.99 (t, *J* = 6.0 Hz, 2H, A), 3.93 (q, *J* = 8.5 Hz, 1H, B), 3.75 (q, *J* = 8.0 Hz, 1H, A), 3.13 (br s, 4H, A + 4H, B), 2.87 – 2.40 (m, 10H, A + 10H, B), 1.95 – 1.66 (m, 4H, A + 4H, B).

^{13}C NMR (101 MHz, $CDCl_3$): δ 170.8, 160.1, 158.6, 141.1, 140.2, 140.0, 138.8, 138.7, 135.8, 134.2, 129.4, 128.9, 128.7, 128.5, 128.0, 127.9, 127.7, 127.6, 127.1, 127.0, 124.9, 119.8, 118.8, 116.5, 116.3, 115.2, 110.0, 107.6, 103.7, 99.6, 68.0, 64.6, 58.3, 53.3, 51.0, 48.5, 47.6, 45.2, 32.5, 29.8, 27.4, 25.5, 24.7.

The experiment DOSY2DLEDBP at 400 MHz in $CDCl_3$ confirmed the presence of a single species in solution with a diffusion coefficient of $6.3 \cdot 10^{-10}$ m^2/s.

HRMS (ESI) Exact mass calculated for $C_{33}H_{38}Cl_2N_3O_2$ $[M+H]^+$: 578.2336, found: 578.2325.

(*S*)-6-chloro-4-(cyclopropylethynyl)-1-((*S*)-2-phenylbut-3-en-1-yl)-4-(trifluoromethyl)-1,4-dihydro-2*H*-benzo[*d*][1,3]oxazin-2-one (38)

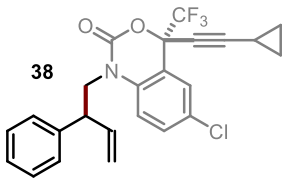

Prepared according to the general procedure, using pre-formed complex **I** as the catalyst, diethyl (*S*)-4-((6-chloro-4-(cyclopropylethynyl)-2-oxo-4-(trifluoromethyl)-2*H*-benzo[*d*][1,3]oxazin-1(4*H*)-yl)methyl)-2,6-dimethyl-1,4-dihydropyridine-3,5-dicarboxylate **2q** (58.1 mg, 100 μmol) and 1-phenylprop-2-en-1-ol **1a** (26.0 μL, 200 μmol) as the substrates, and performing the reaction in $CHCl_3$. The crude mixture was purified by flash column chromatography (isocratic 5% Et_2O in hexane) to afford product **38** (17.3 mg, 39% yield, >20:1 dr) as a colorless wax. This compound was obtained as a single diastereoisomer, as inferred by ^{1}H NMR analyses on both the crude mixture and the isolated compound;

$[\alpha]_D^{26}$ = -61.5 (c = 0.12, CH_2Cl_2). The absolute configuration for the title compound was assigned in comparison to compounds **48** and **49**.

When the reaction was carried out using $[Ir(cod)Cl]_2$/(*S*)-**L1** as the catalytic system, product **38** (12.3 mg, >20:1 dr) was obtained in 28% yield, as a single diastereoisomer.

^{1}H NMR (500 MHz, $CDCl_3$): δ 7.51 (d, *J* = 2.5 Hz, 1H), 7.37 – 7.28 (m, 3H), 7.28 – 7.22 (m, 3H), 6.81 (d, *J* = 9.0 Hz, 1H), 6.06 (ddd, *J* = 17.0, 10.0, 8.0 Hz, 1H), 5.10 (ddd, *J* = 10.0, 1.0, 1.0 Hz, 1H), 5.05 (dt, *J* = 17.0, 1.0, 1.0 Hz, 1H), 4.28 (dd, *J* = 14.5, 8.0 Hz, 1H), 4.16 (dd, *J* = 14.5, 7.0 Hz, 1H), 3.82 (q, *J* = 8.0 Hz, 1H), 1.37 (tt, *J* = 8.0, 5.0 Hz, 1H), 0.94 – 0.87 (m, 2H), 0.87 – 0.81 (m, 2H).

^{13}C NMR (126 MHz, $CDCl_3$): δ 148.2, 140.3, 138.0, 135.4, 131.3, 129.0, 128.8, 128.2, 127.9, 127.4, 122.2 (q, $^1J_{C\text{-}F}$ = 287.5 Hz), 117.7, 117.1, 115.3, 95.5, 77.8 – 76.6 (m), 66.7, 49.1, 48.0, 8.9, 8.8, -0.5.

^{19}F NMR (471 MHz, $CDCl_3$) δ -80.6 (s, 3F).

HRMS (ESI) Exact mass calculated for $C_{24}H_{19}ClF_3NNaO_2$ $[M+Na]^+$: 468.0949, found: 468.0943

(*S*)-6-chloro-4-(cyclopropylethynyl)-1-((*R*)-2-phenylbut-3-en-1-yl)-4-(trifluoromethyl)-1,4-dihydro-2*H*-benzo[*d*][1,3]oxazin-2-one (39)

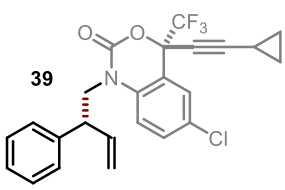

Prepared according to the general procedure, using $[Ir(cod)Cl]_2$/(*R*)-**L1** as the catalytic system, diethyl (*S*)-4-((6-chloro-4-(cyclopropylethynyl)-2-oxo-4-(trifluoromethyl)-2*H*-benzo[*d*][1,3]oxazin-1(4*H*)-yl)methyl)-2,6-dimethyl-1,4-dihydropyridine-3,5-dicarboxylate **2q** (58.1 mg, 100 µmol) and 1-phenylprop-2-en-1-ol **1a** (26.0 µL, 200 µmol) as the substrates, and performing the reaction in $CHCl_3$. The crude mixture was purified by flash column chromatography (isocratic 5% Et_2O in hexane) to afford product **39** (12.5 mg, 28% yield, 1:>20 dr) as a colorless wax. This compound was obtained as a single diastereoisomer, as inferred by ^{1}H NMR analyses on both the crude mixture and the isolated compound; $[\alpha]_D^{26}$ = -64.2 (c = 0.10, CH_2Cl_2). The absolute configuration for the title compound was assigned in comparison to compounds **48** and **49**.

^{1}H NMR (500 MHz, $CDCl_3$): δ 7.54 (d, *J* = 2.5 Hz, 1H), 7.39 (dd, *J* = 9.0, 2.5 Hz, 1H), 7.38 – 7.31 (m, 2H), 7.29 – 7.24 (m, 3H), 6.87 (d, *J* = 9.0 Hz, 1H), 6.04 (ddd, *J* = 17.0, 10.0, 8.0 Hz, 1H), 5.08 (dt, *J* = 10.0, 1.0 Hz, 1H), 5.01 (dd, *J* = 17.0, 1.0 Hz, 1H), 4.62

(dd, *J* = 14.5, 9.5 Hz, 1H), 3.85 (dd, *J* = 14.5, 5.0 Hz, 1H), 3.71 (ddd, *J* = 9.5, 8.0, 5.0 Hz, 1H), 1.38 (tt, *J* = 8.5, 5.0 Hz, 1H), 0.94 – 0.88 (m, 2H), 0.88 – 0.81 (m, 2H).

^{13}C NMR (126 MHz, $CDCl_3$): δ 148.2, 140.8, 137.6, 135.1, 131.4, 129.1, 128.9, 128.6, 127.7, 127.4, 122.3 (q, *J* = 287.5 Hz), 117.6 (*2 signals*), 115.2, 95.5, 77.8 – 76.4 (m), 66.8, 48.7, 47.8, 8.9 (*2 signals*), -0.5.

^{19}F NMR (471 MHz, $CDCl_3$) δ -80.5 (s, 3F).

HRMS (ESI) Exact mass calculated for $C_{24}H_{19}ClF_3NNaO_2$ $[M+Na]^+$: 468.0949, found: 468.0950.

Benzyl (*S*)-benzyl(2-phenylbut-3-en-1-yl)carbamate (40)

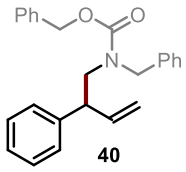

40

Prepared according to the general procedure, using pre-formed complex **I** as the catalyst, diethyl 4-((benzyl((benzyloxy)carbonyl)amino)methyl)-2,6-dimethyl-1,4-dihydropyridine-3,5 dicarboxylate **2r** (50.7 mg, 100 µmol) and 1-phenylprop-2-en-1-ol **1a** (26.0 µL, 200 µmol) as the substrates, and performing the reaction in $CHCl_3$. The crude mixture was purified by flash column chromatography (isocratic PhMe) to afford product **40** (15.1 mg, 41% yield, 96:4 er) as a colorless oil. The enantiomeric ratio was determined by UPC^2 analysis on a CHIRALCEL® OJ-3 column: gradient CO_2/EtOH from 100% CO_2 to 60:40 over 4 minutes, curve 6, flow rate 2 mL/min, λ = 220 nm: τ_{major} = 3.0 min, τ_{minor} = 4.1 min; $[\alpha]_D^{26}$ = +11.5 (c = 0.17, CH_2Cl_2, 96:4 er). The absolute configuration for the title compound was assigned in comparison to compounds **48** and **49**.

^{1}H NMR (500 MHz, $CDCl_3$, *isolated as a 1:1 mixture of rotamers* A *and* B): δ 7.43 – 7.02 (m, 15H, A+B), 6.06 – 5.95 (m, 1H, A), 5.97 – 5.87 (m, 1H, B), 5.22 – 4.93 (m, 4H, A+B), 4.52 (d, *J* = 15.5 Hz, 1H, A), 4.47 (d, *J* = 16.0 Hz, 1H, B), 4.08 (d, *J* = 15.5 Hz, 1H, A), 4.02 (d, *J* = 16.0 Hz, 1H, B), 3.80 – 3.66 (m, 2H, A), 3.65 – 3.51 (m, 2H, B), 3.41 – 3.29 (m, 1H, A+B).

^{13}C NMR (126 MHz, $CDCl_3$, *isolated as a 1:1 mixture of rotamers* A *and* B): δ 156.8, 156.5, 141.7, 141.6, 139.1, 138.9, 137.8, 137.7, 136.9, 136.8, 129.0, 128.9, 128.74, 128.69, 128.66, 128.61, 128.54, 128.50, 128.2, 128.04, 128.02, 127.9, 127.8, 127.5, 127.41, 127.35, 126.94, 126.90, 116.5, 116.4, 67.5, 67.3, 52.3, 51.5, 51.03, 50.96, 49.2, 48.6.

HRMS (ESI) Exact mass calculated for $C_{25}H_{25}NNaO_2$ $[M+Na]^+$: 394.1777, found: 394.1762.

Naphthalen-1-yl (S)-methyl(2-phenylbut-3-en-1-yl)carbamate (41)

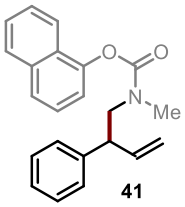

41

Prepared according to the general procedure, using pre-formed complex **I** as the catalyst, diethyl 2,6-dimethyl-4-((methyl((naphthalen-1-yloxy)carbonyl)amino)methyl)-1,4-dihydropyridine-3,5-dicarboxylate **2s** (46.7 mg, 100 μmol) and 1-phenylprop-2-en-1-ol **1a** (26.0 μL, 200 μmol) as the substrates, and performing the reaction in $CHCl_3$. The crude mixture was purified by flash column chromatography (isocratic PhMe) to afford product **41** (15.0 mg, 45% yield, 97:3 er) as a colorless oil. The enantiomeric ratio was determined by HPLC analysis on a Daicel Chiralpak IC-3 column: isocratic hexane/*i*-PrOH 90:10, flow rate 1 mL/min, λ = 225 nm: τ_{minor} = 25.8 min, τ_{major} = 28.9 min; $[\alpha]_D^{26}$ = -0.11 (c = 0.17, CH_2Cl_2, 97:3 er). The absolute configuration for the title compound was assigned in comparison to compounds **48** and **49**.

^{1}H NMR (400 MHz, $CDCl_3$, *isolated as a 1.2:1 mixture of rotamers* A *and* B): □ 7.91 – 7.68 (m, 3H, A+B), 7.53 – 7.41 (m, 3H, A+B), 7.40 – 7.27 (m, 5H, A+B), 7.21 (dd, *J* = 7.5, 1.0 Hz, 1H, A), 7.12 (dd, *J* = 7.5, 1.0 Hz, 1H, B), 6.25 – 6.00 (m, 1H, A+B), 5.28 – 5.14 (m, 2H, A+B), 4.05 – 3.92 (m, 1H, B), 3.93 – 3.77 (m, 2H, A+B), 3.67 – 3.53 (m, 1H, A), 3.13 (s, 3H, A), 2.99 (s, 3H, B).

^{13}C NMR (101 MHz, $CDCl_3$, *isolated as a 1.2:1 mixture of rotamers* A *and* B): □ 155.1, 154.9, 147.5, 147.4, 141.3, 139.1, 138.9, 134.8, 129.0, 128.8, 128.1, 127.60, 127.55, 127.2, 127.0, 126.4, 126.3, 125.6, 121.6, 121.4, 118.4, 118.1, 116.9, 116.5, 54.8, 54.7, 49.2, 48.7, 35.7.

HRMS (ESI) Exact mass calculated for $C_{22}H_{21}NNaO_2$ $[M+Na]^+$: 354.1464, found: 354.1457.

4.12.3 Characterization Data for Products 42-56

(*S*)-9-(2-(4-isopropylphenyl)but-3-en-1-yl)-9*H*-carbazole (42)

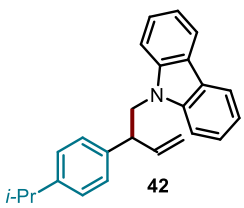

42

Prepared according to the general procedure, using $[Ir(cod)Cl]_2$/(*S*)-**L1** as the catalytic system, diethyl 4-((9*H*-carbazol-9-yl)methyl)-2,6-dimethyl-1,4-dihydro pyridine-3,5-dicarboxylate **2c** (43.3 mg, 100 μmol) and 1-(4-isopropylphenyl)prop-2-en-1-ol **1b** (35.3 mg, 200 μmol) as the substrates, and performing the reaction in acetone. The crude mixture was purified by flash column chromatography (isocratic 5% PhMe in hexane) to afford product **42** (20.0 mg, 58% yield, 93:7 er) as a colorless oil. The enantiomeric ratio

was determined by UPC^2 analysis on a Daicel Chiralpak IB-3 column: gradient CO_2/CH_3CN from 100% CO_2 to 60:40 over 4 minutes, curve 6, flow rate 2 mL/min, λ = 260 nm: τ_{major} = 4.1 min, τ_{minor} = 4.3 min; $[\alpha]_D^{26}$ = +6.6 (c = 0.56, CH_2Cl_2, 93:7 er). The absolute configuration for the title compound was assigned in comparison to compounds **48** and **49**.

^{1}H NMR (400 MHz, $CDCl_3$): δ 8.08 (dt, *J* = 7.5, 1.0 Hz, 2H), 7.39 (ddd, *J* = 8.5, 7.0, 1.0 Hz, 2H), 7.29 – 7.24 (m, 2H), 7.21 (ddd, *J* = 8.0, 7.0, 1.0 Hz, 2H), 7.12 (s, 4H), 6.15 (ddd, *J* = 17.0, 10.5, 7.6 Hz, 1H), 5.01 (dt, *J* = 10.5, 1.0 Hz, 1H), 4.96 (dt, *J* = 17.0, 1.5 Hz, 1H), 4.63 (dd, *J* = 14.5, 8.0 Hz, 1H), 4.48 (dd, *J* = 14.5, 6.5 Hz, 1H), 4.05 – 3.95 (m, 1H), 2.86 (hept, *J* = 7.0 Hz, 1H), 1.23 (d, *J* = 7.0 Hz, 6H).

^{13}C NMR (101 MHz, $CDCl_3$): δ 147.9, 140.7, 138.8, 138.6, 127.8, 126.9, 125.6, 122.9, 120.3, 118.9, 116.9, 109.1, 49.2, 49.1, 33.9, 24.17, 24.16.

HRMS (ESI) Exact mass calculated for $C_{25}H_{26}N$ $[M+H]^+$: 340.2060, found: 340.2056.

(*S*)-9-(2-(4-(*tert*-butyl)phenyl)but-3-en-1-yl)-9*H*-carbazole (43)

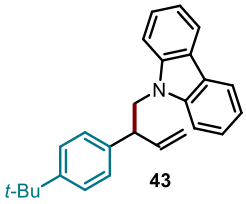

43

Prepared according to the general procedure, using $[Ir(cod)Cl]_2$/(*S*)-**L1** as the catalytic system, diethyl 4-((9*H*-carbazol-9-yl)methyl)-2,6-dimethyl-1,4-dihydro pyridine-3,5-dicarboxylate **2c** (43.3 mg, 100 μmol) and 1-(4-(*tert*-butyl)phenyl)prop-2-en-1-ol **1c** (38.1 mg, 200 μmol) as the substrates, and performing the reaction in acetone. The crude mixture was purified by flash column chromatography (isocratic 5% PhMe in hexane) to afford product **43** (21.0 mg, 60% yield, 92:8 er) as a colorless solid. The enantiomeric ratio was determined by UPC^2 analysis on a Daicel Chiralpak IB-3 column: gradient CO_2/CH_3CN from 100% CO_2 to 60:40 over 4 minutes, curve 6, flow rate 2 mL/min, λ = 260 nm: τ_{major} = 4.2 min, τ_{minor} = 4.3 min; $[\alpha]_D^{26}$ = +5.4 (c = 0.71, CH_2Cl_2, 92:8 er). The absolute configuration for the title compound was assigned in comparison to compounds **48** and **49**.

^{1}H NMR (400 MHz, $CDCl_3$): δ 8.09 (dt, *J* = 7.5, 1.0 Hz, 2H), 7.39 (ddd, *J* = 8.5, 7.0, 1.0 Hz, 2H), 7.31 – 7.24 (m, 4H), 7.21 (ddd, *J* = 8.0, 7.0, 1.0 Hz, 2H), 7.15 – 7.09 (m, 2H), 6.16 (ddd, *J* = 17.0, 10.5, 7.5 Hz, 1H), 5.02 (dt, *J* = 10.5, 1.0 Hz, 1H), 4.97 (dt, *J* = 17.0, 1.5 Hz, 1H), 4.64 (dd, *J* = 14.5, 8.0 Hz, 1H), 4.49 (dd, *J* = 14.5, 6.5 Hz, 1H), 4.01 (app q, *J* = 7.5 Hz, 1H), 1.30 (s, 9H).

^{13}C NMR (101 MHz, $CDCl_3$): δ 150.1, 140.7, 138.5, 138.4, 127.5, 125.7, 125.6, 122.9, 120.3, 118.9, 116.9, 109.1, 49.2, 49.0, 34.6, 31.5.

HRMS (ESI) Exact mass calculated for $C_{26}H_{28}N$ $[M+H]^+$: 354.2216, found: 354.2206.

(*S*)-9-(2-(4-((trimethylsilyl)ethynyl)phenyl)but-3-en-1-yl)-9*H*-carbazole (44)

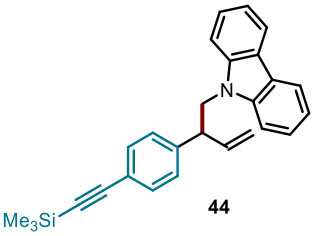

44

Prepared according to the general procedure, using $[Ir(cod)Cl]_2$/(*S*)-**L1** as the catalytic system, diethyl 4-((9*H*-carbazol-9-yl)methyl)-2,6-dimethyl-1,4-dihydro pyridine-3,5-dicarboxylate **2c** (43.3 mg, 100 µmol) and 1-(4-((trimethylsilyl)ethynyl)phenyl)prop-2-en-1-ol **1d** (46.1 mg, 200 µmol) as the substrates, and performing the reaction in acetone. The crude mixture was purified by flash column chromatography (isocratic 10% PhMe in hexane) to afford product **44** (16.5 mg, 40% yield, 86:14 er) as a colorless oil. The enantiomeric ratio was determined by UPC^2 analysis on a Daicel Chiralpak IB-3 column: gradient CO_2/CH_3CN from 100% CO_2 to 60:40 over 4 minutes, curve 6, flow rate 2 mL/min, λ = 260 nm: τ_{major} = 4.3 min, τ_{minor} = 4.5 min; $[\alpha]_D^{26}$ = -41.7 (c = 0.72, CH_2Cl_2, 87:13 er). The absolute configuration for the title compound was assigned in comparison to compounds **48** and **49**.

^{1}H NMR (400 MHz, $CDCl_3$): δ 8.07 (dt, *J* = 8.0, 1.0 Hz, 2H), 7.45 – 7.33 (m, 4H), 7.26 (dt, *J* = 8.0, 1.0 Hz, 2H), 7.22 (ddd, *J* = 8.0, 7.0, 1.0 Hz, 2H), 7.16 – 7.10 (m, 2H), 6.11 (ddd, *J* = 17.0, 10.5, 7.5 Hz, 1H), 5.05 (dt, *J* = 10.5, 1.0 Hz, 1H), 4.97 (dt, *J* = 17.0, 1.5 Hz, 1H), 4.61 (dd, *J* = 14.5, 8.0 Hz, 1H), 4.49 (dd, *J* = 14.5, 7.0 Hz, 1H), 4.04 (app q, *J* = 7.5 Hz, 1H), 0.25 (s, 9H).

^{13}C NMR (101 MHz, $CDCl_3$): δ 141.9, 140.6, 138.0, 132.4, 127.9, 125.7, 123.0, 122.0, 120.4, 119.1, 117.4, 109.0, 105.0, 94.3, 49.2, 48.9, 0.1.

HRMS (ESI) Exact mass calculated for $C_{27}H_{28}NSi$ $[M+H]^+$: 394.1986, found: 394.1984.

(*S*)-9-(2-(naphthalen-2-yl)but-3-en-1-yl)-9*H*-carbazole (45)

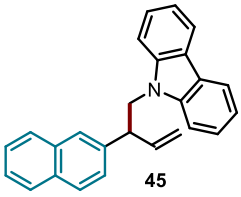

45

Prepared according to the general procedure, using $[Ir(cod)Cl]_2$/(*S*)-**L1** as the catalytic system, diethyl 4-((9*H*-carbazol-9-yl)methyl)-2,6-dimethyl-1,4-dihydro pyridine-3,5-dicarboxylate **2c** (43.3 mg, 100 µmol) and 1-(naphthalen-2-yl)prop-2-en-1-ol **1e** (36.8 mg, 200 µmol) as the substrates, and performing the reaction in acetone. The crude mixture was purified by flash column chromatography (isocratic 5% PhMe in hexane) to afford product **45** (16.0 mg, 46% yield, 86:14 er) as a yellow oil. The enantiomeric ratio was determined by UPC^2 analysis on a Daicel Chiralpak IB-3 column: gradient CO_2/ CH_3CN

from 100% CO_2 to 60:40 over 4 minutes, curve 6, flow rate 2 mL/min, λ = 260 nm: τ_{major} = 5.1 min, τ_{minor} = 5.4 min; $[\alpha]_D^{26}$ = -10.9 (c = 0.65, CH_2Cl_2, 87:13 er). The absolute configuration for the title compound was assigned in comparison to compounds **48** and **49**..

^{1}H NMR (400 MHz, $CDCl_3$): δ 8.08 (dt, *J* = 8.0, 1.0 Hz, 2H), 7.84 – 7.72 (m, 3H), 7.68 (d, *J* = 2.0 Hz, 1H), 7.50 – 7.42 (m, 2H), 7.41 – 7.31 (m, 5H), 7.20 (ddd, *J* = 8.0, 7.0, 1.0 Hz, 2H), 6.21 (ddd, *J* = 17.0, 10.5, 7.5 Hz, 1H), 5.04 (dt, *J* = 10.5, 1.0 Hz, 1H), 4.97 (dt, *J* = 17.0, 1.5 Hz, 1H), 4.74 (dd, *J* = 14.5, 8.5 Hz, 1H), 4.61 (dd, *J* = 14.5, 6.5 Hz, 1H), 4.22 (q, *J* = 7.5 Hz, 1H).

^{13}C NMR (101 MHz, $CDCl_3$): δ 140.7, 138.8, 138.4, 133.7, 132.7, 128.6, 127.80, 127.77, 126.6, 126.3, 126.2, 125.9, 125.7, 123.0, 120.4, 119.0, 117.3, 109.1, 49.5, 49.0.

HRMS (ESI) Exact mass calculated for $C_{26}H_{22}N$ $[M+H]^+$: 348.1747, found: 348.1756.

(*S*)-9-(2-(4-(trimethylsilyl)phenyl)but-3-en-1-yl)-9*H*-carbazole (46)

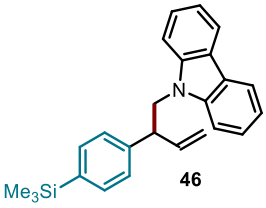

46

Prepared according to the general procedure, using $[Ir(cod)Cl]_2$/(*S*)-**L1** as the catalytic system, diethyl 4-((9*H*-carbazol-9-yl)methyl)-2,6-dimethyl-1,4-dihydro pyridine-3,5-dicarboxylate **2c** (43.3 mg, 100 µmol) and 1-(4-(trimethylsilyl)phenyl)prop-2-en-1-ol **1f** (41.3 mg, 200 µmol) as the substrates, and performing the reaction in acetone. The crude mixture was purified by flash column chromatography (isocratic 5% PhMe in hexane) to afford product **46** (24.8 mg, 66% yield, 91:9 er) as a colorless oil. The enantiomeric ratio was determined by UPC^2 analysis on a Daicel Chiralpak IB-3 column: gradient CO_2/CH_3CN from 100% CO_2 to 60:40 over 4 minutes, curve 6, flow rate 2 mL/min, λ = 260 nm: τ_{major} = 3.9 min, τ_{minor} = 4.1 min; $[\alpha]_D^{26}$ = +7.8 (c = 1.32, CH_2Cl_2, 92:8 er). The absolute configuration for the title compound was assigned in comparison to compounds **48** and **49**.

^{1}H NMR (400 MHz, $CDCl_3$): δ 8.07 (ddd, *J* = 8.0, 1.0, 1.0 Hz, 2H), 7.42 (d, *J* = 8.0 Hz, 2H), 7.38 (ddd, *J* = 8.5, 7.0, 1.0 Hz, 2H), 7.26 (dt, *J* = 8.0, 1.0 Hz, 2H), 7.23 – 7.17 (m, 4H), 6.14 (ddd, *J* = 17.0, 10.5, 7.5 Hz, 1H), 5.00 (dt, *J* = 10.5, 1.0 Hz, 1H), 4.94 (dt, *J* = 17.0, 1.5 Hz, 1H), 4.64 (dd, *J* = 14.5, 8.5 Hz, 1H), 4.49 (dd, *J* = 14.5, 6.5 Hz, 1H), 4.01 (app q, *J* = 7.5 Hz, 1H), 0.25 (s, 9H).

^{13}C NMR (101 MHz, $CDCl_3$): δ 142.0, 140.7, 139.3, 138.3, 133.9, 127.3, 125.6, 123.0, 120.3, 119.0, 117.2, 109.1, 49.5, 49.1, -1.0.

HRMS (ESI) Exact mass calculated for $C_{25}H_{27}NNaSi$ $[M+Na]^+$: 392.1805, found: 392.1795.

(*S*)-9-(2-(4-(4,4,5,5-tetramethyl-1,3,2-dioxaborolan-2-yl)phenyl)but-3-en-1-yl)-9*H*-carbazole (47)

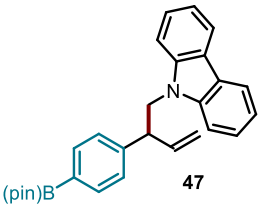

47

Prepared according to the general procedure, using pre-formed complex **I** as the catalyst, diethyl 4-((9*H*-carbazol-9-yl)methyl)-2,6-dimethyl-1,4-dihydro pyridine-3,5-dicarboxylate **2c** (43.3 mg, 100 µmol) and 1-(4-(4,4,5,5-tetramethyl-1,3,2-dioxaborolan-2-yl)phenyl)prop-2-en-1-ol **1g** (52.0 mg, 200 µmol) as the substrates, and performing the reaction in acetone. The crude mixture was purified by rapid filtration on a short pad of silica gel (*eluting with* PhMe), in order to prevent product decomposition, to afford product **47** (26.0 mg, 58% yield, 88:12 er) as a yellow oil. The enantiomeric ratio was determined by UPC^2 analysis on a Daicel Chiralpak IB-3 column: gradient CO_2/EtOH from 100% CO_2 to 60:40 over 4 minutes, curve 6, flow rate 2 mL/min, λ = 260 nm: τ_{major} = 3.9 min, τ_{minor} = 4.0 min; $[\alpha]_D^{26}$ = +52.5 (c = 1.04, CH_2Cl_2, 88:12 er). The absolute configuration for the title compound was assigned in comparison to compounds **48** and **49**.

^{1}H NMR (400 MHz, $CDCl_3$): δ 8.08 (dt, *J* = 8.0, 1.0 Hz, 2H), 7.79 – 7.73 (m, 2H), 7.42 (ddd, *J* = 8.5, 7.0, 1.0 Hz, 2H), 7.34 – 7.26 (m, 4H), 7.22 (ddd, *J* = 8.0, 7.0, 1.0 Hz, 2H), 6.11 (ddd, *J* = 17.0, 10.5, 7.5 Hz, 1H), 4.98 (dt, *J* = 10.5, 1.0 Hz, 1H), 4.89 (dt, *J* = 17.0, 1.5 Hz, 1H), 4.64 (dd, *J* = 14.5, 8.5 Hz, 1H), 4.51 (dd, *J* = 14.5, 6.5 Hz, 1H), 4.06 (app q, *J* = 7.5 Hz, 1H), 1.36 (s, 12H).

^{13}C NMR (101 MHz, $CDCl_3$): δ 144.6, 140.7, 138.2, 135.4, 127.4, 125.7, 123.0, 120.4, 119.0, 117.3, 109.1, 83.9, 49.7, 48.9, 25.02, 24.98.

HRMS (ESI) Exact mass calculated for $C_{28}H_{31}NO_2{}^{10}B$ $[M+H]^+$: 423.2479, found: 423.2489.

(*S*)-9-(2-(4-bromophenyl)but-3-en-1-yl)-9*H*-carbazole (48)

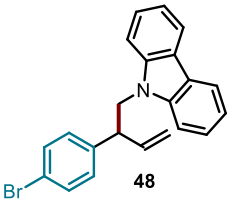

48

Prepared according to the general procedure, using [Ir(cod)Cl]$_2$/(*S*)-**L1** as the catalytic system, diethyl 4-((9*H*-carbazol-9-yl)methyl)-2,6-dimethyl-1,4-dihydropyridine-3,5-dicarboxylate **2c** (43.3 mg, 100 µmol) and 1-(4-bromophenyl)prop-2-en-1-ol **1h** (42.6 mg, 200 µmol) as the

substrates, and performing the reaction in acetone. The crude mixture was purified by flash column chromatography (isocratic 10% PhMe in hexane) to afford product **48** (22.0 mg, 60% yield, 92:8 er) as a colorless oil. The enantiomeric ratio was determined by UPC^2 analysis on a Daicel Chiralpak IB-3 column: gradient CO_2/CH_3CN from 100% CO_2 to 60:40 over 4 minutes, curve 6, flow rate 2 mL/min, λ = 260 nm: τ_{major} = 5.6 min, τ_{minor} = 5.9 min; $[\alpha]_D^{26}$ = -27.3 (c = 1.10, CH_2Cl_2, 92:8 er). Crystals of derivative **51**, suitable for X-ray diffraction analysis, were obtained upon slow evaporation of a CH_2Cl_2 solution of the title compound. This enabled the unambiguous determination of the absolute stereochemical configuration for product **48**.

^{1}H NMR (400 MHz, $CDCl_3$): δ 8.08 (dt, *J* = 7.5, 1.0 Hz, 2H), 7.40 (ddd, *J* = 8.5, 7.0, 1.0 Hz, 2H), 7.38 – 7.33 (m, 2H), 7.27 – 7.18 (m, 4H), 7.06 – 7.00 (m, 2H), 6.11 (ddd, *J* = 17.5, 10.5, 7.5 Hz, 1H), 5.09 (dt, *J* = 10.5, 1.0 Hz, 1H), 5.01 (dt, *J* = 17.0, 1.5 Hz, 1H), 4.61 (dd, *J* = 14.5, 7.5 Hz, 1H), 4.47 (dd, *J* = 14.5, 7.0 Hz, 1H), 4.01 (app q, *J* = 7.5 Hz, 1H).

^{13}C NMR (101 MHz, $CDCl_3$): δ 140.6, 140.3, 137.9, 131.9, 129.7, 125.7, 123.0, 121.0, 120.4, 119.1, 117.4, 109.0, 48.9, 48.7.

HRMS (ESI) Exact mass calculated for $C_{22}H_{19}BrN$ $[M+H]^+$: 376.0695, found: 376.0688.

(*S*)-9-(2-(4-chlorophenyl)but-3-en-1-yl)-9*H*-carbazole (49)

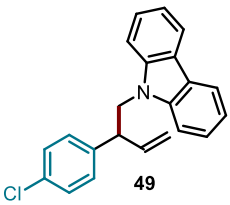

49

Prepared according to the general procedure, using $[Ir(cod)Cl]_2$/(*S*)-**L1** as the catalytic system, diethyl 4-((9*H*-carbazol-9-yl)methyl)-2,6-dimethyl-1,4-dihydro pyridine-3,5-dicarboxylate **2c** (43.3 mg, 100 μmol) and 1-(4-chlorophenyl)prop-2-en-1-ol **1i** (33.7 mg, 200 μmol) as the substrates, and performing the reaction in acetone. The crude mixture was purified by flash column chromatography (isocratic 5% PhMe in hexane) to afford product **49** (21.0 mg, 61% yield, 92:8 er) as a colorless solid. The enantiomeric ratio was determined by UPC^2 analysis on a Daicel Chiralpak IB-3 column: gradient CO_2/CH_3CN from 100% CO_2 to 60:40 over 4 minutes, curve 6, flow rate 2 mL/min, λ = 260 nm: τ_{major} = 4.4 min, τ_{minor} = 4.6 min; $[\alpha]_D^{26}$ = -23.9 (c = 0.12, CH_2Cl_2, 91:9 er). Crystals of derivative **49**, suitable for X-ray diffraction analysis, were obtained upon slow evaporation of a CH_2Cl_2 solution of the title compound. This enabled the unambiguous determination of the absolute stereochemical configuration for product **49**.

^{1}H NMR (400 MHz, $CDCl_3$): δ 8.08 (dt, *J* = 7.5, 1.0 Hz, 2H), 7.41 (ddd, *J* = 8.5, 7.0, 1.0 Hz, 2H), 7.27 – 7.16 (m, 6H), 7.10 – 7.06 (m, 2H), 6.12 (ddd, *J* = 17.5, 10.5, 7.5 Hz, 1H),

5.09 (dt, *J* = 10.5, 1.0 Hz, 1H), 5.02 (dt, *J* = 17.0, 1.5 Hz, 1H), 4.61 (dd, *J* = 14.5, 7.5 Hz, 1H), 4.47 (dd, *J* = 14.5, 7.5 Hz, 1H), 4.02 (app q, *J* = 7.5 Hz, 1H).

^{13}C NMR (101 MHz, $CDCl_3$): δ 140.6, 139.8, 138.0, 133.0, 129.3, 128.9, 125.7, 123.0, 120.4, 119.1, 117.4, 109.0, 48.9, 48.6.

HRMS (ESI) Exact mass calculated for $C_{22}H_{19}ClN$ $[M+H]^+$: 332.1201, found: 332.1201.

(*S*)-9-(2-(3-iodophenyl)but-3-en-1-yl)-9*H*-carbazole (50)

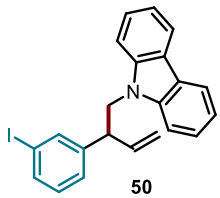

50

Prepared according to the general procedure, using $[Ir(cod)Cl]_2$/(*S*)-**L1** as the catalytic system, diethyl 4-((9*H*-carbazol-9-yl)methyl)-2,6-dimethyl-1,4-dihydro pyridine-3,5-dicarboxylate **2c** (43.3 mg, 100 µmol) and 1-(3-iodophenyl)prop-2-en-1-ol **1j** (52.0 mg, 200 µmol) as the substrates, and performing the reaction in acetone. The crude mixture was purified by flash column chromatography (isocratic 5% PhMe in hexane) to afford product **50** (14.4 mg, 33% yield, 85:15 er) as a colorless oil. The enantiomeric ratio was determined by UPC^2 analysis on a Daicel Chiralpak IB-3 column: gradient CO_2/CH_3CN from 100% CO_2 to 60:40 over 4 minutes, curve 6, flow rate 2 mL/min, λ =260 nm: τ_{major} = 4.7 min, τ_{minor} = 4.8 min; $[\alpha]_D^{26}$ = -14.1 (c = 0.89, CH_2Cl_2, 85:15 er). The absolute configuration for the title compound was assigned in comparison to compounds **48** and **49**.

^{1}H NMR (400 MHz, $CDCl_3$): δ 8.08 (dt, *J* = 8.0, 1.0 Hz, 2H), 7.57 – 7.47 (m, 2H), 7.41 (ddd, *J* = 8.5, 7.0, 1.0 Hz, 2H), 7.28 – 7.18 (m, 4H), 7.06 (dt, *J* = 7.5, 1.5 Hz, 1H), 6.93 (t, *J* = 7.5 Hz, 1H), 6.10 (ddd, *J* = 17.0, 10.5, 7.5 Hz, 1H), 5.08 (dt, *J* = 10.5, 1.0 Hz, 1H), 5.00 (dt, *J* = 17.0, 1.0 Hz, 1H), 4.61 (dd, *J* = 14.5, 8.0 Hz, 1H), 4.48 (dd, *J* = 14.5, 7.0 Hz, 1H), 3.97 (app q, *J* = 7.5 Hz, 1H).

^{13}C NMR (101 MHz, $CDCl_3$): δ 143.7, 140.6, 137.6, 136.9, 136.2, 130.4, 127.4, 125.7, 123.0, 120.4, 119.1, 117.6, 109.0, 94.8, 48.8, 48.8.

HRMS (ESI) Exact mass calculated for $C_{22}H_{19}IN$ $[M+H]^+$: 424.0557, found: 424.0557.

(*S*)-9-(2-(3-methoxyphenyl)but-3-en-1-yl)-9*H*-carbazole (51)

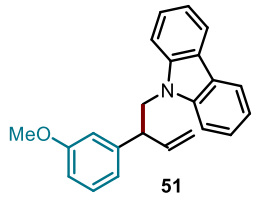

51

Prepared according to the general procedure, using $[Ir(cod)Cl]_2$/(*S*)-**L1** as the catalytic system, diethyl 4-((9*H*-carbazol-9-yl)methyl)-2,6-dimethyl-1,4-dihydro pyridine-3,5-dicarboxylate **2c** (43.3 mg, 100 µmol) and 1-(3-methoxyphenyl)prop-2-en-1-ol **1k** (32.8 mg, 200 µmol) as the substrates, and performing the reaction in acetone. The crude mixture was purified by flash column chromatography (isocratic 30% PhMe in hexane) to afford product **51** (23.0 mg, 68% yield, 92:8 er) as a colorless oil. The enantiomeric ratio was determined by UPC^2 analysis on a Daicel Chiralpak IB-3 column: gradient CO_2/CH_3CN from 100% CO_2 to 60:40 over 4 minutes, curve 6, flow rate 2 mL/min, λ = 260 nm: τ_{major} = 4.3 min, τ_{minor} = 4.5 min; $[\alpha]_D^{26}$ = -0.6 (c = 0.87, CH_2Cl_2, 92:8 er). The absolute configuration for the title compound was assigned in comparison to compounds **48** and **49**.

^{1}H NMR (400 MHz, $CDCl_3$): δ 8.09 (dt, *J* = 7.5, 1.0 Hz, 2H), 7.42 (ddd, *J* = 8.5, 7.0, 1.0 Hz, 2H), 7.29 (dt, *J* = 8.5, 1.0 Hz, 2H), 7.25 – 7.17 (m, 3H), 6.82 (dt, *J* = 7.5, 1.5 Hz, 1H), 6.76 (ddd, *J* = 8.0, 2.5, 1.0 Hz, 1H), 6.68 (dd, *J* = 2.5, 1.5 Hz, 1H), 6.15 (ddd, *J* = 17.0, 10.5, 7.5 Hz, 1H), 5.04 (dt, *J* = 10.5, 1.0 Hz, 1H), 4.99 (dt, *J* = 17.0, 1.5 Hz, 1H), 4.64 (dd, *J* = 14.5, 8.0 Hz, 1H), 4.51 (dd, *J* = 14.5, 7.0 Hz, 1H), 4.01 (app q, *J* = 7.5 Hz, 1H), 3.69 (s, 3H).

^{13}C NMR (101 MHz, $CDCl_3$): δ 160.0, 143.0, 140.7, 138.3, 129.8, 125.6, 123.0, 120.3, 120.2, 119.0, 117.1, 113.9, 112.5, 109.1, 55.3, 49.4, 49.0.

HRMS (ESI) Exact mass calculated for $C_{23}H_{22}NO$ $[M+H]^+$: 328.1696, found: 328.1699.

(*S*)-1-(3-(1-(9*H*-carbazol-9-yl)but-3-en-2-yl)phenyl)ethan-1-one (52)

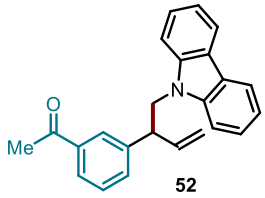

52

Prepared according to the general procedure, using $[Ir(cod)Cl]_2$/(*S*)-**L1** as the catalytic system, diethyl 4-((9*H*-carbazol-9-yl)methyl)-2,6-dimethyl-1,4-dihydropyridine-3,5-dicarboxylate **2c** (43.3 mg, 100 µmol) and 1-(3-(1-hydroxyallyl)phenyl)ethan-1-one **1l** (35.2 mg, 200 µmol) as the substrates, and performing the reaction in acetone. The crude mixture was purified by flash column chromatography (isocratic PhMe) to afford product **52** (17.6 mg, 52% yield, 89:11 er) as a colorless oil. The enantiomeric ratio was determined by UPC^2 analysis on a Daicel Chiralpak IB-3 column: gradient CO_2/CH_3CN from 100% CO_2 to 60:40 over 4 minutes, curve 6, flow rate 2 mL/min, λ =260 nm: τ_{major}

= 4.5 min, τ_{minor} = 4.6 min; $[\alpha]_D^{26}$ = -15.6 (c = 0.91, CH_2Cl_2, 89:11 er). The absolute configuration for the title compound was assigned in comparison to compounds **48** and **49**.

^{1}H NMR (400 MHz, $CDCl_3$): δ 8.06 (dt, *J* = 8.0, 1.0 Hz, 2H), 7.73 (dt, *J* = 7.0, 2.0 Hz, 1H), 7.66 – 7.61 (m, 1H), 7.38 (ddd, *J* = 8.5, 7.0, 1.0 Hz, 2H), 7.34 – 7.27 (m, 2H), 7.25 – 7.16 (m, 4H), 6.19 (ddd, *J* = 17.0, 10.5, 7.5 Hz, 1H), 5.15 (dt, *J* = 10.5, 1.0 Hz, 1H), 5.08 (dt, *J* = 17.0, 1.5 Hz, 1H), 4.67 (dd, *J* = 14.5, 7.5 Hz, 1H), 4.51 (dd, *J* = 14.5, 7.5 Hz, 1H), 4.12 (app q, *J* = 7.5 Hz, 1H), 2.42 (s, 3H).

^{13}C NMR (101 MHz, $CDCl_3$): δ 198.1, 141.9, 140.5, 137.7, 137.5, 132.7, 129.0, 127.8, 127.2, 125.7, 123.0, 120.4, 119.1, 117.6, 109.0, 48.9, 48.8, 26.6.

HRMS (ESI) Exact mass calculated for $C_{24}H_{22}NO$ $[M+H]^+$: 340.1696, found: 340.1692.

(*S*)-*N*-(3-(1-(9*H*-carbazol-9-yl)but-3-en-2-yl)phenyl)acetamide (53)

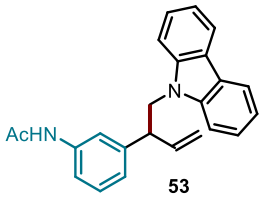

53

Prepared according to the general procedure, using $[Ir(cod)Cl]_2$/(*S*)-**L1** as the catalytic system, diethyl 4-((9*H*-carbazol-9-yl)methyl)-2,6-dimethyl-1,4-dihydropyridine-3,5-dicarboxylate **2c** (43.3 mg, 100 µmol) and *N*-(3-(1-hydroxyallyl)phenyl)acetamide **1m** (38.2 mg, 200 µmol) as the substrates, and performing the reaction in acetone. The crude mixture was purified by flash column chromatography (isocratic 30% PhMe in hexane) to afford product **53** (26.0 mg, 72% yield, 94:6 er) as a colorless solid. The enantiomeric ratio was determined by UPC^2 analysis on a Daicel Chiralpak IB-3 column: gradient CO_2/CH_3CN from 100% CO_2 to 60:40 over 4 minutes, curve 6, flow rate 2 mL/min, λ = 230 nm: τ_{major} = 5.6 min, τ_{minor} = 5.7 min; $[\alpha]_D^{26}$ = -18.4 (c = 0.96, CH_2Cl_2, 94:6 er). The absolute configuration for the title compound was assigned in comparison to compounds **48** and **49**.

^{1}H NMR (400 MHz, $CDCl_3$): δ 8.06 (dt, *J* = 7.5, 1.0 Hz, 2H), 7.44 – 7.34 (m, 3H), 7.35 – 7.25 (m, 3H), 7.24 – 7.15 (m, 4H), 6.92 (d, *J* = 7.5 Hz, 1H), 6.12 (ddd, *J* = 17.5, 10.5, 7.5 Hz, 1H), 5.08 – 4.91 (m, 2H), 4.61 (dd, *J* = 14.5, 8.0 Hz, 1H), 4.50 (dd, *J* = 14.5, 7.0 Hz, 1H), 4.00 (app q, *J* = 7.5 Hz, 1H), 2.13 (s, 3H).

^{13}C NMR (101 MHz, $CDCl_3$): δ 168.4, 142.4, 140.6, 138.4, 138.1, 129.4, 125.7, 123.8, 122.9, 120.3, 119.4, 119.0, 118.6, 117.2, 109.1, 49.3, 49.0, 24.7.

HRMS (ESI) Exact mass calculated for $C_{24}H_{22}N_2NaO$ $[M+Na]^+$: 377.1624, found: 377.1638.

(*S*)-9-(2-(o-tolyl)but-3-en-1-yl)-9*H*-carbazole (54)

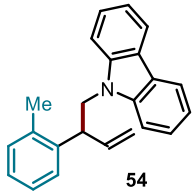

54

Prepared according to the general procedure, using using pre-formed complex **II** as the catalyst, diethyl 4-((9*H*-carbazol-9-yl)methyl)-2,6-dimethyl-1,4-dihydro pyridine-3,5-dicarboxylate **2c** (43.3 mg, 100 µmol) and 1-(o-tolyl)prop-2-en-1-ol **1n** (20.8 mg, 140 µmol) as the substrates, and performing the reaction in acetone. The crude mixture was purified by flash column chromatography (isocratic 5% PhMe in hexane) to afford product **54** (19.8 mg, 61% yield, 85:15 er) as a colorless oil. The enantiomeric ratio was determined by UPC^2 analysis on a Daicel Chiralpak IB-3 column: gradient CO_2/CH_3CN from 100% CO_2 to 60:40 over 4 minutes, curve 6, flow rate 2 mL/min, λ = 260 nm: τ_{major} = 5.1 min, τ_{minor} = 5.4 min; $[\alpha]_D^{26}$ = +14.4 (c = 0.20, CH_2Cl_2, 85:15 er). The absolute configuration for the title compound was assigned in comparison to compounds **48** and **49**.

^{1}H NMR (400 MHz, $CDCl_3$): δ 8.08 (d, *J* = 8.0 Hz, 2H), 7.48 – 7.37 (m, 3H), 7.29 (d, *J* = 8.0 Hz, 3H), 7.25 – 7.19 (m, 2H), 7.14 (td, *J* = 7.5, 1.5 Hz, 1H), 7.05 (d, *J* = 7.5 Hz, 1H), 6.07 (ddd, *J* = 17.0, 10.5, 7.0 Hz, 1H), 4.99 (dt, *J* = 10.5, 1.5 Hz, 1H), 4.89 (dt, *J* = 17.0, 1.5 Hz, 1H), 4.72 (dd, *J* = 14.5, 8.5 Hz, 1H), 4.51 (dd, *J* = 14.5, 6.5 Hz, 1H), 4.29 (dt, *J* = 8.0, 6.5 Hz, 1H), 2.05 (s, 3H).

^{13}C NMR (101 MHz, $CDCl_3$): δ 140.7, 139.7, 138.8, 136.5, 130.8, 127.0, 126.9, 126.5, 125.7, 123.0, 120.4, 119.0, 116.6, 109.0, 48.7, 44.7, 19.6.

HRMS (ESI) Exact mass calculated for $C_{23}H_{22}N$ $[M+H]^+$: 312.1747, found: 312.1745.

(*S*)-9-(2-(2-fluorophenyl)but-3-en-1-yl)-9*H*-carbazole (55)

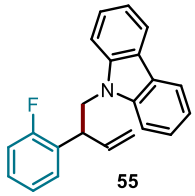

55

Prepared according to the general procedure, using $[Ir(cod)Cl]_2$/(*S*)-**L1** as the catalytic system, diethyl 4-((9*H*-carbazol-9-yl)methyl)-2,6-dimethyl-1,4-dihydropyridine-3,5-dicarboxylate **2c** (43.3 mg, 100 µmol) and 1-(2-fluorophenyl)prop-2-en-1-ol **1o** (30.4 mg, 200 µmol) as the substrates, and performing the reaction in acetone. The crude mixture was purified by flash column chromatography (isocratic 5% PhMe in hexane) to afford product **55** (17.0 mg, 50% yield, 87:13 er) as a colorless oil. The enantiomeric ratio was determined by UPC^2 analysis on a Daicel

Chiralpak IB-3 column: gradient CO_2/CH_3CN from 100% CO_2 to 60:40 over 4 minutes, curve 6, flow rate 2 mL/min, λ = 260 nm: τ_{major} = 3.7 min, τ_{minor} = 4.00 min; $[\alpha]_D^{26}$ = +8.6 (c = 0.43, CH_2Cl_2, 87:13 er). The absolute configuration for the title compound was assigned in comparison to compounds **48** and **49**.

^{1}H NMR (400 MHz, $CDCl_3$): δ 807 (d, *J* = 7.5 Hz, 2H), 7.47 – 7.35 (m, 4H), 7.26 – 7.17 (m, 4H), 7.10 – 6.99 (m, 2H), 6.19 (dddd, *J* = 17.0, 10.0, 8.0, 1.5 Hz, 1H), 5.03 – 4.89 (m, 2H), 4.71 – 4.53 (m, 2H), 4.31 (app q, *J* = 7.5 Hz, 1H).

^{13}C NMR (101 MHz, $CDCl_3$): δ 161.1 (d, $^{1}J_{C\text{-}F}$ = 245 Hz), 140.7, 136.8 (d, $^{4}J_{C\text{-}F}$ = 1.5 Hz), 129.6 (d, $^{3}J_{C\text{-}F}$ = 5.0 Hz), 128.8 (d, $^{3}J_{C\text{-}F}$ = 8.5 Hz), 128.2 (d, $^{2}J_{C\text{-}F}$ = 14.5 Hz), 125.7, 124.6 (d, $^{4}J_{C\text{-}F}$ = 3.5 Hz), 123.0, 120.4, 119.1, 117.8, 116.0 (d, $^{2}J_{C\text{-}F}$ = 22.5 Hz), 109.0, 47.7 (d, $^{3}J_{C\text{-}F}$ = 2.5 Hz), 44.6.

^{19}F NMR (376 MHz, $CDCl_3$): δ -117.0 (s, 1F).

HRMS (ESI) Exact mass calculated for $C_{22}H_{19}FN$ $[M+H]^+$: 316.1496, found: 316.1500.

(*S*)-9-(2-(thiophen-3-yl)but-3-en-1-yl)-9*H*-carbazole (56)

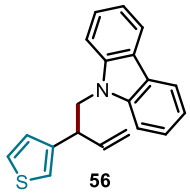

56

Prepared according to the general procedure, using $[Ir(cod)Cl]_2$/(*S*)-**L1** as the catalytic system, diethyl 4-((9*H*-carbazol-9-yl)methyl)-2,6-dimethyl-1,4-dihydropyridine-3,5-dicarboxylate **2c** (43.3 mg, 100 µmol) and 1-(thiophen-3-yl)prop-2-en-1-ol **1p** (28.0 mg, 200 µmol) as the substrates, and performing the reaction in acetone. The crude mixture was purified by flash column chromatography (isocratic 10% PhMe in hexane) to afford product **56** (14.0 mg, 44% yield, 94:6 er) as a colorless oil. The enantiomeric ratio was determined by UPC^2 analysis on a Daicel Chiralpak IB-3 column: gradient CO_2/CH_3CN from 100% CO_2 to 60:40 over 4 minutes, curve 6, flow rate 2 mL/min, λ = 260 nm: τ_{major} = 4.4 min, τ_{minor} = 4.6 min; $[\alpha]_D^{26}$ = +24.7 (c = 0.43, CH_2Cl_2, 94:6 er). The absolute configuration for the title compound was assigned in comparison to compounds **48** and **49**.

^{1}H NMR (400 MHz, $CDCl_3$): δ 8.08 (dt, *J* = 7.5, 1.0 Hz, 2H), 7.41 (ddd, *J* = 8.5, 7.0, 1.0 Hz, 2H), 7.32 – 7.12 (m, 5H), 6.92 (d, *J* = 4.0 Hz, 2H), 6.10 (ddd, *J* = 17.0, 10.5, 7.5 Hz, 1H), 5.07 – 4.96 (m, 2H), 4.63 – 4.47 (m, 2H), 4.17 (app q, *J* = 7.5 Hz, 1H).

^{13}C NMR (101 MHz, $CDCl_3$): δ 141.7, 140.7, 138.1, 127.1, 126.1, 125.7, 123.0, 121.4, 120.4, 119.0, 117.1, 109.0, 48.8, 44.8.

HRMS (ESI) Exact mass calculated for $C_{20}H_{18}NS$ $[M+H]^+$: 304.1154, found: 304.1156.

4.12.4 Mechanistic Studies

4.12.4.1 Electrochemical Characterization of the Reaction Components

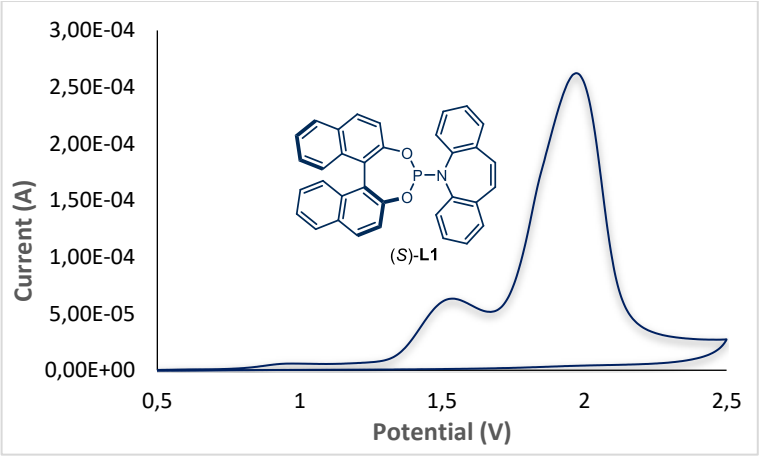

Figure 4.13: Cyclic voltammogram for the chiral ligand (*S*)-**L1** [0.005M] in [0.1 M] $TBAPF_6$ in CH_3CN. Sweep rate: 50 mV/s. Pt electrode working electrode, Ag/AgCl (KCl saturated) reference electrode, Pt wire auxiliary electrode. Irreversible oxidation, $E_p^A = E$ ((*S*)-**L1**/(*S*)-**L1**$^{\cdot+}$) = +1.53 V, E_p^A refers to the anodic peak potential, while the E value describes the electrochemical properties of (*S*)-**L**.

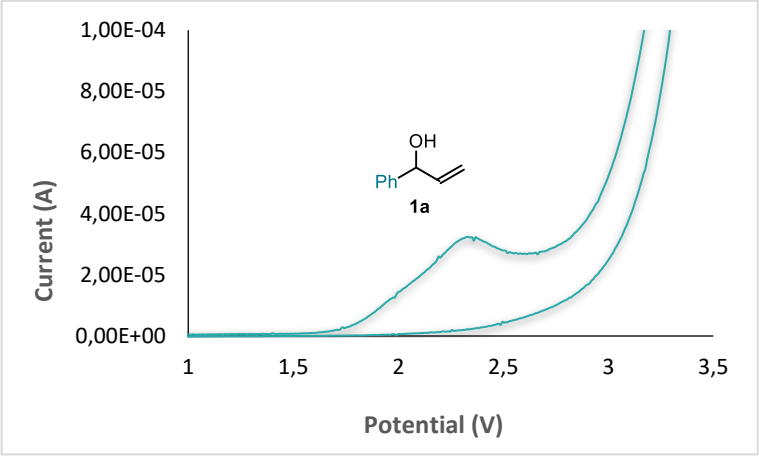

Figure 4.14: Cyclic voltammogram for allylic alcohol **1a** [0.02M] in [0.1 M] $TBAPF_6$ in CH_3CN. Sweep rate: 30 mV/s. Pt electrode working electrode, Ag/AgCl (KCl saturated) reference electrode, Pt wire auxiliary electrode. Irreversible oxidation, $E_p^A = E$ (**1a**/**1a**$^{\cdot+}$) = +2.36 V, E_p^A refers to the anodic peak potential, while the E value describes the electrochemical properties of **1a**.

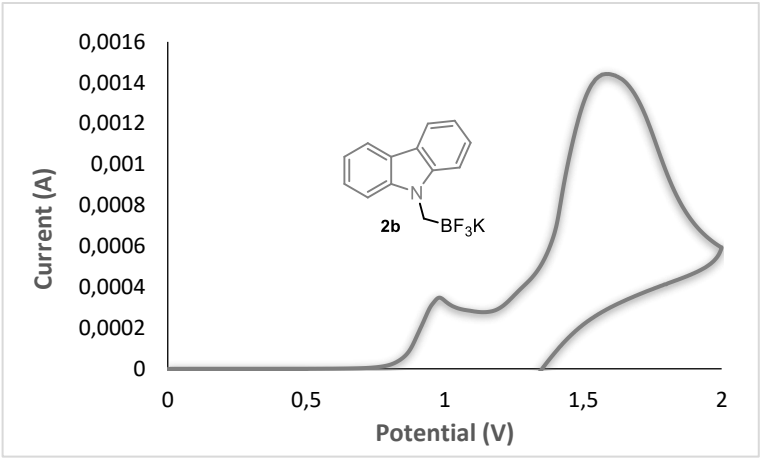

Figure 4.15: Cyclic voltammogram for trifluoroborate salt **2b** [0.02 M] in [0.1 M] $TBAPF_6$ in CH_3CN. Sweep rate: 50 mV/s. Glassy carbon working electrode, Ag/AgCl (KCl saturated) reference electrode, Pt wire auxiliary electrode. Irreversible oxidation peaks, $E_p^A = E$ (**2b**/**2b**$^{\cdot+}$) = +0.98 V, where E_p^A refers to the anodic peak potential, while the E value describes the electrochemical properties of **2b**.

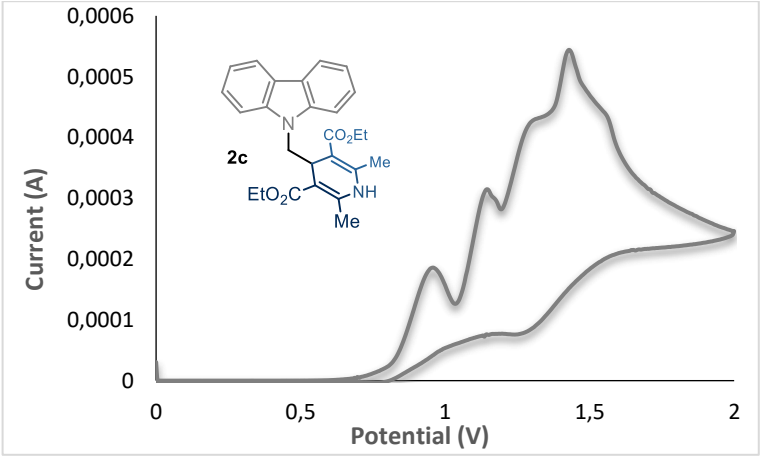

Figure 4.16: Cyclic voltammogram for 1,4-dihydropyridine **2c** [0.02 M] in [0.1 M] $TBAPF_6$ in CH_3CN. Sweep rate: 50 mV/s. Platinum working electrode, Ag/AgCl (KCl saturated) reference electrode, Pt wire auxiliary electrode. Four irreversible oxidation peaks: $E_p^A = E$ (**2c**/**2c**$^{\cdot+}$) = +0.96 V, where E_p^A refers to the anodic peak potential, while the E value describes the electrochemical properties of **2c**.

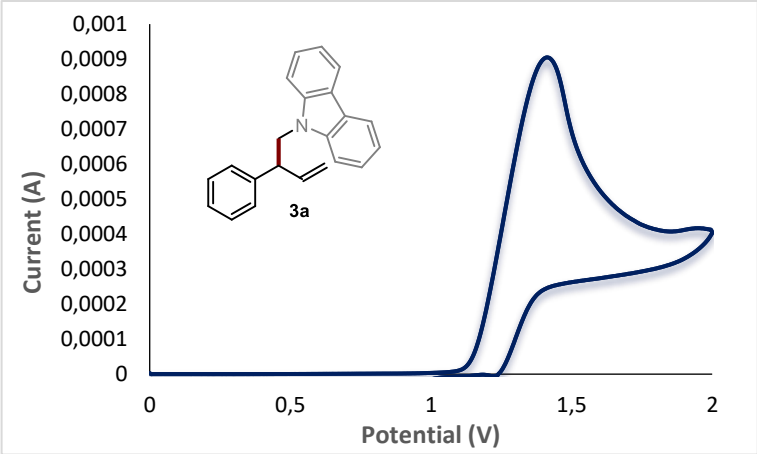

Figure 4.17: Cyclic voltammogram for product **3a** [0.023 M] in [0.1 M] $TBAPF_6$ in CH_3CN. Sweep rate: 200 mV/s. Platinum working electrode, Ag/AgCl (KCl saturated) reference electrode, Pt wire auxiliary electrode. Irreversible oxidation peak, $E_p^A = E$ (**3a**/**3a**$^{\cdot+}$) = +1.42 V, where E_p^A refers to the anodic peak potential, while the E value describes the electrochemical properties of **3a**.

4.12.5 Absorption Spectroscopy Analyses

Solutions at different concentrations of the analyte were introduced into a 1 cm path length quartz cuvette equipped with a Teflon® septum, under an argon atmosphere. All of the analyses were conducted using a UV-vis cary60-TR0 spectrophotometer. The absorbance show a typical Lambert-Beer linear correlation with respect to the concentration.

4.12.5.1 Uv-vis Absorption Spectra of the Reaction Components

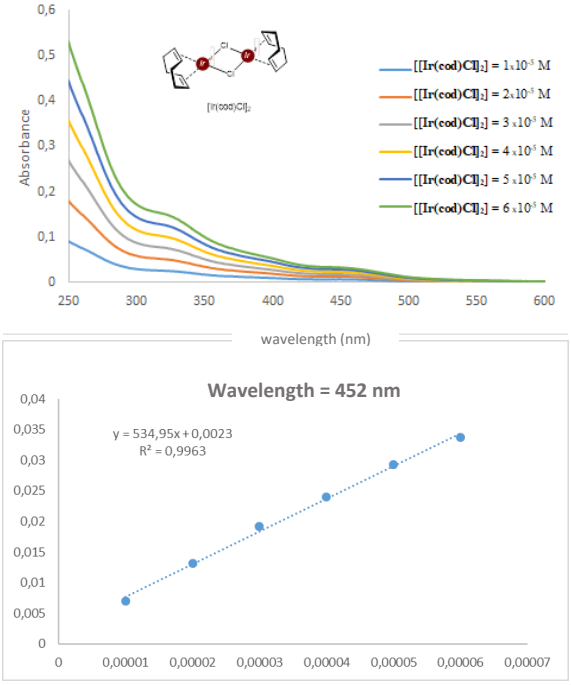

Figure 4.18. UV-vis absorption spectra for pre-catalyst **[Ir(cod)Cl]$_2$**, recorded at different concentrations in anhydrous CH_2Cl_2 (left) and Lambert-Beer linear correlation between absorbance and concentration at 452 nm for the same compound (right). The slope of the line is the molar extinction coefficient ε at 452 nm (ε = 535 M^{-1} cm^{-1}).

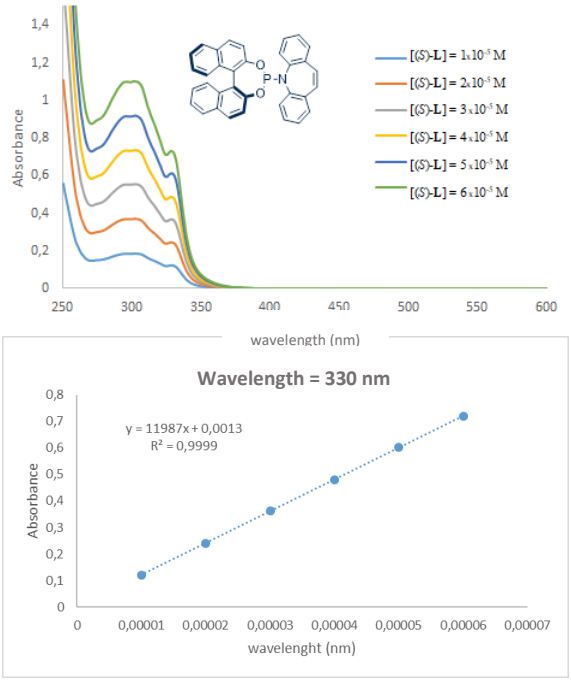

Figure 4.19: UV-vis absorption spectra for chiral ligand (*S*)-**L1**, recorded at different concentrations in anhydrous CH_2Cl_2 (left); and Lambert-Beer linear correlation between absorbance and concentration at 330 nm for the same compound (right). The slope of the line is the molar extinction coefficient ε at 330 nm (ε = 11987 M^{-1} cm^{-1}).

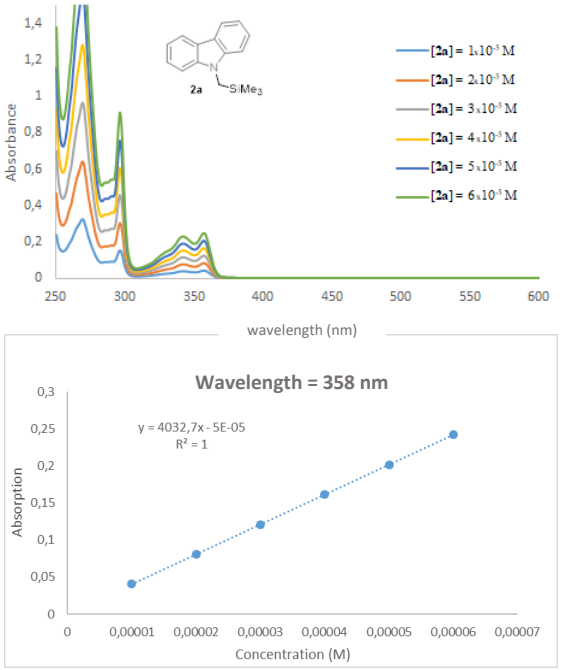

Figure 4.20. UV-vis absorption spectra of silane **2a**, recorded at different concentrations in anhydrous CH_2Cl_2 (left); and Lambert-Beer linear correlation between absorbance and concentration at 358 nm for the same compound (right). The slope of the line is the molar extinction coefficient ε at 358 nm (ε = 4032 M^{-1} cm^{-1}).

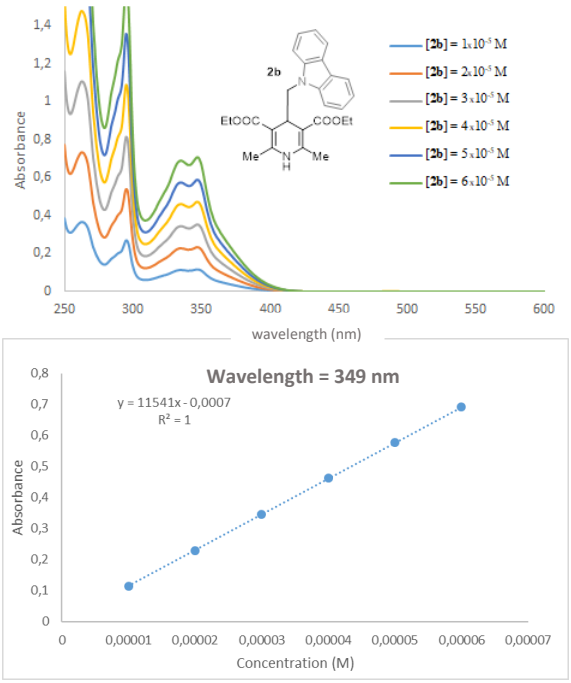

Figure 4.21. UV-vis absorption spectra of 1,4-dihydropyridine **2c**, recorded at different concentrations in anhydrous CH_2Cl_2 (left); and Lambert-Beer linear correlation between absorbance and concentration at 349 nm for the same compound (right). The slope of the line is the molar extinction coefficient ε at 349 nm (ε = 11541 M^{-1} cm^{-1}).

4.12.6 Quantum Yield Determination

A ferrioxalate actinometer solution was prepared by following the Hammond variation of the Hatchard and Parker procedure outlined in the Handbook of Photochemistry.[39,40] The ferrioxalate actinometer solution measures the decomposition of ferric ions to ferrous ions, which are complexed by 1,10-phenanthroline and monitored by UV-vis absorbance at 510 nm. The moles of iron-phenanthroline complex formed are related to moles of photons absorbed.

The following solutions were prepared and stored in a dark laboratory (red light):

[39] Murov, S. L. Ed. Handbook of Photochemistry (Marcel Dekker, New York, 1973).
[40] Hatchard, C. G. & Parker, C. A. "A new sensitive chemical actinometer. II. Potassium ferrioxalate as a standard chemical actinometer" Proc. R. Soc. Lond. A 235, 518–536 (1956).

1. *Potassium ferrioxalate solution*: 294.8 mg of potassium ferrioxalate (commercially available from Alfa Aesar) and 139 µL of sulfuric acid (96%) were added to a 50 mL volumetric flask, and filled to the mark with water (HPLC grade).

2. *Phenanthroline solution*: 0.2% by weight of 1,10-phenanthroline in water (100 mg in 50 mL volumetric flask).

3. *Buffer solution*: 2.47 g of NaOAc and 0.5 mL of sulfuric acid (96%) were added to a 50 mL volumetric flask, and filled to the mark with water (HPLC grade).

4.12.6.1 Quantum Yield for the Reaction between Alcohol 1a and Silane 2a

The actinometry measurements were done as follows:

1) 1 mL of the actinometer solution was added to a screw-cap vial and placed on a single HP LED 1.5 cm away from the light source. The solution was irradiated at 460 nm (irradiance 30 mW/cm^2). This procedure was repeated 5 times, quenching the solutions after different time intervals: 5 sec, 10 sec, 15 sec, 20 sec, and 25 sec.

2) After irradiation, the actinometer solutions were removed and placed in a 10 mL volumetric flask containing 0.5 mL of 1,10-phenanthroline solution and 2 mL of buffer solution. These flasks were filled to the mark with water (HPLC grade).

3) The UV-vis spectra of the complexed actinometer samples were recorded for each time interval. The absorbance of the complexed actinometer solution was monitored at 510 nm.

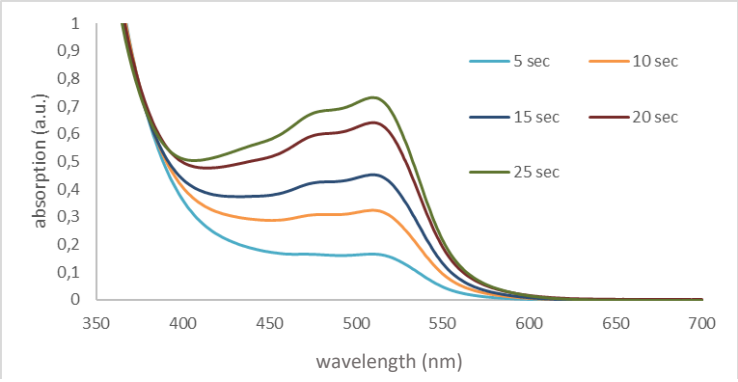

Figure 4.22. Absorbance of the complexed actinometer solutions.

The moles of Fe^{2+} formed for each sample is determined using Beers' Law (Equation S4.1):

$$Mols\ of\ Fe(II) = V_1 \times V_3 \times \Delta A(510\ \text{nm}) / 10^3 \times V_2 \times l \times \varepsilon(510\ nm) \quad \text{[Eq. S4.1]}$$

where V_1 is the irradiated volume (1 mL), V_2 is the aliquot of the irradiated solution taken for the determination of the ferrous ions (1 mL), V_3 is the final volume after complexation with phenanthroline (10 mL), *l* is the optical path-length of the irradiation cell (1 cm), ΔA (510 nm) is the optical difference in absorbance between the irradiated solution and the one stored in the dark, ε(510 nm) is the extinction coefficient the complex $Fe(phen)_3^{2+}$ at 510 nm (11100 L mol^{-1} cm^{-1}). The moles of Fe^{2+} formed (x) are plotted as a function of time (t). The slope of this line was correlated to the moles of incident photons by unit of time ($q^0_{n,p}$) by the use of the following Equation S4.2:

$$\Phi(\lambda) = dx/dt\ q_{n,p}^0\ [1-10^{-A(\lambda)}]\ \text{[Eq. S4.2]}$$

where *dx/dt* is the rate of change of a measurable quantity (spectral or any other property), the quantum yield (Φ) for Fe^{2+} at 458 nm is 1.11,[41] [$1\text{-}10^{-A(\lambda)}$] is the ratio of absorbed photons by the solution, and A(λ) is the absorbance of the actinometer at the wavelength used to carry out the experiments (460 nm). The absorbance at 460 nm A(460) was measured using a UV-vis cary60-TR0 spectrophotometer in a 10 mm path quartz cuvette, obtaining an absorbance of 0.144.

$q_{n,p}^0$, which is the photon flux, was determined to be 8.49 x10^{-8} einstein s^{-1}

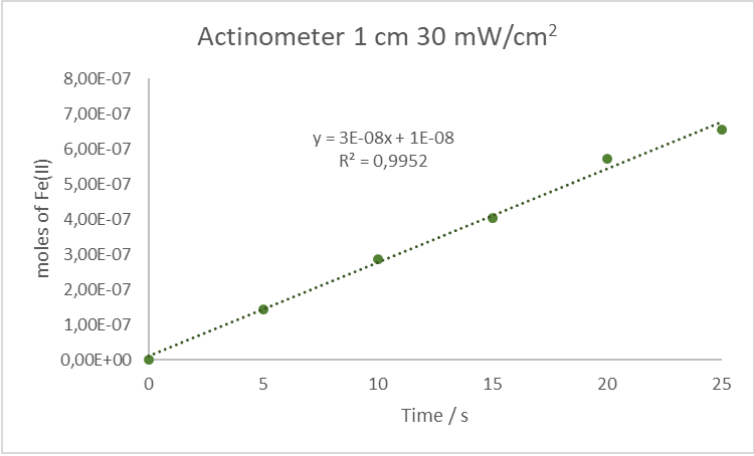

Subsequently, the photochemical reactions were performed: a screw-capped vial, fitted with a rubber septum, was charged with $[Ir(cod)Cl]_2$ (5 mg, 7.5 μmol), chiral ligand (*S*)-**L1** (17 mg, 33.0 μmol) and anhydrous acetone (1 mL), under argon atmosphere. The resulting solution was vigorously stirred for 15 minutes and, then, transferred into a vial containing 9-((trimethylsilyl)methyl)-9*H*-carbazole **2a** (76 mg, 300 μmol) and α-vinyl benzyl alcohol **1a** (79 μL, 600 μmol), affording a yellow solution. To this solution was added TFA (24 μL, 300 μmol), and the vial was sealed with a screw-cap. The vessel was

[41] Hatchard, C. G. & Parker, C. A. "A new sensitive chemical actinometer. II. Potassium ferrioxalate as a standard chemical actinometer" Proc. R. Soc. Lond. A 235, 518–536 (1956).

placed into a 3D-printed plastic support mounted on an aluminum block fitted with a blue high-power single LED (λ = 460 nm, irradiance = 30 mW/cm^2), as controlled by an external power supply (see Supporting Figure S4.1). The reaction was stirred under visible light irradiation at ambient temperature for the time stated. Three different reactions were carried out and quenched at 10 min, 20 min and 30 min, respectively.

The moles of product **3a** formed for the model reaction were determined by gas chromatography measurement (FID detector) using 1,3,5-trimethoxybenzene as internal standard. The moles of product per unit of time are related to the number of photons absorbed. The photons absorbed are correlated to the number of incident photons by the use of Equation 1. According to this, plotting the moles of product (x) versus the moles of incident photons (q_n, ^{0}·dt), the slope is equal to: Φ·(1-10$^{-A(\lambda)(460\ nm)}$), where Φ is the quantum yield to be determined and A(460 nm) is the absorption of the reaction under study. A(460 nm) was measured using a UV-vis cary60-TR0 spectrophotometer in 10 mm path quartz. An absorbance of 0.016 was determined for the model reaction mixture. The quantum yield (Φ) of the photochemical transformation was measured to be **0.14**.

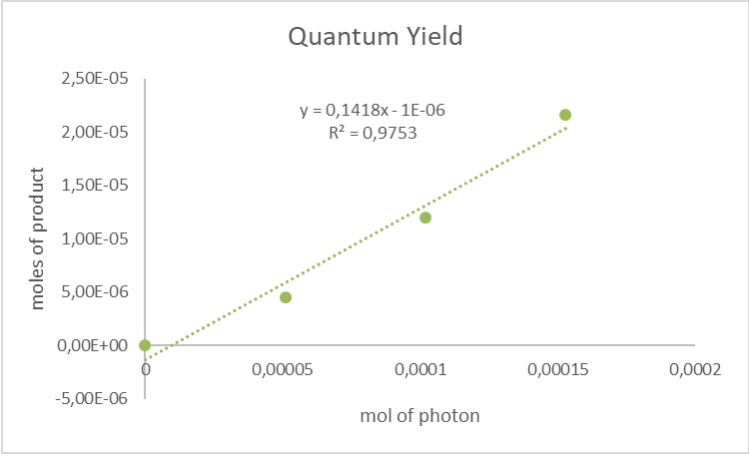

The procedure was repeated a second time to provide an akin value: quantum yield (Φ), at 460 nm of **0.13** (R^2 = 0.916; four points, 15 min, 20 min, 30 min and 40 min).

4.12.6.2 Quantum Yield for the Reaction between Alcohol 1a and 1,4-Dihydropyridine 2c

The actinometry measurements were performed as detailed in Section 4.12.6.1 with modifications relative to the light intensity used, solely:

1) 1 mL of the actinometer solution was added to a screw-cap vial and placed on a single HP LED 1.5 cm away from the light source. The solution was irradiated at 460 nm

(irradiance 11 mW/cm^2). This procedure was repeated 4 times, quenching the solutions after different time intervals: 5 sec, 10 sec, 15 sec, 20 sec, and 25 sec.

2) After irradiation, the actinometer solutions were removed and placed in a 10 mL volumetric flask containing 0.5 mL of 1,10-phenanthroline solution and 2 mL of buffer solution. These flasks were filled to the mark with water (HPLC grade).

3) The UV-Vis spectra of the complexed actinometer samples were recorded for each time interval. The absorbance of the complexed actinometer solution was monitored at 510 nm.

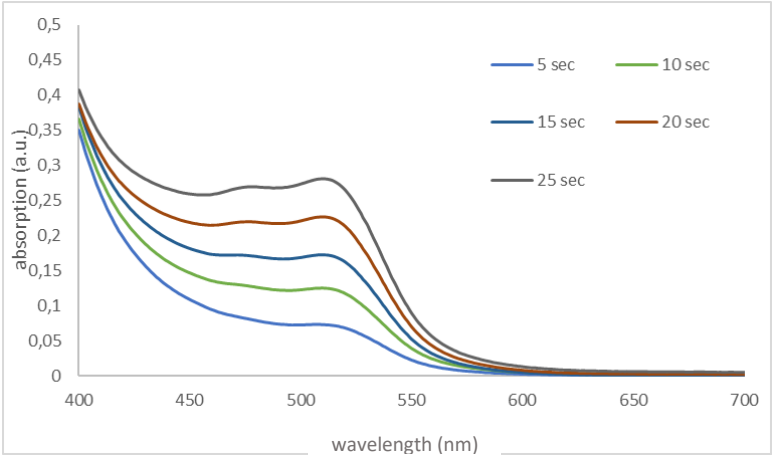

Figure 4.23. Absorbance of the complexed actinometer solutions.

The moles of Fe^{2+} formed for each sample is determined using Beers' Law (Equation S4.1):

$$Mols\ of\ Fe(II) = V_1 \times V_3 \times \Delta A(510\ \text{nm})/10^3 \times V_2 \times l \times \varepsilon(510\ nm) \quad \text{[Eq. S4.1]}$$

where V_1 is the irradiated volume (1 mL), V_2 is the aliquot of the irradiated solution taken for the determination of the ferrous ions (1 mL), V_3 is the final volume after complexation with phenanthroline (10 mL), l is the optical path-length of the irradiation cell (1 cm), ΔA (510 nm) is the optical difference in absorbance between the irradiated solution and the one stored in the dark, ε(510 nm) is the extinction coefficient the complex $Fe(phen)_3^{2+}$ at 510 nm (11100 L mol^{-1} cm^{-1}). The moles of Fe^{2+} formed (x) are plotted as a function of time (t). The slope of this line was correlated to the moles of incident photons by unit of time ($q^0_{n,p}$) by the use of the following Equation S4.2:

$$\Phi(\lambda) = dx/dt\ q_{n,p}{}^0\ [1-10^{-A(\lambda)}] \quad \text{[Eq. S4.2]}$$

where *dx/dt* is the rate of change of a measurable quantity (spectral or any other property), the quantum yield (Φ) for Fe^{2+} at 458 nm is 1.11,[39] $[1\text{-}10^{-A(\lambda)}]$ is the ratio of absorbed photons by the solution, and A(λ) is the absorbance of the actinometer at the wavelength used to carry out the experiments (460 nm). The absorbance at 460 nm A(460) was

measured using a UV-vis cary60-TR0 spectrophotometer in a 10 mm path quartz cuvette, obtaining an absorbance of 0.147.

$q_{n,p}{}^{0}$, which is the photon flux, was determined to be 2.93 $x10^{-8}$ einstein s^{-1}

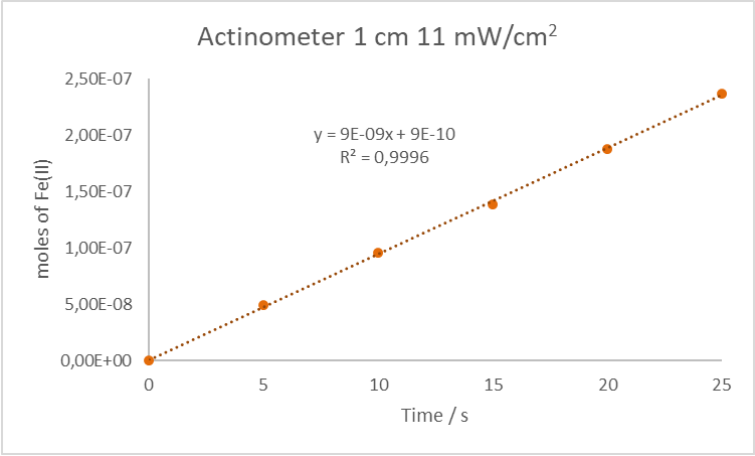

Subsequently, the photochemical reactions were performed: a screw-capped vial, fitted with a rubber septum, was charged with $[Ir(cod)Cl]_2$ (5 mg, 7.5 µmol), chiral ligand (*S*)-**L1** (17 mg, 33.0 µmol) and anhydrous, argon sparged, acetone (1 mL), under argon atmosphere. The resulting solution was vigorously stirred for 15 minutes and, then, transferred to a vial containing diethyl 4-((9*H*-carbazol-9-yl)methyl)-2,6-dimethyl-1,4-dihydropyridine-3,5-dicarboxylate **2c** (130 mg, 300 µmol) and α-vinyl benzyl alcohol **1a** (79 µL, 600 µmol) under argon atmosphere, affording a yellow solution. To this solution was added TFA (24 µL, 300 µmol) and the vial was sealed with a screw-cap. The vessel was placed into a 3D-printed plastic support mounted on an aluminum block fitted with a blue high-power single LED (λ = 460 nm, irradiance = 11 mW/cm^2), as controlled by an external power supply (see Figure S2). The reaction was stirred under visible light irradiation at ambient temperature for the time stated. Four different reactions were carried out and quenched at 2 min, 4 min, 6 min and 8 min, respectively.

The moles of product **3a** formed for the model reaction were determined by gas chromatography measurement (FID detector) using 1,3,5-trimethoxybenzene as internal standard. The moles of product per unit of time are related to the number of photons absorbed. The photons absorbed are correlated to the number of incident photons by the use of Equation 1. According to this, plotting the moles of product (x) versus the moles of incident photons ($q_n, {}^{0} \cdot dt$), the slope is equal to: $\Phi \cdot (1\text{-}10^{-A(\lambda)(460\ nm)})$, where Φ is the quantum yield to be determined and A(460 nm) is the absorption of the reaction under study. A(460 nm) was measured using a UV-Vis cary60-TR0 spectrophotometer in 10 mm path quartz. An absorbance of 0.043 was determined for the model reaction mixture. The quantum yield (Φ) of the photochemical transformation was measured to be **0.80**.

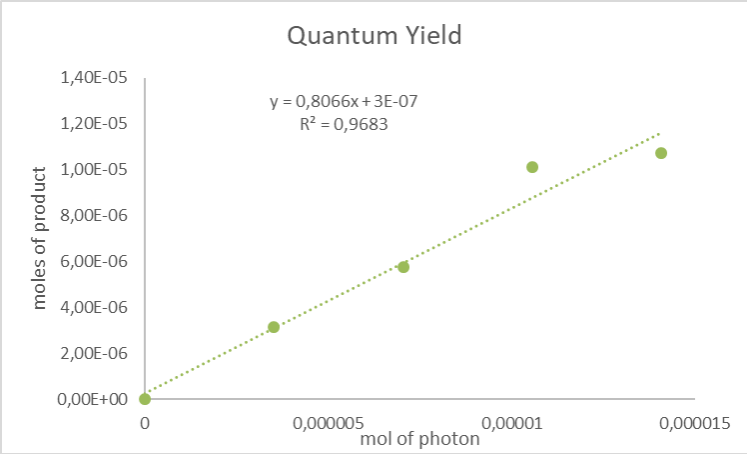

The procedure was repeated a second time to provide an akin value: quantum yield (Φ) at 460 nm of **0.66** (R^2 = 0.98; three points, 5 min, 10 min and 15 min).

4.12.7 Control Experiments

4.12.7.1 Reaction in the Dark

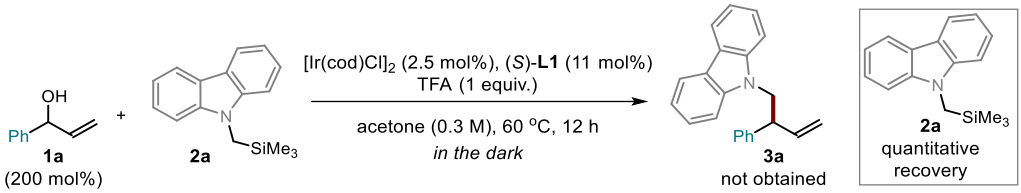

Scheme 4.32: Control experiment reaction in absence of light.

A screw-capped vial, fitted with a rubber septum, was charged with $[Ir(cod)Cl]_2$ (1.7 mg, 2.50 μmol), chiral ligand (*S*)-**L1** (5.6 mg, 11.0 μmol) and anhydrous, argon sparged acetone (300 μL), under an argon atmosphere. The resulting solution was vigorously stirred for 15 minutes and, then, transferred to a Schlenk tube containing alcohol **1a** (26.2 μL, 200 μmol) and 9-((trimethylsilyl)methyl)-9*H*-carbazole **2a** (25.3 mg, 100 μmol), affording a yellow solution. TFA (7.66 μL, 100 μmol) was added to this solution, and the Schlenk tube was sealed with a screw-cap and wrapped in an aluminum foil. The vessel was placed into an oil bath pre-heated at 60 ºC, and stirred for 16 hours. The reaction was allowed to cool down to ambient temperature and the volatiles were removed under reduced pressure. ^{1}H NMR analysis on the crude mixture, using mesitylene (14 μL) as internal standard, revealed that no reaction occurred, while silane **2a** remained completely unreacted.

4.12.7.2 Ability of II to Generate Radicals upon Photoexcitation and Trigger a Radical Allylation

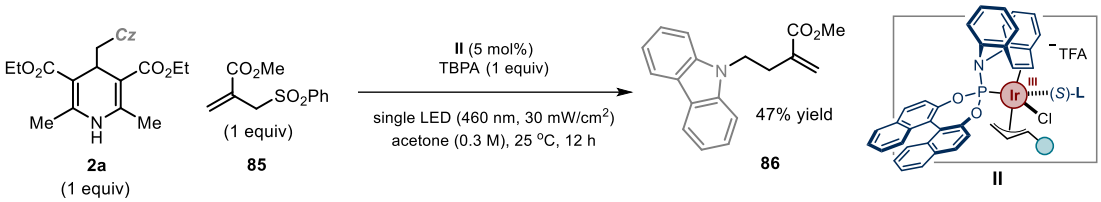

Scheme 4.33: Radical generation and trap under photochemical conditions.

Substrate 2-((phenylsulfonyl)methyl)acrylate **5** was synthesized according to a reported procedure.[42] A Schlenk tube, fitted with a rubber septum, was charged with methyl 2-((phenylsulfonyl)methyl)acrylate **85** (24.0 mg, 100 μmol), diethyl 4-((9*H*-carbazol-9-yl)methyl)-2,6-dimethyl-1,4-dihydropyridine-3,5-dicarboxylate **2c** (43.3 mg, 100 μmol), tris(4-bromophenyl)amine (TBPA, 48.2 mg, 100 μmol), and anhydrous, argon-sparged acetone (200 μL), under argon atmosphere. To this stirring mixture was added dropwise a solution of the preformed complex **I** (7.5 mg, 5 mol%) in anhydrous, argon-sparged acetone (300 μL). The Schlenk tube was sealed with a screw-cap, placed into a 3D-printed plastic support mounted on an aluminum block fitted with a 460 nm high-power single LED (λ = 460 nm, irradiance = 30 mW/cm^2 as controlled by an external power supply, see Figure S2 for details), and stirred under visible light irradiation at ambient temperature for 12 hours. The volatiles were removed under reduced pressure, and the crude mixture was purified by flash column chromatography on silica gel (isocratic 2% Et_2O in hexane) to afford compound **86** (13.1 mg, 47% yield) as an off-white solid. The title compound was previously unknown.

Characterization of compound **86***:*
^{1}H NMR (400 MHz, $CDCl_3$): δ 8.13 – 8.04 (m, 2H), 7.49 – 7.39 (m, 4H), 7.27 – 7.19 (m, 2H), 6.11 (d, *J* = 1.0 Hz, 1H), 5.49 (d, *J* = 1.0 Hz, 1H), 4.51 – 4.44 (m, 2H), 3.80 (s, 3H), 2.84 (ddd, *J* = 8.5, 6.0, 1.0 Hz, 2H).
^{13}C NMR (101 MHz, $CDCl_3$): δ 167.3, 140.4, 137.0, 128.2, 125.8, 123.0, 120.5, 119.1, 108.8, 52.2, 42.4, 32.2.
HRMS (ESI) Exact mass calculated for $C_{18}H_{17}NNaO_2$ $[M+Na]^+$: 302.1151, found: 302.1153.

[42] Rouquet, G., Robert, F., Méreau, R., Castet, F. & Landais, Y. "Allylsilanes in "Tin-Free" Oximation, Alkenylation, and Allylation of Alkyl Halides" *Chem. Eur. J.* **2011** *17*, 13904.

4.12.7.3 Reaction in the Presence of TEMPO as the Radical Scavenger

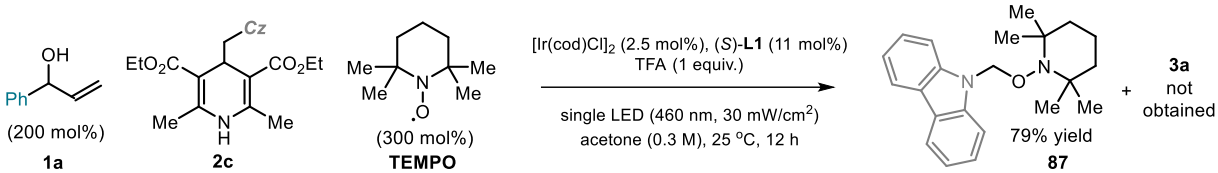

Scheme 4.34: Radical trap with TEMPO under photochemical conditions.

A screw-capped vial, fitted with a rubber septum, was charged with $[Ir(cod)Cl]_2$ (1.7 mg, 2.50 μmol), the chiral ligand (*S*)-**L1** (5.6 mg, 11.0 μmol) and anhydrous, argon-sparged acetone (300 μL), under argon atmosphere. The resulting solution was vigorously stirred for 15 minutes and transferred to a Schlenk tube containing alcohol **1a** (26.2 μL, 200 μmol), diethyl 4-((9*H*-carbazol-9-yl)methyl)-2,6-dimethyl-1,4-dihydropyridine-3,5-dicarboxylate **2c** (43.3 mg, 100 μmol) and the radical scavenger TEMPO (47 mg, 300 μmol), affording a dark orange solution. TFA (7.66 μL, 100 μmol) was added to this solution and the Schlenk tube was sealed with a screw-cap. The vessel was placed into a 3D-printed plastic support mounted on an aluminum block fitted with a 460 nm high-power single LED (λ = 460 nm, irradiance = 30 mW/cm^2 as controlled by an external power supply, see Figure 4.12 for details). The reaction was stirred under visible light irradiation at ambient temperature for 12 hours, prior to removal of the solvent under reduced pressure. ^{1}H NMR analysis on the crude mixture, using mesitylene (14 μL) as the internal standard, revealed that no product **3a** was formed. Purification of the crude mixture by flash column chromatography on silica gel (gradient from hexane to 20% toluene in hexane) provided adduct **87** (26.5 mg, 79% yield, colorless needles), derived from the TEMPO trapping of the radical formed from **2c**. The title compound was previously unknown.

Characterization of compound **87***:*

^{1}H NMR (400 MHz, $CDCl_3$): δ 8.08 (d, *J* = 7.5 Hz, 2H), 7.59 (d, *J* = 8.0 Hz, 2H), 7.48 (ddd, *J* = 8.0, 7.0, 1.0 Hz, 2H), 7.29 – 7.24 (m, 2H), 5.90 (s, 2H), 1.60 – 1.45 (m, 5H), 1.39 – 1.32 (m, 1H), 1.16 (s, 6H), 1.09 (s, 6H).

^{13}C NMR (101 MHz, $CDCl_3$): δ 140.8, 126.0, 123.5, 120.3, 119.8, 110.0, 78.5, 60.2, 40.0, 33.4, 20.3, 17.3.

HRMS (ESI) Exact mass calculated for $C_{22}H_{29}N_2O$ $[M+H]^+$: 337.2274, found: 337.2275.

4.12.8 Evaluating a Potential Radical Chain Propagation

4.12.8.1 Thermal Radical Generation Strategy

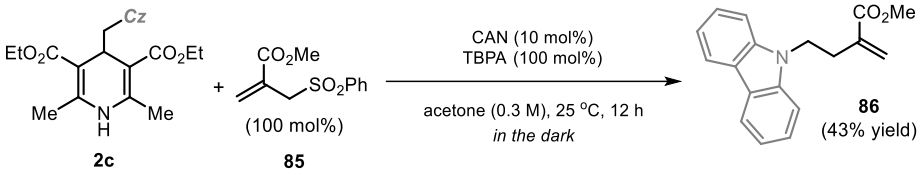

Scheme 4.35: Radical generation and trap under dark conditions using CAN/TBPA combination.

A Schlenk tube, fitted with a rubber septum, was charged with methyl 2-((phenylsulfonyl)methyl)acrylate **85** (24.0 mg, 100 µmol), diethyl 4-((9*H*-carbazol-9-yl)methyl)-2,6-dimethyl-1,4-dihydropyridine-3,5-dicarboxylate **2c** (43.3 mg, 100 µmol), tris(4-bromophenyl)amine (TBPA, 48.2 mg, 100 µmol), and anhydrous, argon-sparged acetone (200 µL), under an argon atmosphere. To this stirring mixture was added dropwise a solution of cerium ammonium nitrate (CAN, 5.48 mg, 10.0 µmol) in anhydrous, argon-sparged acetone (300 µL). The Schlenk tube was sealed with a screw-cap, and the mixture was vigorously stirred for 12 hours in the dark. The crude mixture was filtered through a short pad of silica gel, to remove the insoluble materials, and the filtrate was concentrate under reduced pressure. Purification of the crude material by flash column chromatography on silica gel (isocratic 2% Et_2O in hexane) afforded product **86** (12.1 mg, 43% yield) as an off-white solid.

4.12.8.2 Thermal Radical Generation Strategy in the Asymmetric Ir-Catalyzed Cross-Coupling

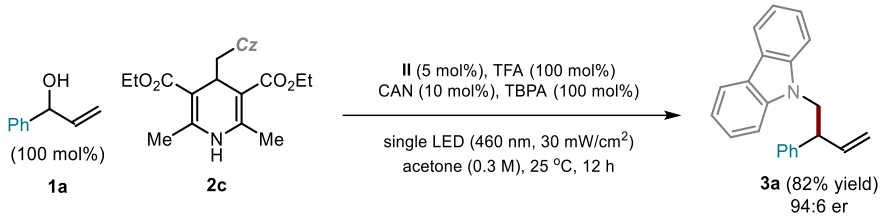

Scheme 4.36: Confirming the compatibility of the CAN/TBPA combination with complex **I**.

A screw-capped vial, fitted with a rubber septum, was charged with pre-formed complex **II** (7.5 mg, 5 mol%) and anhydrous, argon-sparged acetone (200 µL) under argon atmosphere. The resulting solution was transferred to a Schlenk tube containing α-vinyl benzyl alcohol **1a** (26.2 µL, 200 µmol), diethyl 4-((9*H*-carbazol-9-yl)methyl)-2,6-dimethyl-1,4-dihydropyridine-3,5-dicarboxylate **2c** (43.3 mg, 100 µmol) and tris(4-bromophenyl)amine (TBPA, 48.2 mg, 100 µmol), affording a yellow solution. To this solution were sequentially added TFA (7.66 µL, 100 µmol) and a solution of cerium

ammonium nitrate (CAN, 5.5 mg, 10.0 μmol) in anhydrous, argon-sparged acetone (100 μL). The Schlenk tube was sealed with a screw-cap, and placed into a 3D-printed plastic support mounted on an aluminum block fitted with a 460 nm high-power single LED (λ = 460 nm, irradiance = 30 mW/cm^2 as controlled by an external power supply). The reaction was stirred under visible light irradiation at ambient temperature for 12 hours. The crude mixture was filtered through a short pad of silica gel, to remove the insoluble materials, and the filtrate was concentrate under reduced pressure. Purification of the crude material by flash column chromatography on silica gel (isocratic 5% toluene in hexane) provided the enantioenriched product **3a** (24.5 mg, 82% yield, 94:6 er) as a colorless oil.

The same experiment was repeated in the *absence of light radiation*, by placing the reaction vessel on a stirring plate. In this case, ^{1}H NMR analysis on the crude mixture, using mesitylene (14 μL) as the internal standard, revealed substantial consumption of the 1,4-dihydropyridine radical precursor **2c** (75% conversion), but product **3a** was detected only in traces.

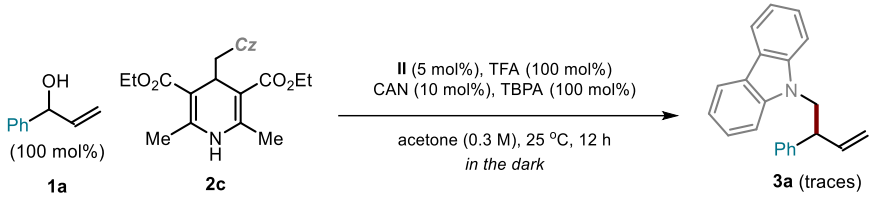

Scheme S4.37: Absence of product formation under the reaction conditions using the CAN/TBPA radicals generation system

The last result suggests that the radical, generated from **2c**, either does not add to the ground-state electrophilic complex **I** or, if it could, this event does not generate an organometallic species suitable for sustaining a radical chain propagation (*i.e.* oxidizing substrate **2c** to reform the propagating radical).

4.12.9. X-ray Crystallographic Data

4.12.9.1 Single Crystal X-ray Diffraction Data for Product 48

X-ray structure determination: stable colorless crystals of compound **48** were obtained by slow evaporation of a dichloromethane solution stored at 4ºC.

Data Collection: Measurements were made on a Rigaku MicroMax-007HF single crystal X-ray diffractometer equipped with a Pilatus 200K area detector, a Rigaku MicroMax-007HF microfocus rotating anode with $Mo_{K\alpha}$ radiation, Confocal Max Flux optics and an Oxford Cryosystems low temperature device Cryostream 700 plus (T = -173 °C). Full-sphere data collection was used with ω and φ scans.

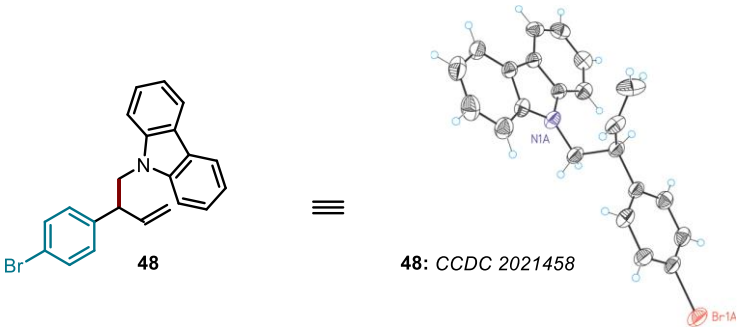

48: *CCDC 2021458*

Table 4.3. Crystal data and structure refinement for **48**. ***CCDC 2021458***

Empirical formula	C22 H18 Br N
Formula weight	376.28
Temperature	296(2)K
Wavelength	0.71073 Å
Crystal system	triclinic
Space group	P 1
Unit cell dimensions	a = 8.3897(3)Å a= 96.917(3)°.
	b = 8.6780(3)Å b = 99.133(3)°.
	c = 13.8659(4)Å g = 117.516(3)°.
Volume	862.06(5) $Å^3$
Z	2
Density (calculated)	1.450 Mg/m^3
Absorption coefficient	2.386 mm^{-1}
F(000)	384
Crystal size	0.200 x 0.100 x 0.100 mm^3
Theta range for data collection	2.714 to 32.130°.
Index ranges	-12<=h<=12,-12<=k<=12,-20<=l<=20
Reflections collected	25785
Independent reflections	11065[R(int) = 0.0255]
Completeness to theta =32.130°	94.2%
Absorption correction	Multi-scan
Max. and min. transmission	1.00 and 0.77
Refinement method	Full-matrix least-squares on F^2
Data / restraints / parameters	11065/ 63/ 472
Goodness-of-fit on F^2	0.998
Final R indices [I>2sigma(I)]	R1 = 0.0320, wR2 = 0.0814
R indices (all data)	R1 = 0.0426, wR2 = 0.0854
Flack parameter	x =-0.002(2)

Largest diff. peak and hole 0.630 and -0.248 e.Å^{-3}

4.12.9.2 Single Crystal X-ray Diffraction Data for Product 49

X-ray structure determination: stable colorless crystals of compound **49** were obtained by slow evaporation of a dichloromethane solution stored at 4ºC.

Data Collection: Measurements were made on a Rigaku MicroMax-007HF single crystal X-ray diffractometer equipped with a Pilatus 200K area detector, a Rigaku MicroMax-007HF microfocus rotating anode with $Mo_{K\alpha}$ radiation, Confocal Max Flux optics and an Oxford Cryosystems low temperature device Cryostream 700 plus (T = -173 °C). Full-sphere data collection was used with ω and φ scans.

Table 4.4. Crystal data and structure refinement for **52**. ***CCDC 2021459***

Empirical formula	C22 H18 Cl N	
Formula weight	331.82	
Temperature	296(2)K	
Wavelength	0.71073 Å	
Crystal system	tetragonal	
Space group	I 41	
Unit cell dimensions	a = 18.4165(2)Å	a= 90°.
	b = 18.4165(2)Å	b = 90°.
	c = 10.6556(3)Å	g = 90°.
Volume	3614.03(13) Å^3	
Z	8	
Density (calculated)	1.220 Mg/m^3	
Absorption coefficient	0.213 mm^{-1}	
F(000)	1392	

Crystal size	0.300 x 0.300 x 0.150 mm^3
Theta range for data collection	3.126 to 32.069°.
Index ranges	-26<=h<=27,-27<=k<=27,-15<=l<=15
Reflections collected	58409
Independent reflections	6115[R(int) = 0.0308]
Completeness to theta =32.069°	98.2%
Absorption correction	Multi-scan
Max. and min. transmission	1.00 and 0.63
Refinement method	Full-matrix least-squares on F^2
Data / restraints / parameters	6115/ 1/ 217
Goodness-of-fit on F^2	0.998
Final R indices [I>2sigma(I)]	R1 = 0.0501, wR2 = 0.1520
R indices (all data)	R1 = 0.0888, wR2 = 0.1805
Flack parameter	x =0.03(2)
Largest diff. peak and hole	0.090 and -0.188 e.$Å^{-3}$

Chapter V

General Conclusions

During my doctoral studies, I have exploited the direct photochemistry as a means to empower asymmetric metal-catalyzed transformations, using 4-alkyl-1,4-dihydropyridines (alkyl-DHPs) as versatile reagents. Chapter III describes a light-driven asymmetric nickel-catalyzed acyl cross-coupling for the synthesis of enantioenriched α,α-disubstituted ketones. The chemistry exploits the ability of photoexcited alkyl-DHPs to serve as strong reductants, sustaining the nickel catalytic cycle, and as radical sources. Easily prepared symmetrical anhydrides provides for the electrophilic partner. This transformation enables the stereoselective installation of biological relevant indole and carbazole moieties as well as benzylic fragments within the final product.

In Chapter IV, we showed that by the means of light excitation we could divert the polar reactivity of a well-established chiral (η^3-allyl)iridium(III) complex, switching on novel catalytic functions. The electrophilic feature of this organo-iridium intermediate is repurposed to trigger SET pathways, enabling the oxidation of 4-alkyl-DHPs serving as ground-state reductants and radical sources. We exploited this findings to realize an enantioselective alkyl-alkyl cross-coupling reaction between allylic alcohol and 4-alkyl-DHPs. This approach enabled the synthesis of a large array of enantioenriched allyl-benzyl products adorned with biological relevant scaffolds. Mechanistic studies confirmed the essential role of (η^3-allyl)iridium(III) complex as competent photooxidant and active catalytic center.

UNIVERSITAT
ROVIRA i VIRGILI